ZANNA MARIA BEHARRY
Characterization of Anthranilate and Benzoate 1,2-Dioxygenase from *Acinetobacter* sp. Strain ADP1
(Under the direction of DONALD M. KURTZ, JR.)

Many oxygen activating enzymes that contain nonheme mononuclear iron active sites catalyze metabolically important reactions that are environmentally and medically significant. In an effort to meet demands for economical and environmentally-friendly oxidation processes and for specific oxidation products, biocatalytic routes are receiving much attention. The Rieske dioxygenases (RDO) catalyze the initial reaction in the microbial degradation of aromatic environmental pollutants. The products of the RDO reaction are also potentially useful intermediates for natural product syntheses. While more than three dozen distinct RDOs have been identified differing in their substrate specificity, few have been isolated due to instability or low expression. The aerobic soil bacterium *Acinetobacter* sp. strain ADP1 (ADP1) is able to utilize the aromatic compounds anthranilate and benzoate as sole carbon sources. The enzyme systems responsible for the initial degradation of these compounds are the chromosomally-encoded Rieske dioxygenases anthranilate 1,2-dioxygenase (AntDO) and benzoate 1,2-dioxygenase (BenDO). In this dissertation, a combination of molecular biological, biochemical and spectroscopic techniques are used to characterize the in vitro substrate specificity of AntDO and BenDO and demonstrate the importance of a highly conserved aspartate residue throughout the RDOs in catalysis. The results presented show that both AntDO and BenDO can dihydroxylate both anthranilate and benzoate to form the expected in vivo products, contrary to previous results that determined AntDO and BenDO are specific for anthranilate and benzoate in vivo, respectively. In addition, the chromosomally-encoded AntDO and BenDO can dihydroxylate a number of substituted

benzoates, which conflicts with the notion that plasmid-encoded RDOs are able to dihydroxylate a much wider range of aromatic compounds than their chromosomally-encoded counterparts.

INDEX WORDS: Rieske Dioxygenase, Substrate Specificity, Aromatic Hydrocarbon Dihydroxylation, *Acinetobacter* sp. Strain ADP1, Nonheme Iron

CHARACTERIZATION OF ANTHRANILATE AND BENZOATE 1,2-DIOXYGENASE FROM *ACINETOBACTER* SP. STRAIN ADP1

by

ZANNA MARIA BEHARRY

B.S., The University of South Carolina, 1997

A Dissertation Submitted to the Graduate Faculty of The University of Georgia in Partial Fulfillment of the Requirements for the Degree

DOCTOR OF PHILOSOPHY

ATHENS, GEORGIA

2002

CHARACTERIZATION OF ANTHRANILATE AND BENZOATE 1,2-DIOXYGENASE FROM *ACINETOBACTER* SP. STRAIN ADP1

by

ZANNA MARIA BEHARRY

Approved

Major Professor: Donald Kurtz

Committee: Ellen Neidle
Robert Phillips
Michael Johnson
Robert Scott

Electronic Version Approved:

Gordhan L. Patel
Dean of the Graduate School
The University of Georgia
August 2002

TABLE OF CONTENTS

Page

CHAPTER 1

INTRODUCTION

Purpose of the Study

These studies focus on the properties of two Rieske dioxygenases, anthranilate 1,2-dioxygenase and benzoate 1,2-dioxygenase, from the soil bacterium *Acinetobacter* sp. strain ADP1. The purpose of these studies was to determine the in vitro substrate preferences of these two enzyme systems, in order to compare them with in vivo results, and to improve our understanding of the mechanism of aromatic dihydroxylation catalyzed by the Rieske dioxygenases. Arene *cis*-dihydroxylation is an exclusive activity of the nonheme iron Rieske dioxygenases, which are responsible for catalyzing the first step in the aerobic biodegradation of aromatic hydrocarbons by bacteria (*1*). An understanding of the substrate preferences and mechanism of the Rieske dioxygenases is essential in devising strategies for their use in bioremediation of environmental aromatic pollutants and for designing more efficient routes for the synthesis of industrially relevant compounds.

A significant number of iron-containing enzymes are involved in dioxygen-dependent metabolism in both prokaryotes and eukaryotes (*1-7*). Many organisms rely on the ability of these enzymes to activate dioxygen for insertion into a hydrocarbon for their growth. The direct oxidation of hydrocarbons by dioxygen (O_2) in the absence of a catalyst is too slow to be of biological significance. Nature has evolved oxygenases that contain only iron in the form of heme, diiron, or nonheme mononuclear iron active sites and those requiring an organic cofactor in addition to nonheme mononuclear iron active

sites (Table 1.1). These oxygenases utilize ferrous iron at their active sites to activate O_2 for insertion into substrate. Representative structures of these active sites are shown schematically in Figure 1.1. The best characterized of these enzymes are the cytochrome P450 monooxygenases, which have been the subject of extensive studies resulting in detailed structural and mechanistic information (*7*). Cytochrome P450 has served as the archetype of O_2 activation by iron enzymes, and the proposed reaction mechanisms for nonheme iron oxygenases generally follow the P450 model.

Cytochrome P450 monooxygenases

Cytochrome P450CAM (P450CAM) is a member of the cytochrome P450 superfamily that catalyzes a diverse array of oxidative transformations including alkane hydroxylation, aromatic hydroxylation, epoxidation, lactonization, demethylation and *N*-, *S*-oxidation. All known P450s contain a cysteine-ligated heme active site, as shown in Figure 1.1. P450CAM catalyzes the hydroxylation of camphor to 5-*exo*-hydroxycamphor (reaction 1.1) (*8*).

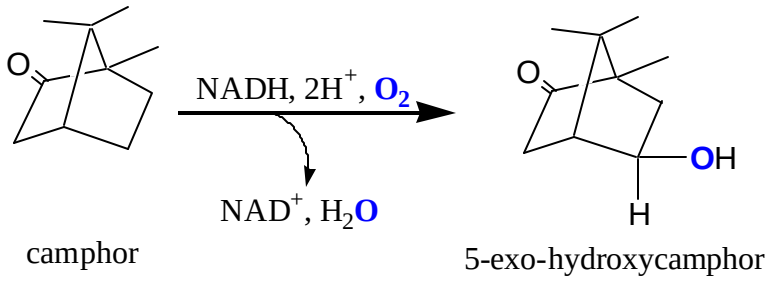

camphor 5-exo-hydroxycamphor **(1.1)**

This reaction is a monooxygenation in which one atom of dioxygen is incorporated into substrate, while the other is reduced to water. The current view of the P450CAM

Table 1.1 Examples of heme and nonheme iron oxygenases.

	Example (reference)	Reaction catalyzed
Heme		
	Cytochrome P450, e.g., P450CAM (*8*)	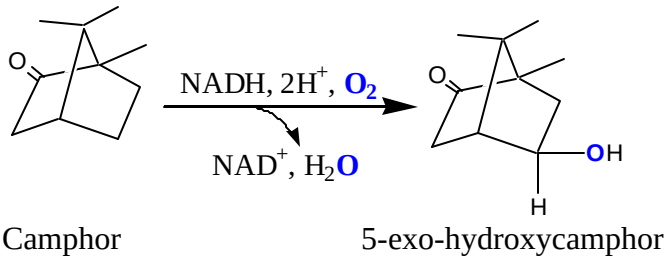 Camphor → 5-exo-hydroxycamphor
Nonheme		
Diiron		
	Methane monooxygenase (*9*)	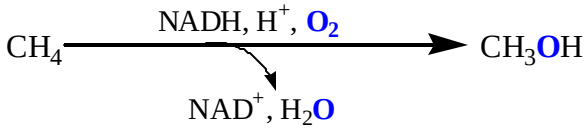 Methane → methanol
Mononuclear iron		
	Intra- and extradiol dioxygenases (*10*)	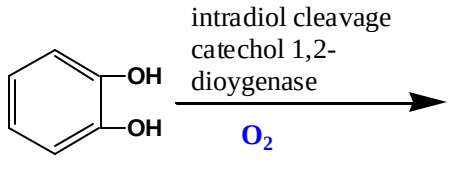 catechol → *cis, cis*-muconate
		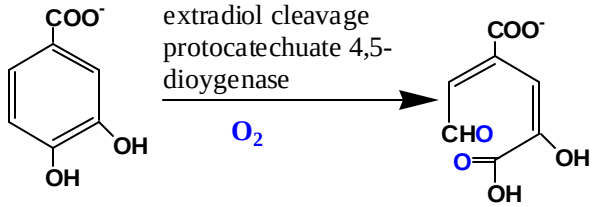 protocatechuate → 2-hydroxy-4-carboxy-muconate semialdehyde

Table 1.1
continued

	Rieske dioxygenase, e.g., naphthalene dioxygenase (*11*)	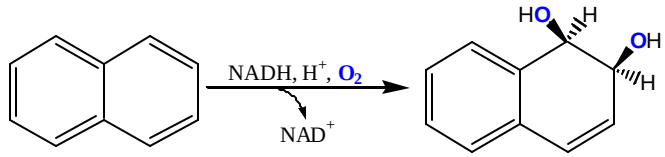 naphthalene → *cis*-1,2-dihydroxy-1,2-dihydronaphthalene
Mononuclear iron and organic cofactor		
Pterin-Dependent	Aromatic amino acid hydroxylase, e.g., tyrosine hydroxylase (*4*)	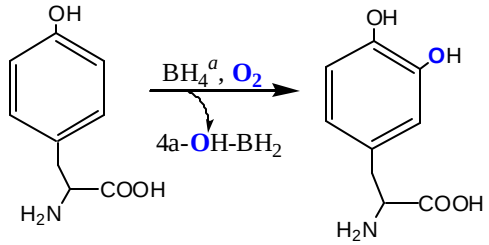 L-tyrosine → L-dopa
α-keto-glutarate-(α-KG) dependent	2,4-dichlorophenoxy-acetate dioxygenase (*6*)	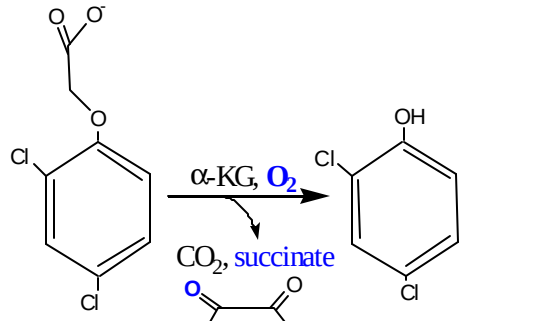 2,4-dichloro-phenoxyacetate → 2,4-dichlorophenol

[a] BH_4, tetrahydrobiopterin

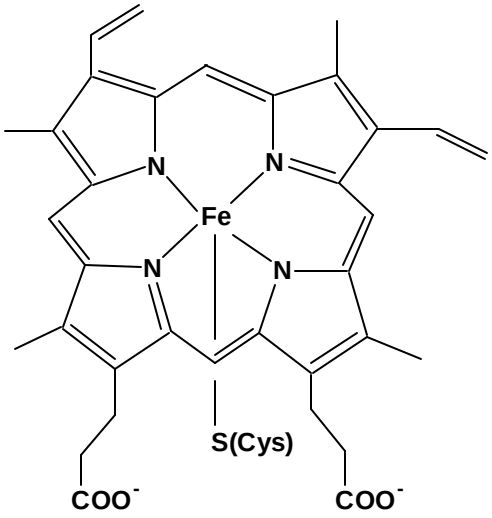

Heme

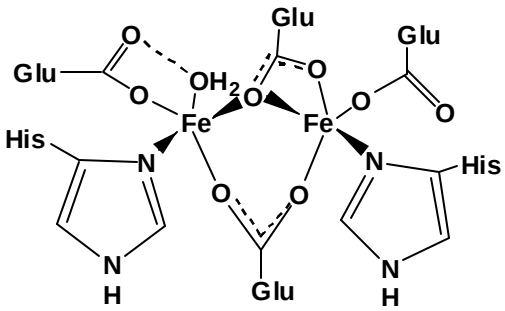

Diiron

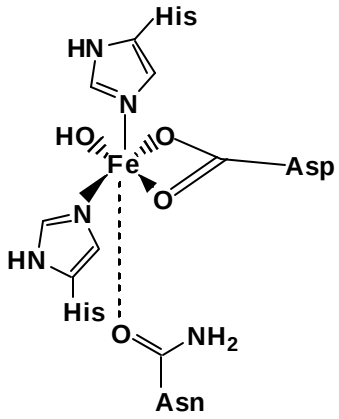

Mononuclear Nonheme Iron

Figure 1.1 Schematic drawings of the ferrous active sites of representative heme (cytochrome P450CAM) (*7*), diiron (methane monooxygenase) (*9*), and mononuclear nonheme iron (naphthalene 1,2-dioxygenase) (*12*) oxygenases.

mechanism of substrate hydroxylation is summarized in Figure 1.2. The catalytic cycle of P450CAM consists of: (i) substrate binding to a hydrophobic pocket within the enzyme resting state, **1**, leading to the ferric enzyme-substrate complex, **2**, which displaces a ferric heme coordinated water (ii) electron transfer from an exogenous source which reduces the enzyme to a ferrous-substrate complex, **3**, (iii) binding of O_2 to the heme iron to generate the ferrous-oxy (or ferric-superoxo) complex, **4**, (iv) a second electron transfer to generate a ferric-peroxo species, **5**, (v) two protonations during which the O-O bond is cleaved, water is released and the putative activated oxygen intermediate, the ferryl porphyrin cation radical species, **7**, is formed, (vi) insertion of the iron-bound oxygen of **7** into camphor to yield the product 5-*exo*-hydroxycamphor, (vii) dissociation of the product and return to the resting state, **1**. Until recently, none of the intermediates in brackets, **(5-7)**, had been directly detected, but were inferred from comparison with other metalloporphyrin enzymes and model systems. However, recently, Schlichting et.al. determined the crystal structures of intermediates in the catalytic cycle of P450CAM using cryotrapping techniques and radiolytic reduction X-ray crystallography (*13*). Their structure of the ferric P450CAM-camphor complex **(2)** was very similar to their structure of the ferrous P450CAM-camphor complex **(3)** (Figure 1.3A), and showed little difference from the originally reported ferric structure (*14*). Diffusion of O_2 into the reduced camphor-bound crystals formed the ferrous-oxy complex, **(4)**, which was confirmed spectroscopically *(10).* Dioxygen is bound end-on with the non-coordinated oxygen atom pointing toward Thr252. This residue in the substrate-binding pocket is believed to be involved in a proton delivery mechanism that facilitates O- O bond

Figure 1.2. Proposed reaction cycle of cytochrome P450CAM. The parallelogram represents the heme (*7*).

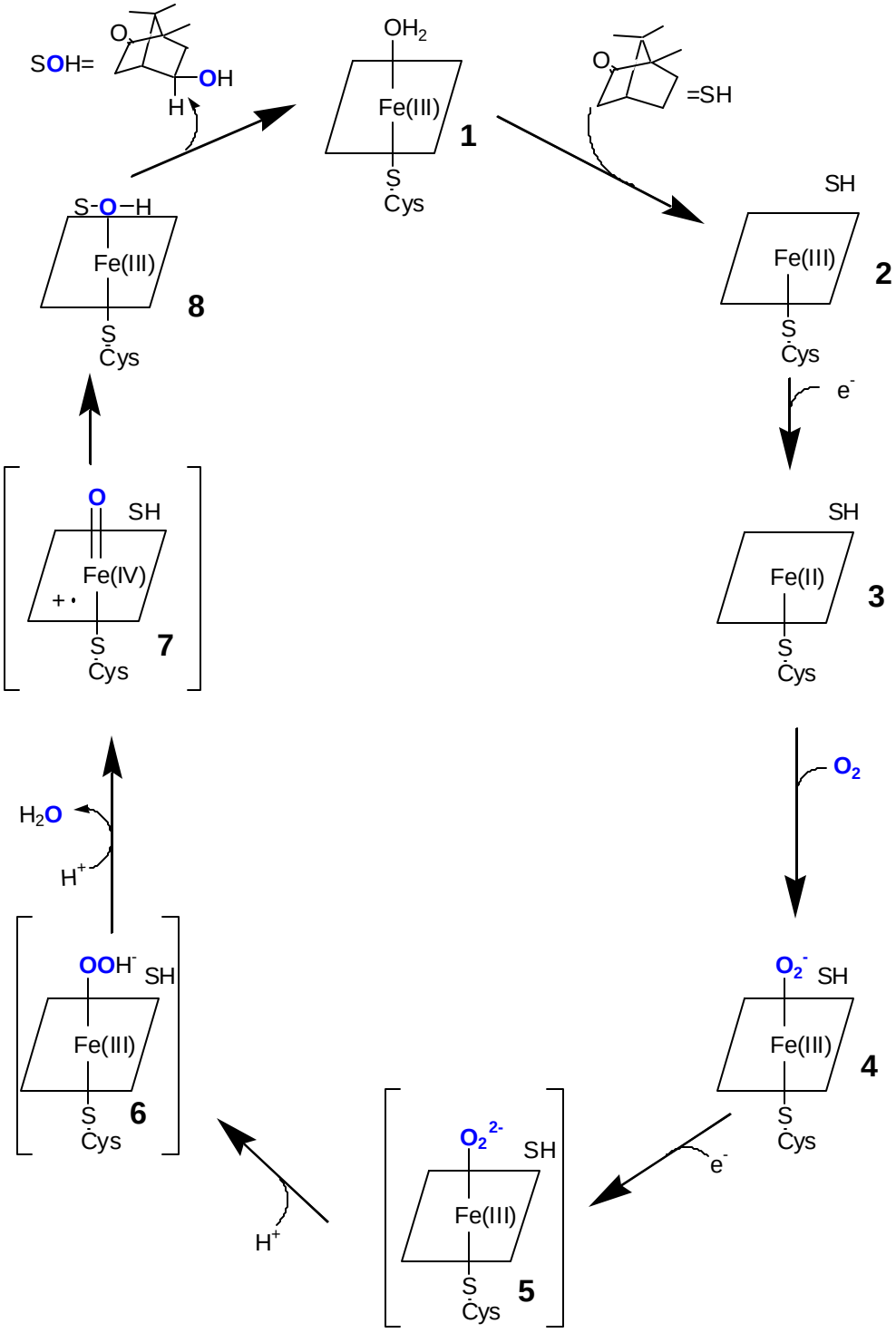
SOH=
O
OH
H
OH2
Fe(III)
1
S
Cys
O
=SH
SH
Fe(III)
2
S
Cys
e-
SH
Fe(II)
3
S
Cys
O2
O2-
SH
Fe(III)
4
S
Cys
e-
O2 2-
SH
Fe(III)
5
S
Cys
H+
OOH-
SH
Fe(III)
6
S
Cys
H2O
H+
O
SH
Fe(IV)
+•
7
S
Cys
S-O-H
Fe(III)
8
S
Cys

Figure 1.3. Wire frame representation of the crystal structures of the active site of P450CAM: (A) ferrous (Protein Databank ID 1DZ6) (*13*), (B) ferrous-oxy, camphor bound (1DZ8) (*13*), and (C) putative high-valent iron-oxo intermediate (1DZ9) (*13*) generated in ViewerLite (Accelrys, Inc.). Water (blue), molecular oxygen (red) and iron (black) are represented as spheres, camphor is shown in green.

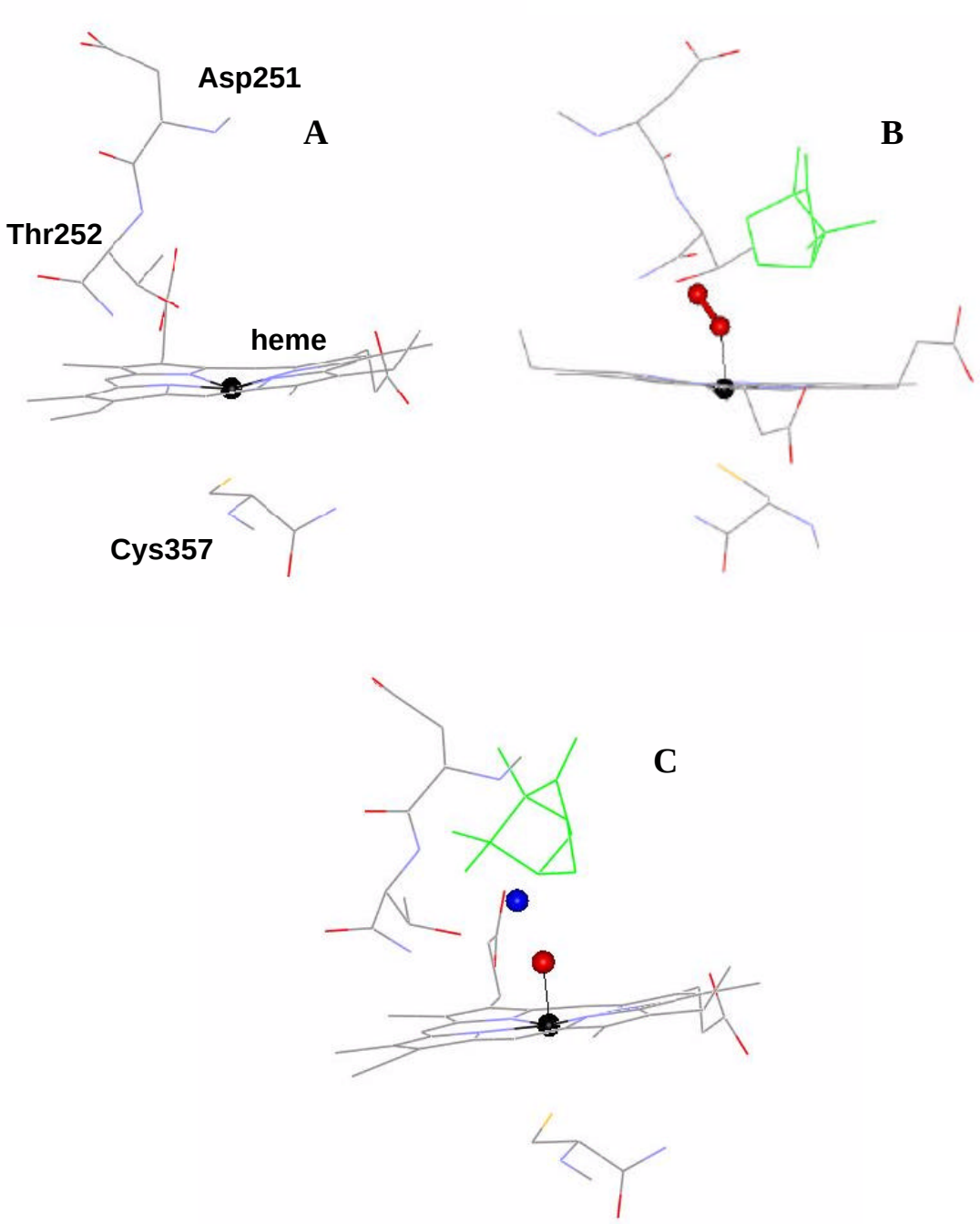
Asp251
A
B
Thr252
heme
Cys357
C

cleavage (Figure 1.3B). Addition of a second electron via radiolytic reduction at cryogenic temperatures resulted in a structure that was interpreted to have undergone O-O bond cleavage, leaving a single oxygen atom coordinated to the iron with an iron-oxygen distance of 1.65 Å (Figure 1.3C). This structure is consistent with the ferryl intermediate, **7**, based on previous time resolved X-ray diffraction studies of the active intermediate of cytochrome c peroxidase and catalase compound I. In the crystal structure of **7**, a new water molecule is observed close to the putative ferryl-bound oxygen and Thr252, which could be the water formed after O-O bond cleavage (Figure 1.3C). In addition, the camphor has moved ~0.2 Å closer to the iron, also consistent with O-O bond cleavage resulting in loss of the distal oxygen atom. The final structure obtained after warming showed electron density extending from C5 of camphor toward the iron, suggesting that the intermediates observed were capable of generating the product 5-*exo*-hydroxycamphor. The formation of 5-*exo*-hydroxycamphor from the cryoreduced crystals was confirmed by gas chromatography.

Schlichting et.al. noted the appearance of a new water molecule in the active site of the ferrous-dioxygen camphor-bound P450CAM structure that was not observed in the structure of the ferric resting state (*13*). This new water is located close to the bound dioxygen and the hydroxyl group of Thr252. In addition, both Asp251 and Thr252 have adopted an altered conformation in the ferrous-oxy complex (Figure 1.3B), in which the backbone carbonyl oxygen of Asp251 has flipped 90° toward another residue, Asn255, and the amide nitrogen of Thr252 has rotated toward the heme. These rearrangements allow for hydrogen bonds between the hydroxyl group of Thr252 and the water molecule and also prevent a conflicting interaction between Asp251 and the water molecule, both

of which would result in stabilization of this water. Previous evidence suggested a role for Thr252 and Asp251 in facilitating O-O bond cleavage via protonation (*15-19*). Mutation of Thr252 to Ala resulted in uncoupling, in which reducing equivalents are funneled into the production of hydrogen peroxide and/or water rather than the product 5-*exo*-hydroxycamphor *(14).* The crystal structure of the Thr252Ala variant showed increased ordered solvent occupancy in the substrate-binding pocket, which may contribute to the destabilization of catalytic intermediates resulting in the formation of hydrogen peroxide or water (*19*). Mutation of Asp251 to Asn resulted in an enzyme that was coupled but generated 5-*exo*-hydroxycamphor at a rate 2% that of the wild type P450CAM (*15*). Analogous to that of the Thr252Ala variant, the crystal structure of the Asp251Asn variant showed a more solvent accessible active site (*15*). Taken together, these results support a critical role for Asp251 and Thr252 in the proton delivery pathway from solvent to the ferric-peroxo intermediate **(5)** in Figure 1.2.

More recently, Davydov et. al. used electron paramagenetic resonance (EPR) and electron nuclear double resonance (ENDOR) spectroscopies to characterize intermediates in the P450CAM cycle. These intermediates were generated at cryogenic temperatures beginning with the one-electron reduced oxygen- and camphor-bound enzyme, i.e., the ferrous-oxy complex, **4**, and using γ-irradiation to introduce the second electron in the reaction cycle (*20, 21*). The Asp251Asn and Thr252Ala variants were investigated by these methods to further determine their roles in catalysis. The ferric-peroxo intermediate, **5**, was the first observed species upon cryoreduction of **4**, followed by formation of a ferric-hydroperoxo species, **6**, and the final observed species was the ferric product complex, **8**. Similar results were observed with the Thr252Ala P450CAM

variant suggesting that the first protonation event was still able to occur in this variant to generate the ferric-hydroperoxo species **(6)**, and that disruption of catalysis to yield the uncoupled product hydrogen peroxide occurs after the first proton delivery step. In contrast, cryoreduction of Asp251Asn P450CAM afforded the ferric-peroxo intermediate, **5**, however at the cryotemperatures used, conversion of **5** to **6** was hindered compared to wild type. This result suggests that the severe reduction in product formation of the Asp251Asn variant may be due to an impaired ability to deliver the first proton. The product 5-*exo*-hydroxycamphor was formed with both wild type and Asp251Asn P450CAM under these cryoconditions, however no product was observed with Thr252Ala P450CAM upon cryoreduction. These product/variant results are consistent with those previously reported at room temperature (*15*, *18*).

While the ferryl intermediate, **(7)**, proposed to be responsible for oxygen insertion into substrate has yet to be directly observed spectroscopically, evidence for its formation in the catalytic cycle of P450CAM comes from the nature of products formed with alternative substrates and from identification of a species similar to **(7)** with synthetic porphyrin models (*8*, *18*). Despite these uncertainties, the proposed reaction cycle for P450CAM has served as a template for the putative reaction cycles of other members of the P450 family and for the diiron and mononuclear nonheme-iron oxygenases.

Methane monooxygenase

Methane monooxygenase (MMO) catalyzes the oxidation of methane to methanol according to reaction 1.2 (*9*).

$$CH_4 + NADH + H^+ + O_2 \rightarrow CH_3OH + NAD^+ + H_2O \qquad \textbf{(1.2)}$$

This reaction constitutes the first step in the metabolic pathway of methanotrophic bacteria that utilize methane as their sole source of carbon and energy. Two types of MMOs are found in methanotrophic bacteria, a copper containing membrane-bound particulate form (pMMO) and an iron containing, soluble form (sMMO). Detailed studies on pMMO have proven difficult due to its instability. sMMO is much easier to purify and more stable than pMMO and therefore, much of what is known about the mechanism of reaction 1.2 comes from studies on sMMO.

sMMO is a multicomponent enzyme system consisting of an oxidoreductase (MMOR) containing both flavin and a plant-type [2Fe-2S] ferredoxin as cofactors that transfer electrons to the hydroxylase component, MMOH, which consists of three non-identical subunits in a $\alpha_2\beta_2\gamma_2$ oligomer (Figure 1.4). Each α subunit contains a carboxylate- and hydroxo-bridged diiron center where methane hydroxylation occurs. sMMO also contains a regulatory protein, MMOB, which has no cofactors and apparently influences MMOH activity by complexing with the hydroxylase component, and allosterically affecting the structure and reactivity of the diiron site (*22-27*).

sMMO has proven to be a worthy system for probing dioxygen activation at a nonheme diiron center. Similar to the studies outlined for P450CAM using artificial electron donors along with rapid spectroscopic techniques, key intermediates in the reaction cycle of MMOH have been identified (Figure 1.5) (*23*). The resting state (diferric, $\mathbf{H_{ox}}$) is reduced via MMOR to the diferrous state ($\mathbf{H_{red}}$), which are the only two stable, isolable states in the catalytic cycle. $\mathbf{H_{red}}$ reacts with dioxygen to yield a peroxo-diferric species (**P**) whose Mössbauer properties compare well with synthetic peroxo-diferric models. One atom of dioxygen is incorporated into a water molecule and

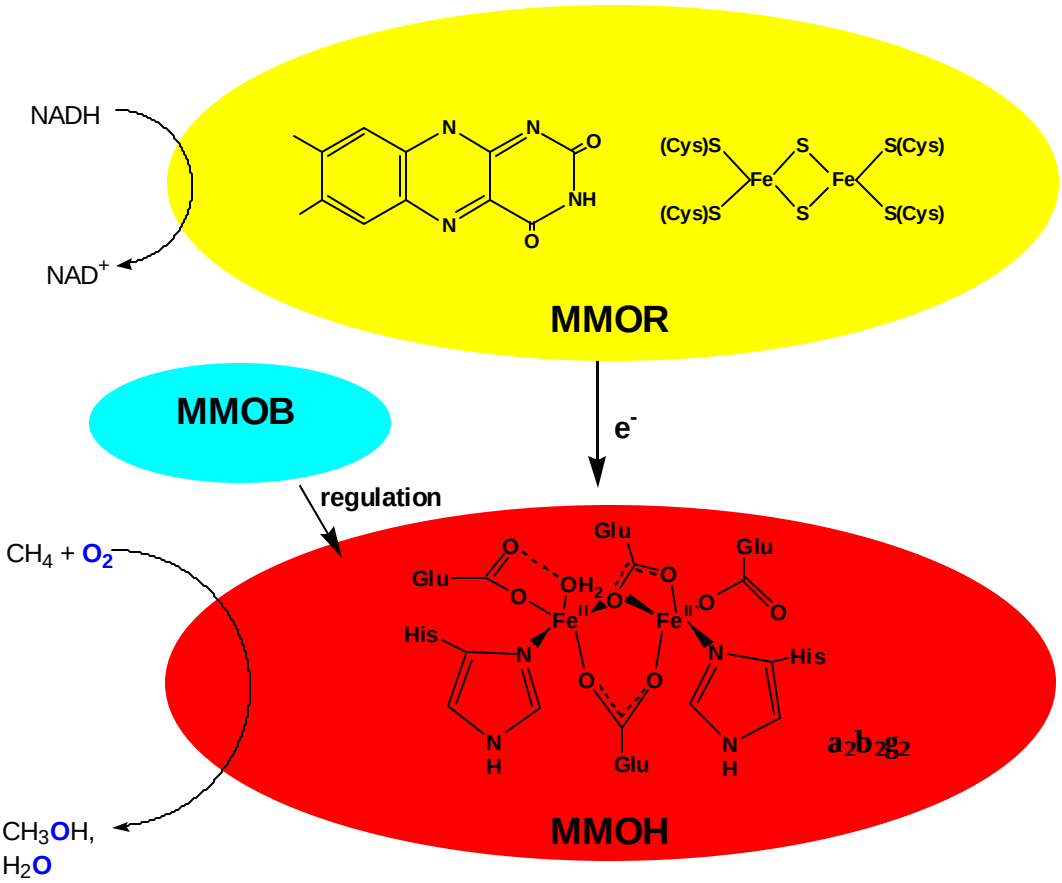

Figure 1.4. Schematic representation of the components of the soluble methane monooxygenase system.

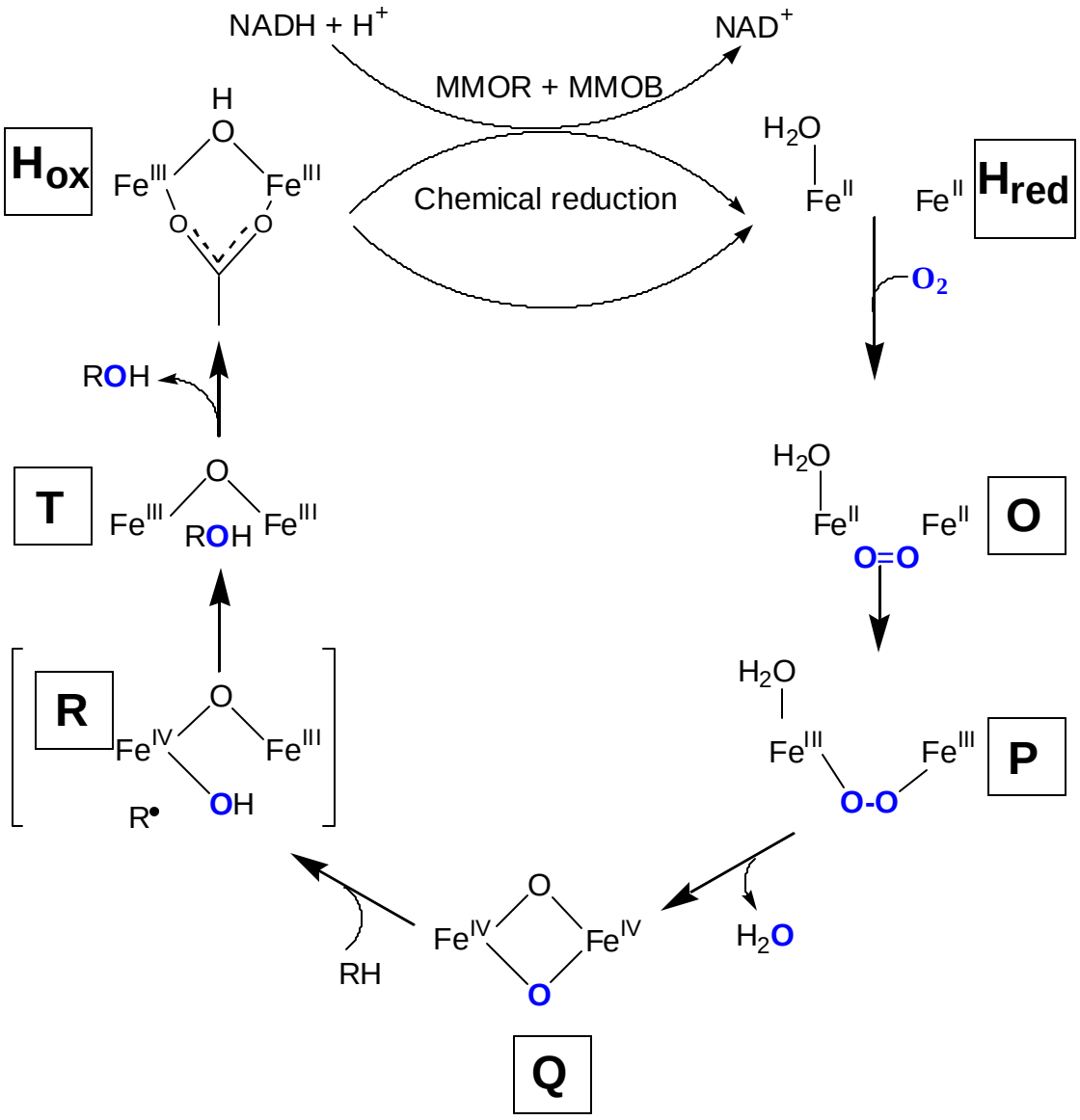

Figure 1.5. Proposed reaction cycle of methane monooxygenase (*22*).

compound **P** decays to the high-valent oxo species, compound **Q**, that has been characterized by Mössbauer and X-ray absorption spectroscopies (*28*). Compound **Q** has been shown to react with methane to yield methanol and is reminiscent of the active oxygenating species in the P450CAM cycle (**(7)**, Figure 1.2). The next species observed following **Q**, is the product-bound diferric species, Compound **T**. Product release returns the enzyme to the resting diferric state (**H_{ox}**).

The mechanism of alkane hydroxylation by compound **Q** is controversial. Three mechanisms have been suggested involving: (i) hydrogen atom abstraction from substrate, RH, generating intermediate **R** as shown in Figure 1.5; (ii) cation formation by electron abstraction of the substrate radical, R•, formed in (i); and (iii); direct oxygen atom insertion into the R-H bond by compound **Q** (*9, 29*). The use of various artificial substrates that yield characteristic products depending on the type of intermediate generated during catalysis (radical versus cation) and observation of significant kinetic isotope effects using deuterated substrates support mechanisms i or ii or a combination of both (*26, 29, 30*).

MMOH in the absence of MMOB is capable of generating product via chemical reduction or NADH/MMOR coupled turnover (*9, 27*). However, the rates of these reactions are greatly decreased, implying a significant role for MMOB in catalysis. Kinetic analyses have shown that MMOB speeds up the formation of compound **P** and the conversion of **P** to **Q**, thereby preventing the unproductive breakdown of **P**. By increasing the rate of conversion of **P** to **Q**, electrons are less likely funneled into the futile reduction of O_2 to form H_2O_2 and/or H_2O (*27*). The mechanism by which MMOB exerts these effects during turnover are not known but believed to occur through the

formation of a complex with the diiron-containing α subunit of MMOH. The formation of the MMOB/MMOH complex results in an alteration of the redox potential of the diiron site and influences the regiospecificity of the hydroxylated products with alternative substrates, suggesting that their binding in the active site is affected by the presence of MMOB (*23*). MMOB has been proposed generally to function by opening a channel for O_2 and methane to be funneled into the active site of MMOH (*26*).

While sMMO is the best studied of the diiron hydroxylases, homologous diiron aromatic hydroxylases, particularly, phenol hydroxylase, which catalyzes the formation of catechol from phenol, and toluene-4-monooxygenase (T4MO) are attracting considerable attention (*31*). These two enzymes are also three-component systems consisting of a reductase, a $\alpha_2\beta_2\gamma_2$ hydroxylase component, and a regulatory component. There is great interest in determining the factors that govern the substrate specificity of these homologous enzymes and particularly why they are unable to hydroxylate methane. Site-directed mutagenesis of amino acids in the regulatory component of phenol hydroxylase that are affected by the presence of phenol have been identified using NMR spectroscopy (*32*). These residues are conserved in the sequences of the two diiron phenol hydroxylases known but differ in the regulatory components of T4MO and MMOB. Considering the putative role of MMOB in opening a channel for substrate and O_2, it has been proposed that the corresponding regulatory components in phenol hydroxylase and T4MO may function in a similar manner and could be manipulated in order to broaden the substrate specificity of the diiron hydroxylases (*32*, *33*).

The Rieske Dioxygenases

While heme and nonheme iron oxygenases can catalyze the monooxygenation of aromatic compounds, *cis*-dihydroxylation of aromatics is a unique reaction catalyzed by the aromatic ring-hydroxylating or Rieske dioxygenases (RDOs). RDOs are multicomponent enzyme systems that catalyze incorporation of dioxygen into an aromatic ring to form *cis*-dihydrodiols (reaction 1.3) (*1*, *34*, *35*).

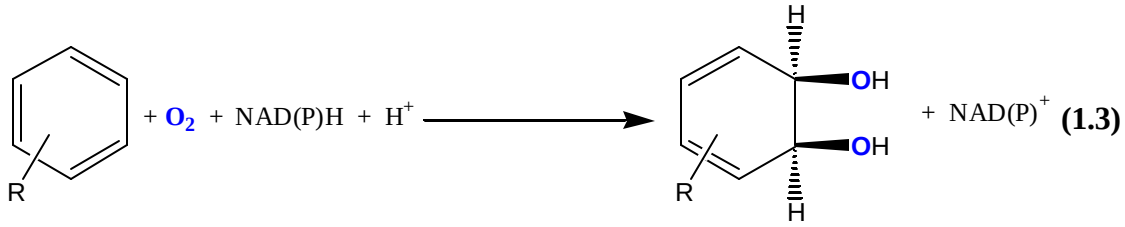

(1.3)

Many RDOs have been found in *Pseudomonas* and *Acinetobacter* species of aerobic soil bacteria, where they catalyze the first step in the aerobic degradation of aromatic compounds (reaction 1.3). These bacteria can, thereby, utilize these aromatics as their sole carbon source, which are degraded via either catechol or protocatechuate (Figure 1.6) (*36*).

The RDOs have received much attention recently because of their potential industrial use (*34*, *35*, *37*, *38*). Aromatic compounds are common environmental pollutants. In fact, many of the organisms harboring the genes for RDOs have been isolated from aromatic hydrocarbon-contaminated sites. These microorganisms, therefore, represent an alternative means by which aromatic hydrocarbons can be removed from the environment, a process termed bioremediation (*31*, *34-40*). In addition, the ability of RDOs to catalyze the stereospecific addition of dioxygen to the aromatic

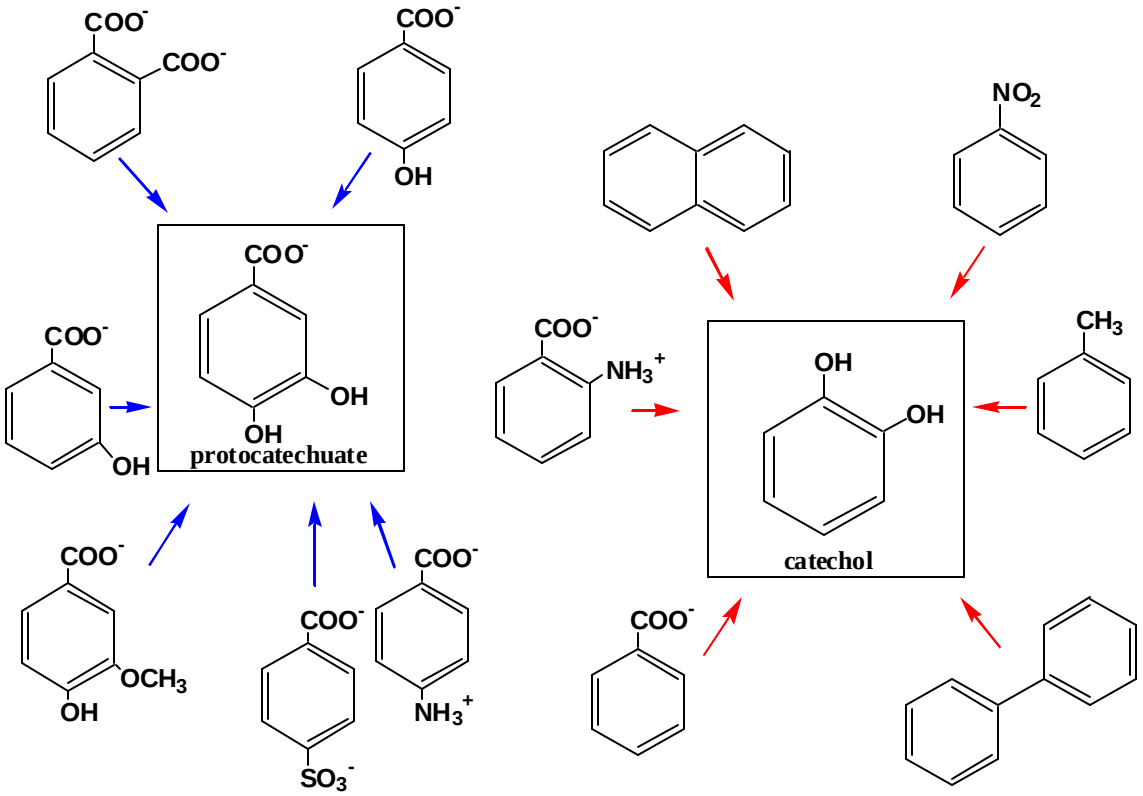

Figure 1.6. Metabolic degradation pathways of various aromatic compounds in *Pseudomonas* and *Acinetobacter* species of bacteria (*1*, *36*).

nucleus represents an environmentally benign synthetic route for the production of enantiomerically pure compounds of industrial and medical relevance (*34*, *35*, *37*) that are essentially impossible to generate using conventional synthetic procedures. For example, the RDO, toluene dioxygenase, which catalyzes the formation of *cis*-2,3-toluene dihydrodiol also catalyzes the *cis*-dihydroxylation of indene to *cis*-1*S*, 2*R*-indandiol (reaction 1.4).

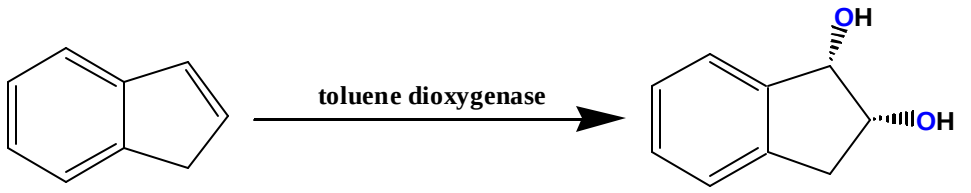

(1.4)

indene **cis-1S,2R-indandiol**

This latter compound, which has been generated in large quantities using a recombinant *E. coli* strain expressing the genes for toluene dioxygenase, is a precursor in the synthesis of Crixivan, an HIV-1 protease inhibitor (*41*). The conditions used for enzymatic synthesis are mild (moderate temperatures, atmospheric pressure, and aqueous solutions), which decrease the energy requirements, organic solvent use and unwanted byproduct formation using conventional synthetic routes, thereby contributing to an environmentally friendly synthetic process, termed “green chemistry”.

RDOs may be classified according to the composition of their protein components as shown in Table 1.2 (*1*). All of the RDOs require a reductase component that transfers electrons from NADH to the oxygenase component using either flavin alone or flavin plus a plant-type [2Fe-2S] cluster as cofactors. Some RDOs also utilize a ferredoxin to transfer electrons between the reductase and oxygenase components. The oxygenase

Table 1.2. Classification of the Rieske dioxygenases (*1, 36*)**.**

Class	Components and prosthetic group(s)			Example (reference)
	Reductase	Ferredoxin	Oxygenase	
I	FAD or FMN, [2Fe-2S]	NONE	$[2Fe\text{-}2S]_{Rieske}$, Fe(II)	Benzoate 1,2-dioxygenase (*42*, *43*)
				Anthranilate 1,2-dioxygenase (*44*)
				Phthalate 4,5-dioxygenase (*45*)
				4-chlorophenylacetate 3,4-dioxygenase (*46*, *47*)
				4-sulphobenzoate 3,4-dioxygenase (*48*)
				Chlorobenzoate 3,4-dioxygenase (*49*)
				2-halobenzoate 1,2-dioxygenase (*50*)
				2-aminobenzenesulfonate 2,3-dioxygenase (*51*)
				Toluate 1,2-dioxygenase (*52*)
II	FAD	[2Fe-2S]	$[2Fe\text{-}2S]_{Rieske}$, Fe(II)	Toluene 2,3-dioxygenase (*53*)
				Benzene 1,2-dioxygenase (*54*)
				Biphenyl 2,3-dioxygenase (*55*)
				Pyrazon dioxygenase (*56*)
				Dibenzofuran 4,4a-dioxygenase (*57*)

Table 1.2 Continued				
				Phenanthrene 3,4-dioxygenase (*58*)
				Isopropylbenzoate 2,3-dioxygenase (*59*)
				Aniline 1,2-dioxygenase (*60*)
				3-phenylpropionate 1,2-dioxygenase (*61*)
III	FAD, [2Fe-2S]	$[2Fe\text{-}2S]_{Rieske}$	$[2Fe\text{-}2S]_{Rieske}$, Fe(II)	Naphthalene 1,2-dioxygenase (*62*)
				Nitrobenzene 1,2-dioxygenase (*63*)
				2-nitrotoluene 2,3-dioxygenase (*64*)
				Carbazole 1,9a-dioxygenase (*65*)

component is comprised of either a single α subunit, or two non-identical subunits, α and β, that assemble to form an oligomeric structure. The smaller β subunit contains no cofactors and shows amino acid sequence homology only to β subunits of other RDOs (or putative RDOs) (*44*). The function of the β subunit is, therefore, thought to be structural. There are reports that in the absence of the β subunit, the α subunit alone is unable to catalyze reaction 1.3 (*66*). The larger α subunit contains both a Rieske-type [2Fe-2S] ferredoxin and a nonheme mononuclear iron center where oxygen activation and substrate hydroxylation are believed to occur (Figure 1.7).

The oxygenase component of naphthalene 1,2-dioxygenase (NDO) from *Pseudomonas* NCIB 9816-4, which catalyzes the conversion of naphthalene to *cis*-1,2-dihydroxy-1,2-dihydronaphthalene (cf. Table 1.1), is the only RDO for which a crystal structure is currently available (*12*, *37*). The two subunits of NDO form a $\alpha_3\beta_3$ hexamer. The structure of the hexamer resembles a mushroom with the β subunits forming the stem and the α subunits forming the cap (Figure 1.8).

The structure of the α subunit of NDO can be divided into two domains: the Rieske domain that contains the Rieske-type [2Fe-2S] cluster and the catalytic domain that contains the mononuclear nonheme iron site (Figure 1.8). A Rieske [2Fe-2S] center differs from the all cysteine-ligated plant-type [2Fe-2S] centers in that one iron is coordinated by two cysteines and the other by two histidines, as shown in Figures 1.7 and 1.9. The mononuclear iron at the active site is coordinated by Nδ2 of two histidines, a bidentate carboxylate from an aspartate and a water molecule. All of the residues furnishing ligands to both iron centers in NDO are strictly conserved in all known RDOs (Figure 1.10) (*11, 37, 39, 40*). The coordination geometry of the mononuclear site can be

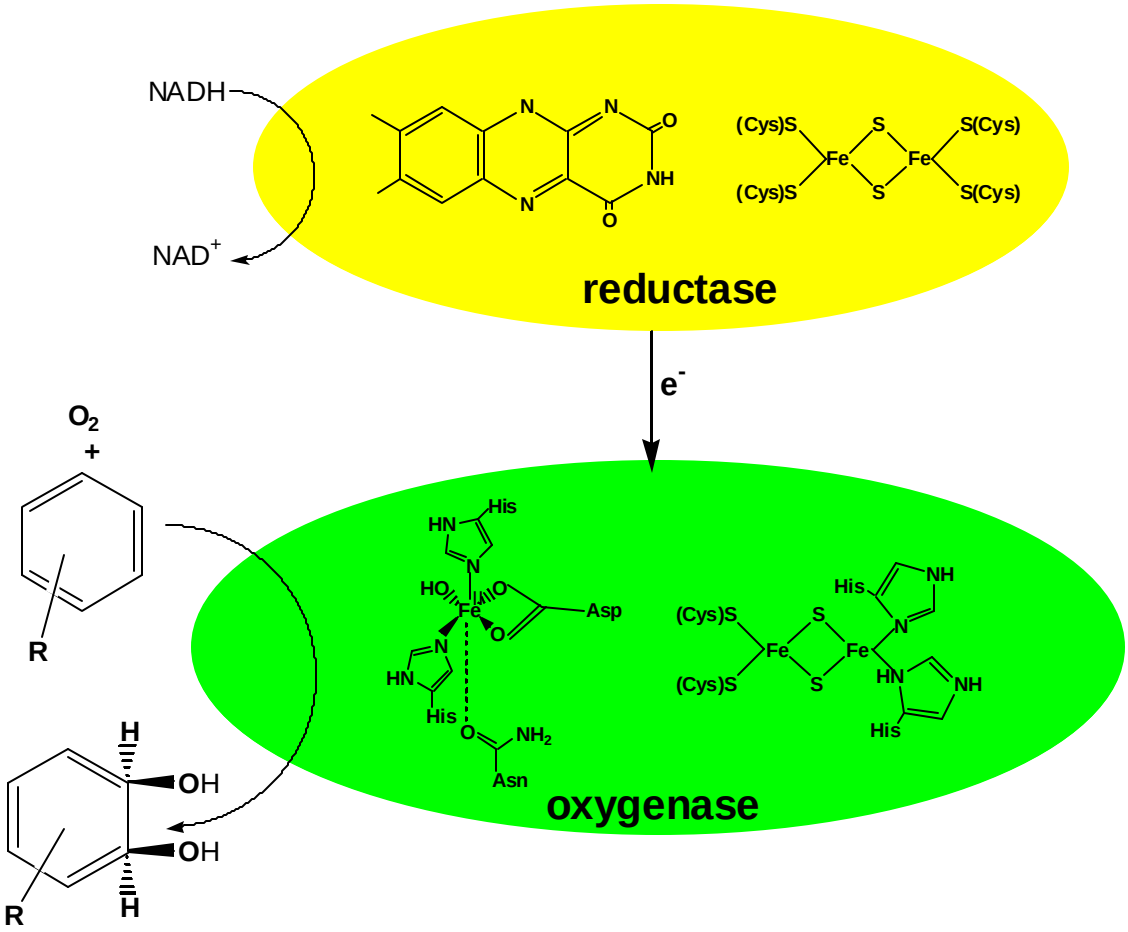

Figure 1.7. Components and cofactors of a class I Rieske dioxygenase.

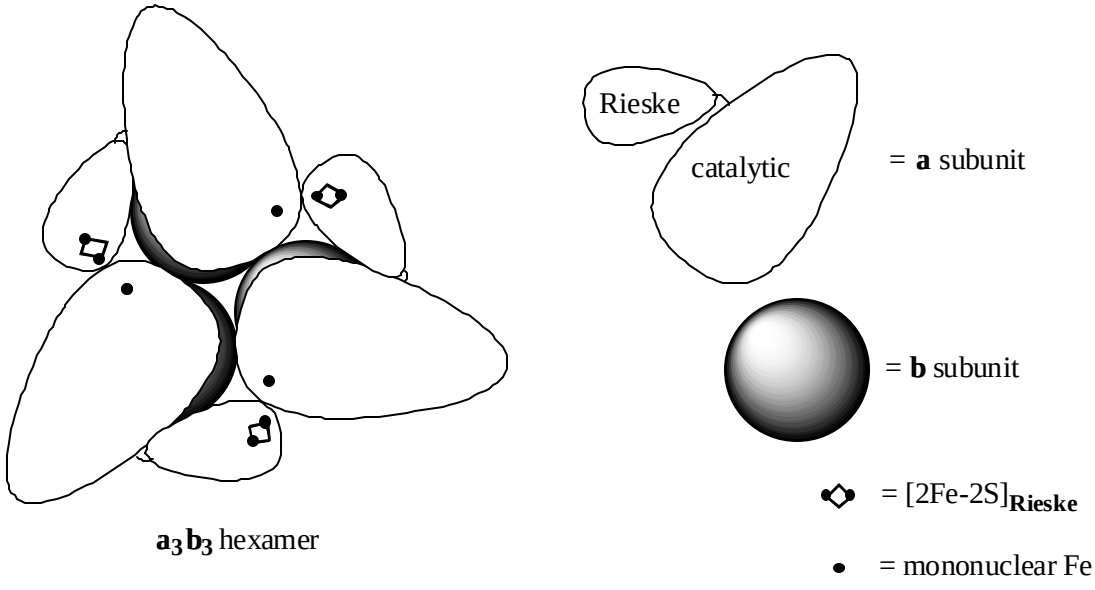

Figure 1.8. Schematic representation of the $\alpha_3\beta_3$ hexamer of naphthalene 1,2-dioxygenase.

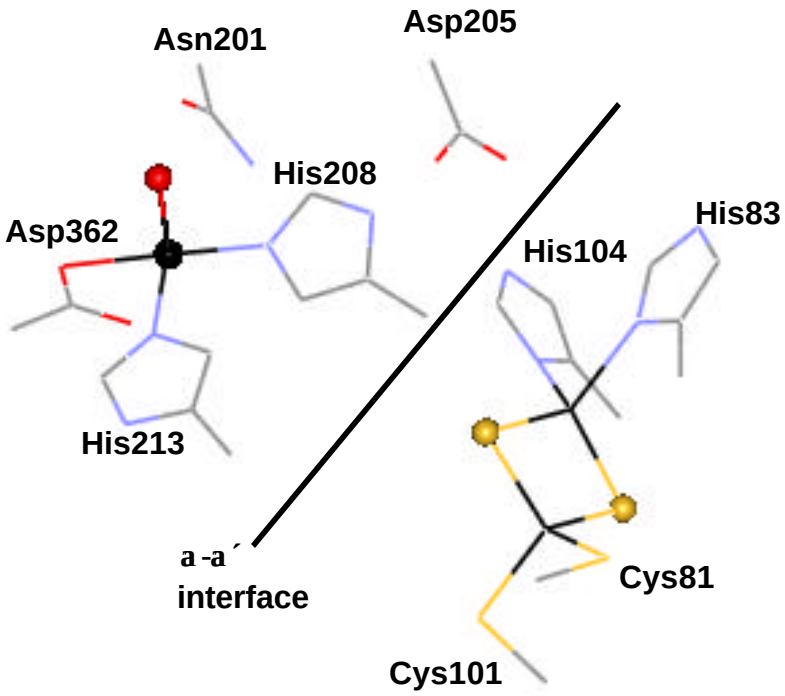

Figure 1.9. Structure of the Rieske and mononuclear iron sites across an α-α´ subunit interface. This drawing was generated in ViewerLite (Accelrys, Inc.) and coordinates from 1NDO in the Protein Data Bank (*12*). Iron atoms are represented as black spheres, inorganic sulfur atoms as orange spheres, and water as a red sphere.

described as distorted octahedral with one ligand missing. The open coordination position points in the direction of the side chain of Asn201 (Figure 1.9). However, the distance between the side chain carbonyl oxygen of Asn201 and the iron (3.75 Å) is considered too long for Asn201 to be a ligand. This 5-coordination apparently contradicts magnetic circular dichroism studies on the RDO, phthalate 4,5-dioxygenase, which indicated a six-coordinate mononuclear site in the absence of the substrate phthalate, and five-coordination upon addition of substrate (reaction 1.5). The loss of a ligand would presumably open a coordination site for O_2 to bind (*67*, *68*).

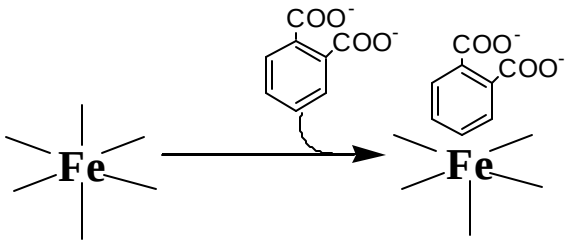

(1.5)

The facial 2-His-1-carboxylate coordination of the mononuclear iron site in NDO is a common structural motif in the mononuclear nonheme iron oxygen-activating enzymes, occurring also in the extradiol ring-cleavage enzymes and in the pterin-dependent tyrosine hydroxylase. Amino acid sequence alignment suggests that this motif is also present in the α-ketoglutarate-dependent 2,4-dichlorophenoxyacetate dioxygenase (*6*, *69*). As shown in Figure 1.10, the residues of this facial triad are conserved in all known RDOs.

The crystal structure of NDO determined that the distance between Rieske and mononuclear iron centers within each α subunit is ~44 Å, whereas the distance between these two centers in adjacent α subunits is much shorter, ~12 Å (*12*). These centers are connected through hydrogen bonds to Asp205 across the α-α′ interface. The Nε1 of the

Figure 1.10. Amino acid sequence alignment of the oxygenase component alpha subunits of RDOs: *Acinetobacter* sp. strain ADP1 anthranilate 1,2-dioxygenase (AntA), *Acinetobacter* sp. strain ADP1 benzoate 1,2-dioxygenase (BenA), *Pseudomonas putida* toluate 1,2-dioxygenase (XylX), *Burkholderia* sp. TH2 2-halobenzoate 1,2-dioxygenase (OhbA), *Pseudomonas putida* isopropylbenzoate 2,3-dioxgyenase (IpbA), *Pseudomonas putida* toluene 2,3-dioxygenase (TolA), *Pseudomonas putida* benzene 1,2-dioxygenase (BedA), *Pseudomonas pseudoalcaligenes* biphenyl 2,3-dioxygenase (BphA), *Pseudomonas putida* naphthalene 1,2-dioxygenase (NdoA), *Pseudomonas* sp. JS42 2-nitrotoluene 2,3-dioxygenase (NtdA), and *Pseudomonas resinovorans* carbazole 1,9a-dioxygenase (CarA). Conserved residues known to furnish ligands to the Rieske and mononuclear site in NdoA are shown in red and blue, respectively. The conserved aspartate, Asp205, that lies at the alpha-alpha´ subunit interface in NdoA is shown in green. Asparagine 201 that lies at the sixth coordination position of the mononuclear site in NdoA is shown in pink. This alignment was generated using the program Multialin (*70*).

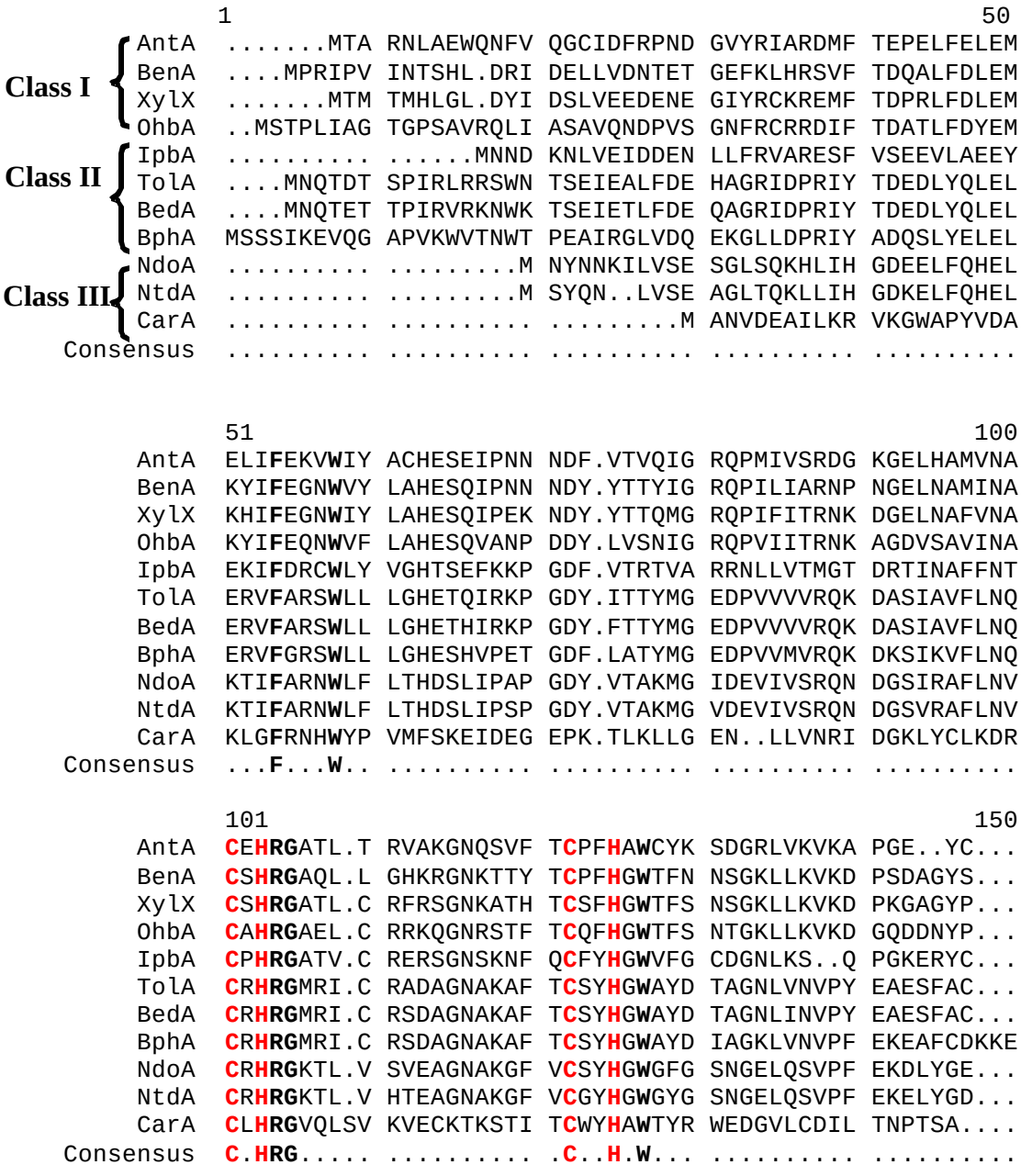
1 50
Class I
AntA .....MTA RNLAEWQNFV QGCIDFRPND GVYRIARDMF TEPELFELEM
BenA ....MPRIPV INTSHL.DRI DELLVDNTET GEFKLHRSVF TDQALFDLEM
XylX .....MTM TMHLGL.DYI DSLVEEDENE GIYRCKREMF TDPRLFDLEM
OhbA ..MSTPLIAG TGPSAVRQLI ASAVQNDPVS GNFRCRRDIF TDATLFDYEM
Class II
IpbA ....MNND KNLVEIDDEN LLFRVARESF VSEEVLAEEY
TolA ....MNQTDT SPIRLRRSWN TSEIEALFDE HAGRIDPRIY TDEDLYQLEL
BedA ....MNQTET TPIRVRKNWK TSEIETLFDE QAGRIDPRIY TDEDLYQLEL
BphA MSSSIKEVQG APVKWVTNWT PEAIRGLVDQ EKGLLDPRIY ADQSLYELEL
Class III
NdoA ....M NYNNKILVSE SGLSQKHLIH GDEELFQHEL
NtdA ....M SYQN..LVSE AGLTQKLLIH GDKELFQHEL
CarA ....M ANVDEAILKR VKGWAPYVDA
Consensus ....
51 100
AntA ELIFEKVWIY ACHESEIPNN NDF.VTVQIG RQPMIVSRDG KGELHAMVNA
BenA KYIFEGNWVY LAHESQIPNN NDY.YTTYIG RQPILIARNP NGELNAMINA
XylX KHIFEGNWIY LAHESQIPEK NDY.YTTQMG RQPIFITRNK DGELNAFVNA
OhbA KYIFEQNWVF LAHESQVANP DDY.LVSNIG RQPVIITRNK AGDVSAVINA
IpbA EKIFDRCWLY VGHTSEFKKP GDF.VTRTVA RRNLLVTMGT DRTINAFFNT
TolA ERVFARSWLL LGHETQIRKP GDY.ITTYMG EDPVVVVRQK DASIAVFLNQ
BedA ERVFARSWLL LGHETHIRKP GDY.FTTYMG EDPVVVVRQK DASIAVFLNQ
BphA ERVFGRSWLL LGHESHVPET GDF.LATYMG EDPVVMVRQK DKSIKVFLNQ
NdoA KTIFARNWLF LTHDSLIPAP GDY.VTAKMG IDEVIVSRQN DGSIRAFLNV
NtdA KTIFARNWLF LTHDSLIPSP GDY.VTAKMG VDEVIVSRQN DGSVRAFLNV
CarA KLGFRNHWYP VMFSKEIDEG EPK.TLKLLG EN..LLVNRI DGKLYCLKDR
Consensus ...F...W.. ....
101 150
AntA CEHRGATL.T RVAKGNQSVF TCPFHAWCYK SDGRLVKVKA PGE..YC...
BenA CSHRGAQL.L GHKRGNKTTY TCPFHGWTFN NSGKLLKVKD PSDAGYS...
XylX CSHRGATL.C RFRSGNKATH TCSFHGWTFS NSGKLLKVKD PKGAGYP...
OhbA CAHRGAEL.C RRKQGNRSTF TCQFHGWTFS NTGKLLKVKD GQDDNYP...
IpbA CPHRGATV.C RERSGNSKNF QCFYHGWVFG CDGNLKS..Q PGKERYC...
TolA CRHRGMRI.C RADAGNAKAF TCSYHGWAYD TAGNLVNVPY EAESFAC...
BedA CRHRGMRI.C RSDAGNAKAF TCSYHGWAYD TAGNLINVPY EAESFAC...
BphA CRHRGMRI.C RSDAGNAKAF TCSYHGWAYD IAGKLVNVPF EKEAFCDKKE
NdoA CRHRGKTL.V SVEAGNAKGF VCSYHGWGFG SNGELQSVPF EKDLYGE...
NtdA CRHRGKTL.V HTEAGNAKGF VCGYHGWGYG SNGELQSVPF EKELYGD...
CarA CLHRGVQLSV KVECKTKSTI TCWYHAWTYR WEDGVLCDIL TNPTSA....
Consensus C.HRG..... ..... .C..H.W... ....

```
          151                                                       200
     AntA  .EDF..DKSS RGLKQGRIAS YRGFVFVSLD TQATDSLEDF LGDAKVFLDL
     BenA  .DCFNQDGSH DLKKVARFES YKGFLFGSLN PVDP.SLQEF LGETTKIIDM
     XylX  .DSFDCDGSH DLKKVARFAS YRGFLFGSLR EDVA.PLEEF LGESRKVIDM
     OhbA  .EGFNVDGSH DLTRVPSFAN YRGFLFGSMN PDAC.PIEEH LGGSKAILDQ
     IpbA  .ADFITGGAG NLVPVPRFDI YAGFCFVSFN AEVE.PLPDY LAGAKEYLEL
     TolA  ....LNKKEW SPLKAR.VET YKGLIFANWD ENAV.DLDTY LGEAKFYMDH
     BedA  ....LDKKEW SPLKAR.VET YKGLIFANWD ENAI.DLDTY LGEAKFYMDH
     BphA  GDCGFDKAEW GPLQAR.VAT YKGLVFANWD VQAP.DLETY LGDARPYMDV
     NdoA  ...SLNKKCL GLKEVARVES FHGFIYGCFD QEAP.PLMDY LGDAAWYLEP
     NtdA  ...AIKKKCL GLKEVPRIES FHGFIYGCFD AEAP.PLIDY LGDAAWYLEP
     CarA  ......QIGR QKLKTYPVQE AKGCVFIYLG DGDPPPLAR. .DTPPNFLDD
Consensus  .......... .......... ..G..... .......... ..........

          201                                                       250
     AntA  MVDQSPTGEL EVLQGKSAYT FAGNWKLQNE N.GLDGYHVS .TVHYNYVS.
     BenA  IVGQSD.QGL EVLRGVSTYT YEGNWKLTAE N.GADGYHVS .AVHWNYAA.
     XylX  VVDQSP.EGL EVLRGSSTYV YEGNWKVQVE N.GADGYHVS .TVHWNYAA.
     OhbA  VIDQTP.GEL EVLRGSSSYI YDGNWKLQIE N.GGDGYHVG .SVHWNYVA.
     IpbA  VSKYSE.SGM GITTGTQEYA IRANWKLLVE N.SIDGYHAV .STHASYLD.
     TolA  MLDRTE.AGT EAIPGVQKWV IPCNWKFAAE QFCSDMYHAG TTSHLSGILA
     BedA  MLDRTE.AGT EVIPGIQKWV IPCNWKFAAE QFCSDMYHAG TTAHLSGIIA
     BphA  MLDRTP.AGT VAIGGMQKWV IPCNWKFAAE QFCSDMYHAG TMSHLSGILA
     NdoA  MF.KHS.GGL ELVGPPGKVV IKANWKAPAE NFVGDAYHVG .WTHASSLRS
     NtdA  TF.KHS.GGL ELVGPPGKVV VKANWKPFAE NFVGDIYHVG .WTHAAALRA
     CarA  ........DM EILGKNQ..I IKSNWRLAVE N.GFDPSHIY IHKDSILVKD
Consensus  .......... .......... ...NW....E ....D..H.. ...H......

          251                                                       300
     AntA  ...TVQHRQQ VNAAKGDELD TLDYSKLGAG DSETDDGWFS FKNGHSVLFS
     BenA  ...TTQHRKE KQA..GDTIR AMSAGSWG.. .KHG.GGSYG FEHGHMLLWT
     XylX  ...TQQQRKL RDA..GDDIR AMTASSWG.. .GDG.GGFYS FENGHQMVWA
     OhbA  ...TIGRRD. .RT..SDTIR TVDVTTWS.. .KKNIGGTYT FEHGHMLLWT
     IpbA  ...YLKNIND .....GFSGA KLEGKSTDLG NGHAVIEFSA PWGRPIASWV
     TolA  ......GLPE DLEMADLAPP ...TVGKQYR ASWGGHGSGF YVGDPNLMLA
     BedA  ......GLPE DLELADLAPP ...KFGKQYR ASWGGHGSGF YIGDPNMMLA
     BphA  ......GMPP EMDLSHAQVP ...TKGNQFR AGWGGHGSGW FVDEPGMLMA
     NdoA  ......GESI FSSLAGNAAL PPEGAGLQMT SKYGSGMGVL WDGYSGVHSA
     NtdA  ......GQSV FSSLAGNAKL PPEGAGLQMT SKYGSGMGLT WDYYSGNFSA
     CarA  ...NDLALPL GFAPGGDRKQ QTRVVDDDVV GRKGVYDLIG .EHGVPVFEG
Consensus  .......... .......... .......... .......... ..........
```

```
           301                                                  350
     AntA  DMPNPTVRPG YNTVMPYLVE KFGEKRAEWA MHRLRNLNLY PSLFFMDQIS
     BenA  QWGNPEDRPN F.PKAAEYTE KFGAAMSKWM IERSRNLCLY PNVYLMDQFG
     XylX  RWGDPKNRPL F.AERDRLAS EFGEARADWM IGVSRNLCLY PNLYLMDQFG
     OhbA  RLPNPEVRPV F.ARREELKA RVGEAVADAI VNQTRNLCIY PNLYVMDQIS
     IpbA  PIWGEEGKQE IDQIYARLVE LHGAEMADRM AYKNRNLLIF PNLIINDIMA
     TolA  IMGPKVTSYW TEGPASEKAA ERLGSVERGS KLMVEHMTVF PTCSFLPGIN
     BedA  MMGPKVTSYL TEGPAAEKAA ERLGSIERGT KIMLEHMTVF PTCSFLPGVN
     BphA  VMGPKVTQYW TEGPAADLAE QRLGHTMPVR RMFGQHMSVF PTCSFLPAIN
     NdoA  DLVPELMAF. .GGAKQERLN KEIGDVRARI YRSHLNCTVF PNNSMLTCSG
     NtdA  DMVPDLMAF. .GAAKQEKLA KEIGDVRARI YRSILNGTVF PNNSFLTGSA
     CarA  TIGGEVVRE. .....GAYGE KIVANDISIW LPGVLKVNPF PNPDMM....
Consensus  .......... .......... .......... .......... P.........

           351                                                  400
     AntA  SQLRIIRPVA WNKTEVISQC IGVKGESSEA RRNRIRQFED FFNVSGLGTP
     BenA  SQIRVLRPIS VNKTEVTIYC IAPVGEAPEA RARRIRQYED FFNASGMATP
     XylX  SQLRITRPLS VDRTEITIYC IAPKGETPR. RARRVRQYED FFNVSGMATP
     OhbA  TQIRVVRPIS VDKTEVTIYC FGPRDESEEV RNSRIRQYED FFNVSGMGTP
     IpbA  ITVRTFYPQA PNYMHVNGWS LAPNEESDWA RKYRLSNFLE FLGPGGFATP
     TolA  T.VRTWHPRG PNEVEVWAFT VVDADAPDDI KEEFRRQTLR TFSAGGVFEQ
     BedA  T.IRTWHPRG PNEVEVWAFT VVDADAPDDI KEEFRRQTLR TFSAGGVFEQ
     BphA  T.IRTWHPRG PNEIEVWAFT LVDADAPAEI KEEYRRHNIR TFSAGGVFEQ
     NdoA  V.FKVWNPID ANTTEVWTYA IVEKDMPEDL KRRLADSVQR TFGPAGFWES
     NtdA  T.FKVWNPID ENTTEVWTYA FVEKDMPEDL KRRLADAAQR SIGPAGFWES
     CarA  .QFEWYVPID ENTHYYFQTL GKPCANDEER KNYEQEFESK WKPMALEGFN
Consensus  .......P.. .......... .......... .......... ..........

           401                                                  450
     AntA  DDLVEFREQQ KGFQG.RIER WSDISRGYHQ WTYGPTQNSQ DLGI....EP
     BenA  DDLEELPRCQ AGYAG.IELE WNDMCRGSKH WIYGPDDAAN EIGL....KP
     XylX  DDLEEFRACQ EGFAG.GGM. .NDMSRGAKH WIEGPDEGAK EIDL....HP
     OhbA  DDLEEFRACQ SGYKG.NAAQ WNDLSRGALR WISGPDDNAR RLGL....AP
     IpbA  DDVEALESCQ NGFSNYRLVP WSDISKGMGK ETANYDDELQ MRAFWTRWNQ
     TolA  DDGENWVEIQ HILRGHKARS .RPFNAEMSM DQTVDNDPVY PGRISNNVYS
     BedA  DDGENWVEIQ HILRGHKARS .RPFNAEMSM GQTVDNDPIY PGRISNNVYS
     BphA  DDGENWVEIQ KGLRGYKAKS .QPLNAQMGL GRSQTGHPDF PGNVGY.VYA
     NdoA  DDNDNMETAS QNGKKYQSRD .SDLLSNLGF GEDVYGDAVY PGVVGKSAIG
     NtdA  DDNENMETLS QNAKKYQSSN .SDQIASLGF GKDVYGDECY PGVVGKSAIG
     CarA  NDDIWAREAM VDFYADDKGW VNEILFEVDE AIVAWRKLAS EHNQGIQTQA
Consensus  .D........ .......... .......... .......... ..........
```

```
          451                                                        501
     AntA  VITGREFTHE GLYVNQHGQW QRLILDGLNK KALKMHDVTF DNQSVMDEV....
     BenA  AISGIKTEDE GLYLAQHQYW LKSMKQAIAA EKEFASRQGE NA..........
     XylX  KLSGVRSEDE GLFVMQHKYW QQQMIKAVKR EQDRLIHAEG V...........
     OhbA  LMSGARMEDE GLFVQQHTYW AETMLRGIEA EPKVFNVQPV EVAQ.........
     IpbA  FIGGAPTPDS GVQYIPTIAL A......... .......... ............
     TolA  EEAARGLYAH WLRMMTSPDW DALKATR... .......... ............
     BedA  EEAARGLYAH WLKMMTSPDW EALKATR... .......... ............
     BphA  EEAARGMYHH WMRMMSEPSW ATLKP..... .......... ............
     NdoA  ETSYRGFYRA YQAHVSSSNW AEFEHASSTW HTELTKTTDR ............
     NtdA  ETSYRGFYRA YQAHISSSNW AEFENASRNW HTELTKTTDR ............
     CarA  HVSG...... .......... .......... .......... ............
Consensus  .......... .......... .......... .......... ............
```

Rieske center ligand, His104, is hydrogen bonded to the carboxylate of Asp205, which is, in turn, hydrogen-bonded to the mononuclear site ligand, His208 (Nδ1). This hydrogen bonding network was proposed as the electron transfer pathway between the Rieske and mononuclear sites. This Asp is strictly conserved in all amino acid sequences of known RDOs (cf. Figure 1.10) (*11, 40, 71*). Mutation of this Asp to Ala in toluene dioxygenase, resulted in an inactive enzyme (*71*). Asp205 has also been changed to Ala, Glu, Asn and Gln in NDO. Crude extracts of the recombinant Asp205Ala, Asp205Glu and Asp205Asn variants expressed in *E. coli* showed very minor product formation that could be detected only by using ^{14}C-naphthalene, while Asp205Gln NDO showed no product formation, again suggesting that Asp205 is necessary for product formation (*72*).

Re-examination of the originally published crystal structure of NDO showed the presence of planar electron density near the mononuclear site, which was modeled as indole, the source of which is most likely the bacterial growth media (*73*). Indole is a substrate for NDO, and is hydroxylated at C2 and C3 to form the product indigo (reaction 1.6). Subsequently, the structure of NDO was re-determined in the absence and presence of indole in an effort to identify residues involved in substrate interactions at the active site (*73*). The resulting indole-bound structure showed very little difference from the indole-free structure except for a 1-Å movement inward of Phe224 located at the entrance to the substrate pocket (Figure 1.11). Electron density for a water molecule that is hydrogen bonded to the iron-bound water molecule and the iron-ligand Asp362 was more clearly observed in the indole-bound structure compared to the NDO structure solved originally. Indole is oriented in the NDO active site such that its NH forms a hydrogen bond to the main chain carbonyl oxygen of Asp205 and is also close to the carbonyl

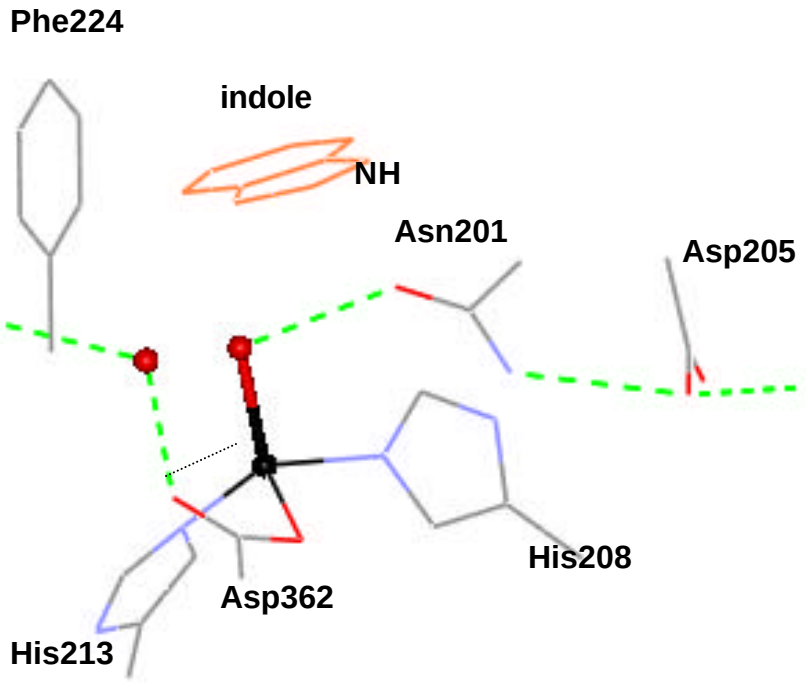

Figure 1.11. Structure of indole bound at the mononuclear iron site of naphthalene 1,2-dioxygenase. This drawing was generated using ViewerLite (Accelrys, Inc.) and coordinates from 1EG9 in the Protein Data Bank *(73)*. Iron is represented as a black sphere and water as red spheres. Hydrogen bonds are indicated by green dashed lines.

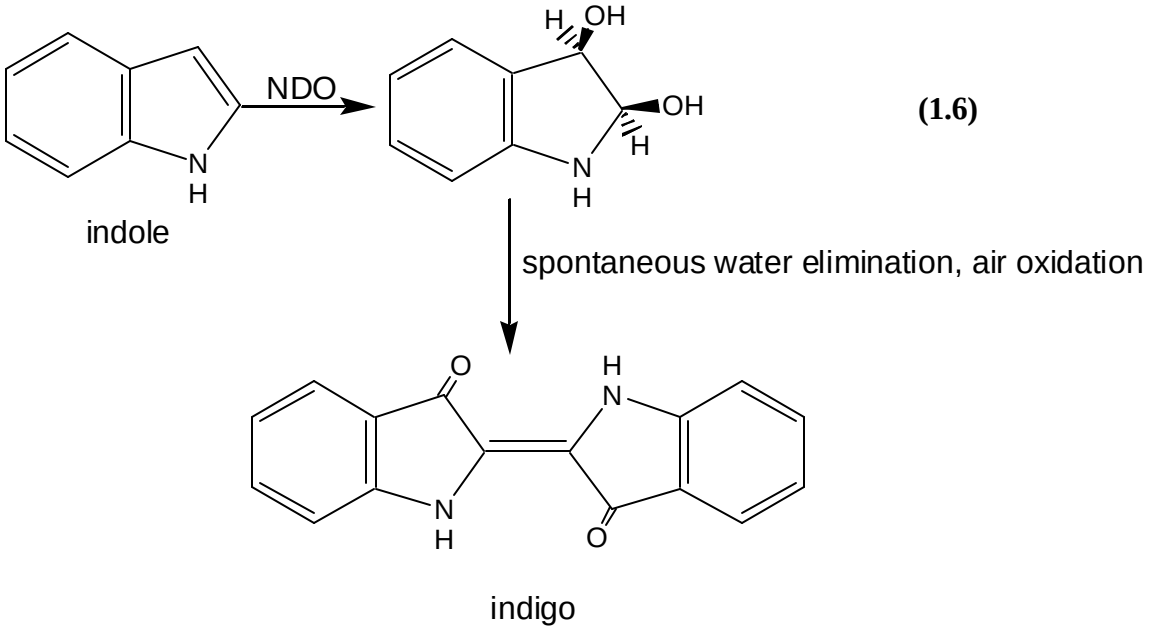

(1.6)

oxygen of Asn201. Computer modeling indicated that naphthalene would have a similar orientation as does indole at the active site, although naphthalene would be unable to form hydrogen bonds.

It was shown many years ago that for RDO-catalyzed reactions, both atoms of O_2 are incorporated into the diol product, which is why RDOs are classified as dioxygenases (*74*). Although there is very little additional information available on the mechanism of aromatic hydrocarbon dihydroxylation, a mechanism for the RDO catalytic cycle has been proposed based on the P450CAM reaction cycle (Figure 1.12) *(3)*. Beginning with the resting ferrous state of the enzyme, substrate and O_2 enter to form a ferrous-oxy (or ferric-superoxo) species, followed by one electron transfer from the Rieske site to generate a ferric-peroxo intermediate. This intermediate may be the active oxygenating species or alternatively, protonation and cleavage of the O-O bond could yield a high-

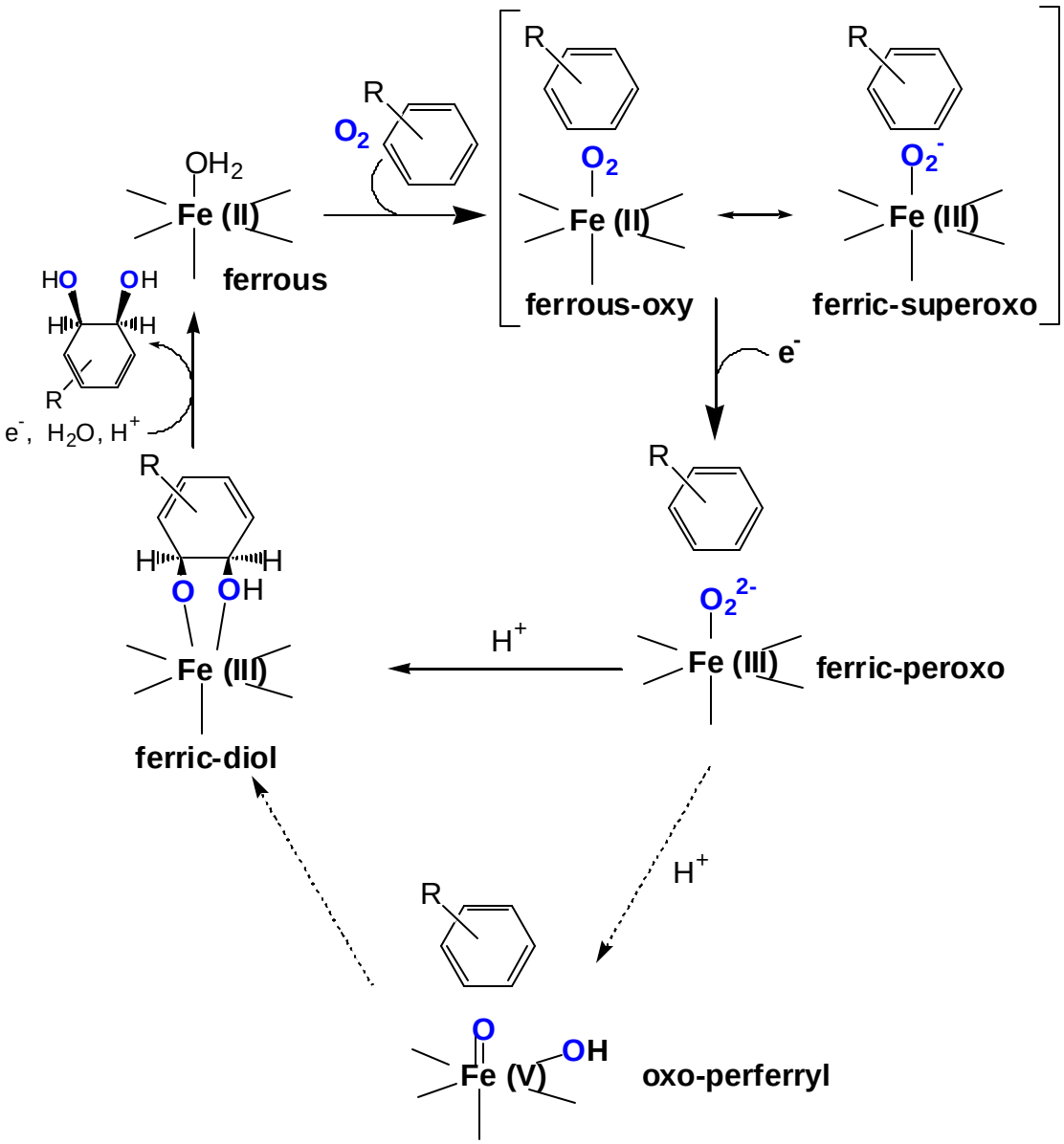

Figure 1.12. Proposed reaction cycle for the Rieske dioxygenases (*1*).

valent iron-oxo/hydroxo intermediate, reminiscent of the active oxygenating species in the P450CAM reaction cycle that may be responsible for substrate hydroxylation. Protonation of the resulting ferric-diol intermediate followed by electron transfer releases product and returns the enzyme back to the resting state. This reaction has been shown to be 1:1:1:1 in aromatic substrate:O_2:NAD(P)H:diol, which demonstrates that RDO-catalyzed dihydroxylation thus, requires two electrons. Unlike P450s, the resting state of the mononuclear iron site is ferrous even in air. Consistent with the proposed RDO reaction cycle, single turnover studies of NDO, in which the oxygenase component was supplied with a single electron per subunit via chemical reduction of the Rieske center and then allowed to react with O_2 and naphthalene, have shown that a stoichiometric amount of the product, *cis*-1,2-dihydroxynaphthalene is formed with respect to the concentration of ferrous mononuclear sites and that the resulting oxidation state of these sites after single turnover is ferric (*75*). This finding would suggest that the second electron consumed in RDO turnover is needed only to return the mononuclear iron site back to the ferrous resting state for subsequent turnovers.

Several synthetic inorganic models have recently provided insight into the mechanism of oxygen activation by mononuclear nonheme iron O_2-activating enzymes (*76-82*). The first synthetic ferrous complex that was able to mimic the reaction catalyzed by RDOs has been prepared and shown to effect the *cis*-dihydroxylation of cyclic alkenes in acetonitrile but required H_2O_2 as the oxidant (*76, 78*). Dihydroxylation occurred only if the model complex presented two labile *cis* coordination sites. As shown in Figure 1.13, this complex catalyzed the conversion of cyclooctene to *cis*-cyclooctane-1,2-diol. The dihydroxylation of cyclooctene by H_2O_2 effected by this complex, when

Figure 1.13. Proposed active intermediates in the *cis*-dihydroxylation of cyclooctene catalyzed by a synthetic mimic of Rieske dioxygenases using ^{16}**O**-water or ^{18}**O**-hydrogen peroxide (*76, 78*).

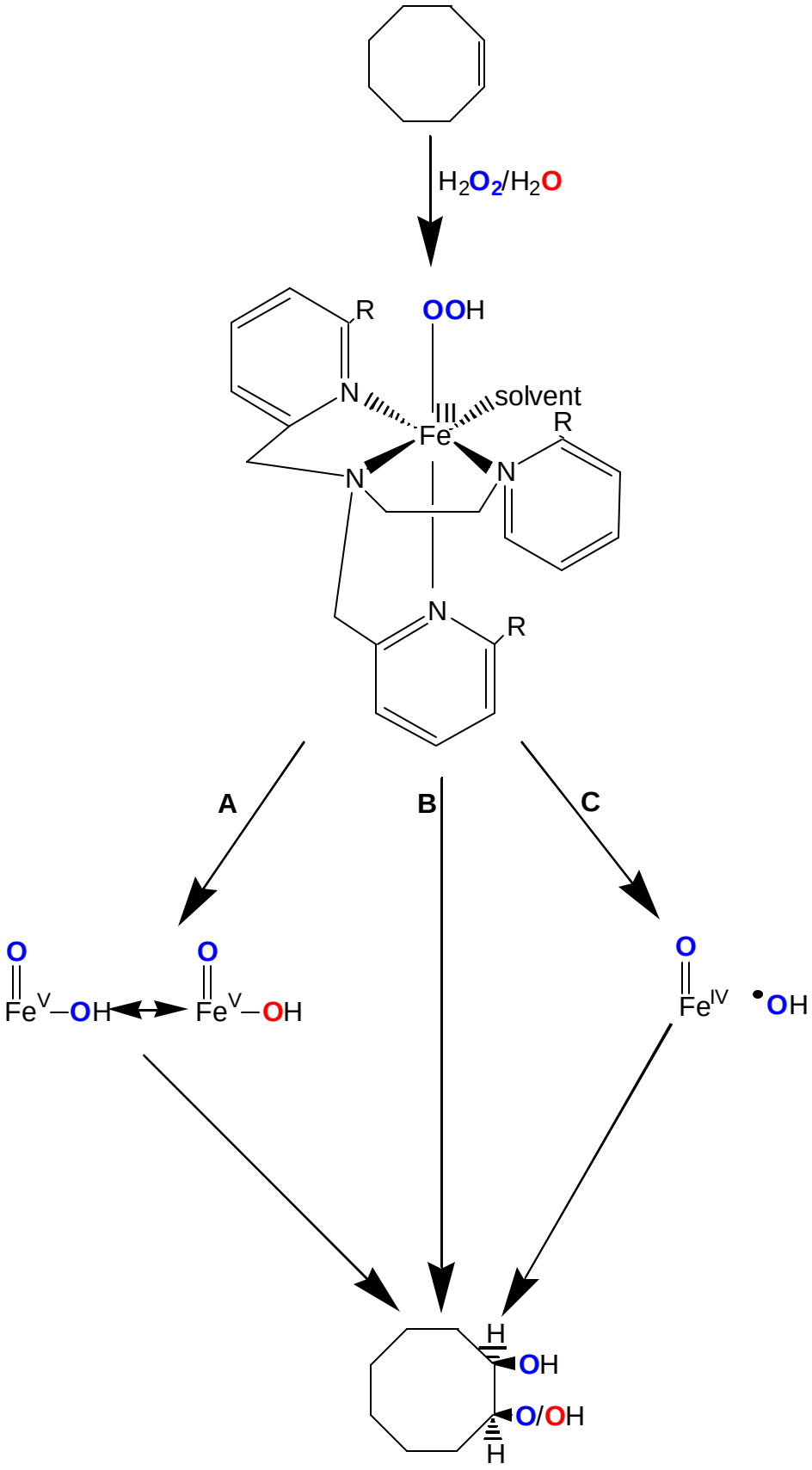
H2O2/H2O
R
OOH
N
III
Fe
solvent
R
N
N
N
R
A
B
C
O
Fe^V–OH
O
Fe^V–OH
O
Fe^IV
•OH
H
OH
O/OH
H

carried out anaerobically, afforded the same amount of stereospecific *cis*-dihydroxylated product, showing that O_2 does not participate. Oxygen incorporation into product using ^{18}O-labeled H_2O_2 and a one hundred-fold excess of $H_2{}^{16}O$ over the complex resulted in 95% of the doubly ^{18}O-labeled *cis*-diol and 4% singly labeled. Alternatively, using $H_2{}^{16}O_2$ and a one-hundred fold excess of $H_2{}^{18}O$ generated only 1 % singly ^{18}O-labeled diol and no doubly ^{18}O-labeled product. These isotopic distributions suggest that the active oxygenating species responsible for stereospecific hydroxylation is capable of a small proportion of oxygen atom exchange with water. The proposed mechanism for alkene hydroxylation based on the above observations is shown in Figure 1.13. This mechanism presents three possible active oxygenating species. However, the stereospecificity of alkane hydroxylation, the lack of involvement of O_2 and the isotope distribution in the products led the authors to favor pathway A, which involves a perferryl intermediate analogous to the proposed active oxygenating species in the P450CAM reaction cycle. This intermediate could be capable of oxygen atom exchange with H_2O, which would account for the formation of a small proportion of singly labeled diol products. In agreement with this proposed mechanism, toluene dioxygenase has been shown to catalyze the monooxygenation of indan to 1-indanol with incorporation of ^{18}O into the alcohol product in the presence of either $^{18}O_2$ and $H_2{}^{16}O$ or $^{16}O_2$ and $H_2{}^{18}O$ (reaction 1.7) (*83*).

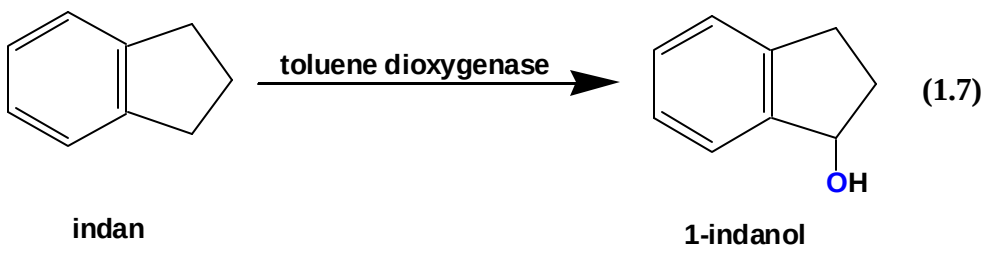

indan **1-indanol** **(1.7)**

In the presence of $^{18}O_2$ gas, 30% of the product incorporated ^{18}O, while in the presence of $^{16}O_2$ and $H_2{}^{18}O$, 68% of the1-indanol formed was ^{18}O-labeled.

At least three dozen distinct RDOs have been described, differing in their substrate specificities (*11, 37, 39, 40*). The potential use of RDOs as tools in bioremediation and green chemistry hinges on the ability of the oxygenase component to bind and subsequently oxygenate the desired substrate. Therefore, determining the factors that govern substrate specificity and developing efficient methods that allow for increased reactivity with alternative substrates is of great importance. A site-directed mutagenesis approach may be the best option for altering substrate specificity if the structure of the enzyme is available. Sequence alignments can help in identifying amino acids that are highly conserved across the classes of RDOs. Alternatively, non-conserved residues may hint at those involved in determining substrate specificity. DNA shuffling, which is the random fragmentation of a set of homologous genes followed by random reassembly, and/or random mutagenesis are alternative approaches (*84*). However, this approach requires a reliable and efficient screen for the activities of the numerous resulting chimeras and protein variants.

There are several reports in which sequence regions between two related RDOs have been exchanged to generate hybrid RDOs (*85-93*). This approach has been applied to the biphenyl dioxygenases (BPDO) from *Pseudomonas pseudoalcaligenes* KF707 (KF707) and *Burkholderia cepacia* LB400 (LB400) to determine specific residues involved in substrate preferences (*89-94*). These two BPDOs are nearly identical in amino acid sequence, however, the LB400 enzyme can dihydroxylate a wider range of substrates compared to the KF707 BPDO. Both enzymes can hydroxylate 2,5,4´-

trichlorobiphenyl but the LB400 enzyme performs a 3,4-dioxygenation of this substrate, whereas the KF707 BPDO dihydroxylates this substrate at the 2´ and 3´ positions (Figure 1.14). Amino acid sequences from the α subunits of the LB400 and KF707 biphenyl oxygenase components were combined to generate hybrid BPDOs. Activity assays of these chimeras using 2,5,4´-trichlorobiphenyl demonstrated that the C-terminal portion of the α subunits were critical in determining the substrate specificity between LB400 and KF707 BPDOs (37). Furthermore, site-directed mutagenesis of amino acids in the C-terminal portion of KF707 BPDO to the corresponding amino acids in LB400 BPDO determined that a single amino acid change in KF707 BPDO, Thr376(KF707) to Asn(LB400) conferred the ability to perform 3,4-dioxygenation of 2,5,4´-trichlorobiphenyl (*92*). However, other sequence regions in the oxygenase components of RDOs have been shown to influence the substrate specificity. Chlorobenzene dioxygenase can dihydroxylate 1,2,4,5-tetrachlorobenzene, but shows no activity toward benzene, while toluene dioxygenase can dihydroxylate benzene but shows no activity toward tetrachlorobenzene (2). Hybrid chlorobenzene/toluene dioxygenase oxygenase components and site-directed mutagenesis identified amino acids in the region of the sequence that contains the histidine ligands to the mononuclear site as crucial for determining reactivity toward these two substrates (*88*). In addition, further studies with BPDO hybrids showed that the β subunit of the oxygenase component was also involved in determining substrate specificity (*89*). There does not appear to be a consensus on the factors that influence substrate preference in the RDOs, suggesting that a combination of factors may determine substrate specificity for each individual RDO.

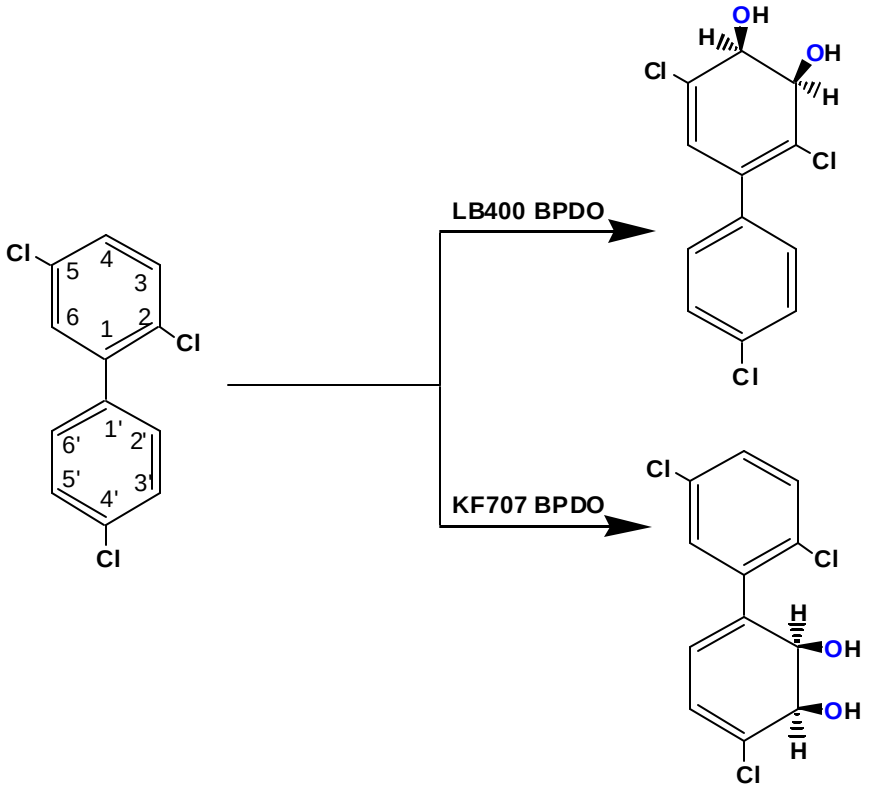

Figure 1.14. Dihydroxylation of 2,5,4´-trichlorobiphenyl catalyzed by KF707 and LB400 biphenyl 2,3-dioxygenases (*92*).

References

1. Barlow, J. N., Baldwin, J. E., Clifton, I. J., Gibson, E., Hensgens, C. M., Hajdu, J., Hara, T., Hassan, A., John, P., Lloyd, M. D., Roach, P. L., Prescott, A., Robinson, J. K., Zhang, Z. H., and Schofield, C. J. (1997) *Biochem. Soc. Trans. 25*, 86-90.
2. Bugg, T. D. (2001) *Curr. Opin. Chem. Biol. 5*, 550-555.
3. Coulter, E. D., and Ballou, D.P. (1999) *Essays in Biochemistry 34*, 31-47.
4. Fitzpatrick, P. F. (2000) *Adv. Enzymol. Relat. Areas Mol. Biol. 74*, 235-294.
5. Jordan, A., and Reichard, P. (1998) *Annu. Rev. Biochem. 67*, 71-98.
6. Lange, S. J., and Que, L., Jr. (1998) *Curr. Opin. Chem. Biol. 2*, 159-172.
7. Sligar, S. G. (1999) *Essays in Biochemistry 34*, 71-82.
8. Kauppi, B., Lee, K., Carredano, E., Parales, R. E., Gibson, D. T., Eklund, H., and Ramaswamy, S. (1998) *Structure 6*, 571-586.
9. Sono, M., Roach, M. P., Coulter, E. D., and Dawson, J. H. (1996) *Chem. Rev. 96*, 2841-2888.
10. Merkx, M., Kopp, D.A., Sazinsky, M.H., Blazyk, J.L., Muller, J., and Lippard, S.J. (2001) *Angew. Chem. Int. Ed. 40*, 2782-2807.
11. Broderick, J. B. (1999) *Essays in Biochemistry 34*, 173-189.
12. Butler, C. S., and Mason, J.R. (1997) *Adv. Microb. Physiol. 38*, 47-84.
13. Schlichting, I., Berendzen, J., Chu, K., Stock, A.M., Maves, S.A., Benson, D.E., Sweet, R.M., Ringe, D., Petsko, G.A., and Sligar, S.G. (2000) *Science 287*, 1615-1622.
14. Poulos, T. L., Finzel, B.C., and Howard, A.J. (1987) *J. Mol. Biol. 195*, 687-700.

15. Vidakovic, M., Sligar, S.G., Li, H., and Poulos, T.L. (1998) *Biochemistry 37*, 9211-9219.

16. Gerber, N. C., and Sligar, S.G. (1994) *J. Biol. Chem. 269*, 4260-4266.

17. Harris, D. L., and Loew, G.H. (1994) *J. Am. Chem. Soc. 116*, 11671-11674.

18. Imai, M., Shimada, H., Watanabe, Y., Matsushima-Hibiya, Y., Makino, R., Koga, H., Horiuchi, T., and Ishimura, Y. (1989) *Proc. Natl. Acad. Sci. USA 86*, 7823-7827.

19. Raag, R., Martinis, S.A., Sligar, S.G., and Poulos, T.L. (1991) *Biochemistry 30*, 11420-11429.

20. Davydov, R., Makris, T.M., Kofman, V., Werst, D.E., Sligar, S.G., and Hoffman, B.M. (2001) *J. Am. Chem. Soc. 123*, 1403-1415.

21. Davydov, R., Macdonald, I.D.G., Makris, T.M., Sligar, S.G., and Hoffman, B.M. (1999) *J. Am. Chem. Soc. 121*, 10654-10655.

22. Gassner, G. T., and Lippard, S.J. (1999) *Biochemistry 38*, 12768-12785.

23. Wallar, B. J., and Lipscomb, J.D. (2001) *Biochemistry 40*, 2220-2233.

24. Froland, W. A., Andersson, K.K., Lee, S.K., Liu, Y., and Lipscomb, J.D. (1992) *J. Biol. Chem. 267*, 17588-17597.

25. Liu, K. E., and Lippard, S.J. (1991) *J. Biol. Chem. 266*, 12836-12839.

26. Brazeau, B. J., Wallar, B.J., and Lipscomb, J.D. (2001) *J. Am. Chem. Soc. 123*, 10421-10422.

27. Liu, Y., Nesheim, J.C., Lee, S.K., and Lipscomb, J.D. (1995) *J. Biol. Chem. 270*, 24662-24665.

28. Shu, L., Nesheim, J.C., Kauffmann, K., Munck, E., Lipscomb, J.D. and Que, L. Jr. (1997) *Science 275*, 515-518.

29. Brazeau, B. J., Austin, R.N., Tarr, C., Groves, J.T., and Lipscomb, J.D. (2001) *J. Am. Chem. Soc. 123*, 11831-11837.

30. Wilkins, P. C., Dalton, H., Samuel, C.J., and Green, J. (1994) *Eur. J. Biochem. 226*, 555-560.

31. Fox, B. G. (1998) in *Comprehensive Biological Catalysis* (Sinnott, M., Ed.) pp. 261-348, Academic Press, Manchester.

32. Qian, H., Edlund, U., Powlowski, J., Shingler, V., and Sethson, I. (1997) *Biochemistry 36,* 495-504.

33. Hemmi, H., Studts, J.M., Chae, Y.K., Song, J., Markley, J.L., and Fox, B.G. (2001) *Biochemistry 40*, 3512-3524.

34. Boyd, D. R., Sharma, N.D., Allen, C.C.R. (2001) *Curr. Opin. Biotechnol. 12*, 564-573.

35. Boyd, D. R., and Sheldrake, G.N. (1998) *Nat. Prod. Rep. 15*, 309-324.

36. Harwood, C. S., and Parales, R.E. (1996) *Annu. Rev. Microbiol. 50*, 553-590.

37. Gibson, D. T., and Parales, R.E. (2000) *Curr. Opin. Biotechnol. 11*, 236-243.

38. Furukawa, K. (2000) *Curr. Opin. Biotechnol. 11*, 244-249.

39. Mason, J. R., and Cammack, R. (1992) *Annu. Rev. Microbiol. 46*, 277-305.

40. Nam, J. W., Nojiri, H., Yoshida, T., Habe, H., Yamane, H., and Omori, T. (2001) *Biosci. Biotechnol. Biochem. 65*, 254-263.

41. Buckland, B. C., Drew, S.W., Connors, N.C., Chartrain, M.M., Lee, C., Salmon, P.M., Gbewonyo, K., Zhou, W., Gailliot, P., Singhvi, R., Olewinski, R.C., Jr.,

Sun, W.J., Reddy, J., Zhang, J., Jackey, B.A., Taylor, C., Goklen, K.E., Junker, B., and Greasham, R.L. (1999) *Metabolic Engineering 1*, 63-74.

42. Eby, D. M., Beharry, Z.M., Coulter, E.D., Kurtz, D.M., and Neidle, E.L. (2001) *J. Bacteriol. 183*, 109-118.

43. Neidle, E. L., Hartnett, C., Ornston, L.N., Bairoch, A., Rekik, M., and Harayama, S. (1991) *J. Bacteriol. 173*, 5385-5395.

44. Neidle, E. L., Shapiro, M.K., and Ornston, L.N. (1987) *J. Bacteriol. 169*, 5496-5503.

45. Batie, C. J., LaHaie, E., and Ballou, D.P. (1987) *J. Biol. Chem. 262*, 1510-1518.

46. Schweizer, D., Markus, A., Seez, M., Ruf, H.H., and Lingens, F. (1987) *J. Biol. Chem. 262*, 9340-9346.

47. Markus, A., Krekel, D., and Lingens, F. (1986) *J. Biol. Chem. 261*, 12883-12888.

48. Locher, H. H., Leisinger, T., and Cook, AM. (1991) *Biochem. J. 274*, 833-842.

49. Nakatsu, C. H., Straus, N.A., and Wyndham, RC. (1995) *Microbiology 141*, 485-495.

50. Fetzner, S., Muller, R., and Lingens, F. (1992) *J. Bacteriol.* ***174***, 279-290.

51. Mampel, J., Ruff, J., Junker, F., and Cook, A. M. (1999) *Microbiology 145*, 3255-3264.

52. Harayama, S., and Rekik, M. (1990) *Mol. Gen. Genet. 221*, 113-120.

53. Heald, S. C., and Jenkins, R.O. (1996) *Appl. Microbiol. Biotechnol. 45*, 56-62.

54. Geary, P. J., Mason, J.R., and Joannou, C.L. (1990) *Methods Enzymol. 188*, 52-60.

55. Haddock, J. D., and Gibson, D.T. (1995) *J. Bacteriol. 177*, 5834-5839.

56. Sauber, K., Frohner, C., Rosenberg, G., Eberspacher, J., and Lingens, F. (1977) *Eur. J. Biochem. 74*, 89-97.

57. Kasuga, K., Habe, H., Chung, J.S., Yoshida, T., Nojiri, H., Yamane, H., and Omori, T. (2001) *Biochem. Biophys. Res. Commun. 283*, 195-204.

58. Saito, A., Iwabuchi, T., and Harayama, S. (2000) *J. Bacteriol. 182*, 2134-2141.

59. Eaton, R. W. (1996) *J. Bacteriol. 178*, 1351-1362.

60. Liu, Z., Yang, H., Huang, Z., Zhou, P., and Liu, S.J. (2002) *Appl. Microbiol. Biotechnol. 58*, 679-682.

61. Diaz, E., Ferrandez, A., and Garcia, J.L. (1998) *J. Bacteriol. 180*, 2915-2923.

62. Simon, M. J., Osslund, T.D., Saunders, R., Ensley, B.D., Suggs, S., Harcourt, A., Suen, W.C., Cruden, D.L., Gibson, D.T., and Zylstra, G.J. (1993) *Gene 127*, 31-37.

63. Lessner, D. J., Johnson, G.R., Parales, R.E., Spain, J.C., and Gibson, D.T. (2002) *Appl. Environ. Microbiol. 68*, 634-641.

64. Parales, J. V., Parales, R.E., Resnick, S.M., and Gibson, D.T. (1998) *J. Bacteriol. 180*, 1194-1199.

65. Nojiri, H., Sekiguchi, H., Maeda, K., Urata, M., Nakai, S., Yoshida, T., Habe, H., and Omori, T. (2001) *J. Bacteriol. 183*, 3663-3679.

66. Jiang, H., Parales, R.E., and Gibson, D.T. (1999) *Appl. Environ. Microbiol. 65*, 315-318.

67. Gassner, G. T., Ballou, D.P., Landrum, G.A., and Whittaker, J.W. (1993) *Biochemistry 32*, 4820-4825.

68. Pavel, E. G., Martins, L.J., Ellis, W.R., and Solomon, E.I. (1994) *Chemistry and Biology 1*, 173-183.

69. Corpet, F. (198) *Nucl. Acids Res. 16*, 10881-10890.

70. Hegg, E. L., and Que, L. (1997) *Eur. J. Biochem. 250*, 625-629.

71. Jiang, H., Parales, R.E., Lynch, N.A., and Gibson, D.T. (1996) *J. Bacteriol. 178*, 3133-3139.

72. Parales, R. E., Parales, J. V., and Gibson, D. T. (1999) *J. Bacteriol. 181*, 1831-1837.

73. Carredano, E., Karlsson, A., Kauppi, B., Choudhury, D., Parales, R. E., Parales, J. V., Lee, K., Gibson, D. T., Eklund, H., and Ramaswamy, S. (2000) *J. Mol. Biol. 296*, 701-12.

74. Kobayashi, S., Kuno, S., Itada, N., Hayaishi, O., Kozuka, S., and Oae, S. (1964) *Biochem. Biophys. Res. Commun. 16*, 556-561.

75. Wolfe, M. D., Parales, J.V., Gibson, D.T., and Lipscomb, J.D. (2001) *J. Biol. Chem. 276*, 1945-1953.

76. Chen, K. C., and Que, L. (1999) *Angew. Chem. Int. Ed. 38*, 2227-2229.

77. Chen, K., and Que, L. (1999) *Chem. Commun. 15*, 1375-1376.

78. Chen, K., Costas, M., Kim, J., Tipton, A.K., and Que, L. (2002) *J. Am. Chem. Soc. 124*, 3026-3035.

79. Wada, A., Ogo, S., Nagatomo, S., Kitagawa, T., Watanabe, Y., Jitsukawa, K., and Masuda, H. (2002) *Inorg. Chem. 41*, 616-618.

80. Zang, Y., Kim, J., Dong, Y., Wilkinson, E.C., Appelman, E.H., and Que, L. (1997) *J. Am. Chem. Soc. 119*, 4197-4205.

81. Kim, C., Chen, K., Kim, J., and Que, L. (1997) *J. Am. Chem. Soc. 119*, 5964-5965.

82. Leising, R. A., Brennan, B.A., and Que, L. (1991) *J. Am. Chem. Soc. 113*, 3988-3990.

83. Wackett, L. P., Kwart, L.D., and Gibson, D.T. (1988) *Biochemistry 27*, 1360-1367.

84. Joern, J. M., Meinhold, P., and Arnold, F. (2002) *J. Mol. Biol. 316*, 643-656.

85. Parales, J. V., Parales, R.E., Resnich, S.M., and Gibson, D.T. (1998) *J. Bacteriol. 180*, 1194-1199.

86. Parales, R. E., Emig, M.D., Lynch, N.A., and Gibson, D.T. (1998) *J. Bacteriol. 180*, 2337-2344.

87. Tan, H.-M., and Cheong, C-M. (1994) *Biochem. Biophys. Res. Commun. 204*, 912-917.

88. Beil, S., Mason, J.R., Timmis, K.N., and Pieper, D.H. (1998) *J. Bacteriol. 180*, 5520-5528.

89. Hurtubise, Y., Barriault, D., and Sylvestre, M. (1998) *J. Bacteriol. 180*, 5828-5835.

90. Chebrou, H., Hurtubise, Y., Barriault, D., and Sylvestre, M. (1999) *J. Bacteriol. 181*, 4805-4811.

91. Bruhlmann, F., and Chen, W. (1999) *Biotechnol. Bioeng. 63*, 544-551.

92. Kimura, N., Nishi, A., Goto, M., and Furukawa, K. (1997) *J. Bacteriol. 179*, 3936-3943.

93. Suenaga, H., Nishi, A., Watanabe, T., Sakai, M., and Furukawa, K. (1999) *J. Biosci. Bioeng. 87*, 430-435.

94. Suenaga, H., Mitsuoka, M., Ura, Y., Watanabe, T., and Furukawa, K. (2001) *J Bacteriol. 183*, 5441-5444.

CHAPTER 2

PURIFICATION AND PROPERTIES OF BENZOATE 1,2-DIOXYGENASE FROM *ACINETOBACTER* SP. STRAIN ADP1[1]

[1] **Beharry, Z.M., Eby, D.M., Coulter, E.D., Neidle, E.L., and Kurtz, D.M., Jr. To be submitted to *Biochemistry*.**

Abstract

The two-component benzoate 1,2-dioxygenase (BenDO) from *Acinetobacter* sp. strain ADP1 was expressed in *E. coli* and purified to homogeneity. This enzyme system catalyzes the conversion of benzoate to the non-aromatic *cis*-1,2-benzoate diol by addition of both atoms of O_2 into the aromatic ring. The as-isolated recombinant oxygenase component (BenAB) formed a $\alpha_3\beta_3$ hexamer of 53-kDa (α) and 25-kDa (β) subunits with one Rieske-type [2Fe-2S] center and an unoccupied nonheme mononuclear iron center in each α subunit. The recombinant reductase component (BenC) contained approximately one FAD and one ferredoxin-type [2Fe-2S] center per 41-kDa monomer. The X-ray crystal structure of BenC was also determined and represents the first structure of a FAD-containing Rieske dioxygenase reductase whose oxygenase component is of $\alpha_3\beta_3$ subunit composition. Activities of BenDO with various substituted benzoates were measured as quantities of NADH and O_2 consumed. Substrate consumption was monitored by HPLC. Catechol and diol products were detected using Gibbs' reagent and the benzoate diol dehydrogenase, BenD and also by HPLC. While conversion of benzoate to the benzoate diol was stoichiometrically coupled to both NADH and O_2 consumption, other substrate analogs exhibited varying degrees of uncoupling. The product of *o*-fluorobenzoate hydroxylation with the related 2-halobenzoate 1,2-dioxygenase was previously shown to be catechol via spontaneous loss of F^- and CO_2. However, in BenDO-catalyzed reactions with *o*-fluorobenzoate, the only product detected was a diol, suggesting that the mode of activated O_2 attack occurs at ring carbons 1 and 6, rather than 1 and 2. These results represent the first thorough study on the substrate

range of a BenDO and the results contradict previous notions that chromosomally encoded BenDOs have relatively narrow substrate specificity.

Introduction

Benzoate is a common intermediate in the aerobic enzymatic degradation of various aromatic compounds by several species of soil bacteria, as diagrammed in Figure 2.1. Catabolism of biphenyl (via the BPH pathway), toluene (via the XYL pathway), and benzonitrile all converge at benzoate, which is subsequently degraded to intermediates of the tricarboxylic acid cycle (Figure 2.2) (*1*). Aerobic degradation of benzoate is initiated by regio- and stereospecific introduction of two dioxygen-derived oxygen atoms onto the aromatic ring to form the non-aromatic *cis*-1*R*,2*S*-dihydroxycyclohexa-3,5-diene-1-carboxylate, hereafter referred to as benzoate diol. This dihydroxylation is catalyzed by the multicomponent Rieske dioxygenase (RDO) benzoate 1,2-dioxygenase (BenDO) (Figure 2.3). The intermediacy of the benzoate diol had been demonstrated previously in a mutant strain of *Alcaligenes eutrophus* blocked in benzoate catabolism, which resulted in the accumulation of the benzoate diol (*2*). The accumulation of the benzoate diol was the result of a defective benzoate diol dehydrogenase (BenD), which catalyzes the conversion of the benzoate diol to catechol (cf. Figure 2.1) (*3, 4*). Furthermore, oxygen incorporation into the diol was shown to originate exclusively from O_2 using $^{18}O_2$ (*2*).

The genes for benzoate conversion to catechol have previously been cloned from *Acinetobacter* sp. strain ADP1 (ADP1) and are part of a 20-kbp supraoperonic cluster that include the genes for catechol degradation (Figure 2.4) (*3, 5*). The *ben* and *cat* genes are regulated by the transcriptional activators BenM and CatM, respectively (*3, 5*). Amino acid sequence comparisons with better-characterized RDOs (cf. Figure 1.10) led to the inferred biological functions and prosthetic groups for the reductase (BenC) and

Figure 2.1. Bacterial aerobic degradation pathways of biphenyl, toluene and benzonitrile leading to formation of benzoate adapted from (*6*).

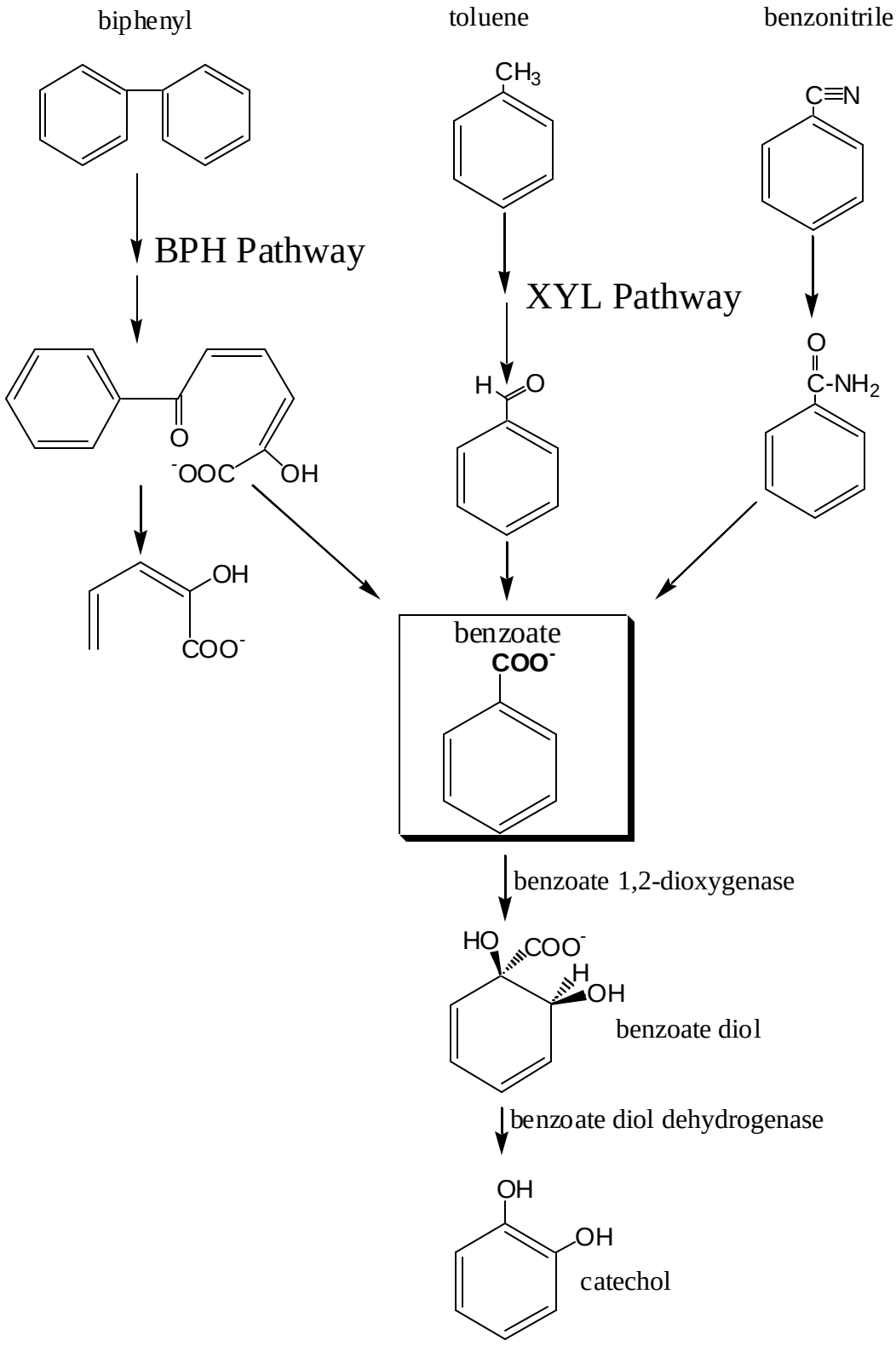
biphenyl
toluene
benzonitrile
BPH Pathway
XYL Pathway
benzoate
benzoate 1,2-dioxygenase
benzoate diol
benzoate diol dehydrogenase
catechol

Figure 2.2. Genes and intermediates in the degradation of benzoate via the chromosomally encoded *ortho* pathway in *Acinetobacter* sp. strain ADP1 (*3*) and the plasmid encoded *meta* pathway in *Pseudomonas putida* (*7, 8*).

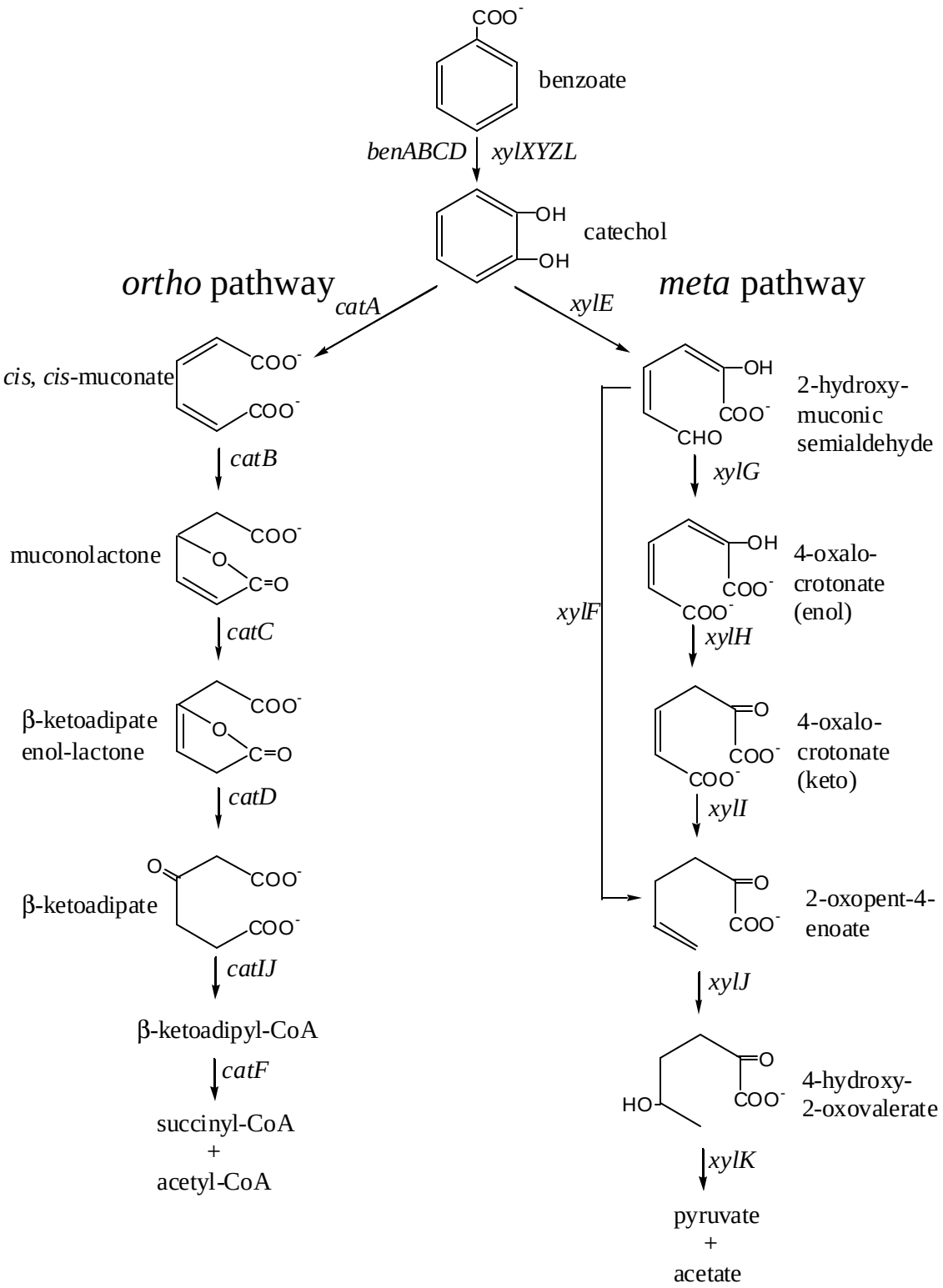
benzoate
benABCD xylXYZL
catechol
ortho pathway
catA
xylE
meta pathway
cis, cis-muconate
catB
muconolactone
catC
β-ketoadipate enol-lactone
catD
β-ketoadipate
catIJ
β-ketoadipyl-CoA
catF
succinyl-CoA + acetyl-CoA
2-hydroxy-muconic semialdehyde
xylG
4-oxalo-crotonate (enol)
xylF
xylH
4-oxalo-crotonate (keto)
xylI
2-oxopent-4-enoate
xylJ
4-hydroxy-2-oxovalerate
xylK
pyruvate + acetate

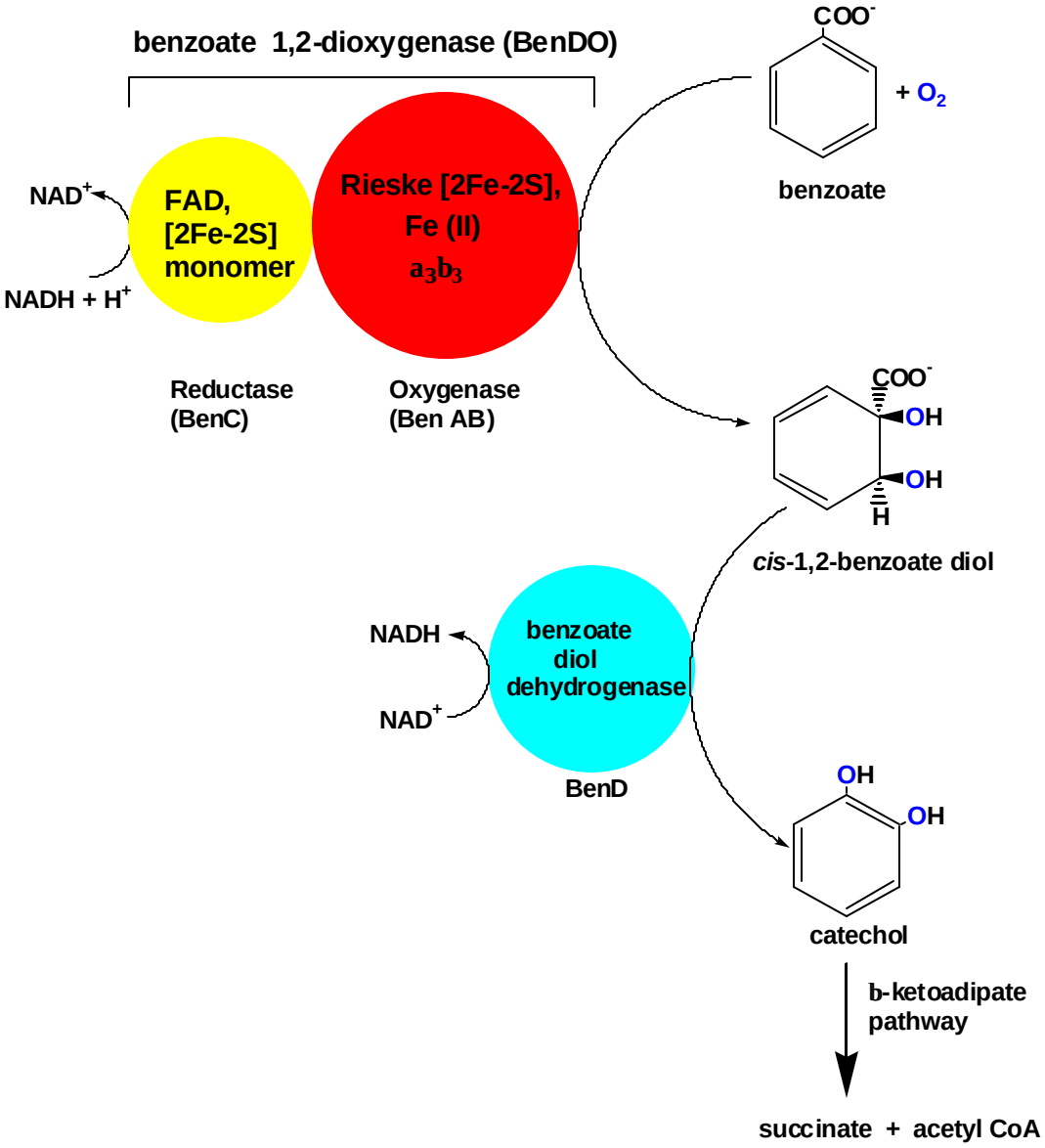

Figure 2.3. Components catalyzing the initial steps of the degradation of benzoate in *Acinetobacter* sp. strain ADP1 via the β-ketoadipate pathway (*ortho* cleavage pathway) (*3*).

Figure 2.4. Organization of the genes involved in benzoate and catechol degradation in *Acinetobacter* sp. strain ADP1 (*3*, *5*).

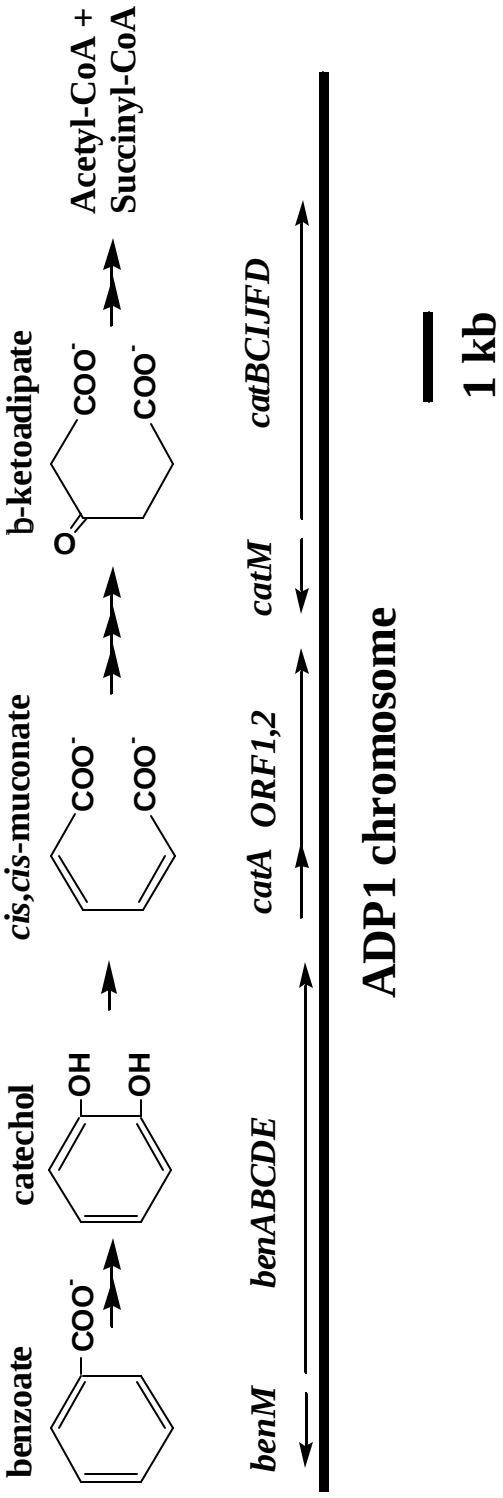
benzoate
catechol
cis,cis-muconate
b-ketoadipate
Acetyl-CoA +
Succinyl-CoA
COO-
OH
O
benM
benABCDE
catA
ORF1,2
catM
catBCIJFD
ADP1 chromosome
1 kb

oxygenase (BenAB) components of BenDO (*9-12*). Oxygenase components of the two best characterized RDOs, phthalate 4,5-dioxygenase (PDO) and naphthalene 1,2-dioxygenase (NDO), contain one Rieske-type [2Fe-2S] center and one mononuclear center per alpha subunit, the latter center being the putative site where O_2 is activated for insertion into the aromatic substrate (*13-16*).

The components of BenDO have been purified from *Pseudomonas putida* (ATCC 23973 and ATCC 23974) (*17, 18*). The oxygenase component was shown to consist of two non-identical subunits in a $\alpha_3\beta_3$ composition, containing Rieske-type [2Fe-2S] centers and mononuclear nonheme iron. The monomeric reductase component of BenDO was shown to contain flavin adenine dinucleotide (FAD) and a plant-type [2Fe-2S] cluster. Based on this biochemical characterization, BenDO belongs to the class I RDOs (see Chapter 1). Activity assays (amounts of NADH consumption only) with various *ortho*-, *meta*-, and *para*-substituted benzoates showed a clear preference by *Pseudomonas* BenDO for *meta*-substituted benzoates. The non-aromatic benzoate diol was determined to be the product with benzoate as the substrate, and the stoichiometry of NADH: O_2:benzoate:benzoate diol was determined 1:1:1:1, indicating a tightly coupled reaction (*18*).

In addition to the chromosomally encoded BenDO, plasmid-encoded genes for benzoate conversion to catechol have been identified (*6, 8, 19, 20*). The ability of certain bacteria to utilize methylbenzoates as sole carbon sources has been attributed to the plasmid-encoded Xyl genes (cf. Figure 2.2). The *xylXYZ* genes encode the oxygenase (XylXY) and reductase (XylZ) components of an RDO (XylDO) that shows very high sequence homology to ADP1 BenABC (77% similarity for the α and β subunits of the

oxygenase components and 71% similarity for the reductases) (*6, 21*). XylDO may, thus, be a BenDO but with broader substrate specificity that includes *meta*- and *para*-methylbenzoates, thereby allowing growth on these compounds as sole carbon sources. *Pseudomonas putida* also contains a chromosomally-encoded BenDO, which apparently allows utilization of benzoate, but not *meta*- or *para*-methylbenzoate as sole carbon sources in the absence of the plasmid-encoded XylDO (*8*). Conversely, mutant ADP1 strains lacking functional BenDO genes cannot grow on benzoate (*3*, *5*), but there are no reports that these strains can utilize methyl-substituted benzoates.

This chapter describes the expression and purification of the components of recombinant *Acinetobacter* sp. strain ADP1 BenDO and the diol dehydrogenase, BenD, from *E. coli,* and the crystal structure of BenC at 1.5 Å-resolution is also presented. Investigations into the substrate specificity of BenDO with various aromatic carboxylates are described.

Experimental

Reagents and general procedures

Substrates were purchased from Sigma. Enzymatically produced benzoate diol was graciously provided by Dr. Albey M. Reiner (Univ. of Massachusetts, Amherst). Oligonucleotides were synthesized by Integrated DNA Technologies. Nucleotide sequencing was performed at the University of Georgia Molecular Genetics Instrumentation Facility (ABI373 sequencer, Applied Biosystems). Protein purity was judged by sodium dodecyl sulfate-polyacrylamide gel electrophoresis (SDS-PAGE) (15%

polyacrylamide gels) with Coomassie blue staining (*22*). Molecular biology procedures followed those in Sambrook et al (*23*).

Plasmids for *ben* gene expression

BenC (1016-bp) was PCR amplified using *Pfu* polymerase (Stratagene) from pIB1354 (*3*) with the primers 5′-ACGATACATATGTCAAACCATCAAGTAGCA-3′ and 5′-ACGATACTCGAGTTAGTTGGCAGAGAA-3′ (with added *Nde*I and *Xho*I restriction sites underlined) and the PCR product was ligated into the *Nde*I/*Xho*I sites of pCYB1 (New England Biolabs), which places *benC* under the control of the P_{tac} promoter to yield pBAC297. *BenAB* (1891-bp) was PCR amplified using *Pfu* polymerase (Stratagene) from pIB1354 (*3*) with the primers 5´-ACGATACCATGGggCCACGTATTCCCGTCATT-3´ and 5´-ACGATAGCTCTTCCGCATTAAATATGATAAATA-3´ (with added *Nco*I and *Sap*I restriction sites underlined; two nucleotides (lowercase) were added to the N-terminal *Nco*I primer so that *benAB* would be translated in frame) or 5´-ATTATAGAATTCATGCCACGTATTCCCG-3´ and 5´-ATCGAGAAGCTTTTAAATATGATAAATATCAATGAC-3´ (with added *EcoR*I and *Hind*III underlined) and ligated into the *Nco*I/*Sap*I sites of pCYB3 (New England Biolabs) or ligated into the *EcoR*I/*Hind*III sites of pKK223-3 (Amersham Pharmacia Biotech), respectively. Both of the resulting constructs and pIB1354 (expressing BenABC from the pUC19 *lac* promoter) showed very little expression of BenAB in *E. coli* with added IPTG. Therefore, attempts were made to subclone *benAB* into the expression vector pCYB1 in a manner similar to that described above for *benC*. B*enA* contains two *Nde*I restriction sites that were removed using silent mutations as follows.

pIB1354 was used as the template for site-directed mutagenesis using the QuikChange Site Directed Mutagenesis kit (Stratagene) with complimentary oligonucleotide primers 5´-TGGTGGCGGTTCCTATGGATTTGAACATGGTCACATGTTGCTCTG-3´ and 5´-CAGAGCAACATGTGACCATGTTCAAATCCATAGGAACCGCCACCA-3´ (with nucleotides used to create silent mutations underlined) to yield pDMK4. Expression from the *lac* promoter of pDMK4 resulted in sufficient production of BenAB in *E. coli* XL1-Blue and, therefore, no further attempts were made to subclone *benAB* into the pCYB1 expression vector. The *benC* and *benAB* nucleotide sequences of pBAC297 and pDMK4, respectively, were confirmed to be the same as in GenBank AF009224.

Expression of ADP1 BenAB, BenC, and BenD in *E. coli* and preparation of cell-free extracts

One-liter cultures of *E. coli* strains XL-1Blue (Stratagene) carrying pDMK4 (encoding BenABC) or pIB1382 (encoding BenD expressed from the pUC19 *lac* promoter) (*3*) or *E. coli* strain BL21-Codon Plus (Stratagene) carrying pBAC297 (encoding BenC) were grown aerobically in Luria-Bertani (LB) medium (XL1-Blue) or M9 minimal medium (BL21-Codon Plus) in an incubator/shaker at 37 °C until OD_{600} ~0.6. The temperature was reduced to 30 °C and isopropyl α-D-thiogalactopyranoside (100 μg/mL) was added to induce expression of the plasmid-borne *ben* genes. Ferrous ammonium sulfate (20 mg) was also added only to cultures in M9 minimal medium at the time of induction. Incubation was continued at this temperature until OD_{600} ~2.5 (~4 hrs). Cells were harvested by centrifugation (5,000g, 5 min, 4 °C) and washed with 25 mM MOPS pH 7.3 (buffer A). Approximately 35 g of cells collected from 12 liters of *E. coli* cultures harboring pDMK4, pIB1382, or pBAC297 were resuspended in 50 mL of buffer

A and sonicated on ice using a Branson sonifier cell disrupter 350 with a 0.5-inch probe tip for 2 min at 10-sec intervals at 20 kHz. Cell debris was removed by centrifugation (12,000g, 30 min, 4 °C). These preparations are referred to as 12 x 1-L cell extracts and were used immediately to isolate the corresponding Ben enzymes.

Purification of BenAB

The procedure described below was carried out at 4 °C on the 12 x 1-L cell extract from *E. coli* XL1-Blue[pDMK4]. Solid ammonium sulfate was added to the cell-free extract (~80 mL) with stirring to 40 % saturation, and the resulting precipitate was pelleted by centrifugation (12,000g, 15 min, 4 °C). The supernatant (containing BenC) was discarded and the pellet containing BenAB, was resuspended in buffer A (~20 mL) and dialyzed against buffer A (4 L x 12 hrs). Column fractions containing BenAB were easily visualized by their red-brown color. The crude BenAB was applied to a HiTrap Q anion-exchange column (Amersham Pharmacia Biotech) equilibrated in 50 mM Tris-HCl pH 7.5 (buffer B). The column was washed with 30 mL of buffer B and bound BenAB was eluted with a linear gradient of NaCl (0-1 M) in buffer B. Fractions containing BenAB were pooled and desalted by repetitive concentration and dilution into buffer A by ultrafiltration in a 50 mL Amicon cell (YM 50 membrane). The desalted BenAB (~ 2 mL) was applied to a Mono Q anion-exchange column equilibrated in buffer A (3 cm X 10 cm, Amersham Pharmacia Biotech). The column was washed with 50 mL of buffer A and bound BenAB was eluted with a linear gradient of NaCl (0-1 M) in buffer A. The purified BenAB (~ 40 mg) was concentrated by ultrafiltration to ~1 mL and stored at –80 °C in 100 µL aliquots.

Purification of BenC

The procedure described below was carried out at 4 °C on the 12 x 1-L cell extract from *E. coli* BL-21 Codon Plus[pBAC297]. The cell-free extract (~60 mL) was applied to a Q Sepharose FF (3 cm x 15 cm, Amersham Pharmacia Biotech) anion-exchange column equilibrated in buffer A. The column was washed with 300 mL of buffer A, and bound BenC was eluted with a step gradient of NaCl (0-400 mM) in buffer A. Active fractions containing BenC (assayed as described below) were pooled and concentrated by ultrafiltration in a 50 mL Amicon cell (YM10 membrane) to 10 mL. Filtered 4 M ammonium sulfate was added with stirring to a final concentration of 1 M. The resulting precipitate was removed by centrifugation (12,000g, 15 min, 4 °C), and the supernatant was applied to an Octyl Sepharose column (1.6 cm x 10 cm, Amersham Pharmacia Biotech) equilibrated in buffer A containing 1 M ammonium sulfate. BenC was eluted with a linear gradient of decreasing ammonium sulfate concentration (1 to 0 M). Fractions containing BenC were concentrated by ultrafiltration to 2 mL and applied to a Sephacryl S100 (1.6 cm X 60 cm, Amersham Pharmacia Biotech) sizing column equilibrated in buffer A containing 250 mM NaCl. BenC was eluted at a flow rate of 0.5 mL/min in the same buffer. Fractions containing BenC were pooled, desalted and concentrated by ultrafiltration in a 50 mL Amicon cell (YM10 membrane) to 2 mL and applied to a Mono Q anion-exchange column (3 cm X 10 cm, Amersham Pharmacia Biotech) equilibrated in buffer A. The column was washed with 50 mL of buffer A, and bound BenC was eluted with a linear gradient of NaCl (0-1M) in buffer A. The purified BenC (~60 mg) was concentrated to by ultrafiltration to ~1 mL and stored at –80 °C in 100 μL aliquots.

Purification of BenD

The procedure described below was carried out at 4 °C on the 12 x 1-L cell extract from *E. coli* XL1-Blue[pIB1382]. Purification of BenD was monitored by the benzoate diol-dependent reduction of NAD^+, as described below. Solid ammonium sulfate was added to the cell-free extract (~60 mL) with stirring to 30 % saturation. The resulting precipitate was removed by centrifugation (12,000g, 15 min, 4 °C). The pellet was discarded and the supernatant was brought to 50 % ammonium sulfate saturation. The precipitated BenD was pelleted by centrifugation (12,000g, 15 min, 4 °C). The pellet was resuspended in 20 mL of buffer A, desalted by dilution to 50 mL in buffer A and concentration to 5 mL by ultrafiltration in a 50 mL Amicon cell (YM10 membrane). This procedure was repeated once more followed by concentration to 2 mL by ultrafiltration. The concentrated BenD was applied to a HiTrap Blue Sepharose (Amersham Pharmacia Biotech) column equilibrated in buffer A. The column was washed with 50 mL of buffer A. BenD was eluted with buffer A containing 1 M NaCl, desalted and concentrated to 2 mL by ultrafiltration and applied to a HiTrap Q (Amersham Pharmacia Biotech) anion-exchange column equilibrated in buffer A. BenD was eluted with a linear gradient of NaCl (0 to 1 M) in buffer A. The purified BenD (~10 mg) was concentrated by ultrafiltration to ~0.5 mL and stored at –80 °C.

Analyses

Protein was quantitated by the method of Bradford (*24*) with bovine serum albumin as the standard (Bio-Rad). The native molecular weights of BenAB, BenC and BenD were determined by gel filtration using a calibrated Sephacryl S300 column (flow rate 0.5 mL/min) equilibrated in buffer A containing 250 mM NaCl. The calibration

proteins were horse spleen ferritin (M_r, 450,000), bovine liver catalase (M_r, 240,000), aldolase (M_r, 158,000), bovine serum albumin (M_r, 68,000), hen egg albumin (M_r, 45,000), chymotrypsinogen A (M_r, 25,000), and horse heart cytochrome *c* (M_r, 12,500). Metal content was determined by inductively coupled plasma atomic emission spectrometry (Chemical Analysis Lab, University of Georgia). The flavin cofactor of BenC was extracted by boiling a 50 μM (1-mL) sample of recombinant BenC for 10 min. Denatured protein was removed by centrifugation. Flavin was identified by thin-layer chromatography, with silica gel coated glass plates, using a mobile phase of butanol: acetic acid: water (4:1:4 volume ratio), and samples were visualized with a hand-held UV light. Commercially obtained flavin adenine dinucleotide (FAD) and flavin mononucleotide (FMN) were used as standards. After its identification as FAD, the amount of flavin present in the supernatant of the boiled BenC sample was determined spectrophotometrically (ε_{450}=11,300 $M^{-1}cm^{-1}$; ε_{375}=9,300 $M^{-1}cm^{-1}$) (*25*).

BenDO activity assays

As-isolated BenAB was inactive. Aerobic incubation of the BenDO components (BenAB, 0.8 μM $\alpha_3\beta_3$; BenC, 0.5 μM), benzoate (0.5 mM), and ferrous ammonium sulfate (50 μM) in 50 mM HEPES pH 7.5 at 4 °C for approximately 30 min, followed by addition of NADH (100 μM) to initiate the reaction, resulted in active protein. In order to determine BenDO activity with other substrates, BenAB was reactivated as described above by replacing benzoate with each of the substrates tested. Substrate-dependent O_2 consumption catalyzed by BenDO was monitored at 23 °C with a Yellow Springs Instruments Model 5300 biological oxygen monitor equipped with a Clark electrode for 5 min. NADH consumption was determined spectrophotometrically at 23 °C by measuring

the decrease in A_{340} (ε_{340}, 6.22 $mM^{-1}cm^{-1}$) for 5 min. In spectrophotometric assays, corrections were made for the absorbance of substrates [anthranilate, (ε_{340}= 1.05 $mM^{-1}cm^{-1}$), *m*-aminobenzoate, (1.3 $mM^{-1}cm^{-1}$) (*18*)], assuming a constant rate of consumption of substrate equal to that of NADH consumption. Assays were carried out in 50 mM HEPES pH 7.5, 100 mM KCl, 0.5 mM substrate, 100 μM NADH, 0.8 μM reactivated BenAB (as described above) and 0.5 μM BenC in a final volume of 1 mL for NADH oxidation assays or 2 mL for oxygen consumption assays. Reactions were monitored for 5 min, at which point 1000 U of bovine liver catalase (Sigma) was added to the reaction mixture monitored with the oxygen electrode. H_2O_2 was determined by the amount of O_2 generated due to the disproportionation of H_2O_2 by catalase as measured with the oxygen electrode.

NADH-cytochrome *c* reductase activity of BenC

The BenC-catalyzed reduction of cytochrome *c* by NADH was detected by the rate of increase in A_{550} (ε_{550}= 19,500 $M^{-1}cm^{-1}$ for reduced minus oxidized cytochrome *c* (*26*)). The assay mixture contained 20 μM cytochrome *c* (horse heart type 6, Sigma), 100 μM NADH, and 0.5 μM pure BenC (or suitable amount of crude enzyme preparation) in buffer A.

Optimization of BenDO activity

A mixed-buffer system was used to determine the pH for maximal BenDO activity. This buffer system contained 50 mM total of equimolar amounts of the following: MES (pK_a 6.1), MOPS (pK_a 7.2), HEPES (pK_a 7.5), N-tris(hydroxmethyl) ethyl-3-aminopropanesulfonic acid (pK_a 8.4), 2-(N-cyclohexylamino) ethanesulfonic acid (pK_a 9.3), and 3-(cyclo-hexylamino)-1-propanesulfonic acid (pK_a 10.4). The pH was

adjusted using either 12 M HCl or 10 M NaOH. Individual NADH oxidation assays were carried out at pH 5.5, 6.0 6.5, 7.0, 8.0, 9.0, otherwise using the conditions described above. After determining the optimal pH for NADH oxidation, assays were repeated in 50 mM HEPES pH 7.5 at four different ionic strengths (0, 50, 100, and 150 mM KCl).

BenD dehydrogenase activity

The BenD-catalyzed conversion of benzoate diol to catechol was monitored as the rate of increase in A_{340} (ε_{340}= 6.22 $mM^{-1}cm^{-1}$) due to reduction of NAD^+ to NADH. Benzoate diol was generated enzymatically using 2 μM ($\alpha_3\beta_3$) reactivated BenAB, 1 μM BenC, 0.1 mM benzoate and 100 μM NADH in 50 mM HEPES pH 7.5. Following consumption of all 100 μM NADH (approximately 4 min), NAD^+ (0.3 mM) and BenD (either 5 μM or suitable amount of crude enzyme preparation) was added and the A_{340} was monitored for 2 min.

Detection of catechol and diol products with substituted benzoates as substrates

Benzoate diol or substituted benzoate diol products were detected by monitoring the increase at A_{340} (ε_{340}= 6.22 $mM^{-1}cm^{-1}$) due to the diol-dependent BenD reduction of NAD^+ (Figure 2.5). Following NADH oxidation assays with BenDO as described above, BenD (5 μM) and NAD^+ (0.2 mM) were added and the increase at A_{340} was monitored for 2 min (longer times resulted in some consumption of NADH by BenDO and excess benzoate or substituted benzoate). Catechol products were detected using Gibbs' reagent (2,6-dichloroquinone-4-chloroimide) (Figure 2.5) (*27*, *28*). Following NADH oxidation reactions, aliquots (~200 μL) were removed and Gibbs' reagent (15 μL of a 2 % (w/v) solution in ethanol) was added and the reaction was incubated at room temperature for 1 hr. Positive reactions were identified by the formation of a blue to purple color.

Figure 2.5. Schematic representation of the methods used to detect diol and catechol products in BenDO-catalyzed reactions (*27*, *28*).

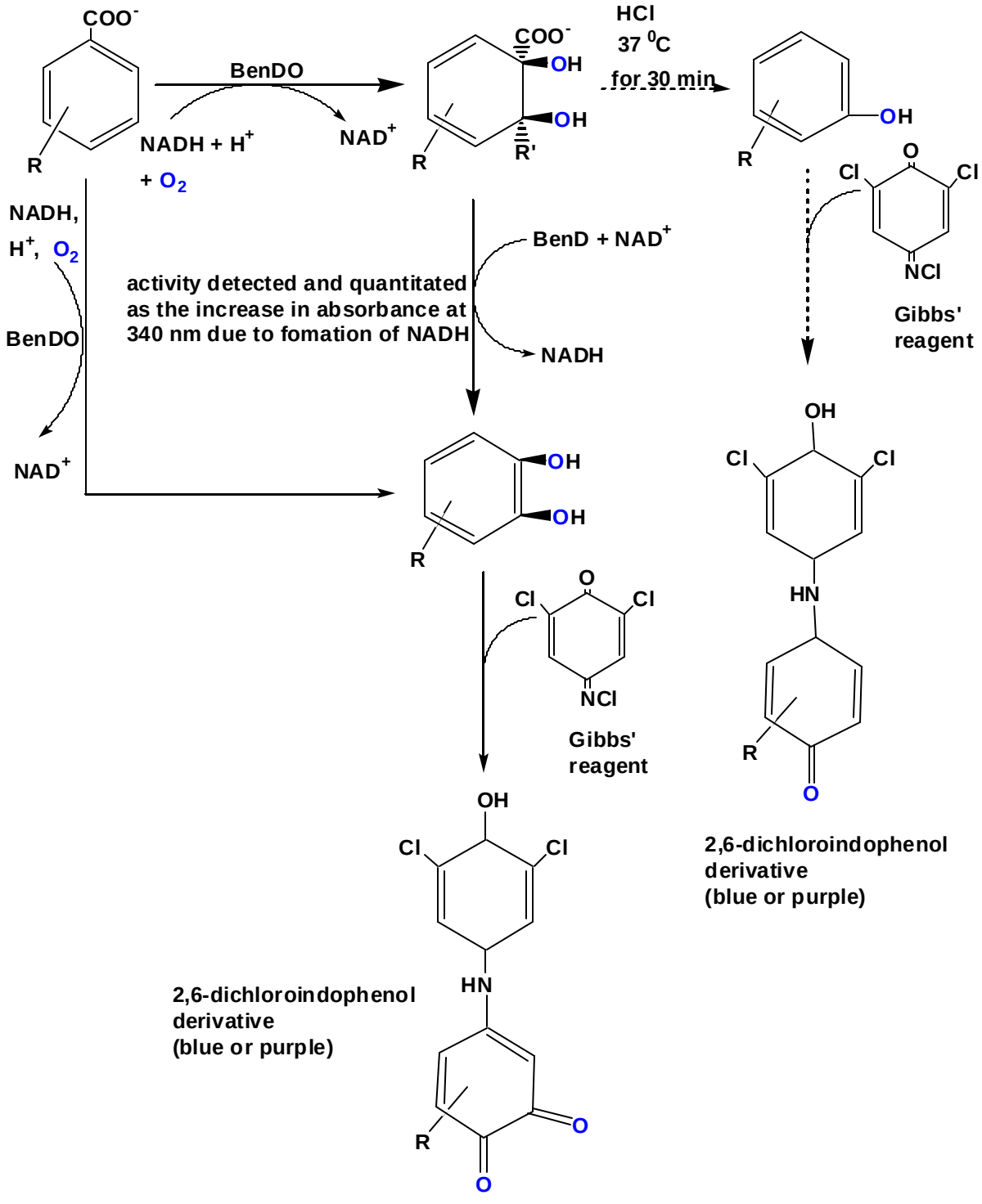
COO-
R
BenDO
NADH + H+
+ O2
NAD+
COO-
OH
OH
R
R'
HCl
37 0C
for 30 min
OH
R
Cl
O
Cl
NCl
Gibbs'
reagent
NADH,
H+, O2
BenDO
NAD+
activity detected and quantitated
as the increase in absorbance at
340 nm due to fomation of NADH
BenD + NAD+
NADH
OH
OH
R
Cl
O
Cl
NCl
Gibbs'
reagent
OH
Cl
Cl
HN
R
O
2,6-dichloroindophenol
derivative
(blue or purple)
OH
Cl
Cl
HN
R
O
O
2,6-dichloroindophenol
derivative
(blue or purple)

Substrates whose products were not positive either in BenD reactions or using Gibbs' reagent were further treated to form the corresponding phenol and allowed to react with Gibbs' reagent. Aliquots (~200 μL) from NADH oxidation reactions were acidified with 0.1 M HCl (100 μL) and incubated at 37 °C for 30 min. The pH was raised by the addition of 0.5 M Tris-HCl pH 8.5 (40 μL) and Gibbs' reagent (15 μL of a 2 % (w/v) solution in ethanol) was added and the reaction was incubated at room temperature for 1 hr.

Quantification of aromatic substrate consumed, catechol formed, and identification of benzoate diol

Aliquots (100 μL) of BenDO assays monitoring NADH consumption (0.8 μM reactivated BenAB (as described previously), 0.5 μM BenC, 0.5 mM substrate, 100 μM NADH in 50 mM HEPES pH 7.5) were applied to an HPLC (Bio-Rad automatic sampling system model AS-100, solvent delivery system 2800, detector uv-1806, and peak integration software) by D. Matthew Eby in the Department of Microbiology, University of Georgia. Compounds were eluted at a rate of 0.8 mL/min from a reverse-phase C_{18} column (Columbus 5 μm, 250 X 4.6 mm) with a mobile phase of 30 % (v:v) acetonitrile:water containing 0.1 % phosphoric acid. The eluate was monitored by absorbance at 210 nm. The concentration of aromatic substrate consumed and catechol formed and the identity of benzoate diol were determined by comparison with known standards and the integration software.

Spectroscopy

EPR spectra were recorded on a Bruker ESP-300E spectrometer equipped with an ER-4116 dual-mode cavity and an Oxford Instrument ESR-9 flow cryostat.

Ultraviolet-visible absorption spectra were obtained in 1-cm pathlength quartz cuvettes on a Shimadzu UV-2401PC scanning spectrophotometer.

Crystallization of BenC

BenC crystals were grown by Andreas Karlsson in the laboratory of Professor Hans Eklund of the University of Sweden using the hanging drop vapor diffusion method at 8 °C. Equal volumes of crystallization solution (2.4 M ammonium sulfate, 0.1 M MES pH 5.8, 3 % 2-methyl-2,4-pentandiol) and protein (7.5 mg/mL in 0.05 M MOPS pH 7) were mixed and allowed to equilibrate for 10 days. BenC crystals grew to a maximum size of 0.5 mm X 0.4 mm X 0.4 mm and belonged to the space group $C222_1$. A native data set was collected at 100 K on a crystal soaked for 30 s in a 90:10 (v/v) mixture of crystallization solution and ethylene glycol to a resolution of 1.5 Å on beamline ID14-EH4 at the ESRF, Grenoble, France.

Multiwavelength anomalous diffraction (MAD)

An ethyl mercury thiosalicylate (EMTS) derivative was prepared by soaking a crystal of BenC in crystallization solution containing 1 mM EMTS for ~4 hrs following removal of excess EMTS by soaking this crystal in crystallization solution containing 10 % (v/v) ethylene glycol prior to cryocooling. Wavelengths suitable for MAD data collection were determined by fluorescence scan of the derivatized crystal at the mercury LIII edge. MAD data were collected and scaled using the programs DENZO and SCALEPACK (*29*).

Structure solution

MAD and native datasets were combined and analyzed using the SOLVE program (*29*) to identify iron and mercury sites in BenC. These sites allowed calculation

of an electron density map at 4 Å resolution. Further averaging, density modification, and phase extension using the program DM (*30*) resulted in an electron density map in which most of the protein could be resolved using the program O (*31*). Refinement of the structure was accomplished by cycles of simulated annealing, energy minimization and *B*-factor minimization using the programs CNS (*32*) and Refmac (*33*). Coordinates for the structure of BenC were deposited in the Protein Data Bank (code 1KRH).

Results

Purification of BenDO

To facilitate the purification of recombinant BenDO and BenD, plasmids containing either the ADP1 *benAB* genes, the *benC* gene or the *benD* gene were used to express the corresponding oxygenase, reductase, and diol dehydrogenase components independently in *E. coli,* a bacterium containing none of the BenDO or BenD genes or activities. The plasmid used to express BenAB, pDMK4, also contained *benC* and a portion of the *benD* gene (*3*). BenAB alone was cloned into two different expression vectors, however, these constructs resulted in either very little or no expression of BenB using a variety of *E. coli* strains. Use of pIB1354, which is the plasmid used to create pDMK4 by removing the *Nde*I restriction sites in *benA*, also resulted in very little expression of BenAB or BenC. Therefore, these restriction sites in *benA* were removed to facilitate cloning of the *benAB* genes into the expression vector pCYB1 or other suitable overexpression vector. However, expression from pDMK4 resulted in sufficient production of BenAB in *E. coli* XL1-Blue and, therefore, no further attempts were made to subclone *benAB* into *E. coli* expression vectors. It is not clear why removing the *Nde*I

sites in *benA* with silent mutations increased expression levels of BenAB. The nucleotides that were mutated did result in codons that are more frequently used in *E. coli*, which may account for increased expression.

Co-expression of the *benAB* genes from pDMK4 in *E. coli* XL1-Blue yielded two overexpressed proteins of ~53 kDa and 25 kDa as monitored by SDS-PAGE (Figure 2.6). These sizes correspond to the α and β subunits of the oxygenase component of BenDO (cf. Table 2.1). In initial attempts to purify BenAB from pDMK4, BenAB and BenC coeluted during anion-exchange and gel filtration chromatography using a Sephacryl S300 column, which based on their native molecular weights (Table 2.1), should have effectively separated the two proteins. Therefore, ammonium sulfate fractionation was used to precipitate BenAB away from BenC. Size-exclusion chromatography of the pure BenAB revealed a single oligomer of approximately 225 kDa. Therefore, BenAB was inferred to be a $\alpha_3\beta_3$ hexamer (Table 2.1). Using the extinction coefficient determined at 463 nm, the 12 x 1-L culture of *E. coli* containing the *benAB* plasmid yielded approximately 40 mg of pure BenAB.

Independent expression of *benC* in *E. coli* BL21-Codon Plus[pBAC297] resulted in abundant production of a protein of the predicted size for BenC. SDS-PAGE and gel filtration indicated that purified BenC was a monomer of ~41 kDa. Approximately 60 mg of pure BenC was obtained from a 12 x 1-L culture. The flavin contained in recombinant BenC was identified as flavin adenine dinucleotide (FAD) by thin layer chromatography using commercially available FAD and flavin mononucleotide (FMN) as standards. As isolated, BenC contained ~0.9 mol FAD/mol protein.

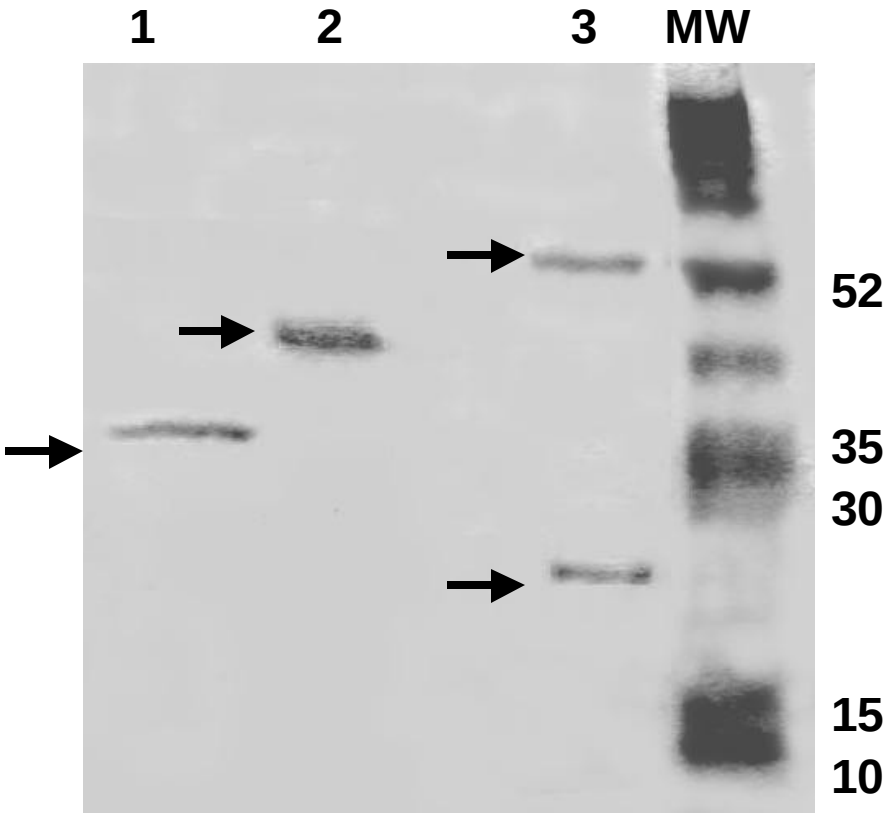

Figure 2.6. SDS-PAGE of purified BenD (lane 1), BenC (lane 2), and BenAB (lane 3). Numbers on the right correspond to the molecular masses (kDa) of the adjacent molecular weight markers (lane MW).

Table 2.1. Molecular and spectroscopic properties of recombinant *Acinetobacter* sp. strain ADP1 BenDO and BenD.

Component	molecular weight (M_r): calc'd from sequence	SDS-PAGE	gel filtration	iron content (mol/mol protein)	flavin content (mol/ mol protein)	UV/vis Absorption λ(ε) nm, ($mM^{-1}cm^{-1}$)
BenAB	52,072 (A) 20,073 (B)	53,000 (A) 25,000 (B)	225,000	5.5 ± 0.7[a]	0	326(sh) 463(15.7)[a] 558(sh)
BenC	38,787	41,000	45,000	1.9 ± 0.5	0.9	334 391 451(23.1) 470
BenD	27,998	30,000	83,000	0	0	280(52.9)

[a]Per $\alpha_3\beta_3$ hexamer, as-isolated (oxidized Rieske center).

Iron Contents of BenDO Components

BenC was determined to contain 1.9 ± 0.5 mol iron/mol BenC monomer, consistent with the prediction of one [2Fe-2S] center based on sequence homology (*12*). The iron content of BenAB was determined to be 5.5 ± 0.7 mol iron/mol protein based on a molecular weight of 225 kDa (Table 2.1). Considering the $\alpha_3\beta_3$ subunit composition and sequence homologies with better characterized RDOs, the iron analysis is consistent with the prediction of one [2Fe-2S] center and an empty mononuclear center per α subunit (*12-14, 16*). BenD was determined to contain no flavin and no appreciable quantities of metals by inductively coupled plasma-atomic emission analysis.

Spectroscopic Properties of BenDO

The visible absorption spectra of oxidized (as-isolated) and dithionite-reduced BenAB are shown in Figure 2.7. The absorption maximum of the oxidized BenAB at 463 nm (ε = 15,700 $M^{-1}cm^{-1}$) and the shoulder at 558 nm are typical of Rieske-type $[2Fe\text{-}2S]^{2+}$ centers (*10, 11, 13, 34*). The absorption spectrum resulting upon anaerobic addition of sodium dithionite also resembled those of other reduced (i.e., $[2Fe\text{-}2S]^{+}$) Rieske-type centers, with a general decrease in absorbance throughout the visible region. In particular, the absorption spectrum in Figure 2.7 closely resembles the corresponding spectra of AntAB discussed in Chapter 3 and the *Pseudomonas putida* BenAB (*18*). Resting oxygenase components of other RDOs are invariably found to have their mononuclear centers in the Fe(II) oxidation state, and this reduced mononuclear center is not expected to contribute to either the oxidized or the reduced visible absorption spectrum (*10, 11, 13, 34*). Accordingly, the addition of a stoichiometric amount (one per mononuclear site) of ferrous iron to BenAB did not result in any changes in the absorption spectrum of

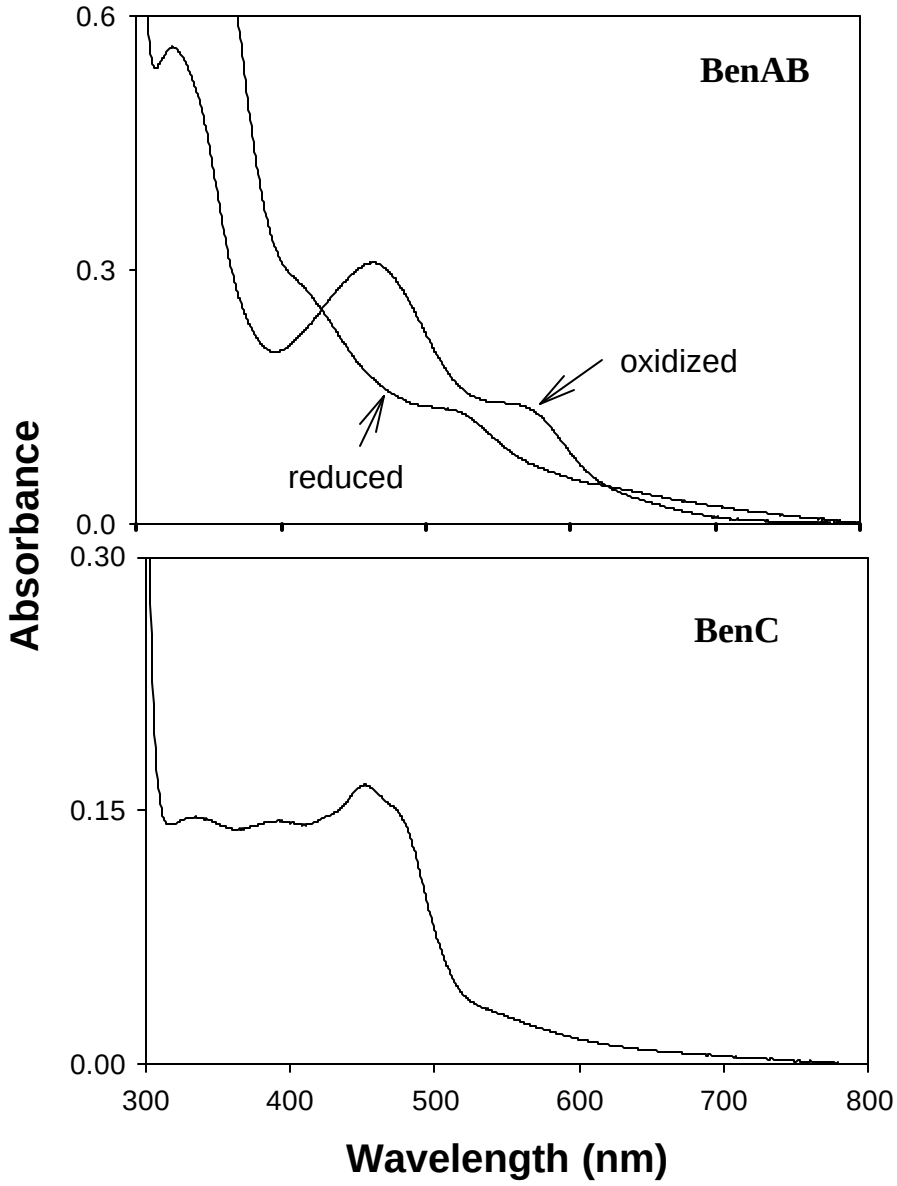

Figure 2.7. UV-visible absorption spectra of oxidized (as-isolated) and dithionite reduced (0.2 mM) BenAB (22 μM $\alpha_3\beta_3$) (top) and oxidized (as-isolated) BenC (8 μM) (bottom) in buffer A.

BenAB. The visible absorption spectrum of as-isolated BenC (Figure 2.7) is consistent with this component containing both FAD and ferredoxin-type [2Fe-2S]$^{2+}$ centers (*10, 35*). The 10-K EPR spectra of the dithionite-reduced BenAB and BenC, shown in Figure 2.8, also confirm the presence of the [2Fe-2S] centers. The BenAB spectrum, with g_{avg} = 1.89, is characteristic of Rieske-type [2Fe-2S]$^{+}$ centers (*36*), and the BenC spectrum with g_{avg} = 1.95, is characteristic of ferredoxin-type [2Fe-2S]$^{+}$ centers (*36*).

Properties of BenD

Molecular weight determinations under non-denaturing and denaturing conditions indicated BenD is a trimer composed of 30 kDa subunits (Table 2.1). This disagrees with that previously reported for partially purified ADP1 BenD, which indicated a dimer of 62 kDa (*3*). The reason for this discrepancy is not known. The absorption spectrum of BenD was featureless throughout the visible region as previously reported for the BenD from *Alcaligenes eutrophus* (*4*).

Catalytic Properties of BenDO

As-isolated BenDO was inactive, consistent with the iron analysis indicating the presence of ~6 irons per hexamer, sufficient to fill the Rieske sites but not the mononuclear sites. Addition of iron as ferrous ammonium sulfate (50 μM) to BenDO assays containing 1.6 μM BenAB mononuclear sites did not reconstitute activity. BenDO activity could be reconstituted, however, by aerobic incubation of BenAB, BenC, ferrous ammonium sulfate and benzoate at 4 °C for 30 min prior to the addition of NADH. BenDO activity was most conveniently measured by monitoring benzoate-dependent consumption of NADH for 5 min. The conditions for maximum activity were found to be at pH 7.5 (50 mM HEPES buffer) and 100 mM KCl. This optimization was

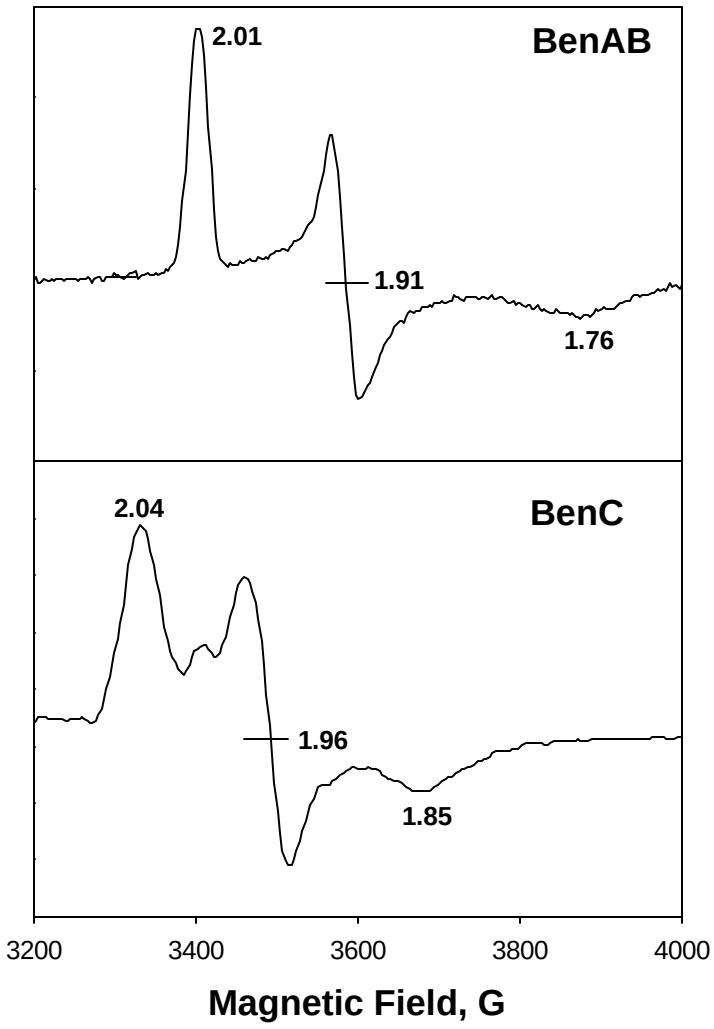

Figure 2.8. EPR spectra of reduced BenAB (100 μM $\alpha_3\beta_3$) and reduced BenC (300 μM) in buffer A. Purified samples of protein were reduced anaerobically with excess sodium dithionite (0.5 mM). Spectra were recorded under the following conditions: temperature, 10K; microwave frequency, 9.58 GHz; modulation amplitude, 6.366 G; microwave power, 4 mW.

determined with saturating NADH, benzoate, and O_2 (typically 100 μM, 0.5 mM, and ~0.25 mM, respectively), and reactivated BenDO (0.8 μM BenAB hexamer, 0.5 μM BenC, 50 μM ferrous ammonium sulfate and 0.5 mM benzoate incubated at 4°C for 30 min). These protein concentrations were chosen for convenience in monitoring NADH consumption. Under these conditions, BenDO consumed NADH at a rate of ~17 μM/min/μM BenAB hexamer. The K_m of BenC for BenAB was determined under the standard assay conditions except with 0.25 mM NADH, 0.05 μM BenAB and variable amounts of BenC from 5 to 50 μM. From a Lineweaver-Burke plot, a K_m for BenC of approximately 32 μM and a turnover number of 5800 min^{-1} were estimated (Figure 2.9).

Activities of BenDO with benzoate derivatives

Table 2.2 summarizes the activities (reported as the concentrations of NADH, O_2, and aromatic substrate consumed in 5 min) of the purified recombinant BenDO with benzoate and various substituted benzoates. Several considerations circumscribe interpretation of the data in Table 2.2. These activities were measured at the pH and salt concentration that had been determined to be optimal with benzoate as substrate. Also, in order to avoid significant background consumption of NADH and O_2 and to allow simultaneous measurements of consumption of several substrates on a reasonable time scale, a sub-saturating concentration of BenC was used.

The reaction of BenDO with benzoate is tightly coupled in NADH:O_2:benzoate consumption (Table 2.2). Clear evidence was found that BenDO consumed NADH and O_2 with several substituted benzoates in addition to benzoate. According to the data in Table 2.2 relative to benzoate, the next best and poorest substrates as judged by NADH consumption rate are *m*-methylbenzoate and *o*-methoxybenzoate, respectively. These

Figure 2.9. Plot of the initial velocity of NADH oxidation of BenAB and varying concentrations of BenC (top) and the corresponding Lineweaver-Burke plot (bottom). Assay conditions: BenAB (0.05 μM $\alpha_3\beta_3$), BenC (5-50 μM), NADH (0.25 mM), benzoate (0.5 mM), ferrous ammonium sulfate (0.01 mM) in 50 mM HEPES containing 100 mM KCl, pH 7.5 at 23 °C.

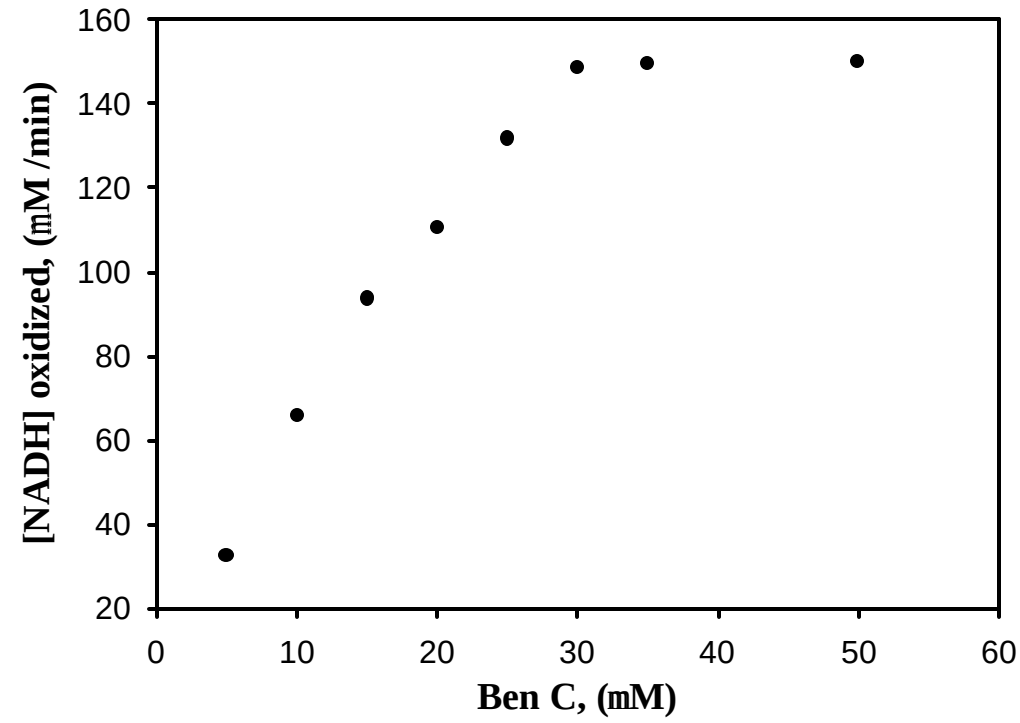
160
140
120
100
80
60
40
20
0
10
20
30
40
50
60
[NADH] oxidized, (mM /min)
Ben C, (mM)

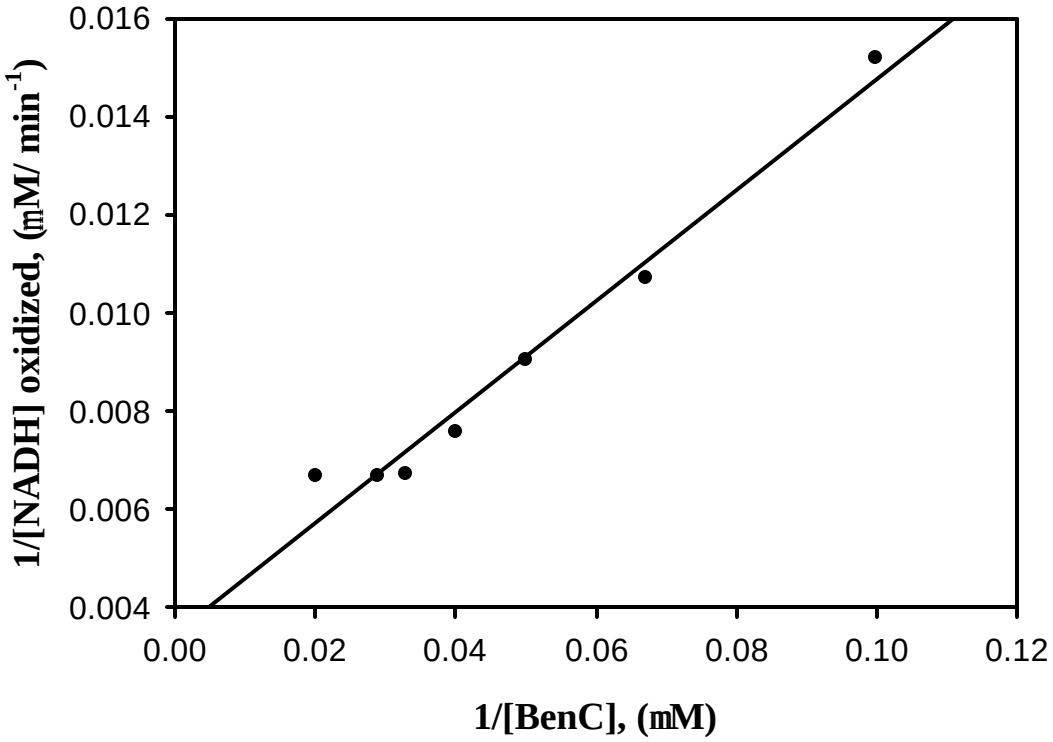
0.016
0.014
0.012
0.010
0.008
0.006
0.004
0.00
0.02
0.04
0.06
0.08
0.10
0.12
1/[NADH] oxidized, (mM/ min-1)
1/[BenC], (mM)

Table 2.2. Activities, reaction stoichiometries and product formation for recombinant *Acinetobacter* sp. ADP1 BenDO with various benzoate derivatives.[a]

Substrate	NADH (μM/5 min) (Rel. act., %)[b]	O_2 (μM/5 min)	H_2O_2 (μM/5 min)	Substrate consumed (μM/ 5 min)[c]	Diol product[d]	Catechol Product[e]
benzoate	67±3 (100)	68±4	-	61±2	+	-
o-aminobenzoate	45±4 (67)	42±2	-	36±2	-	+, 13±1[g]
m-aminobenzoate	55±3 (82)	50±3	10	+[f]	-	+
p-aminobenzoate	36±5 (53)	31±7	-	2±1	-	+
o-fluorobenzoate	38±7 (57)	32±6	-	10±5	+	-
m-fluorobenzoate	50±8 (74)	48±9	-	41±4	+	-
p-fluorobenzoate	53±2 (79)	40±5	7	7±2	+	-
o-chlorobenzoate	26±4 (38)	24±2	5	2±1	-	-
m-chlorobenzoate	49±7 (73)	42±9	3	37±9	+	-
p-chlorobenzoate	21±3 (31)	18±5	5	None	-	-
o-methylbenzoate	30±2 (44)	21±6	7	17±4	-	-
m- methylbenzoate	65±9 (97)	62±2	3	41±19	+	-
p-methylbenzoate	25±6 (37)	21±4	20	None	-	-
o- methoxybenzoate	18±5 (26)	18±2	17	None	-	-
m-methoxybenzoate	21±3 (31)	19±4	3	8±1	-	-
p-methoxybenzoate	23±2 (34)	12±3	3	9±7	-	-
o-hydroxybenzoate	30±4 (44)	23±7	10	13±4	-	-
m-hydroxybenzoate	24±5 (35)	18±2	8	+[f]	-	+
p-hydroxybenzoate	20±1 (30)	14±3	5	10±2	-	+

[a]Assay conditions: 100 μM NADH, 0.25 mM O_2, 0.5 mM aromatic carboxylate, 50 μM ferrous ammonium sulfate, 0.8 μM BenAB ($\alpha_3\beta_3$), 0.5 μM BenC, and in 50 mM

HEPES, 100 mM KCl (pH 7.5) at room temperature (23 ºC). NADH and O_2 consumption values listed are after 5 min.

[b]Relative activities are defined as the percentage of NADH consumed after 5 min relative to BenDO activity with benzoate.

[c]Substrate consumption was monitored by HPLC as described in the Experimental.

[d]Detected by the increase at 340 nm due to formation of NADH upon addition of BenD (5 μM) and NAD^+ (0.2 mM) to reactions monitoring NADH consumption after 5 min. +, indicates generation of NADH; -, no generation of NADH was observed.

[e]Gibbs' reagent (15 μL of a 2% (w/v) solution in ethanol) was added to reactions (200 μL) monitoring NADH consumption after 5 min and determined to be positive (+) by formation of a blue to purple color; -, no color change occured. These analyses were conducted without addition of BenD.

[f]+, substrate consumption was detected but could not be quantified accurately.

[g]Catechol was identified and quantified as the product by HPLC as described in the Experimental section.

relative activities, however, are based on NADH consumption only and do not necessarily correlate with or even signify consumption of the aromatic substrate. For example, the 1:1:1 mol ratio of NADH and O_2 consumed to H_2O_2 produced in reactions with *p*-methylbenzoate and *o*-methoxybenzoate indicates complete uncoupling, i.e., no aromatic substrate was consumed, consistent with the absence of detectable diol or catechol products.

The HPLC conditions used were able to determine that the product of the BenDO reaction with benzoate as substrate is the expected benzoate diol, but these conditions were not optimal for quantification of the amount of diol generated. Therefore, the diol dehydrogenase that catalyzes the conversion of the benzoate diol to catechol was used to quantify the amount of diol formed. The amount of NADH generated upon addition of BenD and NAD^+ to BenDO reactions that consumed 50 μM NADH in the presence of 50 μM benzoate was approximately 50 μM, suggesting formation of a stoichiometric amount of benzoate diol. The amount of benzoate diol formed under standard assay conditions could not be quantitated accurately. Consumption of all 100 μM NADH with benzoate as the substrate was complete after ~10 min. Addition of BenD and NAD^+ to these reactions resulted in the formation of NADH, which was immediately consumed due to the presence of excess benzoate.

Several of the substituted benzoates used as substrates for BenDO assays formed products that either were substrates for BenD (e.g., the fluoro-substituted benzoates), indicating formation of a non-aromatic diol, or tested positive for the formation of a catechol with Gibbs' reagent (e.g., the amino-substituted benzoates) (Table 2.2). The substrate specificity of BenD has not been studied. It is, therefore, possible that the

BenDO reactions that did not indicate the formation of a diol or catechol could be generating a diol product that was unreactive with BenD. Therefore, those BenDO-catalyzed reactions that tested negative with both BenD and Gibbs' reagent (e.g. *o*-chlorobenzoate) were acidified and heated in order to convert any diol to the corresponding phenol, which is detectable using Gibbs' reagent (*27*, *28*). However, no catechol products were detected (data not shown).

Crystal structure of BenC

The crystal structure of BenC was solved using multiwavelength anomalous diffraction and refined to 1.5 Å resolution at the Swedish University of Agricultural Sciences. The BenC structure consists of three domains: iron-sulfur, flavin and NAD^+ binding (Figure 2.10). The fold of the iron-sulfur domain is very similar to that of plant-type [2Fe-2S] ferredoxins. The [2Fe-2S] ferredoxin of BenC is ligated by Cys41, Cys46, Cys49 and Cys83 as predicted from amino acid sequence alignment (*37*).

Structurally, the FAD and NADH domains of BenC are members of the NAD(P)-ferredoxin reductase (FNR) family that contain FAD and NAD^+-binding domains but lack a ferredoxin domain (*38*, *39*). The FAD binding domain of BenC is smaller than those in other members of the FNR family. However, the location of the FAD in BenC is very similar to that in members of the FNR family, where FAD is bound in a bent conformation such that the adenine and ribityl portions are hydrogen-bonded to each other (Figure 2.10). The sequence of the NAD^+-binding domain is shorter in BenC compared to other members of the FNR family. The C-terminus of the NAD^+-binding domain is involved in binding the FAD cofactor via stacking interactions with Phe335, hydrogen bonding interactions with Ser159 and Tyr158 and hydrophobic interactions

Figure 2.10. X-ray crystal structure of *Acinetobacter* sp. strain ADP1 BenC with the three cofactor domains indicated. This figure was generated using ViewerLite (Accelrys, Inc.) and coordinates from 1KRH. Coordination of the [2Fe-2S] center and residues that interact with FAD are shown. Iron atoms are indicated by black spheres and bridging sulfur atoms as orange spheres.


NAD+
FAD
[2Fe-2S]

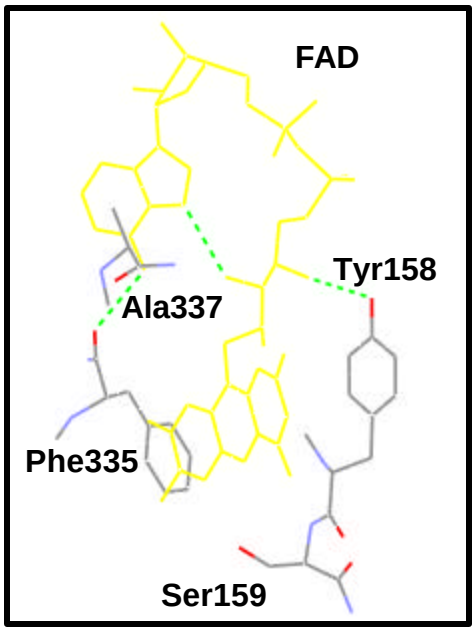
FAD
Tyr158
Ala337
Phe335
Ser159

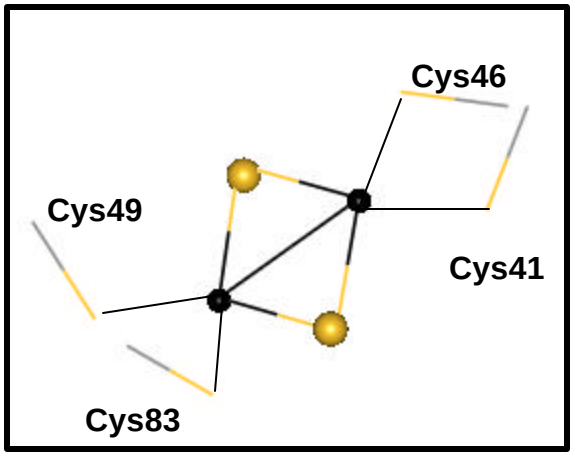
Cys46
Cys49
Cys41
Cys83

with Ala337 (Figure 2.10). The [2Fe-2S] and flavin centers are approximately 9 Å apart, which is well within range for facile electron transfer.

The crystal structure of BenC is the first structure of a RDO reductase whose oxygenase component is of $\alpha_3\beta_3$ composition. BenC can be divided into three domains: an N-terminal [2Fe-2S] domain, a FAD-binding domain and a C-terminal NAD^+-binding domain (Figures 2.10 and 2.11). The structure of the FMN-containing phthalate dioxygenase reductase (PDR), whose oxygenase component (PDO) consists of a single subunit α_4 oligomer, has been solved previously (*40-42*). PDR contains the same domains as BenC but in a different sequential order, as shown in Figure 2.11. For both reductases, catalysis of electron transfer from NADH to the terminal oxygenase component is thought to occur by two-electron transfer of the reductase flavin moiety by NADH, followed by intramolecular electron transfer to the [2Fe-2S] center. The reduced reductase [2Fe-2S] center subsequently transfers electrons to the Rieske-type [2Fe-2S] center in the oxygenase component. It is, therefore, a reasonable assumption that protein-protein interactions between the reductase and oxygenase components would occur in regions near their constituent [2Fe-2S] centers. Examination of the BenC structure, in fact, shows a space between the [2Fe-2S] and FAD domains in BenC that could be available for binding of BenAB (Figure 2.12). In contrast, the open region where PDO could bind to PDR is between the [2Fe-2S] and NAD domains. It is possible that this difference in the arrangement of the flavin, [2Fe-2S], and NAD binding domains within PDR versus BenC are related to the oligomeric composition of their respective terminal oxygenase components. Unfortunately, there is currently no structure of an α_4-type RDO oxygenase available.

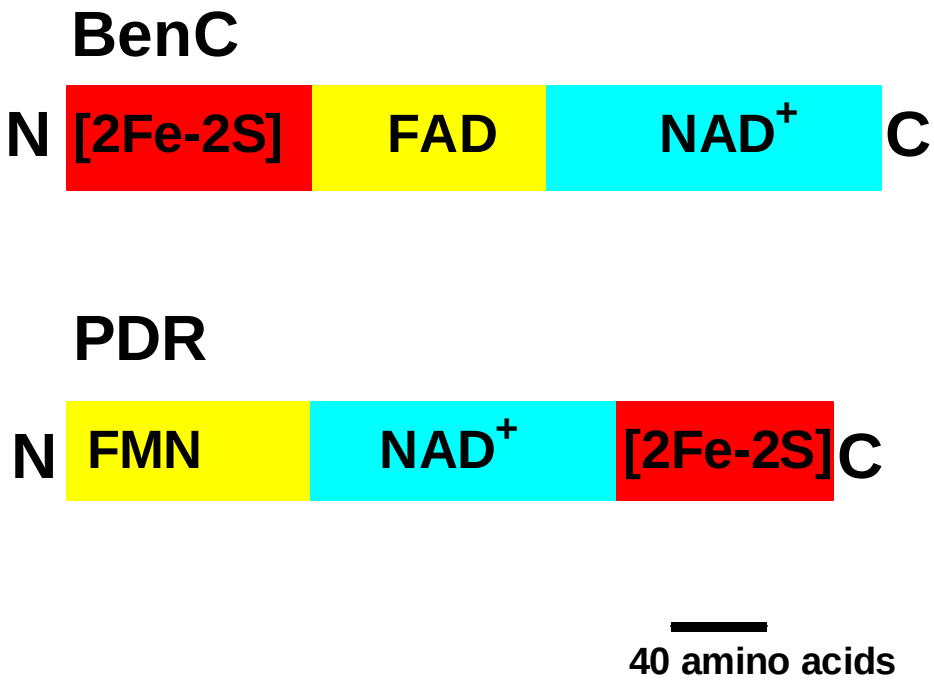

Figure 2.11. Schematic illustration of the sequential arrangements of the cofactor binding domains in BenC (37) and PDR (40). N and C indicate N- and C-termini, respectively.

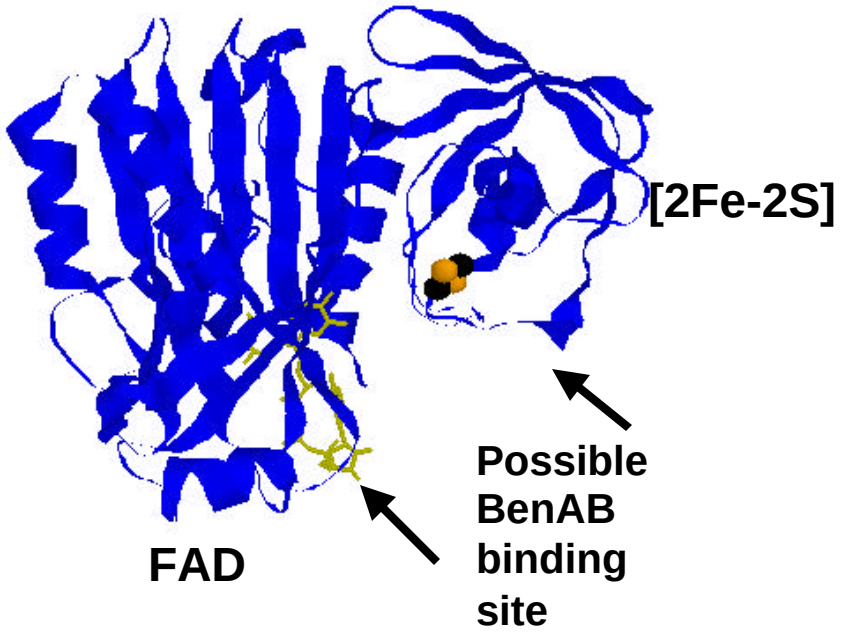

Figure 2.12. Structure of BenC indicating a possible binding site for BenAB between the [2Fe-2S] and FAD binding domains generated using ViewerLite (Accelrys, Inc.) and coordinates from 1KRH.

Discussion

The microbial degradation of a number of aromatic compounds converges at benzoate (cf. Figure 2.1). The Rieske dioxygenase, benzoate 1,2-dioxygenase (BenDO), and the benzoate diol dehydrogenase, BenD, catalyze the transformation of benzoate to catechol. Both chromosomal and plasmid-encoded genes responsible for catalyzing this reaction have been identified. It has been noted that organisms that contain only chromosomally encoded BenDOs are unable to utilize many substituted benzoates as sole sources of carbon, while those with plasmid-encoded BenDOs have the ability to sustain growth on various *meta,* and *para* substituted benzoates (*12, 43*). This distinction has led to the supposition that chromosomal *ben* genes encode for a BenDO with much narrower substrate specificity than their plasmid-encoded counterparts. Therefore, it would appear that organisms have acquired plasmid-encoded pathways for aromatic hydrocarbon degradation in order to increase their catabolic versatility.

Characterization of recombinant *Acinetobacter* sp. strain ADP1 BenAB and BenC

In agreement with the previous characterization of *P. putida* BenDO, the *Acinetobacter* sp. strain ADP1 BenDO (hereafter referred to as ADP1 BenDO) was found to consist of a $\alpha_3\beta_3$ oxygenase component (BenAB) and a monomeric reductase component (BenC) that together catalyze the conversion of benzoate to the benzoate diol (*17, 18*). *P. putida* BenAB was reported to contain 8 and 10 mol iron/mol enzyme for two different preparations of the enzyme (*18, 44*), consistent with fully occupied Rieske and two to three mononuclear iron sites occupied. EPR studies of *P. putida* BenAB showed that the mononuclear iron sites are ferric and the Rieske centers are diferric in the as-isolated protein (*17*). Recombinant ADP1 BenAB, however, contained only enough iron

(~6 irons/$\alpha_3\beta_3$) to account for the three Rieske sites, implying unoccupied mononuclear iron sites. Consistent with this iron analysis, as-isolated BenAB was inactive in assays monitoring benzoate-dependent NADH consumption and addition of ferrous iron did not increase activity. However, incubation of BenAB and BenC in the presence of excess benzoate and ferrous iron restored activity. The importance of BenC-promoted activation of BenDO activity may be attributed to formation of a BenABC complex that is subsequently able to bind substrate and reconstitute iron into empty mononuclear sites. Evidence for formation of a BenABC complex was obtained during initial purification attempts of BenAB. Even though the BenAB $\alpha_3\beta_3$ hexamer is ~175 kDa larger than the monomeric BenC, both BenAB and BenC were observed to co-elute during gel filtration chromatography with an apparent molecular weight greater than 225 kDa.

The K_m of ADP1 BenAB for the reductase, BenC, was determined in this work to be 32 μM, similar to the K_m of 26 μM previously reported for the *P. putida* BenAB/BenC complex (*18*). Under saturating reductase conditions with benzoate as the substrate, ADP1 BenDO had a turnover number of 5800 min^{-1} (on a hexamer basis), while the turnover number of *P. putida* BenDO was reported to be 22,000 min^{-1} (on a hexamer basis) (*18*). However, the turnover number for *P. putida* BenDO was based on a molecular weight of BenAB of 273 kDa (*18*). A second report on *P. putida* BenAB determined the molecular weight as 201 kDa (*44*), which would correspond to a turnover number of ~16,000 min^{-1} (on a hexamer basis).

The product of ADP1 BenDO catalysis with benzoate was identified as the expected non-aromatic benzoate diol by comparison to an authentic sample of benzoate diol using HPLC. However, the amount of diol formed could not be quantitated under the

HPLC conditions used. Therefore, recombinant BenD, which catalyzes the conversion of the benzoate diol to catechol, was isolated and used to quantitate the amount of diol generated. The stoichiometry of benzoate conversion to benzoate diol was shown to be 1:1:1 with respect to NADH, O_2, and benzoate consumed. Furthermore, the amount of NADH generated in these reactions using BenD suggests that a stoichiometric amount of benzoate diol is formed from benzoate. Similarly, the stoichiometry of *P. putida* BenDO-catalyzed dihydroxylation of benzoate was shown to be 1:1:1:1 in reactants consumed and diol formed (*18*).

Substrate specificity of BenDO

In terms of relative NADH consumption rates, *P. putida* BenDO and ADP1 BenDO both showed a clear preference for *meta* substituted benzoates with the exception of the methoxy- and hydroxybenzoates (Table 2.3) (*18*). However, the amount of NADH consumed in these reactions with ADP1 BenDO did not necessarily correlate with diol or catechol formation (Table 2.2). In some cases, electron transfer was diverted from substrate hydroxylation into a futile cycle that reduced some (*m*-aminobenzoate) or all (*p*-methylbenzoate and *o*-methoxybenzoate) of the O_2 consumed to H_2O_2, a process termed uncoupling (which is discussed in more detail in Chapter 3). In these cases, substrate analog binding, thus, triggers electron transfer from the reductase to the oxygenase, even though substrate is not consumed. For *P. putida* BenDO-catalyzed reactions with the substrates listed in Table 2.3 no H_2O_2 was detected (*18*). However, the amounts of O_2 or substrate consumed in the *P. putida* BenDO assays were not reported (except for

Table 2.3. Relative activities of *Acinetobacter* sp. ADP1 BenDO versus *Pseudomonas putida* BenDO.[a]

Substrate	ADP1 BenDO[a]	*P. putida* BenDO[b]
Benzoate	100	100
o-aminobenzoate	67	25
m-aminobenzoate	82	68
p-aminobenzoate	53	11
o-fluorobenzoate	57	28
m-fluorobenzoate	74	89
p-fluorobenzoate	79	68
o-chlorobenzoate	38	11
m-chlorobenzoate	73	71
p-chlorobenzoate	31	1
o-methylbenzoate	44	32
m-methylbenzoate	97	73
p-methylbenzoate	37	5
o-methoxybenzoate	26	1
m-methoxybenzoate	31	6
p-methoxybenzoate	34	0
o-hydroxybenzoate	44	11
m-hydroxybenzoate	35	25
p-hydroxybenzoate	30	15

[a]Relative activities are defined as the percentage of NADH consumed after 5 min relative to BenDO activity with benzoate.

[b]Assay conditions are as described in the footnote of Table 2.2.

[c]Data are from reference (*18*).

benzoate) and therefore, the *P. putida* BenDO activities listed in Table 2.3 are based solely on NADH consumption and may not be representative of substrate hydroxylation.

The products of ADP1 BenDO reactions with *m*- and *p*-fluorobenzoate, *m*-chlorobenzoate, and *m*-methylbenzoate served as substrates for BenD, suggesting formation of non-aromatic *cis*-diols. Addition of BenD to reactions with *o*-fluorobenzoate as the substrate also indicated formation of a non-aromatic *cis* diol. Catechol was not detected as a product with *o*-fluorobenzoate as the substrate with ADP1 BenDO. The 2-halobenzoate 1,2-dioxygenase from *Pseudomonas cepacia* 2CBS was shown to transform *o*-fluorobenzoate to catechol, presumably through spontaneous decarboxylation and dehalogenation of an unstable *cis*-1,2-dihydroxy-2-fluorocyclohexa-3,5-diene-1-carboxylate (2-fluorobenzoate diol) (*25*). The apparent formation of a stable diol in ADP1 BenDO-catalyzed reactions with *o*-fluorobenzoate, suggests that dihydroxylation occurs at C1 and C6 to yield *cis*-1,2-dihydroxy-6-fluorocyclohexa-3,5-diene-1-carboxylate (6-fluorobenzoate diol), which is unable to rearomatize to catechol (Figure 2.13).

BenDO dihydroxylation at the C1, C6 positions of various substrates has been observed with whole cells of a mutant strain of *Alcaligenes eutrophus* B9, which contains a functional BenDO but a defective BenD, allowing accumulation of diol products (*45*). This strain transformed *o*-fluorobenzoate to the corresponding 6-fluorobenzoate diol (Figure 2.13D), whose diacetyl derivative was identified by nuclear magnetic resonance, infrared and ultraviolet absorption spectroscopies. This strain also showed a preference for hydroxylation of *meta* substituted benzoates, which formed both 3- and 5-substituted non-aromatic diols (Figure 2.13A and B). In the *A. eutrophus* strain, the *meta* substituted

Figure 2.13. BenDO products identified in whole cell reactions of *Alcaligenes eutrophus* and *Pseudomonas* sp. B13 (*45, 46*). Dihydroxylation at C1 and C2 of *meta* substituted substrates results in 3- (A) and 5-substituted (B) benzoate diols. Dihydroxylation at C1 and C2 or C1 and C6 of *o*-fluorobenzoate results in 2-fluoro-benzoate diol (C) and 6-fluoro-benzoate diol (D), respectively. Carbon atoms in the products are numbered according to proper nomenclature of these compounds.

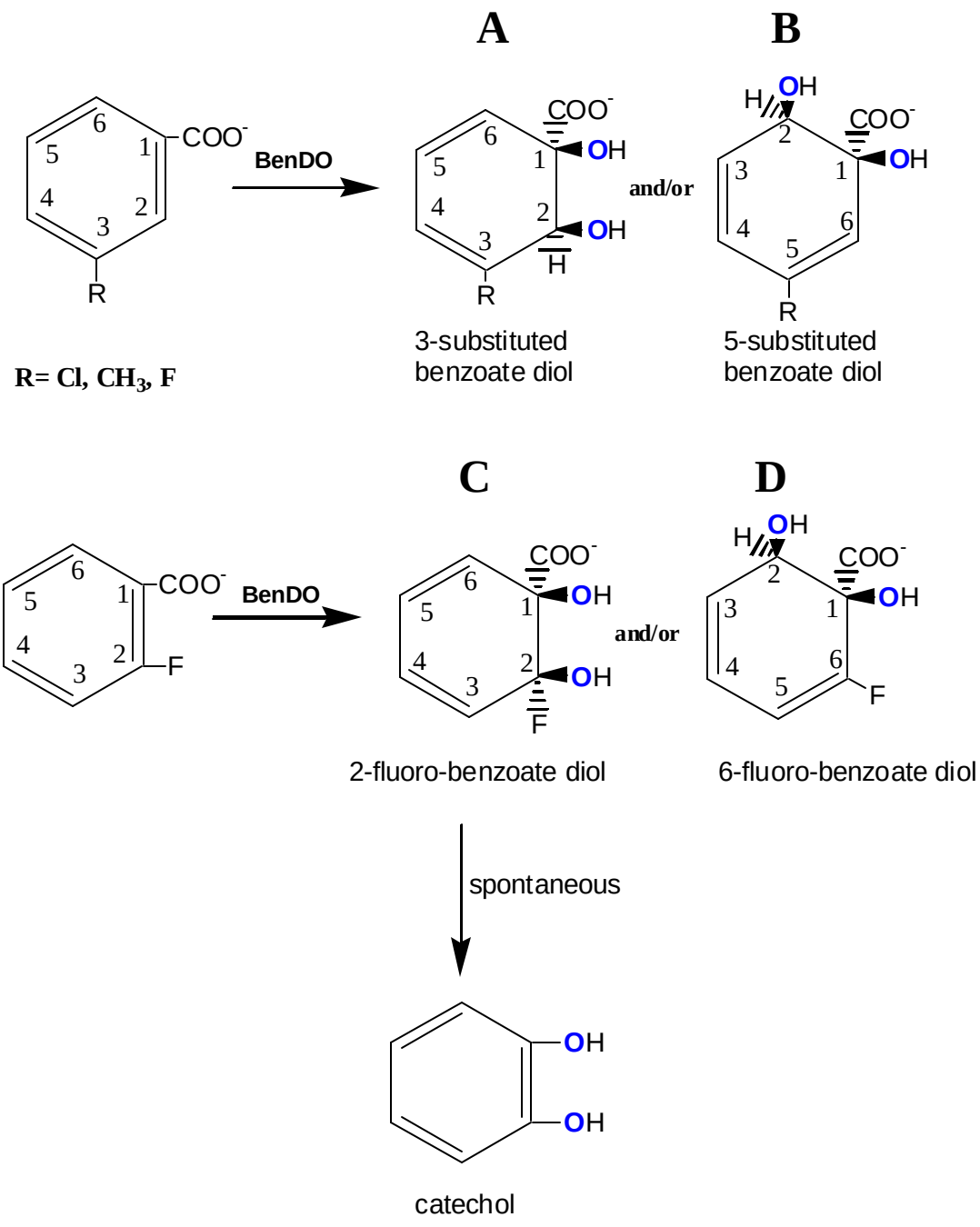
A
B
COO-
BenDO
OH
and/or
H
R
3-substituted
benzoate diol
5-substituted
benzoate diol
R= Cl, CH3, F
C
D
F
2-fluoro-benzoate diol
6-fluoro-benzoate diol
spontaneous
catechol

chloro-, methyl-, and fluorobenzoates were all dihydroxylated at [C1, C2] and also at [C1, C6] to form both 3- and 5-substituted non-aromatic *cis*-diols (Figure 2.13). The ratios of 3- to 5-substituted diol products formed from a mutant strain of *Pseudomonas* sp. B13 also with a defective BenD, showed that *m*-fluorobenzoate and *m*-chlorobenzoate generated approximately equal amounts of either 3- or 5-substituted diols, while the reaction with *m*-methylbenzoate favored formation of the *cis*-1,2-dihydroxy-3-methylcyclohexa-3,5-diene-1-carboxylate (3-methyl benzoate diol) (*46*). It is most likely that ADP1 BenDO catalysis with these *meta* substituted benzoates also generates both 3- and 5-substituted diols, which suggests that these substrates may bind in the BenAB active site either with [C1, C2] or [C1, C6] positioned for dihydroxylation (Figure 2.14).

Comparison of ADP1 chromosomally-encoded BenDO with the plasmid-encoded benzoate/toluate (methylbenzoate) dioxygenase (XylDO)

In vivo studies have shown that chromosomally-encoded BenDO does not act efficiently on methyl substituted benzoates, while the plasmid-encoded XylDO catalyzes the dihydroxylation of benzoate *m*- and *p*-methylbenzoates and many other *meta* and *para* substituted benzoates (*8, 45, 47*). *Pseudomonas putida* contains both a chromosomally encoded BenDO and a plasmid encoded XylDO, which allows this organism to utilize benzoate and *m*- and *p*-methylbenzoate as sole carbon sources (*8, 20*). Accordingly, a *P. putida* strain lacking XylDO and the genes required for further degradation of catechol and substituted catechols via the *meta* pathway are still able to utilize benzoate as the sole carbon source but not *m*- or *p*-methylbenzoate (*8*). However, cells of this strain grown with benzoate as the sole carbon source showed substrate-

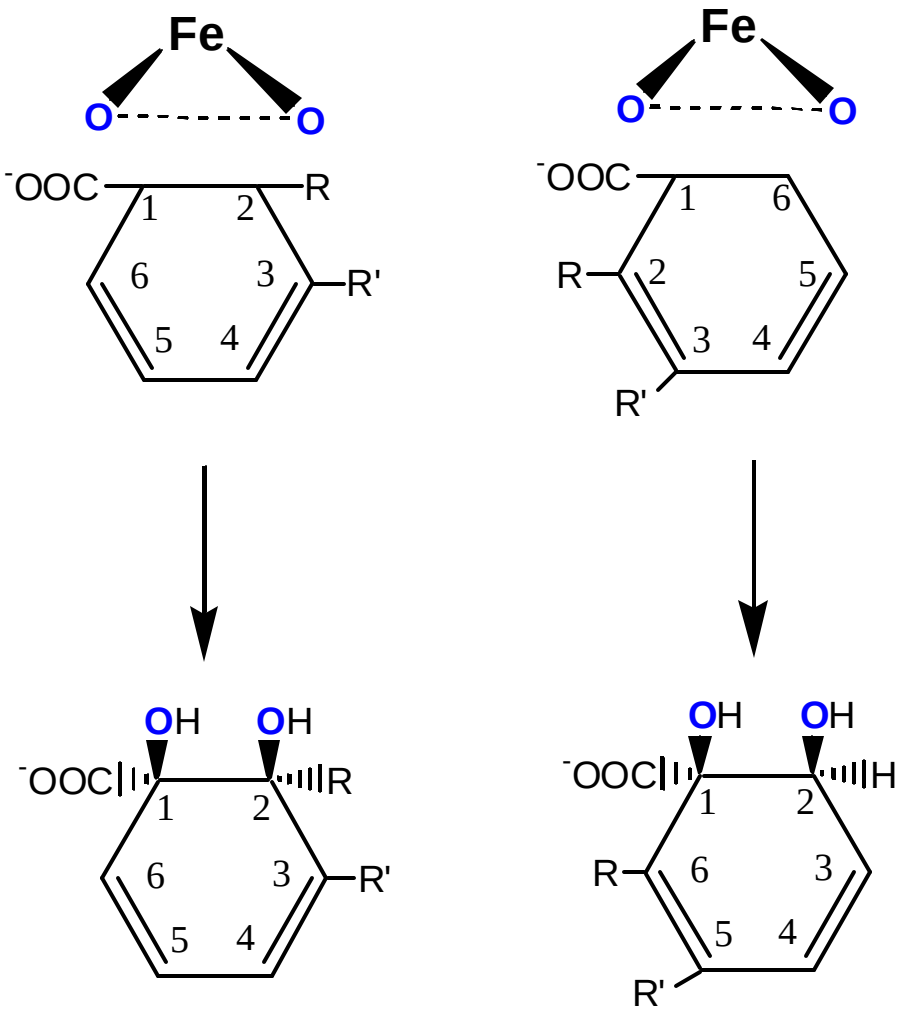

Figure 2.14. Proposed substrate binding at the mononuclear iron site leading to the formation of 2-, 3- and 5-, 6-substituted benzoate diols from *ortho*- or *meta*-substituted benzoate substrates of BenDO. Carbon atoms in the products are numbered according to proper nomenclature of these compounds. For *o*-fluorobenzoate, R=F, R´=H.

dependent O_2 consumption with *m*-methylbenzoate that was ~50% the activity of wild type *P. putida* grown with benzoate (*8*). No activity was seen with *p*-methylbenzoate as the substrate. These results suggest that the chromosomally encoded *P. putida* BenDO was functional but less reactive with *m*-methylbenzoate relative to XylDO and totally inactive with *p*-methylbenzoate. These previous observations agree with the results in Table 2.2 that purified, recombinant ADP1 BenDO exhibited very high activity with *m*-methylbenzoate with formation of a diol product, but showed only uncoupled activity with *p*-methylbenzoate, in which NADH and O_2 but not substrate were consumed to form H_2O_2 (Table 2.2). Despite the observed activity with *m*-methylbenzoate on benzoate grown cells, the inability of the mutant *P. putida* strain to utilize *m*-methylbenzoate as the sole carbon source was attributed to insufficient induction of expression of BenDO during growth with succinate as the carbon source and *m*-methylbenzoate (*8*). Also due to the absence of the genes of the *meta* pathway in this strain, any methylcatechol formed by BenDO could not be further degraded (Figure 2.2) (*8*).

The results presented herein on recombinant ADP1 BenDO are the first detailed studies on the substrate specificity of a chromosomally encoded BenDO. The activities reported for *P. putida* BenDO (*18*) did not measure substrate consumption or detect product formation, and, therefore, the relative activities reported could not be correlated with substrate hydroxylation. It is clear from the data in Table 2.2 that in vitro, ADP1 BenDO is capable of hydroxylating several *o*-, *m*-, and *p*-substituted benzoates, which is inconsistent with previous notions that chromosomally encoded BenDOs have narrow substrate specificity relative to their plasmid encoded counterparts. XylDO has not been purified from any organism, which precludes a detailed comparison of its substrate

specificity relative to ADP1 BenDO in vitro. However, dioxygenase activity with benzoate and several *meta* and *para* substituted benzoates has been demonstrated in *E. coli* expressing a *Pseudomonas putida* XylDO (*47*).

Efforts to broaden the range of aromatic hydrocarbons degraded by microbes has focused on altering the substrate specificity of those enzymes that catalyze the initial ring hydroxylation and ring cleavage reactions in the catabolic pathways. However, it is becoming apparent that other factors including cellular uptake of substrates, the regulation of induction of these enzymes and/or the formation of “dead-end” metabolites must also be considered.

References

1. Ellis, L. B. M., Hershberger, C.D., Bryan, E.M., and Wackett, L.P. (2001) *Nucl. Acids Res.* ***29***, 340-343.
2. Reiner, A. M., and Hegeman., G.D. (1971) *Biochemistry* ***10***, 2530-2536.
3. Neidle, E. L., Shapiro, M.K., and Ornston, L.N. (1987) *J. Bacteriol.* ***169***, 5496-5503.
4. Reiner, A. M. (1972) *J. Biol. Chem.* ***247***, 4960-4965.
5. Collier, L. S., Gaines, G.L. and Neidle, E.L. (1998) *J. Bacteriol.* ***180***, 2493-2501.
6. Williams, P. A., and Sayers, J.R. (1994) *Biodegradation* ***5***, 195-217.
7. Keil, H., Keil, S., Pickup, R.W., and Williams, P.A. (1985) *J. Bacteriol.* ***164***, 887-895.
8. Williams, P. A., and Murray, K. (1974) *J. Bacteriol.* ***120***, 416-423.
9. Bertini, I., Cremonini, M.A., Ferretti, S., Lozzi, I., Luchinat, C., and Viezzoli, M.S. (1996) *Coord. Chem. Rev.* ***151***, 145-160.
10. Butler, C. S., and Mason, J.R. (1997) *Adv. Microb. Physiol.* ***38***, 47-84.
11. Mason, J. R., and Cammack, R. (1992) *Ann. Rev. Microbiol.* ***46***, 277-305.
12. Neidle, E. L., Hartnett, C., Ornston, L.N., Bairoch, A., Rekik, M., and Harayama, S. (1991) *J. Bacteriol.* ***173***, 5385-5395.
13. Batie, C. J., LaHaie, E. and Ballou, D.P. (1987) *J. Biol. Chem.* ***262***, 1510-1518.
14. Coulter, E. D., Moon, N., Batie, C.J., Dunham, W.R., and Ballou, D.P. (1999) *Biochemistry* ***38***, 11062-11072.
15. Tsang, H., Batie, C.J., Ballou, D.P. and Penner-Hahn, J.E. (1996) *J. Biol. Inorg. Chem.* ***1***, 24-33.

16. Kauppi, B., Lee, K., Carredano, E., Parales, R. E., Gibson, D. T., Eklund, H., and Ramaswamy, S. (1998) *Structure **6***, 571-586.

17. Altier, D. J., Fox, B.G., Munck, E. and Lipscomb, J.D. (1993) *J. Inorg. Biochem. **51***, 300.

18. Yamaguchi, M. and Fujisawa, H. (1980) *J. Biol. Chem. **255***, 5058-5063.

19. Harayama, S., Rekik, M. and Timmis, K.N. (1986) *Mol. Gen. Genet. **202***, 226-234.

20. Cowles, C. E., Nichols, N.N. and Harwood, C.S. (2000) *J. Bacteriol. **182***, 6339-6346.

21. Eby, D. M., Beharry, Z.M., Coulter, E.D., Kurtz, D.M., and Neidle, E.L. (2001) *J. Bacteriol. **183***, 109-118.

22. Schagger, H., and Jagow, G. von. (1987) *Anal. Biochem. **166***, 368-379.

23. Sambrook, J., Fritsch, E.F., and Maniatis, T. (1989), Cold Spring Harbor Laboratory Press, Cold Spring Harbor, N.Y.

24. Bradford, M. M. (1976) *Anal. Biochem. **72***, 248-254.

25. Fetzner, S., Muller, R., and Lingens, F. (1992) *J. Bacteriol. **174***, 279-290.

26. Massey, V. (1959) *Biochim. Biophys. Acta 34*, 255-256.

27. Quintana, M. G., Didion, C., and Dalton, H. (1997) *Biotechnol. Tech. **11***, 585-587.

28. Joern, J. M., Sakamoto, T., Arisawa, A., and Arnold, F.H. (2001) *J. Biomol. Screen. **6***, 219-223.

29. Otwinowski, Z. (1993) in *Proceedings of the CCP4 study weekend* (Sawyer, L., Issacs, N. and Bailey, S., Ed.), Daresburry Laboratories, Warrington, UK.

30. Cowtan, K. (1994) *Joint CCP4 and ESF-EACBM Newsletter on Protein Crystallography* ***31***, 34-38.

31. Jones, T. A., Zou, J.Y., Cowan, S. and Kjeldgaard, M. (1991) *Acta Crystallog.* ***47***, 110-119.

32. Brunger, A. T., Adams, P.D., Clore, G.M., DeLano, W.L., Gros, P., Grosse-Kunstleve, R.W. et al. (1998) *Acta Crystallog. Sect. D* ***54***, 905-921.

33. CCP4. (1994) *Acta Crystallog. Sect. D* ***50***, 760-763.

34. Fee, J. A., Findling, K.L., Yoshida, T., Hille, R., Tarr, G.E., Hearshen, O., Dunham, W.R., Day, E.P., Kent, T.A., and Munck,E. (1984) *J. Biol. Chem.* ***259***, 124-133.

35. Hugo, N., Armengaud, J., Gaillard, J., Timmis, K.N., and Jouanneau, Y. (1998) *J. Biol. Chem.* ***273***, 9622-9629.

36. Trumpower, B. L. (1990) *Microbiol. Rev.* ***54***, 101-129.

37. Karlsson, A., Beharry, Z.M., Eby, D.M., Coulter, E.D., Neidle, E.L., Kurtz, D.M., Eklund, H., and Ramaswamy, S. (2002) *J. Mol. Biol. 318*, 261-272.

38. Ingelman, M., Ramaswamy, S., Niviere, V., Fontecave, M. and Eklund, H. (1999) *Biochemistry* ***38***, 7040-7049.

39. Karplus, P. A., Daniels, M.J. and Herriott, J.R. (1991) *Science* ***251***, 60-66.

40. Correll, C. C., Batie, C.J., Ballou, D.P. and Ludwig, M.L. (1985) *J. Biol. Chem.* ***260***, 14633-14635.

41. Correll, C. C., Batie, C.J., Ballou, D.P. and Ludwig, M.L. (1992) *Science* ***258***, 1604-1610.

42. Gassner, G. T., Ludwig, M.L., Gatti, D.L., Correll, C.C. and Ballou, D.P. (1995) *FASEB J.* ***9***, 1411-1418.

43. Harayama, S., Rekik, M., Bairoch, A., Neidle, E.L., and Ornston, L.N. (1991) *J. Bacteriol.* ***173***, 7540-7548.

44. Yamaguchi, M., and Fujisawa, H. (1982) *J. Biol. Chem.* ***257***, 12497-12502.

45. Reineke, W., Otting, W. and Knackmuss, H. (1978) *Tetrahedron* ***34***, 1707-1714.

46. Reineke, W. and Knackmuss, H. (1978) *Biochim. Biophys. Acta*. ***542***, 412-423.

47. Zeyer, J., Lehrbach, P.R. and Timmis, K.N. (1985) *Appl. Environ. Microbiol.* ***50***, 1409-1413.

CHAPTER 3

CHARACTERIZATION AND SUBSTRATE SPECIFICITY OF ANTHRANILATE 1,2-DIOXYGENASE FROM *ACINETOBACTER* SP. STRAIN ADP1[2,3]

[2] **Beharry, Z.M., Eby, D.M., Coulter, E.D., Neidle, E.L., and Kurtz, D.M., Jr. To be submitted to *J. Bacteriol.***

[3] **Eby, D.M., Beharry, Z.M., Coulter, E.D., Kurtz, D.M., Jr., and Neidle, E.L. (2001) *J. Bacteriol. 183,* 109-118.**

Abstract

The two-component anthranilate 1,2-dioxygenase (AntDO) of *Acinetobacter* sp. strain ADP1 (ADP1), which catalyzes the conversion of anthranilate (2-aminobenzoate) to catechol, was expressed in *E. coli* and purified to homogeneity. The terminal oxygenase component (AntAB) formed a $\alpha_3\beta_3$ hexamer of 54- and 19-kDa subunits and was found to contain one Rieske-type [2Fe-2S] cluster and one mononuclear nonheme iron center per α subunit. The recombinant reductase component (AntC), which transfers electrons from NADH to the oxygenase component, contains approximately one FAD and one ferredoxin-type [2Fe-2S] center per 39-kDa monomer. Activities of the combined components were measured as quantities of NADH and O_2 consumed. Anthranilate conversion to catechol was found to be stoichiometrically coupled to both NADH oxidation and O_2 consumption, while other substituted benzoates were determined to exhibit varying degrees of uncoupling. A variant of anthranilate 1,2-dioxygenase, previously shown to exhibit temperature sensitivity in vivo allowing growth of ADP1 at 23 °C but not at 39 °C (*1*), was constructed, purified and shown to be unable to hydroxylate anthranilate in vitro at either temperature. Previous studies have determined that in ADP1, AntDO is unable to substitute for a defective benzoate 1,2-dioxygenase (BenDO) from the same organism and vice versa (*1*). However, results presented herein show, at least in vitro, that anthranilate and benzoate are good, coupled substrates for AntDO, generating the respective in vivo dihydroxylation products, catechol and the non-aromatic *cis*-1,2-benzoate diol.

Introduction

More than three dozen Rieske dioxygenases (RDOs) operating on a wide range of aromatic substrates have been identified, isolated and characterized from several species of soil bacteria (*2*-*5*). These enzymes catalyze reaction 3.1:

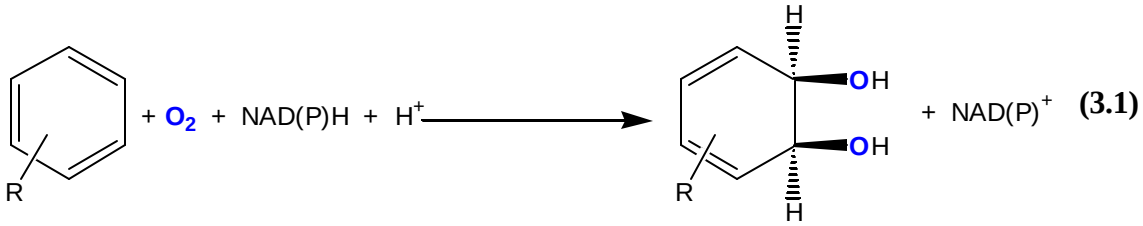

(3.1)

RDOs have typically been isolated following their induction by xenobiotic compounds, whose relationships to preexisting microbial metabolic pathways are usually unclear.

In the early 1960's, it was discovered that crude cell extracts of some *Pseudomonas* species possessed the ability to convert anthranilate (2-aminobenzoate) to catechol via insertion of both atoms of O_2 into the aromatic ring (*6*-*9*). Partial purification of this activity yielded crude preparations of an anthranilate 1,2-dioxygenase (AntDO) (*8*). AntDO was, in fact, one of the first dioxygenase activities of any type to be described. In contrast to most other known RDOs, a connection between AntDO activity and a known metabolic pathway, namely, tryptophan dissimilation, was established many years ago (*10*-*14*). Tryptophan is metabolized via the β-ketoadipate pathway in a strain of *Acinetobacter*, as shown in Figure 3.1 (*13*). Mutants blocked in the ability to metabolize catechol were unable to grow on tryptophan. Similarly, various strains of *Pseudomonas* were shown to metabolize tryptophan via catechol (*10*-*12*). Despite this long history and its metabolic importance, no further characterization of AntDO beyond the early studies cited above has been reported.

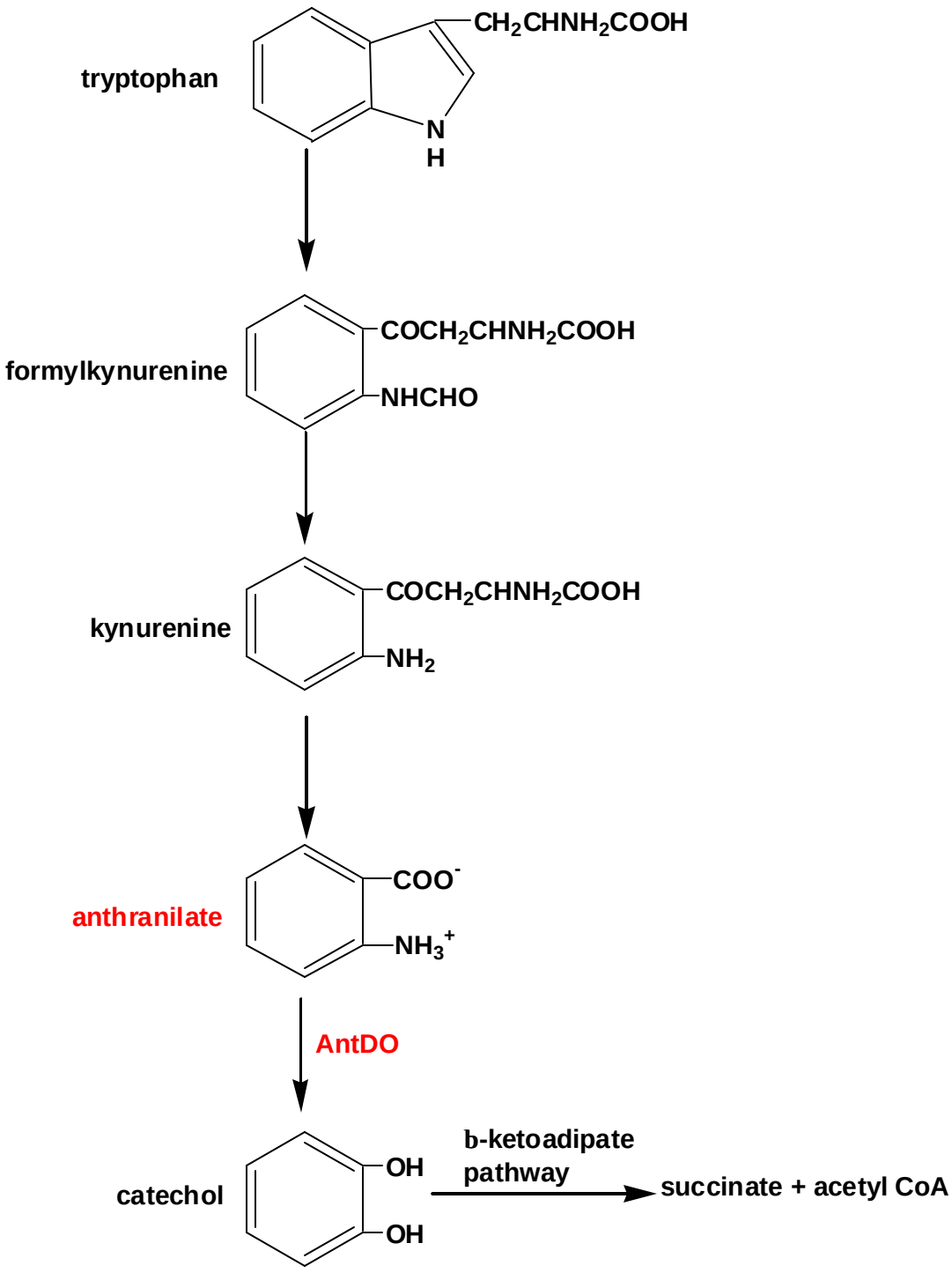

Figure 3.1. Degradation of tryptophan via the β-ketoadipate pathway in *Acinetobacter* (*13*).

The subsequently established components of and reaction catalyzed by AntDO are diagrammed in Figure 3.2. Until recently, the genes encoding AntDO, *antABC* (*antAB*, oxygenase; *antC*, reductase), were known from only one organism, namely the soil bacterium *Acinetobacter* sp. strain ADP1 (ADP1). These three genes are probably co-transcribed and expression of AntA is inducible by anthranilate (Figure 3.3) (*1*). A mutant strain capable of growing on anthranilate at 23 °C but not at 39 °C was used to conclusively identify the *antABC* genes on the ADP1 chromosome (*1*). The temperature sensitivity of this mutant strain was attributed to a point mutation in *antA*, resulting in substitution of a lysine for methionine 43 (M43K AntA). The deduced amino acid sequences of AntA, AntB, and AntC are homologous to those of the class I multicomponent RDOs (*2-5*). Sequence alignments with better characterized RDOs showed conservation of amino acids known to furnish ligands to the mononuclear and Rieske [2Fe-2S] sites of RDO oxygenase components corresponding to AntA (cf. Figure 1.10) and ligands to the [2Fe-2S] center of RDO reductase components corresponding to AntC. Recently, sequence homologies have identified AntDO genes in various strains of *Pseudomonas* (*15-17*), and these putative AntDOs have been implicated in the degradation of carbazole (Figure 3.4), a heterocyclic aromatic compound derived from coal tar and shale oil. Plasmid-borne ADP1 AntDO genes had been expressed in *E. coli* and the resulting cultures gained the ability to convert anthranilate to catechol (*1*). However, until the work described here, no AntDO had been purified (*15*).

The genes encoding AntDO from ADP1, *antABC*, and BenDO, *benABC*, the latter encoding benzoate 1,2-dioxygenase (BenDO) from the same organism, share a high

Figure 3.2. Degradation of anthranilate and benzoate in *Acinetobacter* sp. strain ADP1 via catechol and the β-ketoadipate pathway. Relevant compounds and the roles of AntDO and BenDO are indicated (*1*, *18*).

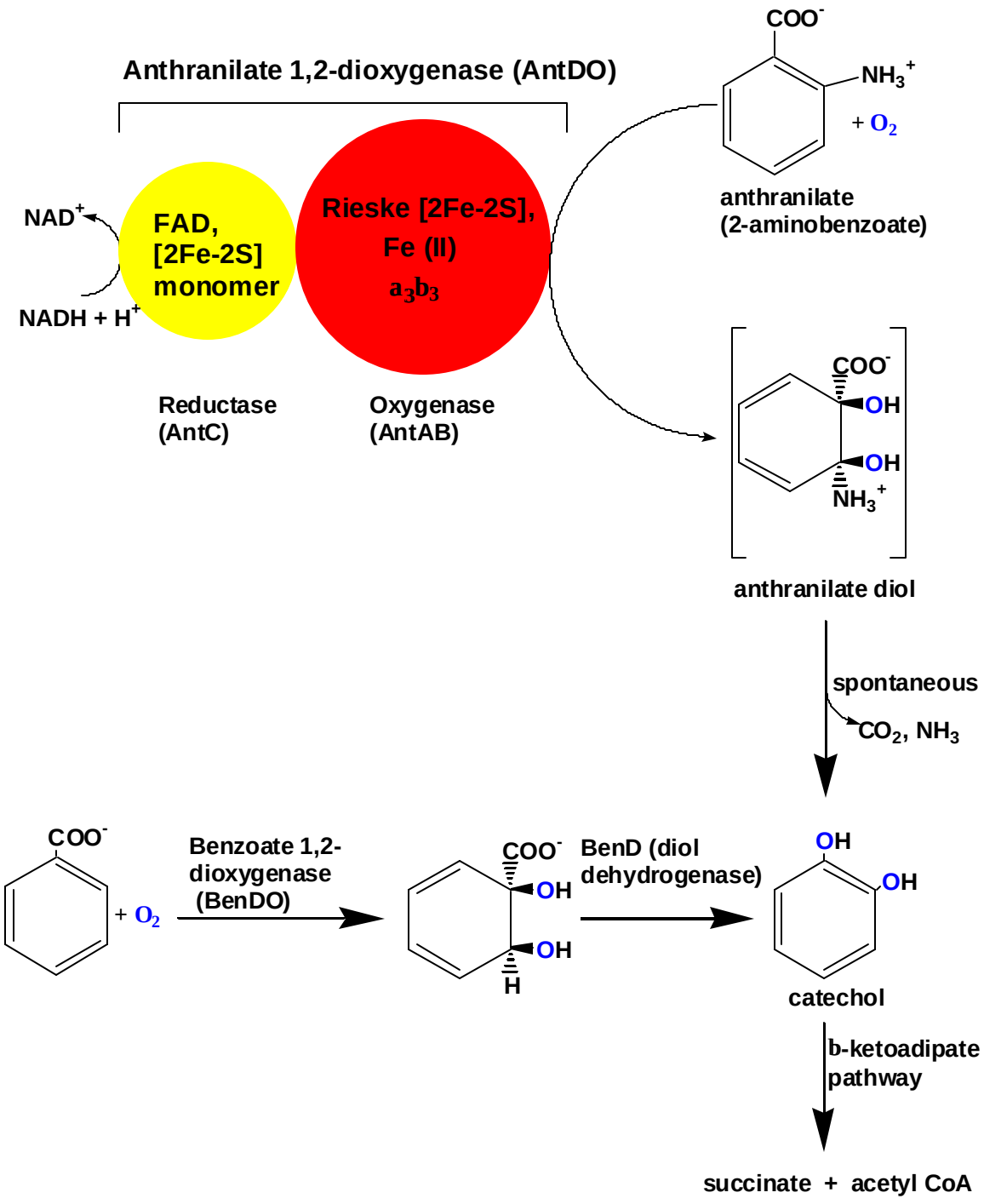
Anthranilate 1,2-dioxygenase (AntDO)
NAD+
NADH + H+
FAD, [2Fe-2S] monomer
Rieske [2Fe-2S], Fe (II)
a3b3
Reductase (AntC)
Oxygenase (AntAB)
COO-
NH3+
+ O2
anthranilate (2-aminobenzoate)
COO-
OH
OH
NH3+
anthranilate diol
spontaneous
CO2, NH3
COO-
+ O2
Benzoate 1,2-dioxygenase (BenDO)
COO-
OH
OH
H
BenD (diol dehydrogenase)
OH
OH
catechol
b-ketoadipate pathway
succinate + acetyl CoA

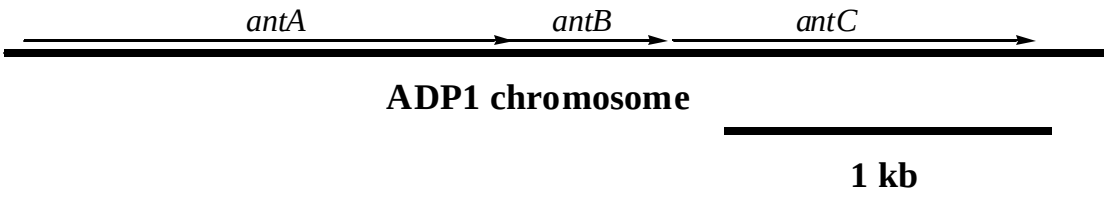

Figure 3.3. Organization of the genes involved in anthranilate degradation in *Acinetobacter* sp. strain ADP1 (*1*).

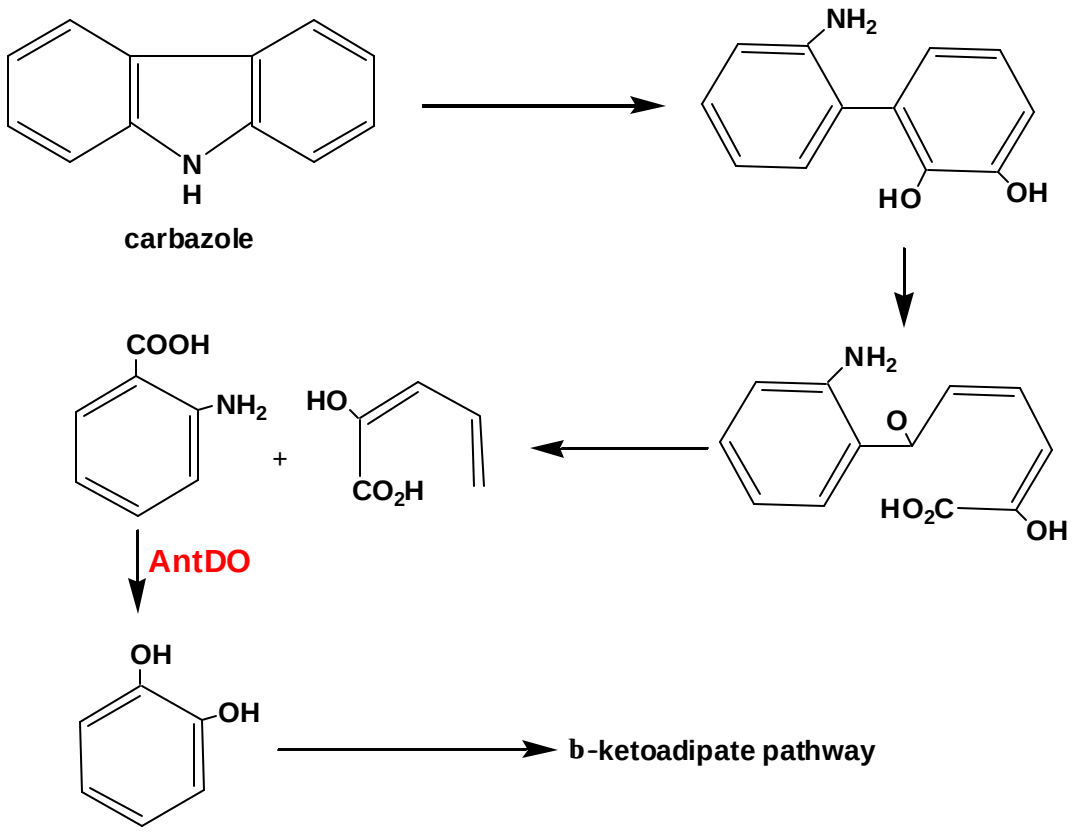

Figure 3.4. Degradation of carbazole in *Pseudomonas* sp. strain CA10 (*15*).

degree of sequence homology (65% and 59% similarity for the alpha and beta subunits, respectively, of the oxygenase components, and 61% similarity for the reductase components) indicating a common evolutionary origin for both sets of genes (*1*). From metabolic studies (*1, 18*), it was established that, whereas dihydroxylation of benzoate yields a stable non-aromatic *cis* diol, dihydroxylation of anthranilate results in spontaneous conversion to catechol by loss of ammonia and carbon dioxide (cf. Figure 3.2). Furthermore, the benzoate and anthranilate degradative pathways utilizing these RDOs converge at catechol. It has been demonstrated that regulatory and catabolic mutants of ADP1 in which either the *ant* or *ben* genes were disrupted lost the ability to utilize anthranilate or benzoate, respectively (*1, 18, 19*). This suggests that in vivo AntDO and BenDO act efficiently only on anthranilate and benzoate, respectively, despite the similar chemical structures of these substrates and the sequence homology noted above. The mutant strain of ADP1 used to isolate *antABC* contained a point mutation in the 43rd codon of *antA* resulting in the substitution of lysine for methionine in AntA (*1*). This strain could grow on anthranilate at 23 °C but not at 39 °C (*1*). Disruption of *antC* in this temperature sensitive strain resulted in a strain that could still grow on anthranilate, suggesting that another RDO reductase could substitute for AntC (*1*). Disruption of *antC* and *benC* together eliminated growth on anthranilate indicating that BenC, the reductase component of BenDO, was most likely substituting for AntC (*1*). Expression of the *ben* genes is regulated by the transcriptional regulator, BenM. Disruption of *antC* along with *benM* also resulted in a mutant strain of ADP1 no longer able to grow on anthranilate (*1*). It was, therefore, inferred that BenC substitution for AntC required the expression of BenC in the presence of anthranilate, although it is

known that expression of the *ben* operon is inducible. A low level of constitutive expression of BenC was suggested to allow formation of sufficient catechol to induce BenM-activated *ben* gene expression. Since *benAB* is co-transcribed with *benC*, it was reasoned that there should also be some low-level expression of BenAB. Assuming some low-level expression of BenAB in the presence of anthranilate, the M43K variant of AntA resulting in a mutant strain of ADP1 no longer able to grow on anthranilate at 39 °C, implied that BenAB (the oxygenase component of BenDO) could not substitute for a defective AntA.

This chapter describes the expression in *E. coli* and isolation of the components of recombinant AntDO from *Acinetobacter* sp. strain ADP1. The potentially temperature sensitive variant of the oxygenase component, M43K AntAB, was generated using site-directed mutagenesis and was also purified to homogeneity. The results of biochemical and spectroscopic characterizations of the recombinant AntDO and M43K AntDO and investigations into the substrate preference of AntDO for various aromatic carboxylic acids are presented. The in vitro reactivity of AntDO and BenDO with anthranilate and benzoate as substrates are compared with each other and to in vivo studies of the degradation of these two aromatic compounds in ADP1.

Experimental

Reagents and general procedures

Substrates were purchased from Sigma. Enzymatically produced 1*R*,2*S*-1,2-dihydroxycyclohexa-3,5-diene carboxylate (benzoate diol) was graciously provided by Dr. Albey M. Reiner (Univ. of Massachusetts, Amherst). Other reagents were the highest

commercially available grade. Restriction enzymes and polymerases were purchased from either Promega, Inc. or New England Biolabs, Inc. Oligonucleotides were synthesized by Integrated DNA Technologies. Nucleotide sequencing was carried out at the University of Georgia Molecular Genetics Instrumentation Facility (ABI373 sequencer, Applied Biosystems, Inc). Molecular biology procedures not described in detail below followed those in Sambrook et al. (*20*). All plasmid-bearing *E. coli* strains were cultured in Luria-Bertani medium containing 100 μg/mL ampicillin. Purity of proteins was judged by SDS-PAGE (12.5% polyacrylamide gels) with Coomassie blue staining (*21*).

Plasmids for high-level expression of the ADP1 *antABC* genes in *Escherichia coli*

The *antAB* (1912-bp) and *antC* (1031-bp) genes from *Acinetobacter* sp. strain ADP1, on plasmid pBAC103 (*1*), were PCR-amplified with *Pfu* polymerase (Stratagene) and the primers*:* ANTAnde, 5′ ggacttcatATGACTGCACGTAACCTCGC-3′ and ANTBtaa, 5′-ataatagctcttccgcaTTAGACGTGATAGAAATCGAGTAC-3′ for amplification of *antAB* or with primers ANTCnde, 5′-ggggaccatATGAATCATTCTGTTGCACTCAA-3′ and ANTCtaa, 5′-attatagctcttccgcATTAAGTTTTTGCGGTATTACTTTG-3′ for amplification of *antC*. In these primers, sequences duplicating those at the 5′ end of *antA* or *antC* and the 3′ end of *antB* or *antC*, respectively, are capitalized and added *Nde*I and *Sap*I restriction sites, respectively, underlined. The purified PCR products were ligated into the multiple cloning sites of pCYB1 (New England Biolabs) to yield plasmids pBAC209 (*antAB*) and pBAC208 (*antC*). These plasmids place the *antAB* and *antC* genes under the control of the lactose-inducible P_{tac} promoter. Nucleotide sequencing confirmed that the plasmid-

borne *ant* regions were wild type (duplicating sequences deposited in Genbank, accession number AF071556).

Construction of M43K *antA*

An *antA* gene encoding a change from methionine to lysine at residue 43 was constructed using the QuikChange Site Directed Mutagenesis kit (Stratagene). Plasmid pBAC209 was used as the template with the complementary mutagenic oligonucleotide primers, 5´-TTTGAACTTGAAAAAGAACTCATTTTTG-3´, and 5´-CAAAAATGAGTTCTTTTTCAAGTTCAAA-3´ (with mutational codon underlined). Incorporation of M43K into the *antAB* sequence of the resulting plasmid, pDMK3, was verified by nucleotide sequencing.

Expression of AntAB, AntC and M43K AntAB in *E. coli* and preparation of cell-free extract

One-liter cultures of *E. coli* strains DH5α (Gibco BRL) carrying the recombinant *antC* (pBAC208) or BL21Gold (Stratagene) carrying the recombinant *antAB* (pBAC209), or M43K AntAB (pDMK3) plasmids were grown aerobically in Luria-Bertani (LB) medium in an incubator/shaker at 37 ºC until OD_{600} ~0.6. The temperature was then reduced to 30 ºC and isopropyl α-D-thiogalactopyranoside (100 μg/mL) was added to induce expression of the plasmid-borne *ant* genes. After ~5 hrs incubation at 30 ºC, cells were harvested by centrifugation (5,000g, 5 min, 4 ºC). Due to the previously observed temperature sensitivity of M43K AntAB, cells harboring pDMK3 were grown at 23°C using an otherwise identical procedure to that described for the wild type AntAB. Approximately 40 g of cells collected from six 1-L *E. coli* cultures were resuspended in 50 mL of 25 mM MOPS pH 7.3 (buffer A) and sonicated on ice using a Branson sonifier

cell disrupter 350 with a 0.5-inch probe tip for 2 min at 30-sec intervals at 20 kHz. Cell debris was removed by centrifugation (12,000g, 30 min, 4 ºC) resulting in either red-brown or yellow-orange supernatants from cells containing AntAB or AntC, respectively. These preparations are referred to as 6 x 1-L cell-free extracts and were used immediately.

Purification of AntAB

The procedure described below was used both for wild type and M43K AntAB. All steps were carried out at 4 ºC on the 6 x 1-L cell-free extracts. Column fractions containing AntAB or M43K AntAB were easily visualized by their red-brown color. The cell-free extract was applied to a 3 x 15-cm Q Sepharose FF anion-exchange column (Amersham Pharmacia Biotech) equilibrated in buffer A. The column was washed with 200 mL of buffer A and AntAB was eluted with a step gradient of NaCl (0-400 mM) in buffer A. Fractions containing AntAB were pooled, desalted and concentrated by ultrafiltration to ~2 mL (Amicon YM10 membrane). The concentrated AntAB was applied to a 2 x 8-cm Mono Q anion-exchange column (Amersham Pharmacia Biotech) equilibrated in buffer A. The column was washed with 50 mL of buffer A and bound AntAB was eluted with a 250-mL linear gradient of NaCl (0-1 M) in buffer A. Fractions containing AntAB were pooled and concentrated by ultrafiltration to ~2 mL and applied to a HiPrep 16/60 Sephacryl S300 size-exclusion column (Amersham Pharmacia Biotech) equilibrated in buffer A containing 250 mM NaCl. The column was eluted at a flow rate of 0.5 mL/min. The fractions containing AntAB were pooled and concentrated by ultrafiltration to ~2 mL and stored at –80 ºC in 100 µL aliquots. Approximately 15 mg of purified AntAB or 6 mg of M43K AntAB was obtained per liter of *E. coli* culture.

Purification of AntC

This purification was carried out at 4 ºC under low light conditions to minimize loss of flavin. The 6 x 1-L cell-free extract from *E. coli* DH5$_\alpha$[pBAC208] (30 mL) was applied to the same Q Sepharose FF anion-exchange column used for AntAB purification, and the column was washed with 200 mL of buffer A. Bound AntC was eluted with a 250-mL linear gradient of NaCl (0-250 mM) in buffer A at 2.0 mL/min. Active fractions (assayed as described below) were pooled and concentrated by ultrafiltration (Amicon YM10 membrane) to 10 mL. Filtered 4 M $(NH_4)_2SO_4$ was added to a final concentration of 1 M. The precipitate was removed by centrifugation (12,000g, 15 min, 4 °C), and the supernatant, containing AntC was applied to a Butyl Sepharose column (2 cm X 11.5 cm, Amersham Pharmacia Biotech) equilibrated in buffer A containing 1 M ammonium sulfate. AntC was eluted with a linear gradient of decreasing ammonium sulfate (0-1 M). Fractions containing AntC were pooled and concentrated by ultrafiltration to 10 mL and equilibrated in 50 mM MOPS, pH 7.0. Samples were dialyzed against the same buffer containing 5 % (v/v) glycerol and 1 mM FAD (4 L x 12 hrs). The sample was concentrated by ultrafiltration, applied to a Sephacryl S100 column (1.6 cm X 60 cm, Pharmacia) equilibrated in buffer A containing 200 mM NaCl, and eluted at a flow rate of 0.5 mL/min. Purified AntC (~10 mg per liter of *E. coli* culture) was concentrated by ultrafiltration to ~2 mL and stored at -80 ºC in 100 µL aliquots.

Analyses

Protein was quantitated by the method of Bradford (*22*) using bovine serum albumin as the standard (Bio-Rad). The native molecular weights of AntAB, AntC and M43K AntAB were determined by gel filtration using a calibrated Sephacryl S300

column (1.6 cm X 60 cm, flow rate 0.5 mL/min, Amersham Pharmacia Biotech) equilibrated in 50 mM HEPES (pH 7.3) containing 100 mM NaCl. The calibration proteins were horse spleen ferritin (M_r 450,000), bovine catalase (M_r 240,000), aldolase (M_r 158,000), bovine serum albumin (M_r 68,000), hen egg albumin (M_r 45,000), chymotrypsinogen A (M_r 25,000) and horse heart cytochrome *c* (M_r 12,500). The molecular weights of enzyme subunits were determined under denaturing conditions using SDS-PAGE (*21*). Iron content was determined with a colorimetric ferrozine method based on that of Batie et al (*23*) (as described below) or by inductively coupled plasma atomic emission (ICP-AE) spectrometry at the University of Georgia Chemical Analysis Facility. For the ferrozine method, a 200-µl protein sample (approximately 10 µM AntAB hexamer or AntC monomer) was added to an eppendorf tube containing 250 µl 0.02% ascorbic acid, 30 µl 6 M HCl and 25 µl of a 5 mg/mL solution of ferrozine. The sample was mixed by vortexing and 1 mL of 8 M guanidine-HCl was added. Saturated ammonium acetate (200 µl) was added and A_{562} was measured. A standard curve was prepared using a ferrous ammonium sulfate solution, and the molar absorption coefficient was determined to be 28,000 $M^{-1}cm^{-1}$ for the ferrous iron-ferrozine complex (*23*). The same concentrations of proteins were also submitted for ICP-AE in 1 mL. The flavin cofactor was extracted by boiling a 50-µM (1 mL) sample of the purified AntC for 10 min. Precipitated protein was removed by centrifugation. Flavin was identified by thin-layer chromatography, with silica gel-coated glass plates, using a mobile phase of butanol: acetic acid: water (4:1:4 volume ratio), and samples were visualized with a hand-held UV light. Commercially obtained FAD and flavin mononucleotide were used as standards. After its identification as FAD, the amount of flavin present in the supernatant

of the boiled AntC sample was determined spectrophotometrically using ε_{450}=11,300 $M^{-1}cm^{-1}$ and ε_{375}=9,300 $M^{-1}cm^{-1}$ (*24*).

Oxygen consumption and NADH oxidation assays for AntDO

Substrate-dependent O_2 consumption catalyzed by AntDO was monitored with a Yellow Springs Instruments Model 5300 biological oxygen monitor equipped with a Clark electrode. NADH oxidation was determined spectrophotometrically by measuring the decrease in A_{340} (ε_{340} = 6.22 $mM^{-1}cm^{-1}$). Unless stated otherwise, assays were carried out in 50 mM MES (pH 6.3), 100 mM KCl, 0.5 mM substrate, 100 μM NADH, 0.5 μM purified AntAB ($\alpha_3\beta_3$) and 0.18 μM AntC in a final volume of 1 mL for NADH oxidation assays or 2 mL for O_2 consumption assays in air-saturated buffer at 23 °C. All rates were corrected for small background NADH oxidation or O_2 consumption in the absence of substrate. In spectrophotometric assays, corrections were made for the absorbance of aromatic substrates (anthranilate, ε_{340} = 1050 M^{-1} cm^{-1} and *m*-aminobenzoate, ε_{340} = 1300 $M^{-1}cm^{-1}$ (*25*)), assuming a constant rate of consumption of substrate equal to that of NADH consumption. Reactions were monitored for 5 min, at which point 1000 U bovine liver catalase (Sigma) was added to those assays monitoring O_2 consumption in the oxygraph. The amount of O_2 generated in response to catalase from H_2O_2 present in the mixture was measured with the oxygen electrode. Activities are reported as the concentration of NADH consumed/ 5 min.

NADH-cytochrome *c* reductase activity of AntC

AntC activity was measured as the reduction of cytochrome *c* in the presence of NADH by the increase in A_{550} (ε_{550} = 19,500 $M^{-1}cm^{-1}$ for reduced minus oxidized cytochrome *c* (*26*)). The assay mixture contained 20 μM oxidized cytochrome *c* (horse

heart type 6, Sigma), 100 μM NADH, 0.5 μM pure AntC (or a suitable amount of a crude enzyme preparation) in 100 mM potassium phosphate buffer, pH 7.

Optimization of AntDO Activity

A mixed buffer system was used to determine the optimal pH for assaying AntDO activity. This buffer system contained 50 mM total of equimolar amounts of the following six Good's buffers: MES (pK_a 6.1), MOPS (pK_a 7.2), HEPES (pK_a 7.5), N-tris(hydroxmethyl) ethyl-3-aminopropanesulfonic acid (pK_a 8.4), 2-(N-cyclohexylamino) ethanesulfonic acid (pK_a 9.3), and 3-(cyclo-hexylamino)-1-propanesulfonic acid (pK_a 10.4). The pH was adjusted using 12 M HCl or 10 M NaOH. Individual NADH oxidation assays were carried out at pH 5.5, 6.0, 6.5, 7.0, 8.0, and 9.0, using the assay conditions described above. After determining the optimal pH, assays were repeated in 50 mM MES buffer at pH 6.3 at four different ionic strengths (0, 50, 100, or 150 mM KCl).

HPLC monitoring of substrate consumption and product formation in AntDO reactions

Samples from AntDO-catalyzed reactions (100 μL) were applied to an HPLC (Bio-Rad automatic sampling system model AS-100, solvent delivery system 2800, detector uv-1806, and peak integration software) by D. Matthew Eby in the Department of Microbiology, University of Georgia. Compounds were eluted at a rate of 0.8 mL/min from a reverse-phase C_{18} column (Columbus 5 μm, 250 X 4.6 mm) with a mobile phase of 30 % (v:v) acetonitrile:water containing 0.1 % phosphoric acid. The eluate was monitored by absorbance at 210 nm. The concentrations and identities of substrates and products were determined by comparison with known standards.

Detection of catechol and diol products

Diol products were detected by monitoring the increase at A_{340} (ε_{340}, 6.22 $mM^{-1}cm^{-1}$) due to the diol-dependent BenD reduction of NAD^+ (cf. Figure 2.5). BenD is the *cis*-1,2-benzoate diol dehydrogenase that converts this diol to catechol. Recombinant *Acinetobacter* sp. strain ADP1 BenD was purified as described in Chapter 2. Following NADH oxidation reactions as described above, BenD (5 μM) and NAD^+ (0.2 mM) were added and the increase at A_{340} was monitored for 2 min. Catechol products were detected using Gibbs' reagent (2,6-dichloroquinone-4-chloroimide) (Figure 3.5) (*27, 28*). Following NADH oxidation reactions, aliquots (~200 μL) were removed and Gibbs' reagent (15 μL of a 2 % (w/v) solution in ethanol) was added and the reaction was incubated at room temperature for 1 hr. Positive reactions were identified by the formation of a blue to purple color. Substrates whose products were not positive either in BenD reactions or using Gibbs' reagent were further treated as follows. Aliquots (~200 μL) from NADH oxidation reactions were acidified with 0.1 M HCl (100 μL) and incubated at 37°C for 30 min to allow conversion of diol products to phenols. The pH was raised by the addition of 0.5 M Tris-HCl pH 8.5 (40 μL) and Gibbs' reagent (15 μL of a 2 % (w/v) solution in ethanol) was added and the reaction was incubated at room temperature for 1 hr.

Spectroscopy

EPR spectra were recorded on a Bruker ESP-300E spectrometer equipped with an ER-4116 dual-mode cavity and an Oxford Instrument ESR-9 flow cryostat. Ultraviolet-visible absorption spectra were obtained in 1-cm pathlength quartz cuvettes on a Shimadzu UV2101-PC scanning spectrophotometer. To obtain absorption spectra of

reduced [2Fe-2S] centers, oxidized proteins (250 μM) were reduced by anaerobic addition of an excess of sodium dithionite. Other conditions are listed in the figure legends.

Results

Purification of AntDO

Purification of ADP1 AntDO from *E. coli*, a bacterium whose genome contains no known AntDO genes or activity, was accomplished using plasmids containing either the ADP1 *antAB* genes or the *antC* gene that express the corresponding oxygenase or reductase components independently. The oxygenase and reductase components were each purified to homogeneity by anion-exchange chromatography, ammonium sulfate fractionation, hydrophobic interaction chromatography and size-exclusion chromatography. A curious qualitative observation was that, when anthranilate and excess ferrous iron were added to the 1-L *E. coli* cultures during expression of AntAB, the medium gradually turned a dark purple color that was identical to the color produced when catechol and iron were added to LB with no bacterial inoculation. Apparently, the expressed recombinant AntAB is able to use an endogenous source of electrons in *E. coli* to catalyze conversion of anthranilate to catechol even in the absence of AntC. This color development, which is presumably due to formation of a ferric-catechol/quinone complex, served as a convenient visual indicator of expression of active AntAB. No such color development occurred if anthranilate was omitted or if anthranilate and ferrous iron were added to uninoculated LB.

The *antA* and *antB* genes are adjacent to each other on the ADP1 chromosome (*1*). Co-expression of these *antAB* genes in *E. coli* yielded high levels of two proteins

that corresponded in size to the deduced amino acid sequences of the α (54 kDa) and β (19 kDa) subunits, respectively, of AntDO (Figure 3.6). Size-exclusion chromatography of the pure AntAB revealed a single oligomer of approximately 220 kDa, consistent with a hexameric $\alpha_3\beta_3$ subunit composition (Table 3.1). Using the extinction coefficient determined at 454 nm, 6 x 1-L culture of *E. coli* containing the *antAB* plasmid yielded approximately 90 mg of pure AntAB. Due to the previously observed temperature dependence, M43K AntAB was expressed at 23 °C in an effort to obtain active protein. The addition of anthranilate and ferrous iron to cultures expressing M43K AntAB did not show the color change indicative of catechol formation at either 23 °C or 37 °C. Regardless, M43K AntAB was purified by analogous procedures to wild type AntAB and found to contain two subunits of the same size as for the wild type protein. SDS-PAGE analysis of the cell-free extract showed the presence of more AntB relative to M43K AntA. Furthermore, SDS-PAGE of the pellet demonstrated that a significant amount of M43K AntA was insoluble (Figure 3.6). Nevertheless, the M43K AntAB purified from the cell-free extract (40 mg) migrated identically to the wild type enzyme on the same size-exclusion column and was, therefore, also inferred to be a $\alpha_3\beta_3$ hexamer.

Independent expression of *antC* in *E. coli* resulted in abundant production of a protein of the predicted size for AntC. Initial attempts to isolate and purify AntC resulted in loss of flavin, a process that was visually evident during column chromatography as a yellow-colored fraction eluting prior to the AntC protein. By minimizing its exposure to light during purification, AntC could be purified with retention of the majority of its flavin (Table 3.1). SDS-PAGE and gel filtration indicated that purified AntC was a monomer of 39 kDa (Table 3.1, Figure 3.6). Approximately 75 mg of pure AntC was

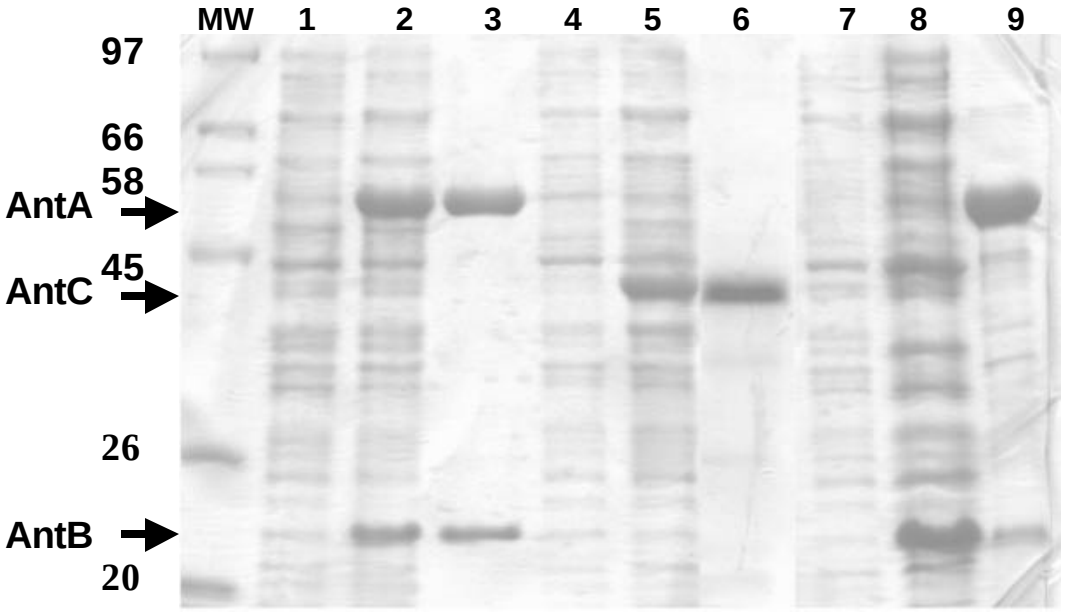

Figure 3.6. SDS-PAGE of the expression and purification of recombinant ADP1 AntAB, AntC, and M43K AntAB. Lanes 1,4,7: whole cells from uninduced *E. coli* cultures harboring pBAC209 (AntAB), pBAC208 (AntC), and pDMK3 (M43K AntAB), respectively. Lanes 2,5,8: induced whole cells from *E. coli* cultures harboring pBAC209, pBAC208, and pDMK3, respectively. Lanes 3 and 6, purified AntAB and AntC, respectively. Lane 9, pellet of M43K AntAB following sonication and centrifugation. Numbers at left correspond to molecular masses (kDa) of the adjacent molecular weight markers (lane MW).

Table 3.1. Molecular and spectroscopic properties of recombinant *Acinetobacter* sp. ADP1 AntDO.

Component	molecular weight (M_r): calc'd from sequence	SDS-PAGE	gel filtration	iron content (mol/ mol protein)	Flavin content (mol/ mol protein)	UV/vis Absorption $\lambda(\varepsilon)$ (nm, ($mM^{-1}cm^{-1}$))
AntAB	53,936 (A) 19,330 (B)	54,000 (A) 19,000 (B)	220,000	8.8 ± 1[a]	0	320(sh) (31)[a] 454(14.4)[a] 555(sh)(7)[a]
AntC	38,548	39,000	45,000	2.3 ± 0.5	0.7[b], 1.5[c]	330 (25)[c] 370 (23)[c] 450(22)[c] 410,462[d]

[a]Per $\alpha_3\beta_3$ hexamer, as-isolated

[b]As FAD from low-light isolation.

[c]After reconstitution with FAD as described in Experimental.

[d]Low-flavin form; ε not determined

typically obtained from a 6 x 1-L culture of *E. coli* harboring the AntC expression plasmid.

Identification and quantitation of the flavin in AntC

The flavin contained in recombinant AntC was identified as flavin adenine dinucleotide (FAD) by thin layer chromatography using commercially available FAD and flavin mononucleotide as standards. When isolated under low light conditions, AntC contained 0.7 mol FAD per mol of AntC monomer (Table 3.1). The reductase activity of AntC could be increased by dialysis against FAD followed by passage over a Sephadex G-25 column to remove excess FAD. When reconstituted in this fashion, AntC contained 1.5 mol FAD per mol AntC (Table 3.1). Further additions of FAD did not increase AntC activity in the assays used in this work. The AntC isolated in normal room light contained less than 4% of the flavin found in the low-light-isolated AntC on a protein basis. The FAD-depleted AntC, when substituted for a comparable amount of the FAD-enriched AntC, showed no detectable catalytic activity in enzymatic assays.

Iron content of AntDO components

AntC was determined to contain 2.3 ± 0.5 mol iron/mol AntC monomer, consistent with the prediction of one [2Fe-2S] center based on sequence homology to BenC (cf. Chapter 2). The iron content of AntAB was determined to be 8.8 ± 1 mol iron/mol protein based on a protein mole weight of 220 kDa (Table 3.1). Considering the $\alpha_3\beta_3$ subunit composition, the iron analysis is consistent with the prediction of one [2Fe-2S] center and one mononuclear center per α subunit, as expected from the amino acid sequence alignment (cf. Figure 1.10) (*2, 29*). The purified M43KA AntAB also contained close to its full complement of iron, 8.1 ± 0.2 mol iron/$\alpha_3\beta_3$.

Spectroscopic properties of AntDO

The visible absorption spectra of oxidized (as-isolated) and dithionite-reduced recombinant AntAB are shown in Figure 3.7 (top panel). The absorption maximum of the oxidized AntAB at 454 nm (ε = 14,400 $M^{-1}cm^{-1}$) and the shoulder at 555 nm are typical of Rieske-type $[2Fe\text{-}2S]^{2+}$ centers (*2, 23, 29, 30*). Furthermore, the absorption spectrum of dithionite-reduced AntAB also resembled those of other reduced (i.e., $[2Fe\text{-}2S]^{+}$) Rieske-type centers (*2, 23, 29, 30*). Also shown in Figure 3.7 (inset) is the visible absorption spectrum of the as-isolated M43K AntAB. The spectrum is consistent with a perturbation, but not destruction of the oxidized Rieske center.

The visible absorption spectra of low-light purified, FAD-enriched AntC (Figure 3.7, bottom panel) and the FAD-depleted AntC isolated under normal room light show that this component contains both FAD and ferredoxin-type $[2Fe\text{-}2S]^{2+}$ centers (*2, 31*). The ratios of absorption intensities at 330 or 370 nm relative to that at 450 nm in the FAD-enriched reductase are somewhat higher than those reported for the reductase component of phthalate 4,5-dioxygenase, which also contains one flavin and one $[2Fe\text{-}2S]^{2+}$ chromophore (*23, 32*). Presumably, the excess of FAD (1.5 mol/mol AntC) is responsible for the altered absorption intensities of AntC.

The 10-K EPR spectra of the dithionite-reduced AntAB and AntC, shown in Figure 3.8, also confirms the presence of the [2Fe-2S] centers with g_{avg} = 1.91 and g_{avg} = 1.97 for AntAB and AntC, respectively, which are typical for Rieske-type $[2Fe\text{-}2S]^{+}$ centers and ferredoxin-type $[2Fe\text{-}2S]^{+}$ centers (*33*).

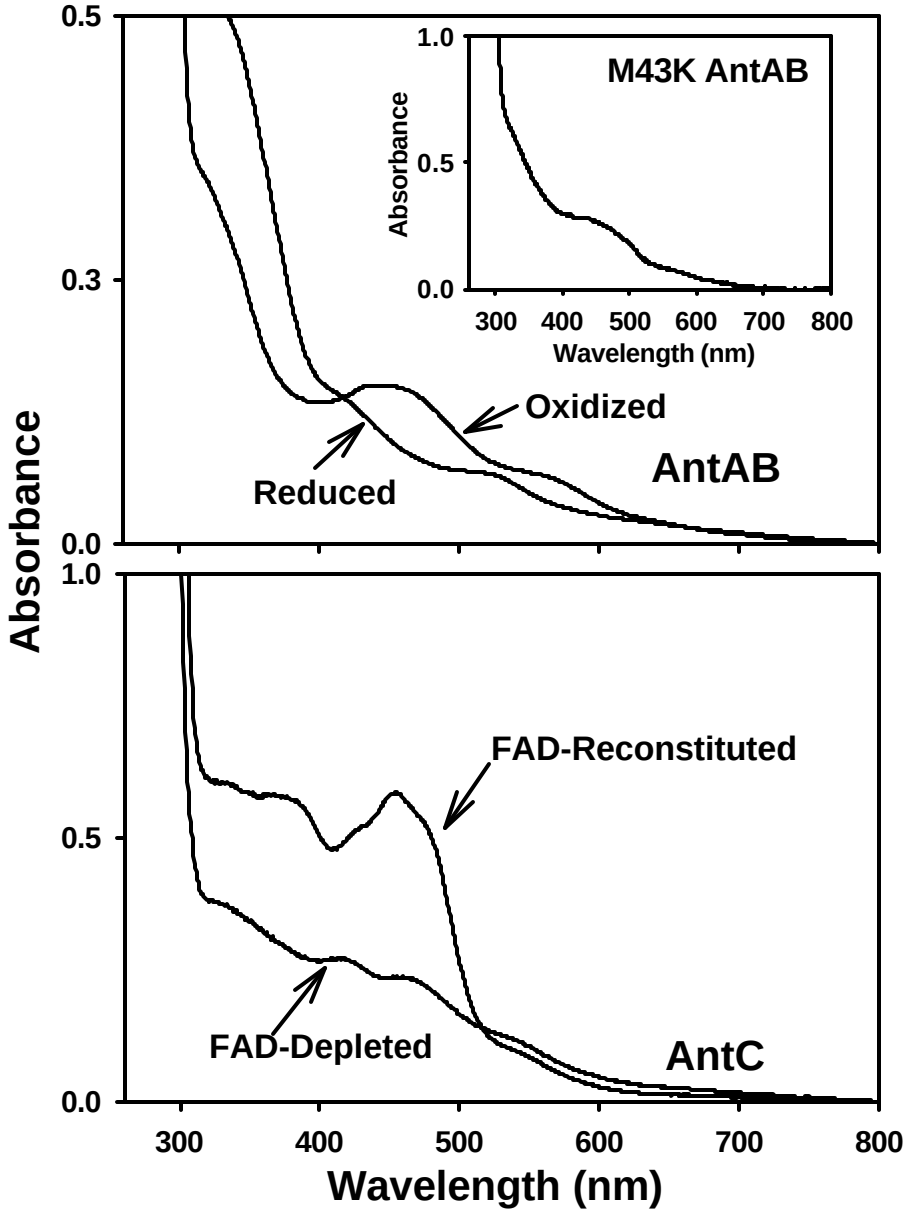

Figure 3.7. UV-visible absorption spectra of (top) oxidized (as-isolated) and dithionite-reduced (0.2 mM) recombinant AntAB (12 μ M $\alpha_3\beta_3$) and oxidized (as-isolated) M43K AntAB (15 μM $\alpha_3\beta_3$) (inset) and (bottom) oxidized (as-isolated) AntC either reconstituted with FAD (FAD-reconstituted) or as-isolated in normal room light (FAD-depleted). All spectra were recorded in buffer A.

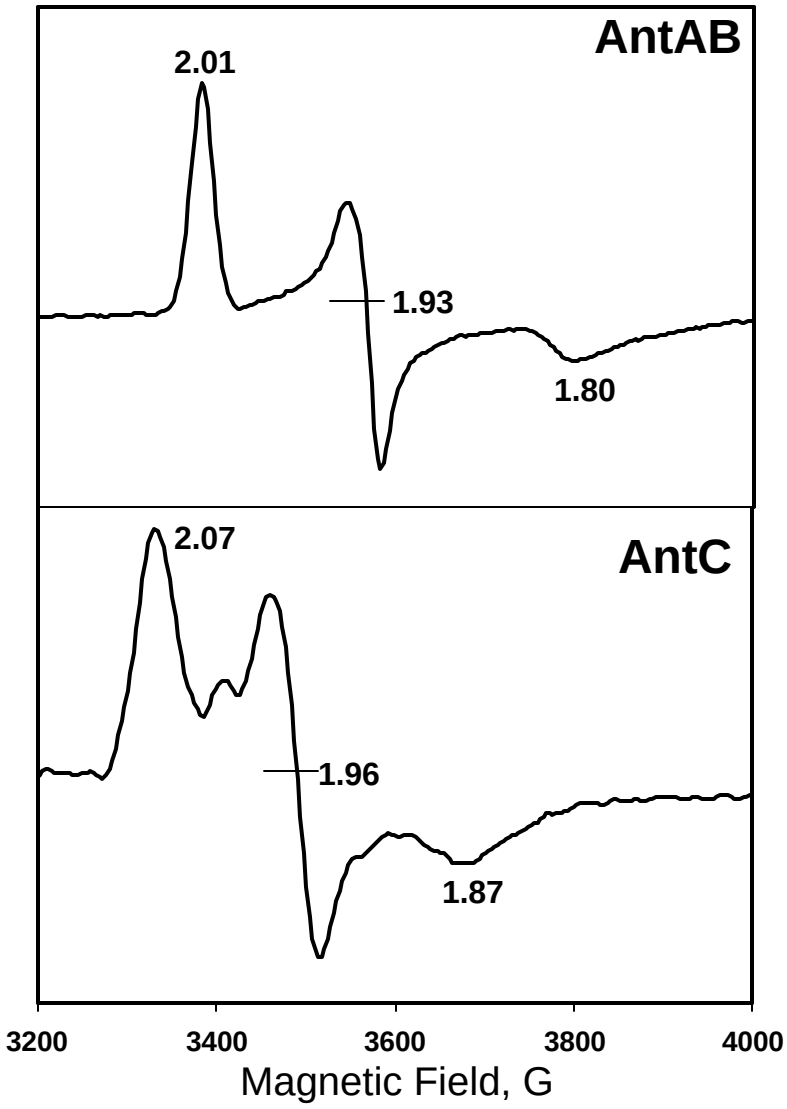

Figure 3.8. EPR spectra of reduced AntAB (top) and AntC (bottom). Purified samples of protein (250 μM in buffer A) were reduced anaerobically with excess sodium dithionite (0.5 mM). Spectra were recorded under the following conditions: temperature, 10 K; microwave frequency, 9.59 GHz; modulation amplitude, 6.366 G; microwave power, 4 mW.

Catalytic properties of AntDO

AntDO activity was most conveniently measured by monitoring anthranilate-dependent consumption of NADH. The optimal conditions of pH and salt concentration for this activity were found to be at pH 6.3 (50 mM MES buffer) and 100 mM KCl. This optimization was performed with saturating NADH, aromatic substrate, and O_2 (typically 100 μM, 0.5 mM, and ~0.25 mM, respectively), 0.5 μM AntAB (hexamer) and 0.18 μM AntC. These reagent concentrations were chosen mostly for convenience in monitoring NADH consumption via absorbance at 340 nm, which was complete after 5 min. Under these conditions (i.e., non-saturating AntC) AntAB oxidized 40 μM NADH/min/μM AntAB hexamer with anthranilate as the substrate. The K_m of AntC for AntAB was determined under the standard assay conditions except with 0.01 μM AntAB and variable amounts of AntC from 0.1 to 2 μM. From a Lineweaver-Burke plot, a K_m for AntC of approximately 2 μM and a turnover number of 3200 min^{-1} were estimated (Figure 3.9). With saturating (2 μM) AntC, 0.01 μM AntAB and 100 μM NADH, the rate of NADH oxidation was linear down to 1 μM anthranilate. The small absorbance change for NADH consumption at ≤ 1 μM anthranilate precluded accurate rate measurements below this concentration. Therefore, the K_m of AntDO for anthranilate was assumed to be <1 μM ($k_{cat}/K_m \geq 1066\ min^{-1}\mu M^{-1}$ per site). The K_m of AntAB for benzoate was determined under standard assay conditions except with 0.01 μM AntAB, 2 μM AntC and variable amounts of benzoate from 10 to 100 μM. From a Lineweaver-Burke plot, a K_m of approximately 12 μM and a turnover number of 1500 min^{-1} (k_{cat}/K_m= 42 $min^{-1}\mu M^{-1}$ per site) were estimated (Figure 3.10).

Figure 3.9. Plot of the initial velocity of NADH oxidation of AntAB and varying concentrations of AntC (top) and the corresponding Lineweaver-Burke plot (bottom). Assay conditions: AntAB (0.01 μM $\alpha_3\beta_3$), AntC (0.1-4 μM), NADH (0.1 mM), anthranilate (0.5 mM) in 50 mM MES containing 100 mM KCl, pH 6.3 at 23 °C.

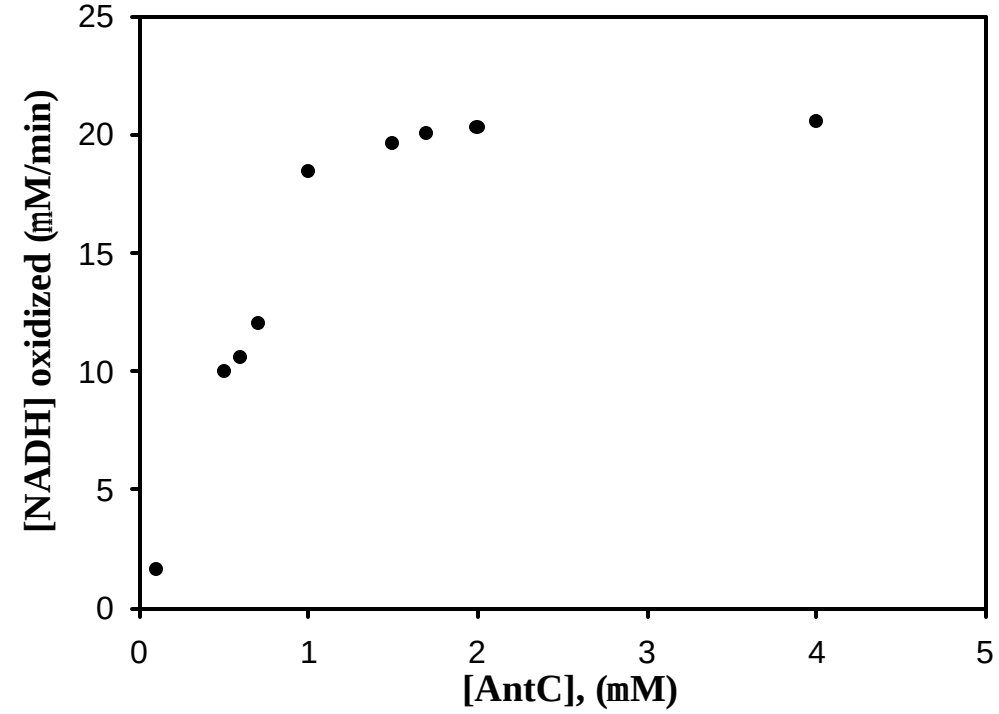
25
20
15
10
5
0
0
1
2
3
4
5
[NADH] oxidized (mM/min)
[AntC], (mM)

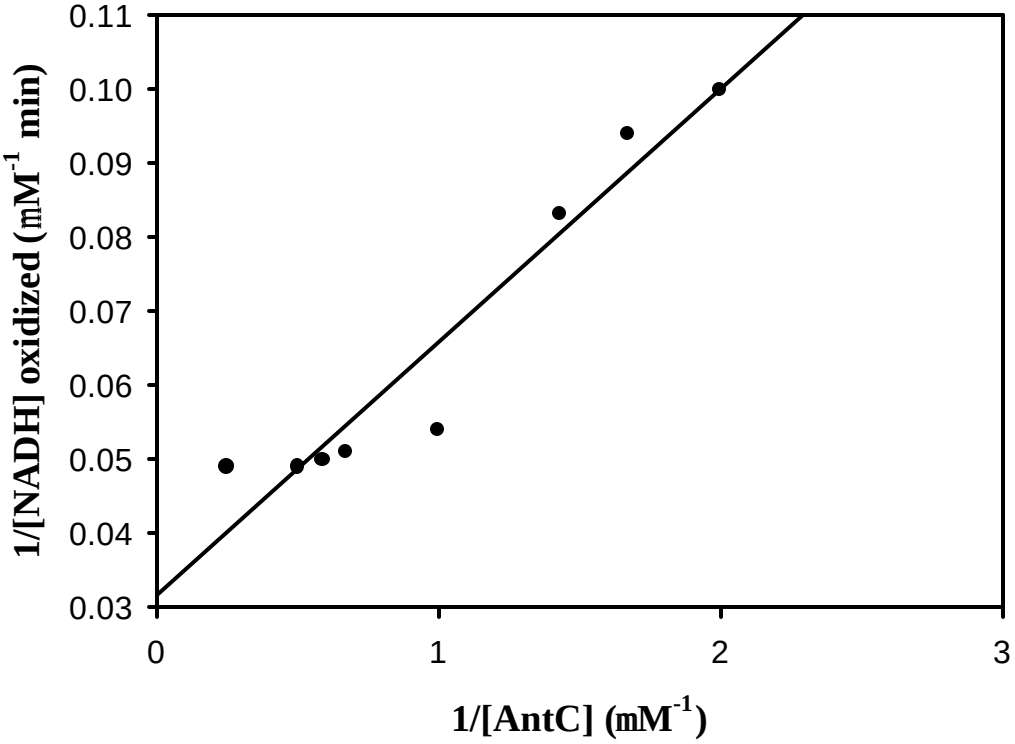
0.11
0.10
0.09
0.08
0.07
0.06
0.05
0.04
0.03
0
1
2
3
1/[NADH] oxidized (mM-1 min)
1/[AntC] (mM-1)

Figure 3.10. Plot of the initial velocity of NADH oxidation of AntDO with varying concentrations of benzoate (top) and the corresponding Lineweaver-Burke plot (bottom). Assay conditions: AntAB (0.01 μM $\alpha_3\beta_3$), AntC (2 μM), NADH (0.1 mM), benzoate (10-100 μM) in 50 mM MES containing 100 mM KCl, pH 6.3 at 23 °C.

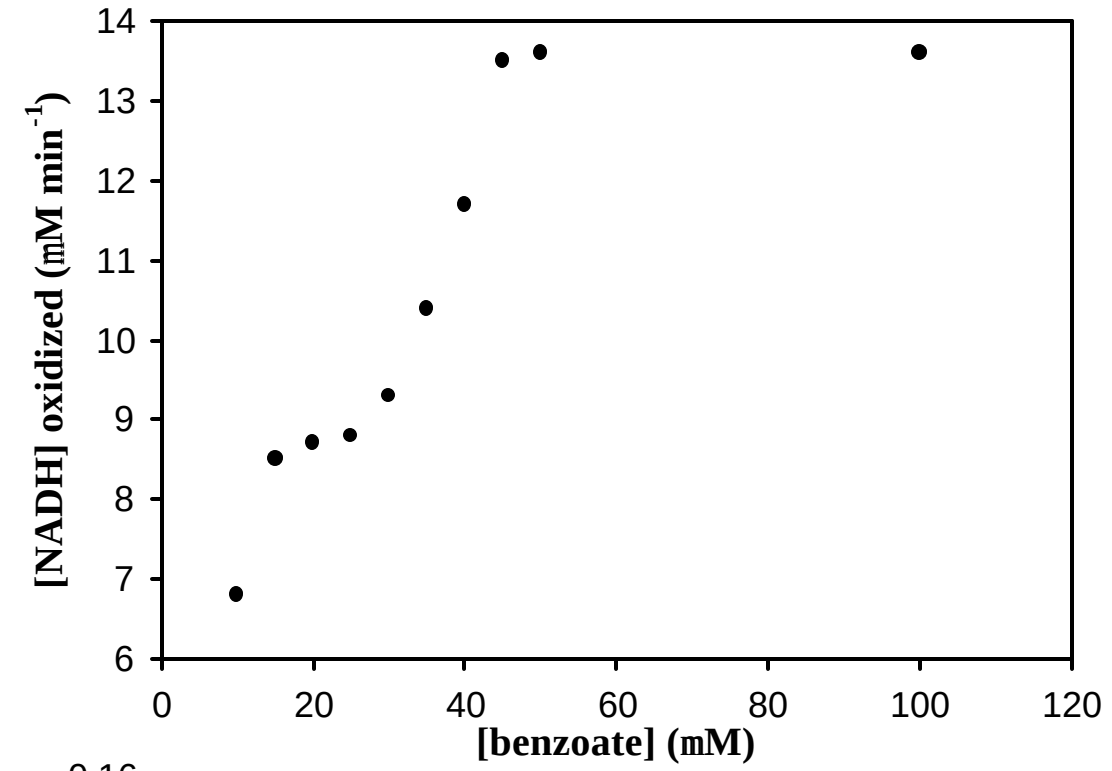
14
13
12
11
10
9
8
7
6
0
20
40
60
80
100
120
[NADH] oxidized (mM min-1)
[benzoate] (mM)

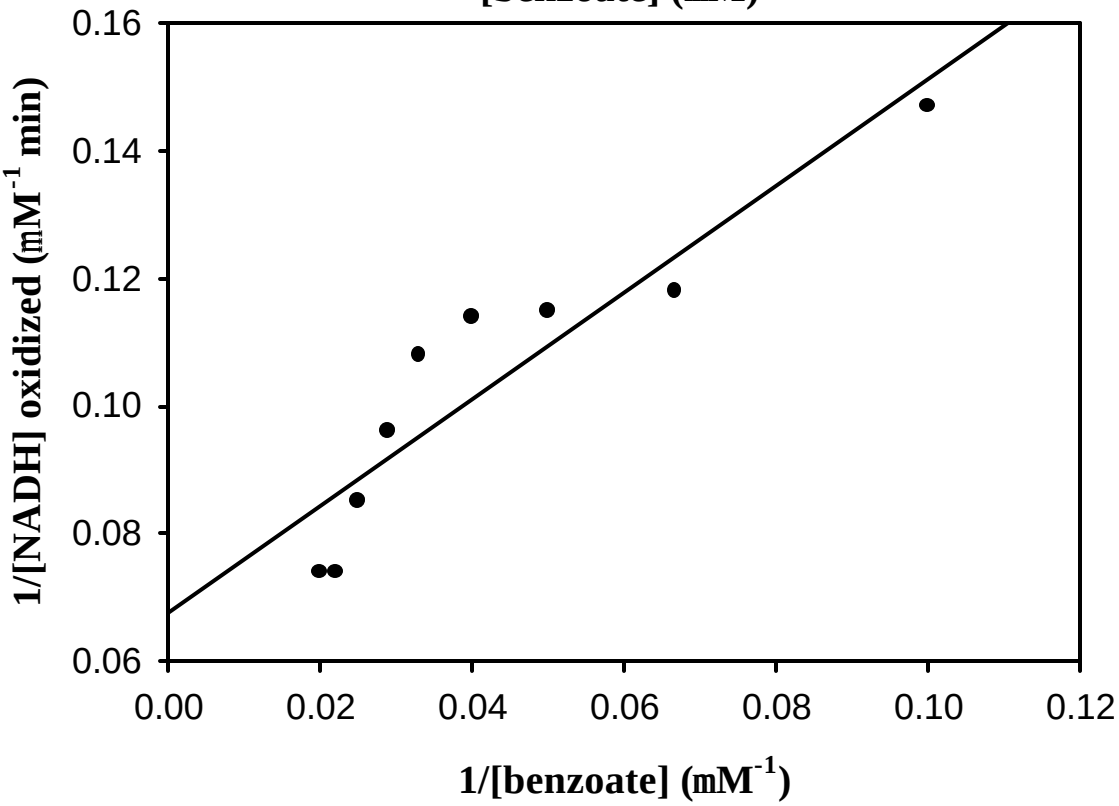
0.16
0.14
0.12
0.10
0.08
0.06
0.00
0.02
0.04
0.06
0.08
0.10
0.12
1/[NADH] oxidized (mM-1 min)
1/[benzoate] (mM-1)

Activities of AntDO with substituted benzoates

Table 3.2 shows that the stoichiometry of the AntDO-catalyzed conversion of anthranilate to catechol is 1:1:1:1 in reactants consumed and product formed. Benzoate is also a tightly coupled substrate for AntDO, forming the same non-aromatic *cis*-1,2-benzoate diol (verified using HPLC and authentic *cis*-1,2-benzoate diol), as has been observed for benzoate 1,2-dioxygenase from ADP1 (BenDO) (cf. Chapter 2). The activity (reported as the amount of NADH consumed/5 min) of AntDO with benzoate is 89% relative to activity with anthranilate as the substrate. The benzoate diol could not be quantified with the HPLC conditions used here. However, AntDO reactions using 100 μM NADH and 100 μM benzoate consumed 89 μM NADH and 86 μM O_2 and addition of the benzoate diol dehydrogenase, BenD, resulted in the generation of 80 μM NADH, indicating that 80 μM benzoate diol was formed. This concentration of benzoate was used in order to accurately quantify the amount of NADH generated upon addition of BenD. In the presence of excess benzoate, formation of NADH by BenD was accompanied by its consumption by AntDO, thereby precluding an accurate quantification of the benzoate diol formed. For comparison of the reactivity of AntDO and BenDO with anthranilate and benzoate, the amounts and stoichiometries of NADH, O_2, and substrate consumed and product formed are listed in Table 3.2. Although the standard assay conditions used for AntDO and BenDO activity assays differ with respect to the concentrations of oxygenase and reductase employed and pH, Table 3.2 shows that benzoate is a tightly coupled substrate for both AntDO and BenDO. Anthranilate is a tightly coupled substrate for AntDO, however, a substoichiometric amount of catechol is

Table 3.2. Stoichiometry of AntDO and BenDO activity with anthranilate and benzoate.[a]

	Substrate	Relative activity (%)	NADH (μM/5 min)	O_2 (μM/5 min)	H_2O_2	Substrate consumed[b] (μM/5 min)	Product Formed (μM/5 min)[b,c]
AntDO[a]	Anthranilate	100	100±6	102±7	None	101±3	96±2, catechol
	Benzoate	89	89±9	86±8	None	83±9	80±5, BD
BenDO	Anthranilate	67	45±4	42±2	None	36±1	13±4, catechol
	Benzoate	100	67±2	68±5	None	61±2	65±7, BD

[a]Assay conditions: 100 μM NADH, 250 μM O_2, 0.5 mM anthranilate or 0.1 mM benzoate, 23 °C and 0.5 μM AntAB, 0.18 μM AntC in 50 mM MES, 100 mM KCl (pH 6.3) or (for BenDO) 0.8 μM BenAB, 0.5 μM BenC, 50 μM Fe(II) in 50 mM HEPES, 100 mM KCl (pH 7.5); values listed are the average of three determinations after 5 min. Relative activities are defined as the percentage of NADH consumed in 5 min relative to activity with anthranilate for AntDO or relative to activity with benzoate for BenDO.

[b]Anthranilate and benzoate consumption and formation of catechol was monitored by HPLC as described in Experimental.

[c]Benzoate diol (BD) was identified using HPLC as described in Experimental; the amount of benzoate diol formed was determined by the amount of NADH generated upon addition of BenD (5 μM) and NAD^+ (0.2 mM) to activity assays after 5 min.

formed (with respect to NADH, O_2, and anthranilate) by BenDO with anthranilate as the substrate. Under standard AntDO assay conditions, the activity was 89 μM NADH oxidized/ 5 min/ 0.5 μM AntAB hexamer with benzoate as the substrate versus 100 μM NADH oxidized/ 5 min/ 0.5 μM AntAB hexamer with anthranilate as the substrate. The activity of BenDO-catalyzed dihydroxylation of benzoate and anthranilate under the standard assay conditions were 67 μM NADH oxidized/ 5 min/ 0.8 μM BenAB hexamer and 45 μM NADH oxidized/ 5 min/ 0.8 μM BenAB hexamer, respectively (cf. Table 3.2).

Table 3.3 summarizes the relative activities (defined as the concentration of NADH consumed/ 5 min) of the purified recombinant AntDO with anthranilate and various other analogs. Several of these substrates exhibited varying degrees of "uncoupling", a process in which some or all of the electrons consumed in substrate-dependent AntDO-catalyzed reactions may be used to reduce O_2 without hydroxylation of substrate. The most often observed products of uncoupling are H_2O_2 and/or H_2O (*34-36*). Uncoupling with production of H_2O_2 has been observed previously in the reaction of naphthalene 1,2-dioxygenase with benzene (*34*). H_2O_2 is conveniently detected and quantitated by the addition of catalase to reactions and monitoring the amount of O_2 liberated due to the catalase-catalyzed disproportionation of H_2O_2. H_2O produced from uncoupling cannot be determined directly. However, reduction of O_2 to H_2O requires four electrons or two equivalents of NADH per O_2. Therefore, a ratio of 2:1 in NADH: O_2 consumed would be expected for reactions with substrates that are completely uncoupled to form H_2O compared to 1:1 to form H_2O_2. AntDO-catalyzed dihydroxylation of anthranilate and benzoate are tightly coupled, with NADH:O_2 stoichiometries of 1:1, and

Table 3.3. Activities, reaction stoichiometries and product formation of recombinant *Acinetobacter* sp. ADP1 AntDO with various benzoate derivatives.[a]

	Substrate consumed (μM/5 min)			Product formed (μM/5 min)		
Substrate	NADH[b]	O_2 [b]	Aromatic substrate[c]	H_2O_2	Diol product[d]	Catechol product[e]
Anthranilate	100±6	102±7	101±3	n.d.[f]	-	+, 96±2[g]
Benzoate	89±9	86±8	80±11	n.d.[f]	+, 80±5[h]	-
m-aminobenzoate	47±10	47±10	n.d.[f]	5	-	+
p-aminobenzoate	21±5	11±1	6±2	2	+	+
o-fluorobenzoate	47±9	40±9	18±2	5	+	-, 12±2[g]
m-fluorobenzoate	36±6	33±6	+	5	+	-
p-fluorobenzoate	45±8	42±6	+	2	+	-
o-chlorobenzoate	42±9	30±9	n.d.[f]	3	-	-
m-chlorobenzoate	48±7	43±2	+	15	+	-
p-chlorobenzoate	32±5	23±5	+	13	+	-
o-methylbenzoate	47±7	39±6	13±2	5	+	+
m-methylbenzoate	48±6	36±7	+	5	+	-
p-methylbenzoate	28±4	19±9	+	7	+	-
o-methoxybenzoate	43±4	42±5	23±4	3	+	+,19±3[g]
m-methoxybenzoate	57±3	43±7	ND	7	+	-
p-methoxybenzoate	12±7	10±4	ND	12	-	-
o-hydroxybenzoate	63±4	60±8	48±4	5	-	-[i]
m-hydroxybenzoate	42±5	30±3	ND	5	-	+
p-hydroxybenzoate	20±3	18±7	ND	7	-	-
M43KAntAB with anthranilate	23±4	24±2	n.d.[f]	14	-	-

[a]Assay conditions: 100 μM NADH, 0.25 mM O_2, 0.5 mM aromatic carboxylate, 0.5 μM AntAB, 0.18 μM AntC, and in 50 mM MES, 100 mM KCl (pH 6.3) at room temperature (23 ºC). Values listed are after 5 min.

[b]Relative activities are defined as the percentage of NADH or O_2 consumed after 5 min relative to AntDO activity with anthranilate. Since AntDO activity with anthranilate consumed 100 μM NADH in 5 min, the amount of NADH consumed with other substrates also reflects the relative activity (%).

[c]+, substrate consumption was detected by HPLC but could not be quantified accurately; ND, not determined.

[d]Detected by the increase at 340 nm due to formation of NADH upon addition of BenD (5 μM) and NAD^+ (0.2 mM) to reactions monitoring NADH consumption after 5 min. +, indicates generation of NADH; -, no generation of NADH was observed.

[e]Gibbs' reagent (15 μL of a 2 % (w/v) solution in ethanol) was added to AntDO reactions (200 μL) and judged to be positive (+) by formation of a blue to purple color; -, no color change occurred. These analyses were conducted without BenD.

[f]None detected.

[g]Product was detected and identified as catechol and quantified by HPLC.

[h]Benzoate diol was identified as the product using HPLC as described in Experimental; the amount of benzoate diol formed was determined by the amount of NADH generated upon addition of BenD (5 μM) and NAD^+ (0.2 mM) to activity assays (described in Experimental except with 0.1 mM benzoate) after 5 min.

[I]Product was detected using HPLC but could not be detected using Gibbs' reagent or BenD.

no H_2O_2 was detected (cf. Tables 3.2 and 3.3). As shown in Table 3.3, however, the reaction of AntDO with *p*-methoxybenzoate is completely uncoupled to H_2O_2 generation, while the ratio of NADH:O_2 consumption with *o*-chlorobenzoate as substrate is greater than 1:1, most likely indicating uncoupling with formation of H_2O from O_2. For both of these substrates, no diol or catechol product was detected and in the case of the reaction with *o*-chlorobenzoate, no substrate consumption was observed when monitoring this reaction using HPLC.

Most of the substrates tested did generate either a diol or catechol product or both, as detected using BenD, the benzoate diol dehydrogenase of the BenDO system, or Gibbs' reagent (Table 3.3). Several other substrates did not appear to form either a diol or catechol. Since the substrate specificity of BenD is not known, it is possible that a diol is generated in AntDO reactions with some of the benzoate derivatives, which is not a substrate for BenD. Therefore, these reactions were treated further to convert any diol to the corresponding phenol, which can be detected by Gibbs' reagent (cf. Figure 3.5) (*27, 28*). However, none of these treated reactions gave a positive result. In addition, the amount of substrate consumed in reactions with *ortho*-substituted substrates was monitored using HPLC. With the exception of *o*-chlorobenzoate, substrate was consumed in activity assays with all of the *ortho*-substituted benzoates tested. Catechol was detected as the product of the AntDO-catalyzed dihydroxylation of *o*-fluorobenzoate and *o*-methoxybenzoate. In addition, some non-aromatic diol product was formed with *o*-fluorobenzoate and *o*-methoxybenzoate as substrates, as determined by the BenD-dependent reduction of NAD^+ in AntDO reactions. Catechol-like products were detected in reactions with *o*-methylbenzoate and *o*-hydroxybenzoate using HPLC, but the

identities of these products were not determined. Apparently, the product formed with *o*-hydroxybenzoate that was detected by HPLC is unreactive with Gibbs' reagent since no color formation was observed.

Activity of M43K AntAB

Activity assays of M43K AntAB with anthranilate as substrate were performed under the standard optimized assay conditions established for wild type AntAB. The amount of NADH and O_2 consumed was 25 % that of wild type AntAB in 5 min. At 23 °C the ratio of NADH:O_2 was 1:1, but this activity was uncoupled to form H_2O_2 and no anthranilate was consumed (Table 3.3). Similarly completely uncoupled activity was observed with benzoate as the substrate for M43K AntAB. Activity assays were also performed at 39 °C for both wild type and M43K AntAB. Both enzymes were inactive at the elevated temperature, presumably due to thermal instability.

Discussion

Anthranilate is an intermediate in the dissimilation of tryptophan in *Acinetobacter* and *Pseudomonas* species (*10-14*). Recently, anthranilate has been demonstrated to be an intermediate in the degradation of carbazole, a recalcitrant aromatic carcinogen (*37*) by *Pseudomonas* sp. strain CA10 (*15*). The Rieske dioxygenase, anthranilate 1,2-dioxygenase (AntDO), catalyzes the conversion of anthranilate to catechol, which is further degraded by the *ortho* pathway (cf. Figure 2.2) (*1, 15*). Chromosomally-encoded AntDO genes have been identified in *Acinetobacter* sp. strain ADP1 (ADP1) (*1*) and *Pseudomonas aeruginosa* (*16*). AntDO activity had been demonstrated in cell extracts of

some *Pseudomonas* species (*6-9*), however, AntDO had not previously been purified to homogeneity from any organism.

Characterization of AntDO and M43K AntAB

The recombinant AntDO oxygenase component (AntAB) from ADP1 was found to contain both mononuclear non-heme iron and Rieske-type [2Fe-2S] centers, while the reductase component (AntC) contains both FAD and a [2Fe-2S] center.

The three-dimensional structure of the terminal oxygenase component of naphthalene 1,2-dioxygenase (NDO), a three-component (class III) RDO, was determined and found to be a $\alpha_3\beta_3$ hexamer (*38*). Sequence similarity to the oxygenase component of AntDO (cf. 1.10) includes conservation of the residues furnishing ligands to the mononuclear and Rieske [2Fe-2S] centers, making it likely that the AntDO structure is very similar to the NDO structure. Based on sequence alignment, Met43 in AntA corresponds to Leu31 in NDO and, as shown in Figure 3.11, Leu31 lies at the α_3 trimer interface and is ~3.6 Å away from Arg379 in an adjacent α subunit. This Arg is conserved in AntA (Arg396) based on sequence alignment. Mutation of Met43 to Lys in AntA could result in unfavorable steric or electrostatic interactions between Lys43 and amino acids in the adjacent α subunit (possibly Arg396), which may alter the quaternary structure of the hexamer, possibly destroying the ability of the α subunits to form a trimer. However, purified soluble M43K AntAB was shown by gel filtration chromatography to be hexameric. SDS-PAGE analysis of the cell-free extract and pellet of cultures expressing M43K AntAB, however, did show a significant amount of insoluble AntA localized in the pellet, while the majority of wild type AntB was soluble

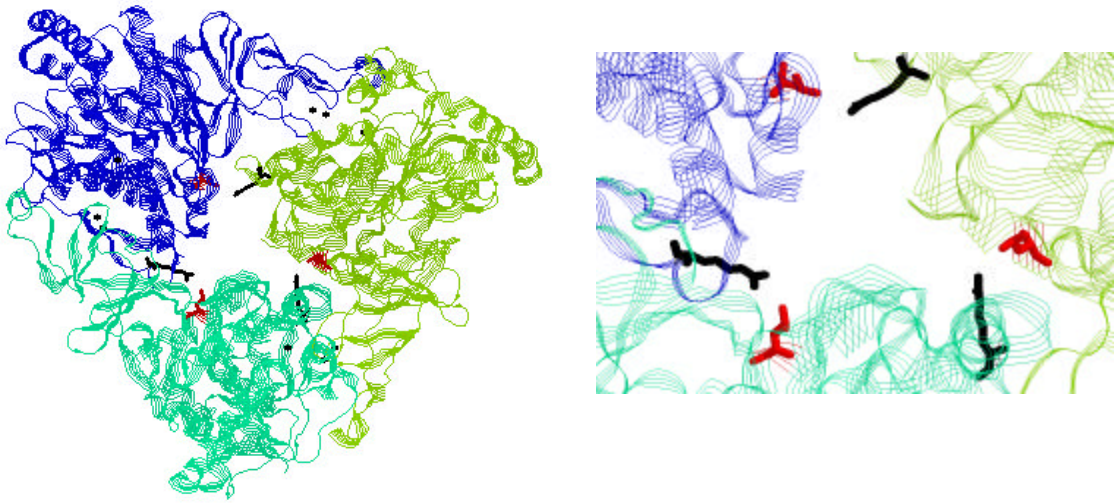

Figure 3.11. Structure of the α_3 trimer of naphthalene 1,2-dioxygenase (NDO) generated using ViewerLite (Accelrys, Inc.) and coordinates from 1NDO in the Protein Data Bank *(38)*. The α subunits are shown in blue, green, and cyan. The mononuclear and Rieske [2Fe-2S] iron atoms are represented as black spheres. Leu31, which aligns to Met43 in AntA, is shown in red. Arg379 in NDO is shown in black. The distance between Leu31 and Arg379 in an adjacent α subunit is 3.6 Å.

(Figure 3.6). Hence, substitution of Lys for Met43 may result in the equilibrium:

$$\alpha_3\beta_3 \rightleftharpoons \alpha_n \text{ or } (\alpha\beta)_n$$

which could lead to formation of insoluble α_n or $(\alpha\beta)_n$ oligomers.

The activity of M43K AntAB with anthranilate was shown to be completely uncoupled to generate H_2O_2 and no catechol, which is not easily reconciled with the previously observed in vivo results showing that M43K AntAB could support growth of ADP1 at 23 °C but not at 39 °C (*1*). Expression of the *ant* genes in ADP1 at the lower temperature may be slower than at 39 °C, allowing more time for correct folding of M43K AntAB to yield mostly $\alpha_3\beta_3$, resulting in active protein. In *E. coli,* however, the *antAB* containing plasmid used was designed for relatively high-level expression of the *ant* genes. Expression of recombinant M43K AntAB in *E. coli* at 23 °C may, therefore, still be too fast to allow proper folding, resulting in uncoupled enzyme activity.

Substrate preferences of AntDO and mechanistic implications

The relative activities of AntDO-catalyzed reactions, reaction stoichiometries under standard assay conditions and detection of diol or catechol products indicates that AntDO is able to hydroxylate several substituted benzoates, but, with varying degrees of uncoupling (Table 3.3). AntDO catalyzed the conversion of anthranilate to catechol in a tightly coupled manner, i.e., 1:1:1:1 NADH:O_2:anthranilate:catechol product. Most of the substrates tested with AntDO that were partially uncoupled generated some diol and/or catechol products with the exceptions of *o*-chlorobenzoate and *p*-hydroxybenzoate. The RDO, 2-halobenzoate dioxygenase, whose amino acid sequence

shows high homology to that of AntDO (cf. Figure 1.10), has been shown to catalyze the transformation of *o*-chlorobenzoate to catechol, most likely by spontaneous loss of CO_2 and Cl^- (*24*). However, *o*-chlorobenzoate is not a substrate for ADP1 AntDO, even though NADH and O_2 were consumed in a *o*-chlorobenzoate-dependent manner. These substituted benzoates, therefore, still presumably bind at the anthranilate binding site of AntDO.

In the AntDO-catalyzed reaction with *o*-hydroxybenzoate, product could not be detected using either BenD or Gibbs' reagent, although assays monitored by HPLC showed consumption of *o*-hydroxybenzoate and formation of an unidentified product. Hydroxylation of *o*-hydroxybenzoate (salicylate) to catechol is catalyzed by a flavin-containing monooxygenase, salicylate hydroxylase (*39*). In addition, a salicylate 5-hydroxylase activity has been detected for a putative RDO from *Ralstonia* sp. strain U2 that converts salicylate to 2,5-dihydroxybenzoate (gentisate) (*40*). In the event that AntDO-catalyzed reactions with *o*-hydroxybenzoate form the monooxygenated product gentisate, it is possible that this compound would not react with Gibbs' reagent and therefore appear to form no product using this detection method.

Of the *ortho*-, *meta*-, *para*-substituted benzoates, AntDO appears to be least active with the *para*-substituted substrates. *p*-Aminobenzoate and *p*-methoxybenzoate were highly uncoupled in AntDO reactions. While some substrate was consumed and diol and catechol products were detected in the reaction with *p*-aminobenzoate, the ratio of NADH:O_2 was nearly 2:1, suggesting that, in addition to some product formation, the uncoupled four-electron reduction of O_2 to H_2O was also occurring. No diol or catechol product could be detected in AntDO reactions with *p*-methoxybenzoate; the substrate and

NADH:O_2 consumption was completely uncoupled to generate H_2O_2. An RDO that uses *p*-methoxybenzoate as the substrate, putidamonooxin (*p*-methoxybenzoate *O*-demethylase) is a two-component RDO homolog that consists of a reductase with a plant-type [2Fe-2S] center and FMN and an oligomeric, single subunit oxygenase component that contains one Rieske-type [2Fe-2S] center and one mononuclear nonheme iron center per subunit (*41*). Putidamonooxin catalyzes the demethylation of *p*-methoxybenzoate to yield *p*-hydroxybenzoate and formaldehyde (*41*).

Substrates that are completely or partially uncoupled can hint at possible intermediates in the catalytic cycle of AntDO. Figure 3.12 shows a proposed reaction cycle for the RDOs based on mechanistic and structural results obtained with better characterized RDOs (cf. Chapter 4) (*42*). Substrate binding near the mononuclear site is required for reaction of O_2 with the mononuclear Fe(II) followed by electron transfer from the reduced Rieske center generating a ferric-peroxo intermediate. This intermediate could either hydroxylate substrate or be converted to an oxo-perferryl intermediate by protonation and heterolytic cleavage of the O-O bond, which could hydroxylate substrate. A second electron transfer from the Rieske site and product release returns the product-bound mononuclear iron site back to the resting state. In the uncoupled pathways (dashed arrows) protonation of the ferric-peroxo species can uncouple electron transfer from substrate hydroxylation to form H_2O_2 (unc-2), followed by electron transfer to return the enzyme to the resting state. Alternatively, protonation and two-electron reduction of the ferric-peroxo intermediate and subsequent electron transfer would form H_2O (unc-1) and return the enzyme to the resting state. AntDO reactions with substrates

Figure 3.12. Schematic representation of the RDO reaction cycle (solid arrows) and uncoupling pathways (dashed arrows) leading to the formation of H_2O_2 and H_2O.

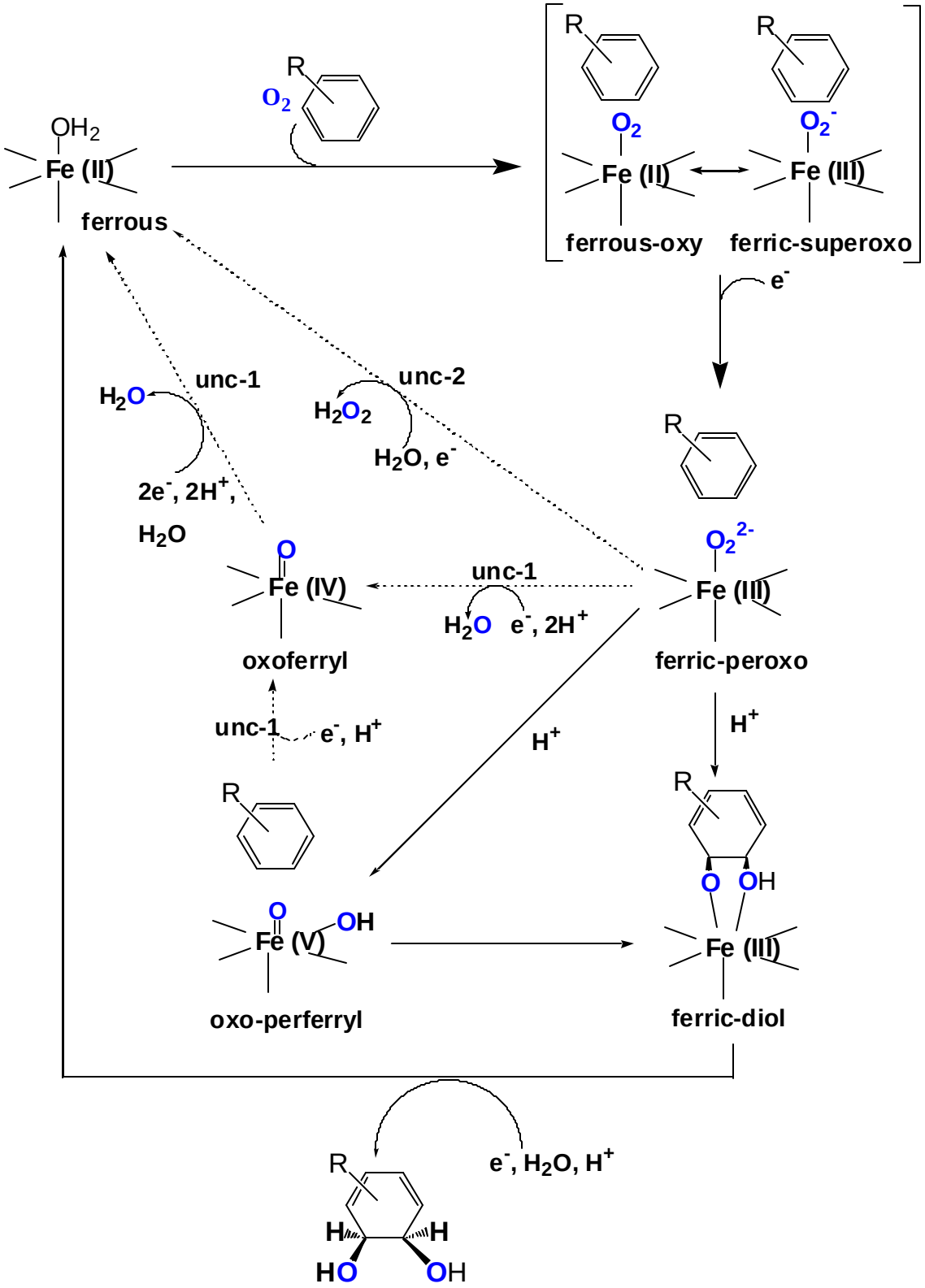
OH2
Fe (II)
ferrous
R
O2
R
O2
Fe (II)
ferrous-oxy
R
O2-
Fe (III)
ferric-superoxo
e-
R
unc-1
H2O
2e-, 2H+,
H2O
unc-2
H2O2
H2O, e-
O2 2-
Fe (III)
ferric-peroxo
O
Fe (IV)
oxoferryl
unc-1
H2O
e-, 2H+
unc-1
e-, H+
H+
H+
R
R
O
OH
Fe (V)
oxo-perferryl
Fe (III)
ferric-diol
e-, H2O, H+
R
H
H
HO
OH

that form both H_2O_2 and product, such as *m*-chlorobenzoate (15 μM H_2O_2), *p*-chlorobenzoate (13 μM H_2O_2), and *p*-methoxybenzoate (12 μM H_2O_2), suggest that a ferric-peroxo intermediate is involved in the AntDO reaction cycle. The stoichiometries of NADH to O_2 consumed in AntDO reactions with *p*-aminobenzoate and *o*-chlorobenzoate suggest formation of either a ferric-peroxo species or a high-valent iron-oxo complex in the AntDO reaction cycle that generates product in the case of *p*-aminobenzoate, but is most likely reduced to form H_2O with *o*-chlorobenzoate. The factors that give rise to either type of uncoupling are most likely a combination of the inherent properties of the substrate itself and how it interacts within the active site.

Both a non-aromatic diol and catechol were detected in the AntDO-catalyzed reaction with *o*-fluorobenzoate. In addition, the NADH:O_2 ratio in these reactions was greater than 1:1 and some H_2O_2 was detected, both suggesting some uncoupling of electron transfer in addition to product formation. Dihydroxylation of *o*-fluorobenzoate catalyzed by 2-halobenzoate dioxygenase has been shown to yield catechol (*24*), most likely from spontaneous loss of CO_2 and F^- from an unstable *cis*-1,2-dihydroxy-2-fluorocylcohexa-3,5-diene-1-carboxylate (2-fluoro-1,2-benzoate diol) intermediate, while benzoate dioxygenase from *Pseudomonas putida* converts *o*-fluorobenzoate to the stable non-aromatic *cis*-1,2-dihydroxy-6-fluorocyclohexa-3,5-diene-1-carboxylate (6-fluoro-1,6-benzoate diol (*43*, *44*). These results along with the formation of both catechol and a non-aromatic diol in AntDO reactions, suggest that *o*-fluorobenzoate can bind to the active site of AntDO in two alternative binding modes leading to either 1,2 or 1,6 dihydroxylation, as shown in Figure 3.13. Presumably the fluoro substituent is small

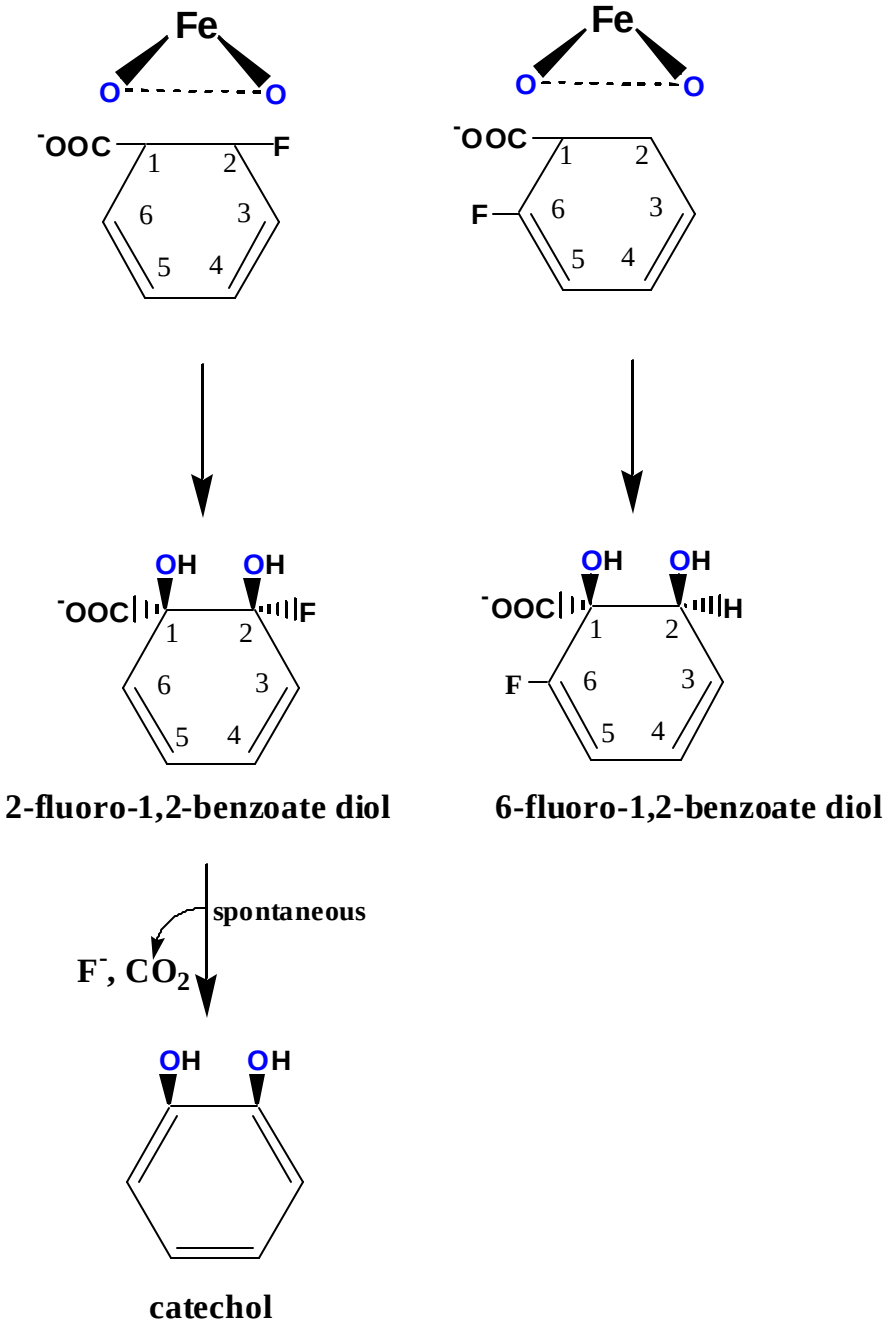

Figure 3.13. Schematic representation of two possible conformations of *o*-fluorobenzoate binding at the mononuclear iron site of AntDO leading to the formation of catechol and a nonaromatic fluorobenzoate diol.

enough not to engage in sterically restricted interactions with the enzyme in either binding mode.

AntDO and BenDO activity with anthranilate and benzoate

Both anthranilate and benzoate are converted to catechol and the non-aromatic *cis*-1,2-benzoate diol, respectively, by both AntDO or BenDO (Chapter 2) in vitro, suggesting that AntDO could substitute for BenDO in vivo. However, the specific activities reported were measured under a set of conditions that were optimized for each RDO separately with respect to pH, substrate and enzyme concentrations, which most likely does not reflect true intracellular conditions. Regardless, separate *ben* and *ant* operons appear to be specific for benzoate and anthranilate, respectively, in vivo (*1, 18*).

The results in Table 3.3 indicate that AntDO is nearly as active with benzoate as substrate as with anthranilate. The question then arises as to why AntDO cannot support growth on benzoate in vivo. Benzoate conversion to catechol requires the diol dehydrogenase, BenD, in addition to BenDO (cf. Figure 3.2) (*18*). In ADP1, expression of BenDO and BenD is regulated by the transcriptional regulator BenM, which induces expression of the *ben* genes in the presence of benzoate and *cis*, *cis*-muconate (the latter being the product of intradiol cleavage of catechol carried out by catechol 1,2-dioxygenase) (*19*). The *ben* and *ant* operons are separated by one-third of the ADP1 chromosome and the *ben* operon is not induced by anthranilate. No homolog to BenM or BenD has been identified in the region of the *ant* operon. Expression of *antA* has been shown to be induced by anthranilate, but not benzoate (*1*). Therefore, despite the in vitro activities reported herein, AntDO and BenDO may not be able to substitute for each other in vivo due to insufficient anthranilate-mediated expression of the *ben* genes and/or

insufficient benzoate-mediated expression of the *ant* genes. In vivo results showed that the reductase component of BenDO, BenC, could substitute for a defective AntC and allow growth on anthranilate as the sole carbon source (*1*). This was attributed to anthranilate-mediated expression of AntAB and low level constitutive expression of BenC for AntAB/BenC-catalyzed dihydroxylation of anthranilate to catechol. However, in the absence of functional *antAB* genes, BenAB cannot substitute for AntAB (*1*) suggesting that the low constitutive level concentrations of BenAB and BenC are not sufficient for BenDO-catalyzed dihydroxylation of anthranilate. Otherwise, any BenDO conversion of anthranilate to catechol would most likely result in catechol-induced expression of the catechol degradation genes, leading to conversion of catechol to *cis,cis*-muconate, which is an inducer of BenM-mediated *ben* gene expression. Alternatively, *ben* gene expression may be repressed in the presence of anthranilate. Consistent with this notion, previous studies have determined that ADP1 shows a preference for carbon source utilization (*19, 45*). When benzoate and *p*-hydroxybenzoate are provided together, ADP1 preferentially degrades benzoate first. However, disruption of *benM* results in rapid utilization of *p*-hydroxybenzoate in the presence of benzoate, suggesting that BenM may play a role in regulating *p*-hydroxybenzoate degradation. In the presence of four carbon sources, shikimate, anthranilate, benzoate and *p*-hydroxybenzoate, wild type ADP1 showed a lag in the degradation of benzoate. After 8 hrs, approximately 90% of the benzoate that was provided as a carbon source remained, while approximately 50% of shikimate and anthranilate were degraded. After this lag period, all of the benzoate was consumed within 3 hrs. ADP1 strains with *benM* disrupted are still able to utilize anthranilate, which suggests that BenM does not regulate expression of the *ant* genes

(*19*). However, the above results may suggest that the regulatory mechanisms of AntDO (as yet to be identified) may influence the ability of AntDO to degrade benzoate in vivo and possibly influence BenDO-catalyzed degradation of anthranilate.

The components of AntDO have been purified to homogeneity for the first time from any organism and determined to be a class I RDO. Contrary to expectations from previous in vivo results, AntDO and BenDO can dihydroxylate anthranilate and benzoate to the expected products catechol and benzoate diol, respectively in a tightly coupled manner in vitro. The assay conditions employed in these studies probably do not reflect true intracellular conditions and therefore, the specific activities reported may not accurately represent in vivo enzymatic activities. However, as discussed above, in the presence of multiple carbon sources, ADP1 shows a preference for which compound is utilized initially and transcriptional regulators may play a role in governing the preferential utilization of a given carbon source. Future studies may identify additional genes involved in anthranilate degradation in ADP1 thereby shedding light on the mechanisms that govern substrate utilization of AntDO and BenDO in vivo.

References

1. Bundy, B. M., Campbell, A. L., and Neidle, E. L. (1998) *J. Bacteriol. 180*, 4466-4474.
2. Butler, C. S., and Mason, J.R. (1997) *Adv. Microb. Physiol. 38*, 47-84.
3. Bertini, I., Cremonini, M.A., Ferretti, S., Lozzi, I., Luchinat, C., and Viezzoli, M.S. (1996) *Coord. Chem. Rev. 151*, 145-160.
4. Gibson, D. T., and Parales, R.E. (2000) *Curr. Opin. Biotechnol. 11*, 236-243.
5. Nam, J., Nojiri, H., Yoshida, T., Habe, H., Yamane, H., and Omori, T. (2001) *Biosci. Biotechnol. Biochem. 65*, 254-263.
6. Ichihara, A., Adachi, K., Hosokawa, K., and Takeda, Y. (1962) *J. Biol. Chem. 237*, 2296-2302.
7. Kobayashi, S., Kuno, S., Itada, N., Hayaishi, O., Kozuka, S., and Oae, S. (1964) *Biochem. Biophys. Res. Commun. 16*, 556-561.
8. Kobayashi, S., and Hayaishi, O. (1970) *Methods Enzymol. 17A*, 505-510.
9. Taniuchi, H., Hatanaka, M., Kuno, S., Hayaishi, O., Nakajima, M., and Kurihara, N. (1964) *J. Biol. Chem. 239*, 2204-2211.
10. Stanier, R. Y., Hayaishi, O., and Tsuchida, M. (1951) *J. Bacteriol. 62*, 355-366.
11. Stanier, R. Y., and Hayaishi,O. (1951) *J. Bacteriol. 62*, 367-375.
12. Hayaishi, O., and Stanier, R.Y. (1951) *J. Bacteriol. 62*, 691-709.
13. Wheelis, M. L. (1972) *Arch. Mikrobiol. 87*, 1-9.
14. Cohn, W., and Crawford, I.P. (1976) *J. Bacteriol. 127*, 367-379.
15. Nojiri, H., Sekiguchi, H., Maeda, K., Urata, M., Nakai, S., Yoshida, T., Habe, H., and Omori, T. (2001) *J. Bacteriol. 183*, 3663-3679.

16. Zhang, C., Huang, M. and Holloway, B.W. (1993) *FEMS Microbiol. Lett. 108*, 303-310.

17. Zhang, C., Huang, M. and Holloway, B.W. (1993) *FEMS Microbiol. Lett. 112*, 255-260.

18. Neidle, E. L., Shapiro, M.K., and Ornston, L.N. (1987) *J. Bacteriol. 169*, 5496-5503.

19. Collier, L. S., Gaines, G.L. and Neidle, E.L. (1998) *J. Bacteriol. 180*, 2493-2501.

20. Sambrook, J., Fritsch, E.F., and Maniatis, T. (1989) Cold Spring Harbor Laboratory Press, Cold Spring Harbor, N.Y.

21. Schagger, H., and Jagow, G. von. (1987) *Anal. Biochem. 166*, 368-379.

22. Bradford, M. M. (1976) *Anal. Biochem. 72*, 248-254.

23. Batie, C. J., LaHaie, E., and Ballou, D.P. (1987) *J. Biol. Chem. 262*, 1510-1518.

24. Fetzner, S., Muller, R., and Lingens, F. (1992) *J. Bacteriol. 174*, 279-290.

25. Yamaguchi, M., and Fujisawa, H. (1980) *J. Biol. Chem. 255*, 5058-5063.

26. Massey, V. (1959) *Biochim. Biophys. Acta 34*, 255-256.

27. Joern, J. M., Sakamoto, T., Arisawa, A., and Arnold, F.H. (2001) *J. Biomol. Screen. 6*, 219-223.

28. Quintana, M. G., Didion, C., and Dalton, H. (1997) *Biotechnol. Tech. 11*, 585-587.

29. Mason, J. R., and Cammack, R. (1992) *Ann. Rev. Microbiol. 46*, 277-305.

30. Fee, J. A., Findling, K.L., Yoshida, T., Hille, R., Tarr, G.E., Hearshen, O., Dunham, W.R., Day, E.P., Kent, T.A., and Munck,E. (1984) *J. Biol. Chem. 259*, 124-133.

31. Hugo, N., Armengaud, J., Gaillard, J., Timmis, K.N., and Jouanneau, Y. (1998) *J. Biol. Chem. 273,* 9622-9629.

32. Gassner, G. T., Ludwig, M.L., Gatti, D.L., Correll, C.C., and Ballou, D.P. (1995) *FASEB J. 9*, 1411-1418.

33. Trumpower, B. L. (1990) *Microbiol. Rev. 54*, 101-129.

34. Lee, K. (1999) *J. Bacteriol. 181*, 2719-2725.

35. Kadkhodayan, S., Coulter, E.D., Maryniak, D.M., Bryson, T.A., and Dawson, J.H. (1995) *J. Biol. Chem. 270*, 28042-28048.

36. Gorsky, L. D., Koop, D.R., and Coon, M.J. (1984) *J. Biol. Chem. 259*, 6812-6817.

37. Arcos, J. C., and Argus, M.F. (1968) *Adv. Cancer Res. 11*, 305-471.

38. Kauppi, B., Lee, K., Carredano, E., Parales, R. E., Gibson, D. T., Eklund, H., and Ramaswamy, S. (1998) *Structure 6*, 571-586.

39. Suzuki, K., Asao, E., Nakamura, Y., Nakamura, M., Ohnishi, K., and Fukuda, S. (2000) *J. Biochem. (Tokyo) 128*, 293-299.

40. Zhou, N., Al-Dulayymi, J., Baird, M.S., and Williams, P.A. (2002) *J. Bacteriol. 184*, 1547-1555.

41. Bernhardt, F., Bill, E., Trautwein, A., and Twilfer, H. (1988) *Methods Enzymol. 161*, 281-294.

42. Coulter, E. D. and Ballou, D.P. (1999) *Essays in Biochemistry 34*, 31-47.

43. Reineke, W., Otting, W. and Knackmuss, H. (1978) *Tetrahedron 34*, 1707-1714.

44. Reineke, W. and Knackmuss, H. (1978) *Biochim. Biophys. Acta. 542*, 412-423.

45. Gaines, G. L., Smith, L. and Neidle, E.L. (1996) *J. Bacteriol. 178*, 6833-6841.

CHAPTER 4

PROTON AND ELECTRON TRANSFER IN THE RIESKE DIOXYGENASES: ROLE OF A CONSERVED ASPARTATE IN ANTHRANILATE DIOXYGENASE[4]

[4] **Beharry, Z.M., Eby, D.M., Coulter, E.D., Neidle, E.L., Phillips, R.S., and Kurtz, D.M., Jr. To be submitted to *Biochemistry*.**

Abstract

The Rieske dioxygenase anthranilate 1,2-dioxygenase (AntDO) from *Acinetobacter* sp. strain ADP1 catalyzes the dihydroxylation of anthranilate with release of ammonia and carbon dioxide leading to catechol. The oxygenase consist of a $\alpha_3\beta_3$ hexamer containing Rieske-type [2Fe-2S] and mononuclear iron sites. Based on the inter- and intra-α subunit distances between the Rieske and mononuclear iron sites of the related oxygenase component of naphthalene dioxygenase (NDO), it was proposed that the most efficient route of electron transfer between these two centers occurs across adjacent α subunit interfaces via a conserved aspartate residue that bridges two iron sites. Mutation of this aspartate residue to glutamine resulted in an inactive NDO variant with spectral properties identical to those of wild type NDO (*1*). This report describes mutation of the corresponding aspartate residue in AntDO (Asp218) to alanine, asparagine, and glutamate and characterization of these variant AntDOs. All three AntDO variants when overexpressed in *E. coli* retained a stable $\alpha_3\beta_3$ structure with a full complement of Rieske and mononuclear iron (except for the glutamate variant, whose mononuclear site was unoccupied). However, none of these Asp218 variants showed any detectable ability to catalyze the transformation of anthranilate to catechol, or uncoupled NADH consumption by dioxygen. Single turnover experiments monitored by stopped-flow spectrophotometry, electron paramagnetic resonance spectroscopy, and HPLC suggest that Asp218 is not essential for electron transfer between the Rieske and mononuclear iron sites of AntDO and that a product is formed but it is not the expected product catechol. A role for this residue in proton transfer to activated intermediates resulting

from reaction of the mononuclear site with dioxygen in the catalytic reaction cycle is proposed.

Introduction

Rieske dioxygenases (RDOs) catalyze the initial step in aerobic degradation of aromatic compounds by several *Pseudomonas* and *Acinetobacter* species of soil bacteria according to the transformation shown in reaction 4.1. Both atoms of O_2 are inserted into the aromatic ring yielding cyclic *cis*-dihydrodiols or *cis*-diol carboxylic acids (*2*-*4*). Substituent R can be hydrogens or any of several other substituents.

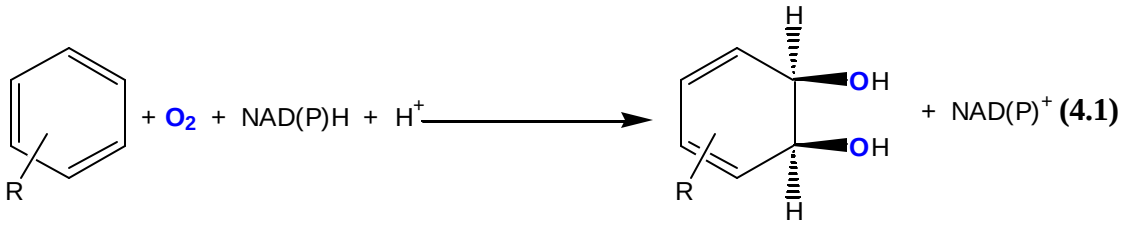

(4.1)

RDOs consist of a reductase, an oxygenase, and, in some cases, an additional ferredoxin that mediates electron transfer between the former two components. The oxygenase component catalyzes the insertion of both atoms of molecular oxygen into the aromatic substrate. This insertion is believed to occur from an activated species resulting from reaction of O_2 with a mononuclear ferrous site followed by reduction of the $[Fe\text{-}O_2]^{2+}$ species by a Rieske-type $[2Fe\text{-}2S]^{+}$ site (*5*). Formation of this activated species is "gated", occurring only after binding of the aromatic substrate.

The X-ray crystal structure of the oxygenase component of the related RDO, naphthalene dioxygenase (NDO) (*6*) from *Pseudomonas putida*, revealed a mushroom-shaped, three-fold rotationally symmetric $\alpha_3\beta_3$ hexamer (cf. Figure 1.8). The distance between the Rieske and mononuclear sites within each α subunit is ~44 Å, whereas a much shorter distance, ~12 Å, occurs between these two metal centers across

adjacent α-subunit interfaces (cf. Figure 1.9). This intersubunit route was, therefore, proposed to be the most efficient for the catalytically essential electron transfer between Rieske and mononuclear iron sites (*6*). The carboxylate of a conserved aspartate residue, Asp205 in NDO, was found to lie between the Rieske and mononuclear iron sites across each of the three α/α´ subunit interfaces and to be hydrogen-bonded to a ligand histidine of the Rieske site and a ligand histidine of the mononuclear iron site. This aspartate residue is conserved in all known RDOs (cf. Figure 1.10) (*2*) and, based on its location in NDO, was proposed to facilitate electron transfer between the Rieske and mononuclear iron sites (*1, 6*). Crude *E. coli* extracts expressing engineered NDO variants in which Asp205 was replaced by Ala, Glu, Asn or Gln showed little or no ability to hydroxylate naphthalene and no ability to consume substrate or dioxygen under conditions where the wild type NDO *E. coli* extract did show these activities (*1*). The Asp205Gln NDO variant was isolated and found to retain the native $\alpha_3\beta_3$ quaternary structure and an intact Rieske center capable of being reduced by NADH via its reductase component. Iron analysis indicated the presence of ~2.7 Fe/αβ for both wild type NDO and the Asp205Gln variant i.e., that the mononuclear site was also occupied.

Anthranilate 1,2-dioxygenase (AntDO) is a two-component RDO from the soil bacterium *Acinetobacter* sp. strain ADP1 (ADP1) that catalyzes the conversion of anthranilate (2-aminobenzoate) to catechol, as diagrammed in Figure 4.1. Although AntDO activity was reported as early as 1964 (*7, 8*), its oxygenase (AntAB) and reductase (AntC) components were only recently purified to homogeneity as described in Chapter 3 (*9*). The composition of the oxygenase component, AntAB, mimicked that of

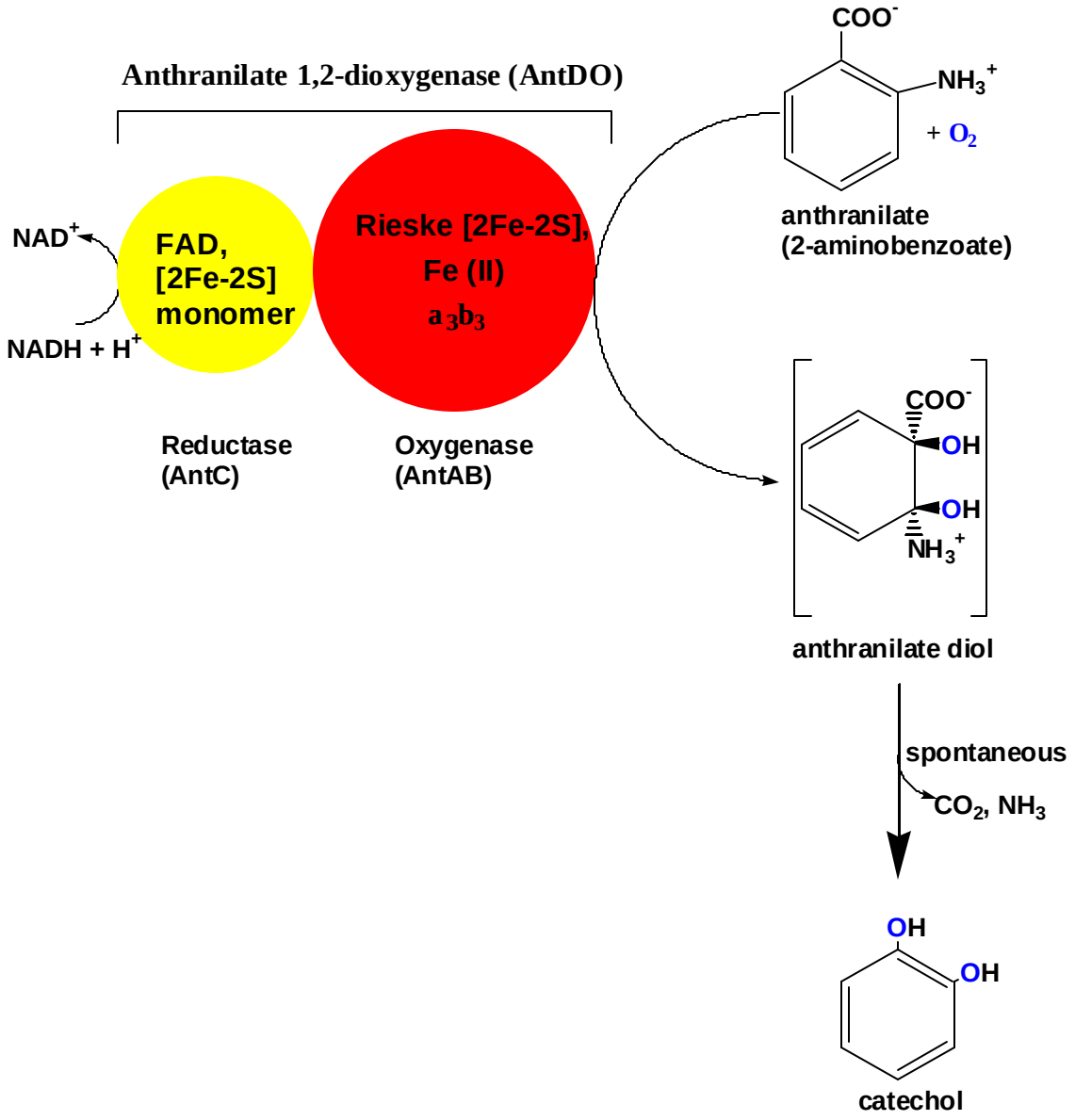

Figure 4.1. Components and reaction catalyzed by *Acinetobacter* sp. strain ADP1 AntDO (*9*, *10*).

NDO, i.e., a $\alpha_3\beta_3$ hexamer with one Rieske-type [2Fe-2S] center and mononuclear ferrous site per α subunit. All residues contributing ligands to the Rieske and mononuclear iron sites of NDO are conserved in AntDO (*9*). Also conserved is the homologue to Asp205 in NDO, namely, Asp218 in the α subunit of AntDO (AntA) (cf. Figure 1.10).

This chapter describes the characterization of three Asp218 variants of AntAB and provides evidence for an essential role of this conserved residue in proton rather than electron transfer during RDO catalysis of aromatic ring dihydroxylation.

Experimental

Reagents and general procedures

Anthranilate and ultrapure grade ammonium sulfate were purchased from Sigma Chemical Company. Oligonucleotides were synthesized by Integrated DNA Technologies. Nucleotide sequencing was performed at the University of Georgia Molecular Genetics Instrumentation Facility (ABI373 sequencer, Applied Biosystems). Protein purity was judged by sodium dodecyl sulfate-polyacrylamide gel electrophoresis (SDS-PAGE) (15% polyacrylamide gels) with Coomassie blue staining (*11*). Standard molecular biology procedures followed those in Sambrook et al. (*12*) or Ausubel et al. (*13*). Protein was quantitated using the Bio-Rad protein assay (Bio-Rad) with bovine serum albumin as the standard. Native protein molecular weights (gel filtration) and iron quantitation (ferrozine method) were determined as previously described (*9*). Other metals in the proteins were quantitated by inductively coupled plasma-atomic emission spectrometry at the University of Georgia Chemical Analysis Laboratory. For

examination of the reduced Rieske center by EPR spectroscopy, excess sodium dithionite (~3 mM) was added to buffered AntAB samples that had been made anaerobic by purging with N_2 gas. The reduced samples were then transferred via gas-tight syringe to EPR tubes that were continuously purged with N_2 gas and then frozen in liquid N_2.

Construction of D218 AntAB variants

Substitution of the aspartate-218 codon with that of alanine (D218A) in *antA* from *Acinetobacter* sp. strain ADP1 was carried out using the QuikChange Site Directed Mutagenesis kit (Stratagene) following the procedures described in the product manual. Plasmid pBAC209 (*9*), which contains *antAB*, was used as the template with the complementary mutagenic oligonucleotide primers 5´-GAAAATGGCCTCgctGGCTACCACGTC-3´ and 5´-GACGTGGTagcCAGCGAGGCCATTTTC-3´ (with variant codon in lower case), resulting in plasmid, pDMK5. The D218N and D218E *antAB* variants were constructed analogously, using mutagenic primer pairs 5´-GAAAATGGCCTCaatGGCTACCACGTC-3´/5´-GACGTGGTAGCCattGAGGCCATTTTC-3´, resulting in plasmid, pDMK8 for D218N, and 5´-GAAAATGGCCTCgaaGGCTACCACGTC-3´/5´-GACGTGGTAGCCttcGAGGCCATTTTC-3´ resulting in plasmid pDMK9 for D218E. Successful substitution of the codons in all *antA* variant-encoding plasmids was verified by nucleotide sequencing.

Construction of a D218A AntA mutant of *Acinetobacter* sp. strain ADP1

The plasmid, pDMK5, containing the D218A *antAB* gene was digested with *Bgl*II to linearize the plasmid via the unique *Bgl*II restriction site within the vector. The

linearized plasmid was used as donor DNA in an *Acinetobacter* transformation assay adapted from Neidle and Ornston (*14*). Wild-type *Acinetobacter sp.* strain ADP1 was grown in 1 mL minimal salts media containing succinate (*15*). When the culture reached early log phase, approximately 1 μg of donor DNA was added and the culture was incubated for an additional 5 hours. Serial dilutions of the culture were plated to minimal agar media with succinate and colonies were first screened for loss of growth on minimal agar containing anthranilate, then for ampicillin sensitivity on Luria Broth agar with 150 mg/L ampicillin to ensure that the plasmid was neither retained in the cell nor incorporated into the chromosome. Cell-free lysates of colonies that were ampicillin-sensitive and unable to grow on anthranilate as sole carbon source were prepared (*14*), and *antA* was PCR-amplified using these cell-free lysates as template and primers duplicating the nucleotide sequences of the 5´ and 3´ ends of *antA*. Sequencing of the resulting PCR amplicon confirmed the presence of a mutation in *antA* that was identical to that encoding the D218A AntAB as found in pDMK5. The new ADP1 strain with the D218A mutation in *antA* on the chromosome was designated ACN476.

Expression of recombinant enzymes in *E. coli* and preparation of cell-free extracts

One-liter cultures of *E. coli* strain BL21-Codon Plus (Stratagene) carrying pBAC208 (containing *antC*) (*9*), pBAC209 (*antAB*), pDMK5 (D218A *antAB*), pDMK8 (D218N *antAB*) or pDMK9 (D218E *antAB*) were grown aerobically in M9 minimal medium containing 100 mg/L ampicillin in an incubator/shaker at 37 ºC until OD_{600} ~0.6. The temperature was reduced to 30 ºC and ferrous ammonium sulfate (20 mg/L of culture) and IPTG (100 mg/L) were added. Incubation continued at this temperature until OD_{600} ~2.5 (~4 hrs). Cells were harvested by centrifugation and washed with 25 mM

MOPS pH 7.3 (buffer A). Approximately 25 g of cells collected from six liters of *E. coli* culture were resuspended in 25 mL of buffer A containing 1 mg of DNase and sonicated on ice using a Branson sonifier cell disrupter 350 with a 0.5-inch probe tip for 2 min at 30-sec intervals at 20 kHz. Cell debris was removed by centrifugation (12,000 g, 30 min, 4 ºC). This preparation is referred to as 6 x 1-L cell-free extract and was used immediately for isolation of enzymes.

Isolation and purification of wild type and variant AntABs

The procedure described below is modified from that described earlier (*9*) and was used to isolate and purify both wild type and D218 variant AntABs. All steps were carried out at 4 ºC on the 6 x 1-L cell-free extracts described above. Column fractions containing AntAB were easily visualized by their red-brown color. The cell-free extract was applied to a 3 x 15-cm Q Sepharose FF anion-exchange column (Amersham Pharmacia Biotech) equilibrated in buffer A. The column was washed with 200 mL of buffer A and AntAB was eluted with a step gradient of NaCl (0-400 mM) in buffer A. Fractions containing AntAB were pooled, desalted and concentrated by ultrafiltration to ~2 mL (Amicon YM10 membrane). The concentrated mixture was applied to a 2 x 8-cm Mono Q anion-exchange column (Amersham Pharmacia Biotech) equilibrated in buffer A. The column was washed with 50 mL of buffer A and bound AntAB was eluted with a 250-mL linear gradient of NaCl (0-1 M) in buffer A. Fractions containing AntAB were pooled and concentrated by ultrafiltration to ~2 mL and applied to a HiPrep 16/60 Sephacryl S300 column (Amersham Pharmacia Biotech) equilibrated in buffer A containing 250 mM NaCl. The column was eluted at a flow rate of 0.5 mL/min. The eluted fractions containing AntAB were pooled and concentrated by ultrafiltration

(YM10 membrane) to ~2 mL and stored at –80 ºC in 100 μL aliquots. Approximately 15 mg of purified enzyme per liter of *E. coli* culture was obtained for the both wild type and D218 variant AntABs.

Purification of AntC

The procedure described below is modified from that described earlier (*9*). AntC was isolated from 6 X 1-L cell-free extracts at 4 ºC under low light conditions to minimize loss of flavin (*9*). Fractions containing AntC were readily visualized by their bright orange color. Anion-exchange chromatography followed the same procedure described above for AntAB. Size-exclusion chromatography was performed as described for AntAB using a HiPrep 16/60 Sephacryl S100 (Amersham Pharmacia Biotech) column. Purified AntC was dialyzed against buffer A containing 1 mM FAD (4 L x 12 hrs) and then dialyzed against buffer A (4 L x 12 hrs). The purified flavin-reconstituted AntC was concentrated by ultrafiltration (YM10 membrane) to ~2 mL and stored at -80 ºC in aliquots. Approximately 12 mg of purified AntC was obtained per liter of *E. coli* culture.

Activity assays

The concentrations of AntAB, the D218A AntAB and AntC were routinely determined spectrophotometrically (AntAB, ε_{454}=14.4 $mM^{-1}cm^{-1}$; D218A AntAB, ε_{454}=14.9 $mM^{-1}cm^{-1}$; AntC, ε_{450}=22 $mM^{-1}cm^{-1}$). Substrate-dependent O_2 and NADH consumption activities of wild type and variant AntABs and AntC activities were measured as previously described (*9*). Thin-layer chromatography (TLC) was used to identify catechol produced in more concentrated AntDO assay mixtures: 30 μM in wild type or variant AntAB $\alpha_3\beta_3$ combined with 5 μM AntC, 1 mM anthranilate, 1 mM

NADH, in 50 mM MES, 100 mM KCl pH 6.3. After one-hour incubation at room temperature, assay mixtures were spotted directly on silica gel-coated glass TLC plates, which were then developed with a mobile phase of butanol-acetic acid-water (4:1:4, vol/vol/vol). Catechol was visualized on the TLC plates by staining with 20 % phosphomolybdic acid in ethanol (weight/volume) (*16*). Products from single turnover assays were detected using HPLC as follows. AntAB or D218A AntAB (50 μM mononuclear sites each) were reduced anaerobically in buffer A (0.5 mL) by careful anaerobic spectrophotometric titration with NADH in the presence of 0.3 μM AntC and anthranilate (0.2 mM). An equal volume of O_2-saturated buffer A was added (0.5 mL) and the reaction was allowed to proceed for 30 min followed by addition of concentrated phosphoric acid (100 μL) or trichloroacetic acid to a final concentration of 1 %. Products were detected by HPLC as previously described (*9*).

Removal and reconstitution of the mononuclear site iron

In order to remove a portion of apparently unreducible mononuclear iron, the mononuclear iron of either wild type or D218A AntAB (~10 mL of 100 μM $\alpha_3\beta_3$) was completely removed by dialysis against buffer A containing 5 mM EDTA (4 L x 12 hrs) at 4 °C. The resulting enzyme (apoAntAB or apoD218A AntAB) was exchanged into buffer A by repetitive concentration and dilution by ultrafiltration in a 50 mL Amicon cell (YM10 membrane). Iron/protein analyses, retention of the Rieske EPR signal, and loss of catalytic activity (for wild type AntAB) were used to verify removal of only the mononuclear site iron. The mononuclear site was then reconstituted as follows. ApoAntAB (200 μM $\alpha_3\beta_3$) (or apoD218A AntAB) in buffer A (2 mL) was made anaerobic by purging with nitrogen gas. Nine-tenths to one molar equivalent of either

Fe(II) or Co(II) per AntA mononuclear site (quantitated from the Bio-Rad protein assay) was added from anaerobic 10-mM stock solutions of either ferrous ammonium sulfate or cobaltous chloride.

Nitric oxide adducts of AntAB and D218A AntAB

All steps were carried out using anaerobic solutions and gas-tight syringes. Iron-reconstituted AntAB (165 μM $\alpha_3\beta_3$) or D218A AntAB (150 μM $\alpha_3\beta_3$) in buffer A (using 0.9 molar equivalents of Fe(II) per mononuclear site) was divided into two portions and anthranilate from an anaerobic stock solution was added to a final concentration of 1 mM to one portion. Diethylammonium (Z)-1-(*N*,*N*-diethlyamino)diazen-1-ium-1,2-diolate (DEAENONOate) (Cayman Chemicals) from a 25 mM stock solution in 0.01 M NaOH was added to both portions to a final concentration of 1 mM. DEAENONOate is stable at high pH but decomposes to release NO gas at ~pH 7. The samples were incubated for ~30 min before being transferred via gas-tight syringe to EPR tubes and frozen in liquid nitrogen.

Stopped-flow spectrophotometry

Reduction of apoAntAB (12 μM $\alpha_3\beta_3$) and apoD218A AntAB (16 μM $\alpha_3\beta_3$) in buffer A (2 mL) was accomplished by careful anaerobic spectrophotometric titration with NADH in the presence of 0.1 μM AntC. The titrations were continued until the UV-vis absorption spectra of Rieske-reduced AntAB or D218A AntAB were reached and no additional absorbance at 340 nm was observed due to excess NADH. Where appropriate, anthranilate was added to a final concentration of 0.2 mM and one molar equivalent of iron(II) or cobalt(II) was added to reconstitute empty mononuclear sites. Stopped-flow spectrophotometry was performed on an RSM 1000 rapid-scanning spectrophotometer

(OLIS Inc., Bogart, Ga). One syringe was made anaerobic and loaded with 1 mL of reduced wild type or variant AntAB solution and the other syringe was loaded with an equal volume of O_2-saturated buffer A (~1.2 mM O_2 at 23 °C). Following stopped-flow mixing, the reaction was monitored with a diode array spectrophotometric detector and the absorbance versus time data were analyzed using software supplied by OLIS Inc.

H_2O_2 detection upon reoxidation of wild type and D218A AntAB in the presence of anthranilate

AntAB (12 μM $\alpha_3\beta_3$) or D218A AntAB (16 μM $\alpha_3\beta_3$) samples were reduced anaerobically in the presence of 200 μM anthranilate, as described above (see "stopped-flow spectrophotometry" section), and then reoxidized by rapid manual mixing with an equal volume of O_2-saturated buffer A. H_2O_2 was detected by the method of Atkins and Sligar (*16*). Briefly, 2 mL of ice-cold 3 % trichloroacetic acid was added to 1 mL of reoxidized protein (approximately 2 min after the addition of O_2-saturated buffer A). After 15 min, the precipitated protein was removed by centrifugation and 1 mL of the supernatant was added to 1 mL of 10 mM ferrous ammonium sulfate and 200 μL of 0.5 M potassium thiocyanate. After 2 min, the A_{480} was measured and the concentration of H_2O_2 was determined from a standard curve of known H_2O_2 concentrations. This procedure was repeated with AntAB samples that had been allowed to reoxidize for 30 min.

Other spectroscopies

EPR spectra were recorded on a Bruker ESP-300E spectrometer equipped with an ER-4116 dual-mode cavity and an Oxford Instruments ESR-9 flow cryostat. Ultraviolet-

visible absorption spectra were obtained in 1-cm pathlength quartz cuvettes on a Shimadzu UV-2401PC scanning spectrophotometer.

Results

Lack of growth of D218A AntAB *Acinetobacter* ADP1 strain

The mutant strain ACN476 grew identically to the wild type ADP1 strain on succinate minimal medium (*15*) at either 37 ºC or room temperature, but, unlike the wild type, this mutant strain failed to grow on anthranilate minimal medium (*14*) either at 37 ºC or room temperature, either in liquid culture or on agar plates. Presumably, D218A AntAB is expressed in this mutant strain, but is insufficiently active to sustain growth on anthranilate. The ability of ACN476 to grow with benzoate as the sole carbon source demonstrates that the genes required for the degradation of catechol via the *ortho* pathway are functional (cf. Figure 2.2).

Expression, purification and characterization of D218 AntAB variants

As noted previously (*9*), expression of enzymatically active recombinant ADP1 AntAB in *E. coli* could be qualitatively detected as gradual formation of an unidentified purple iron-catechol complex in cultures containing added anthranilate (~2 mM) and ferrous iron. Apparently, an *E. coli* reductase is able to supply electrons to AntAB for this conversion in the absence of its native reductase component, AntC. No such color change was observed in the induced *E. coli* cultures containing plasmids encoding D218A, -N or –E AntABs respectively, qualitatively indicating a diminished ability of these cultures to convert anthranilate to catechol. SDS-PAGE of cell extracts of the *E. coli* cultures expressing the D218 variant AntABs showed the presence of two prominent

bands corresponding to the expected sizes of the α (54 kDa) and β (19 kDa) subunits of AntAB, as shown for the D218A AntAB-expressing culture in Figure 4.2. Therefore, the apparent lack of AntDO activity in *E. coli* cultures containing plasmids encoding the D218 variant AntABs is not due to lack of expression of the recombinant enzymes. The analogous procedures that were used to express and purify wild type AntAB gave approximately the same yields of D218 variant AntABs.

Table 4.1 compares the properties of purified wild type and D218 variant AntABs. Size-exclusion chromatography of purified D218A, -N and –E AntABs gave molecular masses indistinguishable from that of wild type AntAB, i.e., ~220 kDa, indicating that the D218 variants retained the $\alpha_3\beta_3$ hexameric quaternary structure. Iron analyses of D218A and D218N AntAB showed ~9 Fe/$\alpha_3\beta_3$ (cf. Table 4.1), respectively, indicating full occupancy of the Rieske and mononuclear sites by iron, as was found previously for the recombinant wild type AntAB (*9*). Iron analysis of the D218E AntAB gave ~6 Fe/$\alpha_3\beta_3$, indicating (together with the UV-vis absorption spectra) that the mononuclear iron sites were not occupied by iron. Neither the wild type nor any of the D218 variant AntABs contained other transition metals in mol ratios exceeding 0.2 metal/$\alpha_3\beta_3$.

Spectroscopic properties of D218 variant AntABs

The near UV-visible absorption spectra of wild type and D218A AntABs in their as-isolated forms, are shown in Figure 4.3. The visible absorption spectrum of wild type AntAB is due to the oxidized ($[2Fe\text{-}2S]^{2+}$) Rieske center. In the corresponding D218A AntAB spectrum, the broad absorption maximum of wild type AntAB at ~454 nm has partially resolved into two features with maxima at ~419 nm and ~474 nm. In addition,

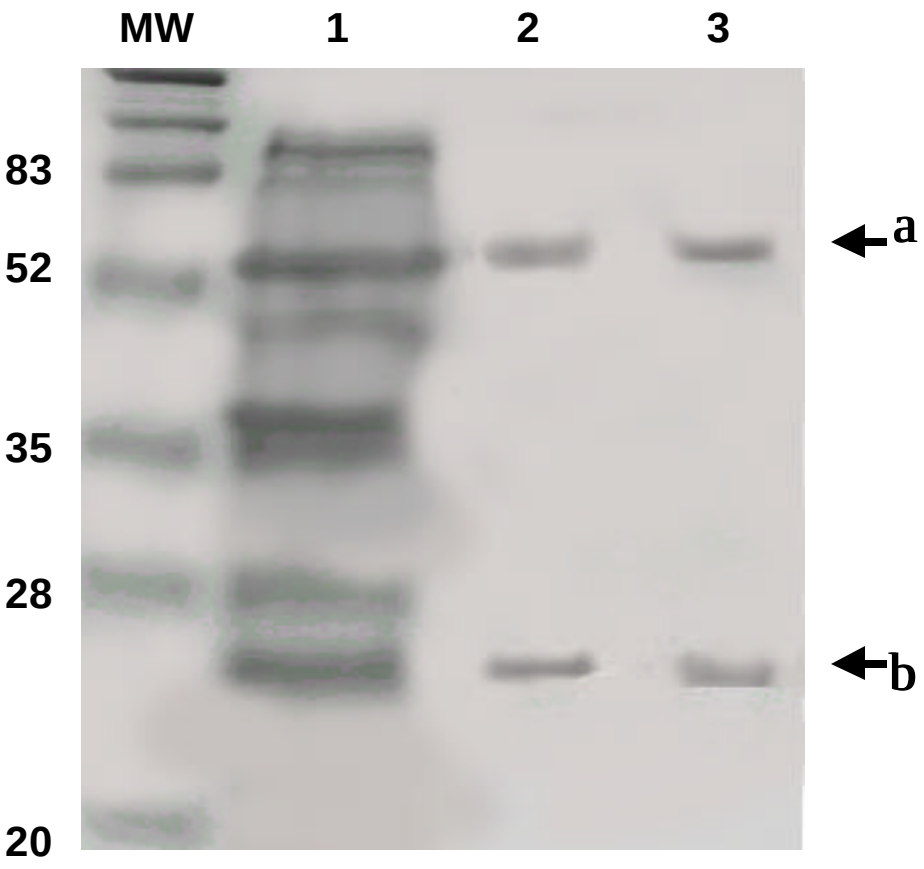

Figure 4.2. SDS-PAGE monitoring expression and purification of recombinant wild type and D218A AntABs from *E. coli* BL21-Codon Plus. Lane 1, crude cell extract containing D218A AntAB; lane 2, purified wild type; lane 3, purified D218A AntAB. Numbers at left indicate molecular masses (kDa) corresponding to the adjacent markers (lane MW). Arrows indicate positions of the α and β subunits.

Table 4.1. Properties of recombinant *Acinetobacter* sp. ADP1 AntAB, D218 variants, and AntA.[a]

	molecular weight (kDa)		iron/ protein[b]	UV/vis, nm(ε, $mM^{-1}cm^{-1}$)[b]	Rieske EPR g values	specific activities[d] (μM/5 min)	
	SDS-PAGE	Gel Filtration				NADH	O_2
Wild type AntAB	52 (α) 24 (β)	220	8.8±1.0	320(31) 454(14.4) 555 (7)	2.01 1.93 1.80	190 ± 10	200 ± 7
D218A AntAB	52 (α) 24 (β)	220	9.2±0.7	320 (36) 419(17.6) 454 (14.9) 474 (16) 555(9.6)	2.01 1.93 1.80	0	0
D218N AntAB	52 (α) 24 (β)	220	8.7±0.7	N.D.[c]	N.D.[c]	0	0
D218E AntAB	52 (α) 24 (β)	220	5.8±1.2	N.D.[c]	N.D.[c]	0	0

[a]Data from this work, except for wild type AntAB, which are taken from Eby et al. (*9*), described in Chapter 3.

[b]Per $\alpha_3\beta_3$, as isolated.

[c]Not determined.

[d]Assay conditions: 100 μM NADH, 250 μM O_2, 500 μM anthranilate, 0.5 μM oxygenase $\alpha_3\beta_3$ or α_3, 0.18 μM AntC, and in 50 mM MES, 100 mM KCl (pH 6.3) at room temperature (~23 °C). NADH consumption activity was monitored as $\Delta A_{340\ nm}$ and reported as μM NADH oxidized/5 minutes/μM oxygenase $\alpha_3\beta_3$. O_2 consumption was monitored with an O_2 electrode and reported as μM O_2 consumed/5 minutes/μM oxygenase $\alpha_3\beta_3$ or α_3. Listed activities are the averages of three determinations.

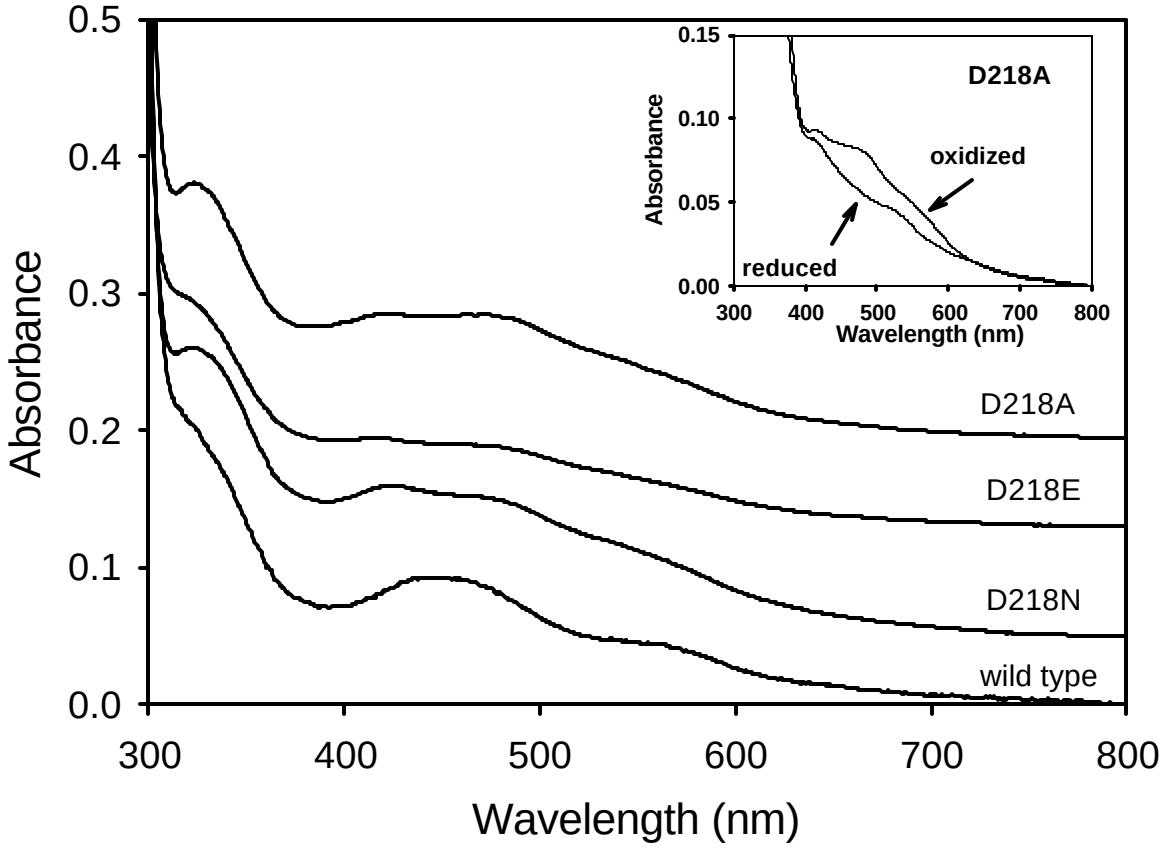

Figure 4.3. UV-visible absorption spectra of as-isolated wild type AntAB (7 μM $\alpha_3\beta_3$), D218A AntAB (6 μM $\alpha_3\beta_3$), D218E AntAB (4 μM $\alpha_3\beta_3$), and D218N AntAB (7 μM $\alpha_3\beta_3$) in buffer A. Spectra of variants are offset vertically for clarity. **Inset:** UV-visible absorption spectra of oxidized and enzymatically reduced D218A AntAB (6 μM $\alpha_3\beta_3$) by AntC (1 μM) and NADH (50 μM) in buffer A. Absorption features below 400 nm are obscured by the absorbance of NADH. The reduction was performed anaerobically.

the shoulders at ~320 nm and ~550 nm in the wild type AntAB spectrum have become better and less well defined, respectively, in the D218A AntAB spectrum. The same absorption spectral perturbations were found for the D218N and -E variants. Addition of ferricyanide to the as-isolated D218A AntAB did not result in any changes in the absorption spectrum of the Rieske center, indicating that the spectral perturbation relative to wild type is not due to partial reduction of the Rieske center. Also, the EPR spectrum of as-isolated D218A AntAB (Figure 4.4) (without any added reducing or oxidizing agents) shows essentially no reduced Rieske sites and only a small g = 4.3 signal. The 4-K EPR spectrum of dithionite-reduced D218A AntAB (Figure 4.4) showed *g*-values identical to those of reduced wild type AntAB at 2.01, 1.93, and 1.80, which are characteristic of Rieske-type $[2Fe\text{-}2S]^{+}$ centers. Thus, the visible absorption spectrum of the oxidized Rieske site in AntAB was perturbed upon mutation of Asp218, whereas the reduced-Rieske visible absorption and EPR spectra were not detectably perturbed. As shown in the inset to Figure 4.3, the Rieske site of D218A AntAB could be reduced anaerobically with a catalytic amount of AntC and excess NADH, resulting in a spectrum with significantly decreased absorption between 400 nm and 600 nm, and which is essentially identical to that of reduced ($[2Fe\text{-}2S]^{+}$) wild type AntAB (*9*). Essentially identical absorption spectral changes occurred for D218N and -E AntABs when they were anaerobically treated with the same amounts of NADH and AntC (not shown). These results demonstrate that electron transfer from AntC to the Rieske sites remains intact in the D218 variant AntABs.

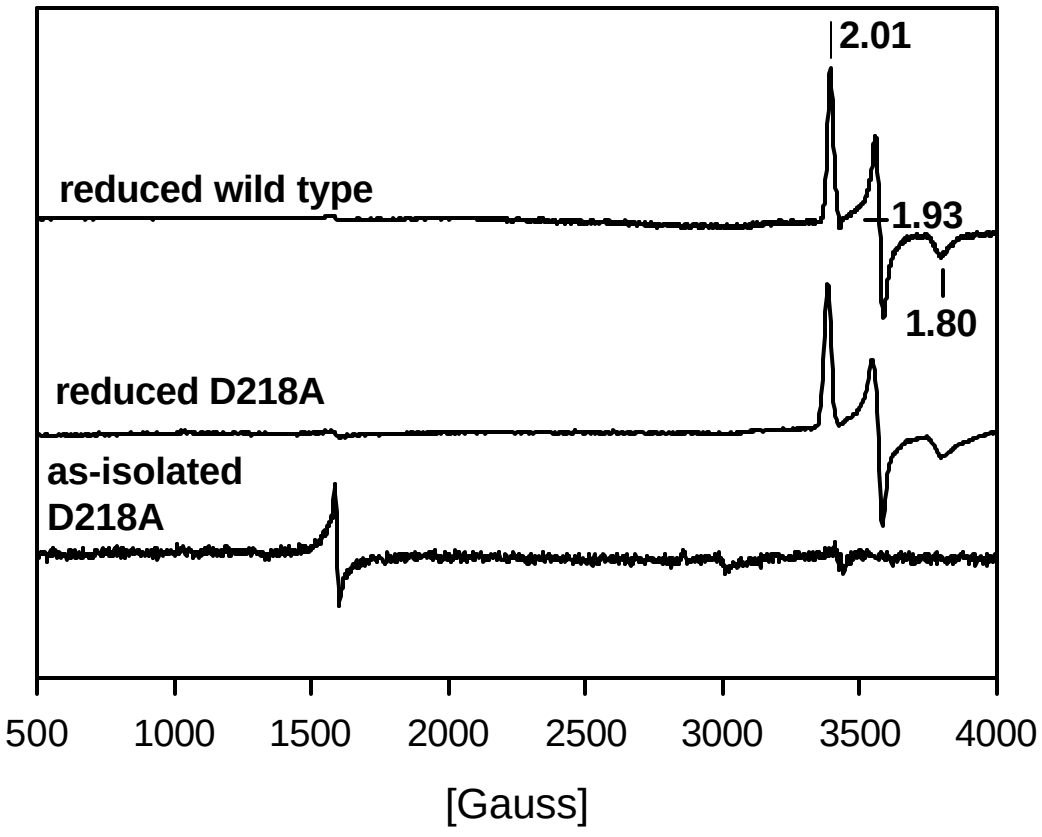

Figure 4.4. EPR spectra of dithionite-reduced wild type AntAB (250 μM $\alpha_3\beta_3$), dithionite-reduced D218A AntAB (200 μM $\alpha_3\beta_3$) and D218A AntAB as-isolated (200 μM $\alpha_3\beta_3$) all in buffer A. Samples were prepared as described in the Experimental section. EPR conditions: temperature, 10K; microwave frequency, 9.60 GHz; modulation amplitude, 6.366 G; microwave power, 2 mW.

Activities of D218 variant AntABs

Activities of the D218 variant AntABs were measured by monitoring the anthranilate-dependent oxidation of NADH under conditions previously optimized for wild type AntAB (*9*). The conversion of anthranilate to catechol by wild type AntDO under these assay conditions is a tightly coupled two-electron process in which NADH, O_2 and anthranilate are consumed to form catechol in a 1:1:1:1 molar stoichiometry. Under these conditions (0.5 μM AntAB $\alpha_3\beta_3$, 0.2 μM AntC, 0.5 mM anthranilate, and 100 μM NADH in 50 mM MES and 100 mM KCl, pH 6.3), wild type AntAB oxidized 40 μM NADH/min/μM AntAB $\alpha_3\beta_3$ (cf. Chapter 3). Under the same conditions none of the D218 variant AntABs showed any detectable NADH consumption, O_2 consumption, or catechol formation, i.e., none of the D218 variants showed any evidence of anthranilate dioxygenase activity. Omission of anthranilate also did not result in any detectable NADH consumption, i.e., the D218 variant AntABs also showed no uncoupled NADH oxidase activity. The absorption spectra in the inset to Figure 4.3 verify that this lack of activity is not due to an inability of AntC to reduce the Rieske sites of D218A AntAB. Addition of ferrous iron (100 μM) did not stimulate any NADH oxygenase or oxidase activity of the D218 variant AntABs in either the presence or absence of anthranilate. D218A AntAB activity assays were conducted with the same enzyme and reagent concentrations listed above at pH 5.5, 6, 6.5, 7, 8, and 9, and no NADH consumption was observed at any of these pHs. Solutions containing up to 30 μM D218A AntAB $\alpha_3\beta_3$, catalytic AntC and excess NADH qualitatively showed no catechol formation when reaction mixtures were spotted on TLC plates after ~1 hour incubation at

room temperature. Under analogous conditions, catechol could be readily visually detected for wild type AntAB by TLC.

Nitrosyl adducts of wild type and D218A AntABs

To more directly probe O_2 and substrate access to the mononuclear Fe(II) site, nitric oxide adducts of the wild type and D218A AntAB were generated both in the presence and absence of anthranilate. Nitric oxide has been employed as an O_2-mimic in other non-heme iron dioxygenases, where it reacts with mononuclear ferrous centers to yield EPR-active S=3/2 $[FeNO]^7$ complexes (*17-20*). Prior to formation of the NO adducts, iron was removed from the mononuclear sites of both wild type AntAB and D218A AntAB by dialysis against EDTA, and then reconstituted by anaerobic addition of 0.9 molar equivalents of ferrous iron. ApoAntAB and apoD218A AntAB showed no activity under standard assay conditions. Iron-reconstituted AntAB, however, showed the same activity (40 μM NADH oxidized/min/μM AntAB) as the as-isolated AntAB. Iron-reconstituted D218A AntAB, cobalt-reconstituted AntAB, and cobalt-reconstituted D218A AntAB showed no activity under standard assay conditions. The iron removal/reconstitution procedure was carried out in order to ensure that essentially all mononuclear sites were occupied and in the ferrous form. This procedure was found to minimize an interfering EPR resonance at g=4.3 in the as-isolated AntAB, which is presumably due either to adventitiously bound Fe(III) or to a minor portion of irreversibly oxidized mononuclear sites. Reconstitution of apoAntAB or apoD218A AntAB with Fe(II) followed by anaerobic exposure to NO yielded adducts showing nearly axial EPR spectra near g = 4 consistent with the expected S=3/2 species (Figure

Figure 4.5. EPR spectra of wild type AntAB-nitrosyl complexes (165 μM $\alpha_3\beta_3$) (top panel) and D218A AntAB-nitrosyl complexes (150 μM $\alpha_3\beta_3$) (bottom panel) in the absence and presence of anthranilate (1 mM) in buffer A (top panel). EPR conditions: temperature, 4K; microwave frequency, 9.59 GHz; modulation amplitude, 6.366 G; microwave power, 2 mW.

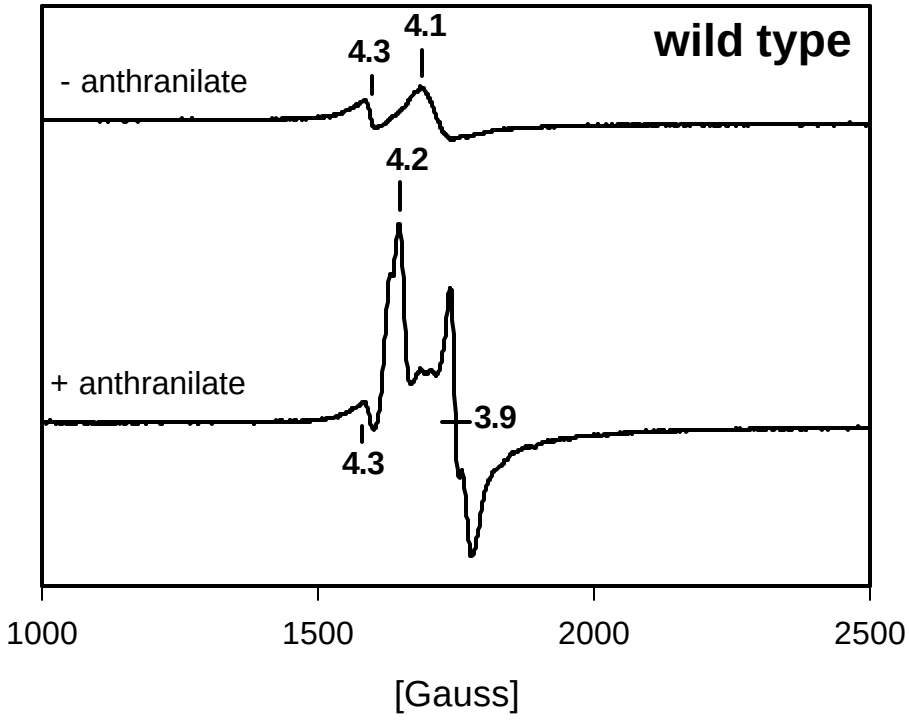
wild type
4.1
4.3
- anthranilate
4.2
+ anthranilate
3.9
4.3
1000
1500
2000
2500
[Gauss]

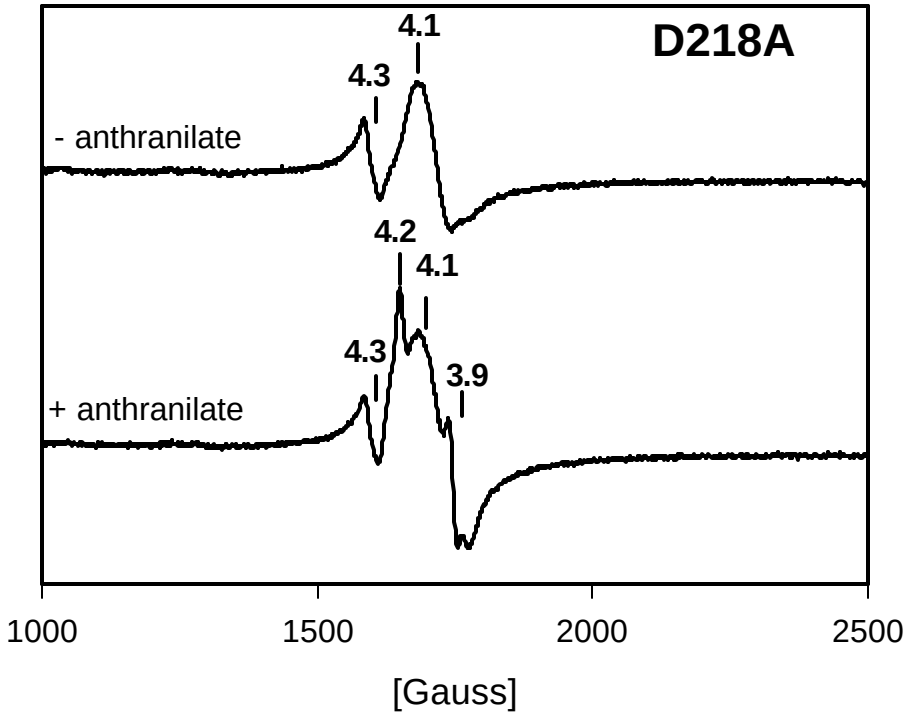
D218A
4.1
4.3
- anthranilate
4.2
4.1
4.3
3.9
+ anthranilate
1000
1500
2000
2500
[Gauss]

4.5 spectra labeled "- anthranilate"), and a weak residual Fe(III) signal at g = 4.3. Upon addition of anthranilate, the spectra of both enzymes became distinctly rhombic (Figure 4.5 spectra labeled "+ anthranilate"). At least two S=3/2, substrate-perturbed spectral components are observed in both cases. The EPR spectrum of the D218A AntAB/anthranilate/NO sample appeared to retain a significant portion of the substrate-free component, most likely indicating that 1 mM anthranilate was insufficient to saturate the substrate binding site. Alternatively, the concentration of anthranilate used may be sufficient to saturate the substrate binding site but this binding does not perturb most of the $[FeNO]^7$ complex at the D218A AntAB mononuclear site. Either way, the D218A substitution does not appear to greatly perturb the ligand environment of the NO-bound mononuclear site in the substrate free form. For both wild type and D218A AntAB, at least one coordination site on the mononuclear Fe(II) can be occupied by NO, and a NO coordination site remains available, but is perturbed to some extent upon binding of substrate. The EPR signal of the wild type "+ anthranilate" NO adduct appears to be significantly larger than the "-anthranilate" signals, implying that substrate binding increases access of NO to the mononuclear site. This increased signal intensity is not apparent in the case of D218A AntAB. The EPR spectra in Figure 4.5 are of Rieske-oxidized enzymes. Analogous EPR experiments on NO-reacted Rieske-reduced enzymes showed considerably different $[FeNO]^7$ EPR signals for wild type and D218A AntABs, but neither signal was perturbed by substrate addition (Figure 4.6). The D218A Rieske-reduced $[FeNO]^7$ signal closely resembled the substrate-free signal in Figure 4.5 and also appears to be much less intense than the corresponding wild type signals in Figure 4.6.

Figure 4.6. EPR spectra of enzymatically reduced wild type AntAB-nitrosyl complexes (200 μM $\alpha_3\beta_3$) (top panel) and enzymatically reduced D218A AntAB-nitrosyl complexes (125 μM $\alpha_3\beta_3$) (bottom panel) in the absence and presence of anthranilate (1 mM) in buffer A. EPR conditions: temperature, 10K; microwave frequency, 9.60 GHz; modulation amplitude, 6.366 G; microwave power, 2 mW.

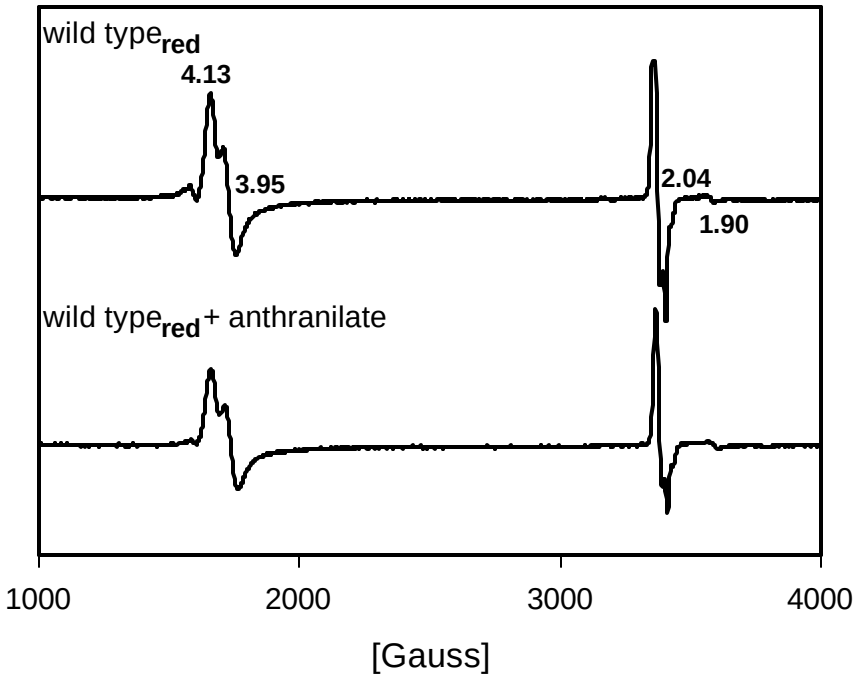
wild type red
4.13
3.95
2.04
1.90
wild type red + anthranilate
1000
2000
3000
4000
[Gauss]

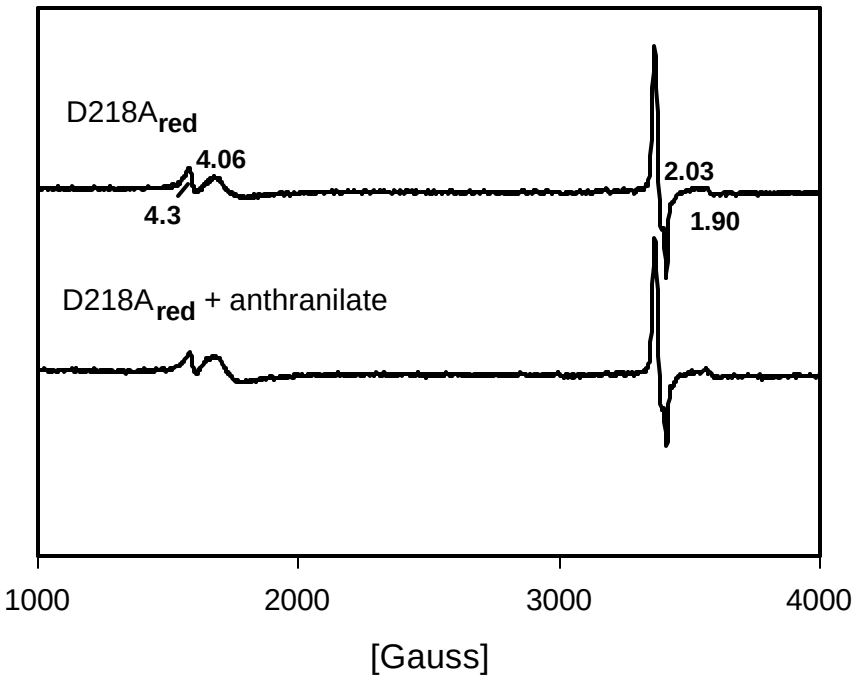
D218A red
4.06
4.3
2.03
1.90
D218A red + anthranilate
1000
2000
3000
4000
[Gauss]

However, these EPR spectra also showed that NO reacted with the reduced Rieske sites, as has been reported for NDO and benzoate 1,2-dioxygenase (*18*). This reaction complicates interpretation of NO binding to the mononuclear sites when the Rieske sites are reduced.

O_2 re-oxidation of wild type and D218A AntABs

In order to determine whether the D218 substitution affects electron transfer from the reduced Rieske to the mononuclear iron sites of AntAB, oxidations of enzymatically reduced wild type and D218A AntABs were monitored by stopped-flow spectrophotometry. Reduction under anaerobic conditions was monitored by titration of the Rieske absorption spectrum with NADH in the presence of catalytic amounts of AntC. The time courses for reoxidation of the reduced Rieske sites upon rapid mixing with O_2-saturated buffer were then monitored by the increase in absorbance at 454 nm. The following sets of conditions were examined: Fe(II)-reconstituted mononuclear sites with and without anthranilate; apoAntAB and apoD218A AntAB with anthranilate, and cobalt(II)-reconstituted mononuclear sites with and without anthranilate all in buffer A. Cobalt(II) incorporation into the mononuclear site of apoAntAB was confirmed using cobalt- X-ray absorption spectroscopy (R. A. Scott, N. Cosper, D. M. Eby, E D. Coulter, Z. Beharry, E. Neidle, D. M. Kurtz, Jr., unpublished results). The spectral changes at 454 nm following stopped-flow mixing of Fe(II)-reconstituted, Rieske-reduced wild type or D218A AntAB solutions containing 100 μM anthranilate (which is well above saturating for wild type AntDO turnover (*9*)) with excess O_2 are shown in Figure 4.7. Approximately 46 % and 31 % (using ε_{454}) of the Rieske sites, respectively, were oxidized within the mixing time (~1-2 msec) followed by a slower phase of oxidation

Figure 4.7. Kinetic traces monitoring absorbance at 454 nm following stopped-flow mixing of one-electron enzymatically reduced iron-reconstituted wild type or D218A AntAB solutions containing either no anthranilate (-anthranilate) or 200 μM anthranilate with saturated O_2 solutions. All solutions were in buffer A. All experiments were performed at 25 °C. Concentrations after mixing were: wild type AntAB, 6 μM $\alpha_3\beta_3$; D218A AntAB, 8 μM $\alpha_3\beta_3$; anthranilate (when present), 100 μM; O_2, 600 μM. The left and right panels show initial portions of time courses spanning 2 sec and 10 minutes, respectively. Filled circles in the left panels represent the absorbance of the reduced Rieske sites determined by stopped-flow mixing the same solutions of reduced AntABs with the same volumes of anaerobic buffer A used for the reaction with O_2. Filled circles in the right panels indicate the absorbance of fully reoxidized Rieske sites.

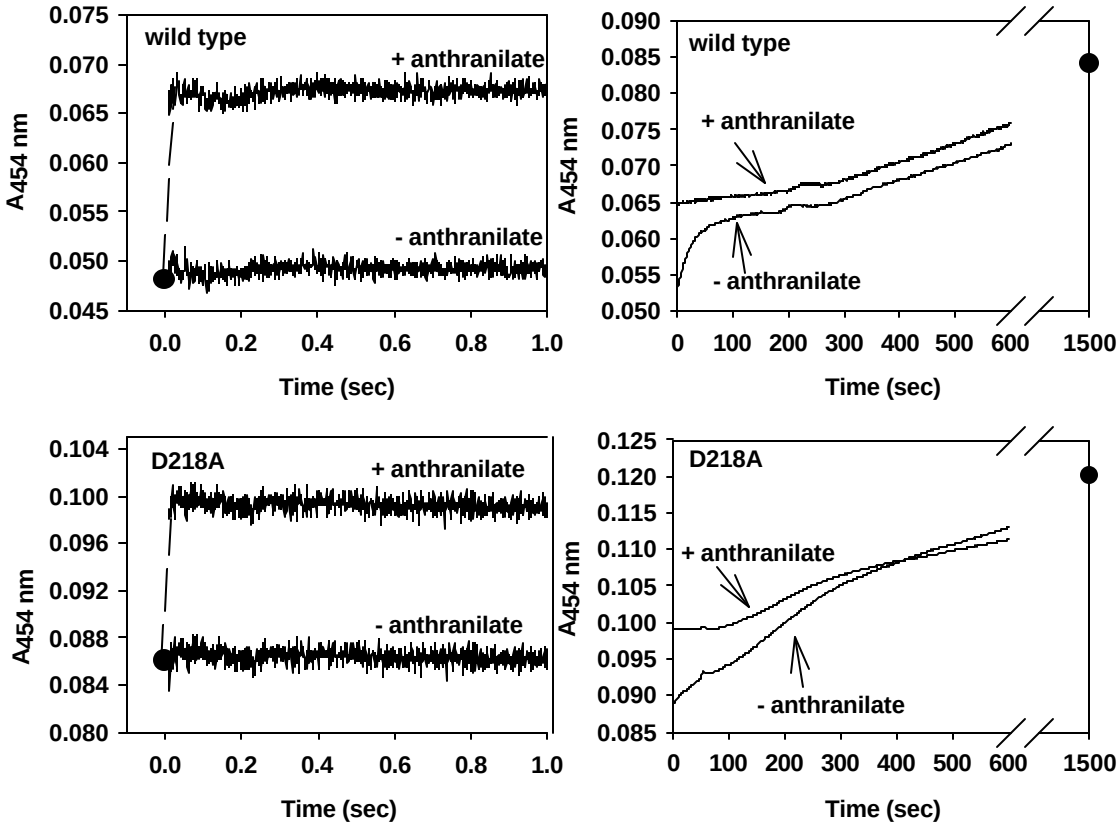
wild type
+ anthranilate
- anthranilate
A454 nm
Time (sec)
0.075
0.070
0.065
0.060
0.055
0.050
0.045
0.0
0.2
0.4
0.6
0.8
1.0
0.090
0.085
0.080
0.075
0.070
0.065
0.060
0.055
0.050
0
100
200
300
400
500
600
1500
D218A
0.104
0.100
0.096
0.092
0.088
0.084
0.080
0.125
0.120
0.115
0.110
0.105
0.100
0.095
0.090
0.085

which could be fit to first order rate constants of 0.005 s^{-1} for wild type AntAB and 0.003 s^{-1} for D218A AntAB. In analogous stopped-flow experiments, the initial fast phase of Rieske oxidation (i.e., within the mixing dead time) for the Fe(II)-reconstituted AntABs was not observed without anthranilate (cf. Figure 4.7) or for the apoAntABs in the presence of 100 μM anthranilate, or the cobalt(II)-substituted AntABs with or without anthranilate (Figure 4.8). All of these latter samples showed two phases of A_{454} increases which could be fit to first order rate constants of ~0.04 s^{-1} and 0.002 s^{-1} for wild type AntAB and 0.01 s^{-1} and 0.004 s^{-1} for D218A AntAB (Figure 4.7). These results demonstrate that the fast phase of reduced Rieske site oxidation by O_2 (~>350 s^{-1}) observed for both wild type AntAB and D218A AntAB requires the presence of both Fe(II) and anthranilate at the mononuclear sites. The enzymatically reduced Rieske sites of both wild type and D218A AntABs could undergo a second cycle of reduction and re-oxidation by O_2. Samples that had undergone Rieske-site re-oxidations by O_2 as described above were made anaerobic and stoichiometrically re-reduced by NADH/AntC. Re-mixing of these solutions with O_2-saturated buffer gave similar percentages of rapid and slower phases of Rieske center re-oxidation to those described above. O_2-reoxidation assays in the presence of anthranilate by manual mixing of more concentrated as-isolated AntAB and D218A AntAB (~9 Fe/$\alpha_3\beta_3$) showed similar results obtained using stopped-flow spectrophotometry and iron-reconstituted enzyme (Figure 4.9). The substrate-dependent rapid re-oxidation of only a portion of the Rieske sites during a rapid phase followed by a slower phase for oxidation of the remaining Rieske sites parallels the behavior seen for single turnovers of chemically reduced NDO (*18*). This behavior in NDO was attributed to partial occupancy of the mononuclear sites by iron. The metal

Figure 4.8. Kinetic traces monitoring absorbance at 454 nm following stopped-flow mixing of one-electron enzymatically reduced apoAntAB or cobalt-reconstituted AntAB with 200 μM anthranilate with O_2 saturated solutions (top panel) and one-electron enzymatically reduced apoD218A AntAB or cobalt-reconstituted D218A AntAB with 200 μM anthranilate with O_2 saturated solutions (bottom panel). All solutions were in buffer A. All experiments were performed at 25 °C. Concentrations after mixing were: AntAB, 6 μM $\alpha_3\beta_3$; D218A AntAB, 8 μM $\alpha_3\beta_3$; anthranilate, 100 μM; O_2, 600 μM. Filled circles represent the absorbance after the rapid absorbance increase of iron-reconstituted wild type AntAB or D218A AntAB following stopped-flow mixing with O_2-saturated buffer A in the presence of anthranilate (cf. Figure 4.9).

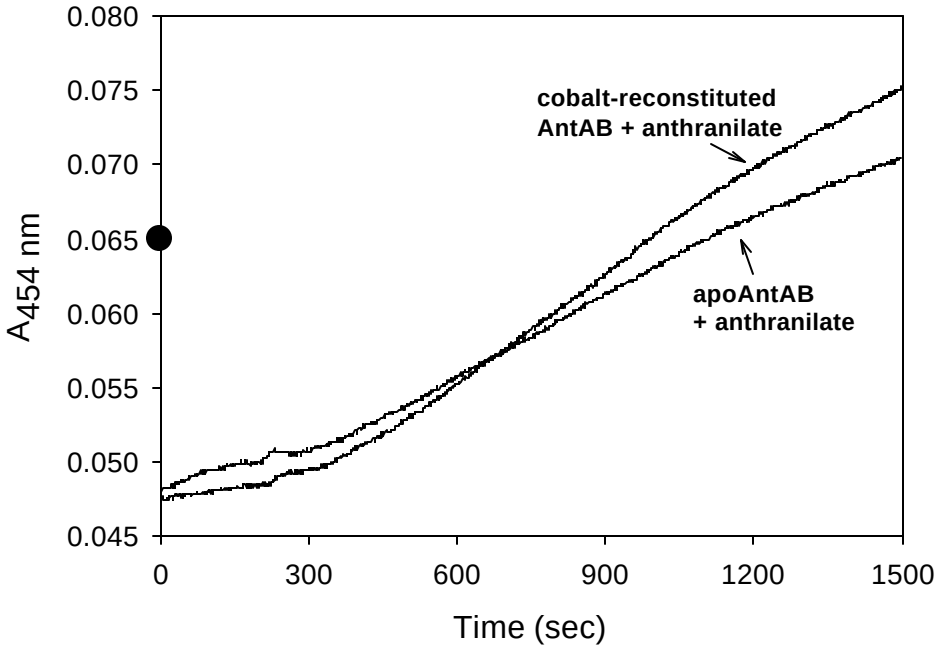
0.080
0.075
0.070
0.065
0.060
0.055
0.050
0.045
A454 nm
cobalt-reconstituted
AntAB + anthranilate
apoAntAB
+ anthranilate
0
300
600
900
1200
1500
Time (sec)

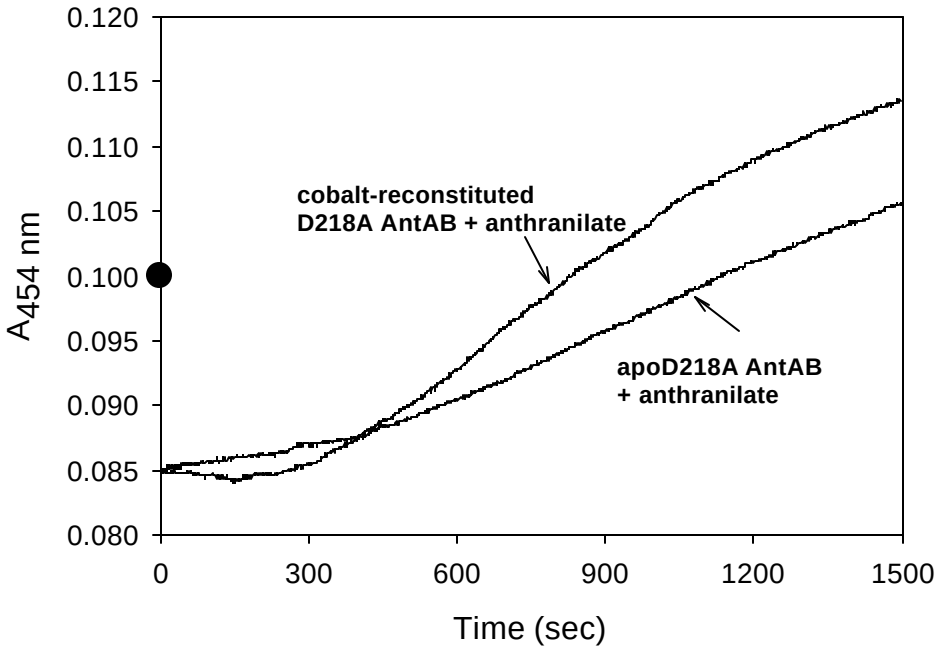
0.120
0.115
0.110
0.105
0.100
0.095
0.090
0.085
0.080
A454 nm
cobalt-reconstituted
D218A AntAB + anthranilate
apoD218A AntAB
+ anthranilate
0
300
600
900
1200
1500
Time (sec)

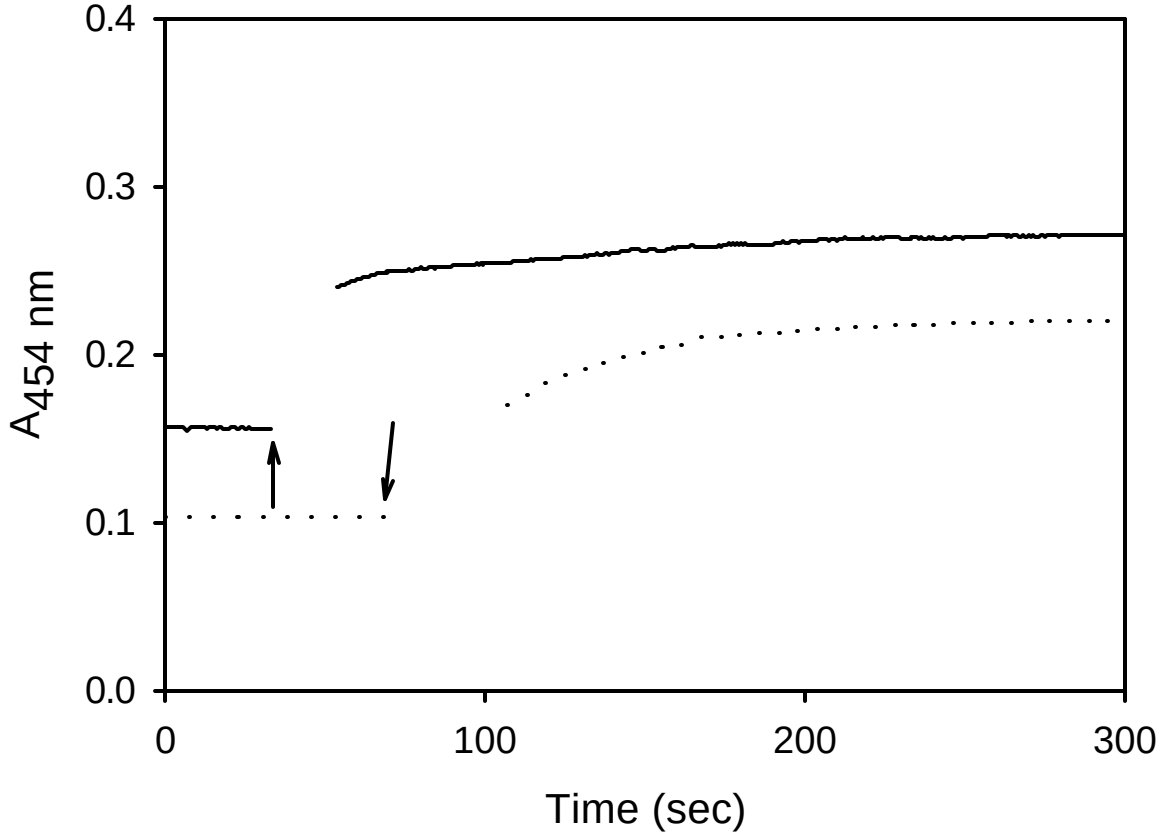

Figure 4.9. Reoxidation of one-electron enzymatically reduced as-isolated wild type (solid line) or as-isolated D218A AntAB (dotted line) in the presence of anthranilate (200 μM) with O_2 saturated solutions performed by manual mixing. All solutions were in buffer A. All experiments were performed at 23 °C. Concentrations after mixing were: wild type AntAB, 20 μM $\alpha_3\beta_3$; D218A AntAB, 16 μM $\alpha_3\beta_3$; anthranilate, 100 μM; O_2, 600 μM. Arrows indicate the times O_2-saturated buffer was added. The traces were corrected for dilution.

analyses of the as-isolated and iron-reconstituted AntAB and D218A AntAB, however, indicate full occupancy of the mononuclear sites. The most important results in the present context are that similar kinetics were observed for Rieske site re-oxidation in both wild type and D218A AntABs and that the rapid phase of this re-oxidation required mononuclear sites occupied by iron.

In order to verify that both Rieske and mononuclear sites had re-oxidized during the single turnovers, analogous reactions of the reduced Rieske sites with O_2 in the presence of anthranilate were monitored by EPR, as shown in Figure 4.10. Enzymatically reduced samples of Fe(II)-reconstituted wild type AntAB and D218A AntAB showed the expected EPR signals due to the reduced Rieske sites and a weak signal at g = 4.3, which may be due to adventitiously bound Fe(III) and/or some Fe(III) remaining unreduced in the mononuclear sites. After 5-minute reactions of the Rieske-reduced AntABs with excess O_2, the Rieske EPR signal had lost most of its intensity, and the g = 4.3 signal had increased in intensity, consistent with Rieske center re-oxidation and concomitant formation of high-spin Fe(III) at the mononuclear sites. These EPR results verify that Rieske and mononuclear site re-oxidations by O_2 exhibit similar kinetics in wild type and D218A AntABs.

No hydrogen peroxide was detected from the reoxidations of NADH/AntC-reduced wild type or D218A AntABs (using the same reaction conditions as outlined for the stopped-flow spectrophotometric experiments, i.e., 8 μM D218A AntAB $\alpha_3\beta_3$, 6 μM AntAB $\alpha_3\beta_3$) either 1 min or 30 min after manual mixing with O_2-saturated buffer A. These reactions would be expected to generate, at most, concentrations of H_2O_2 equal to the concentration of mononuclear sites (i.e., 24 μM for D218A AntAB and 18 μM for

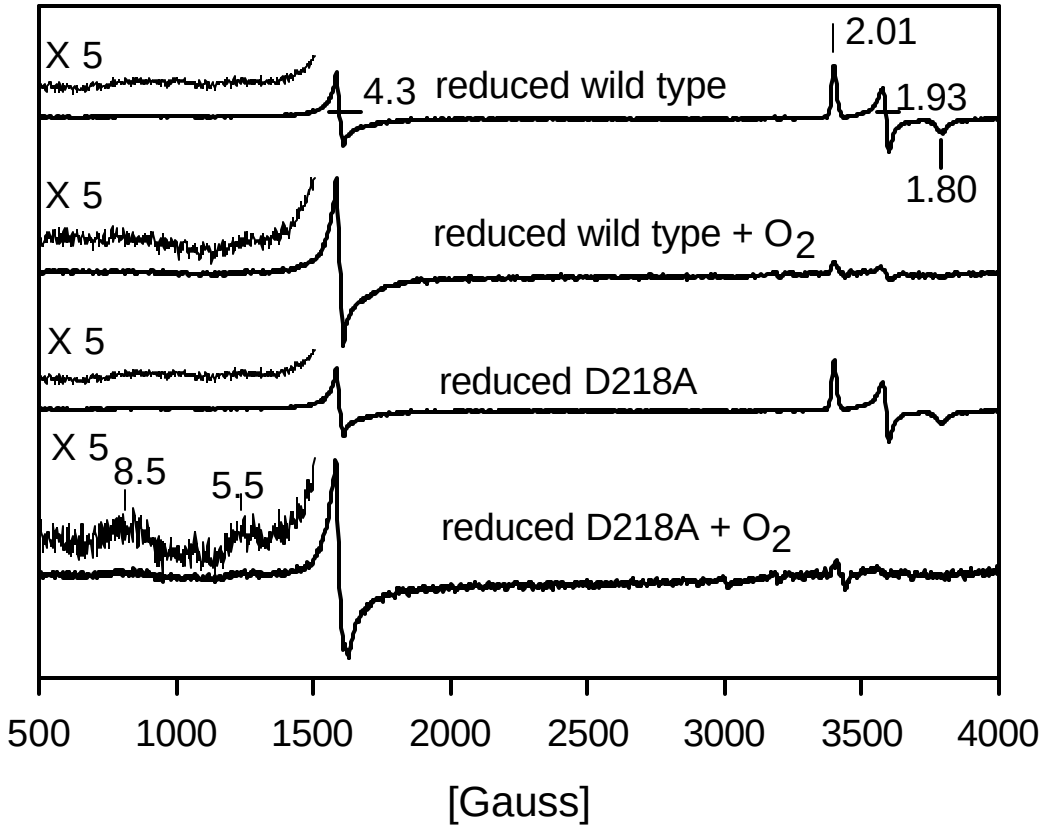

Figure 4.10. EPR spectra of one-electron enzymatically reduced wild type AntAB (200 μM $\alpha_3\beta_3$) and D218A AntAB (125 μM $\alpha_3\beta_3$) in the presence of 10 mM anthranilate in buffer A. The "+ O_2" indicates spectra of the reduced enzyme solutions after mixing with an equal volume of O_2-saturated buffer A and reaction at room temperature for ~5 min. Spectral intensities for the O_2-mixed solutions were corrected for dilution. EPR conditions: temperature, 10K; microwave frequency, 9.60 GHz; modulation amplitude, 6.366 G; microwave power, 2 mW.

antAB). The lower detection limit for H_2O_2 using the method described in experimental was found empirically to be ~5 μM.

The single turnover reoxidation of wild type AntAB (50 μM mononuclear sites) in the presence of anthranilate generated a stoichiometric amount (50 μM) of the expected product catechol, as detected by HPLC (Figure 4.11). The corresponding reoxidation of D218A AntAB, however, showed no catechol formation, but did show accumulation of an unidentified peak in the HPLC chromatogram at a retention time of 2.9 min, indicating product formation (Figure 4.11).

Discussion

Based on the X-ray crystal structure of NDO (cf. Figure 1.9), Asp218 in AntAB was predicted to interact with the Rieske site across the three α/α´ subunit interfaces of the $\alpha_3\beta_3$ oligomer. Since the three D218 variant AntABs retained the $\alpha_3\beta_3$ oligomeric structure of the wild type enzyme, Asp218 cannot play an essential role in maintaining the quaternary structure. On the other hand, the UV-visible absorption spectrum of the oxidized Rieske site of D218A AntAB is perturbed from that of wild type (cf. Figure 4.5), confirming the expected interaction. The reduced Rieske EPR signal, however, is not detectably altered in the D218A variant. These observations could indicate that interactions between the Rieske site and D218 are stronger in the oxidized than reduced form of the Rieske site. Nevertheless, the Rieske sites in the D218 variant AntABs were still able to receive electrons from NADH via the reductase component, AntC.

All three D218 variants were completely inactive both in catalysis of anthranilate 1,2-dihydroxylation and in uncoupled NADH oxidase activity under standard assay

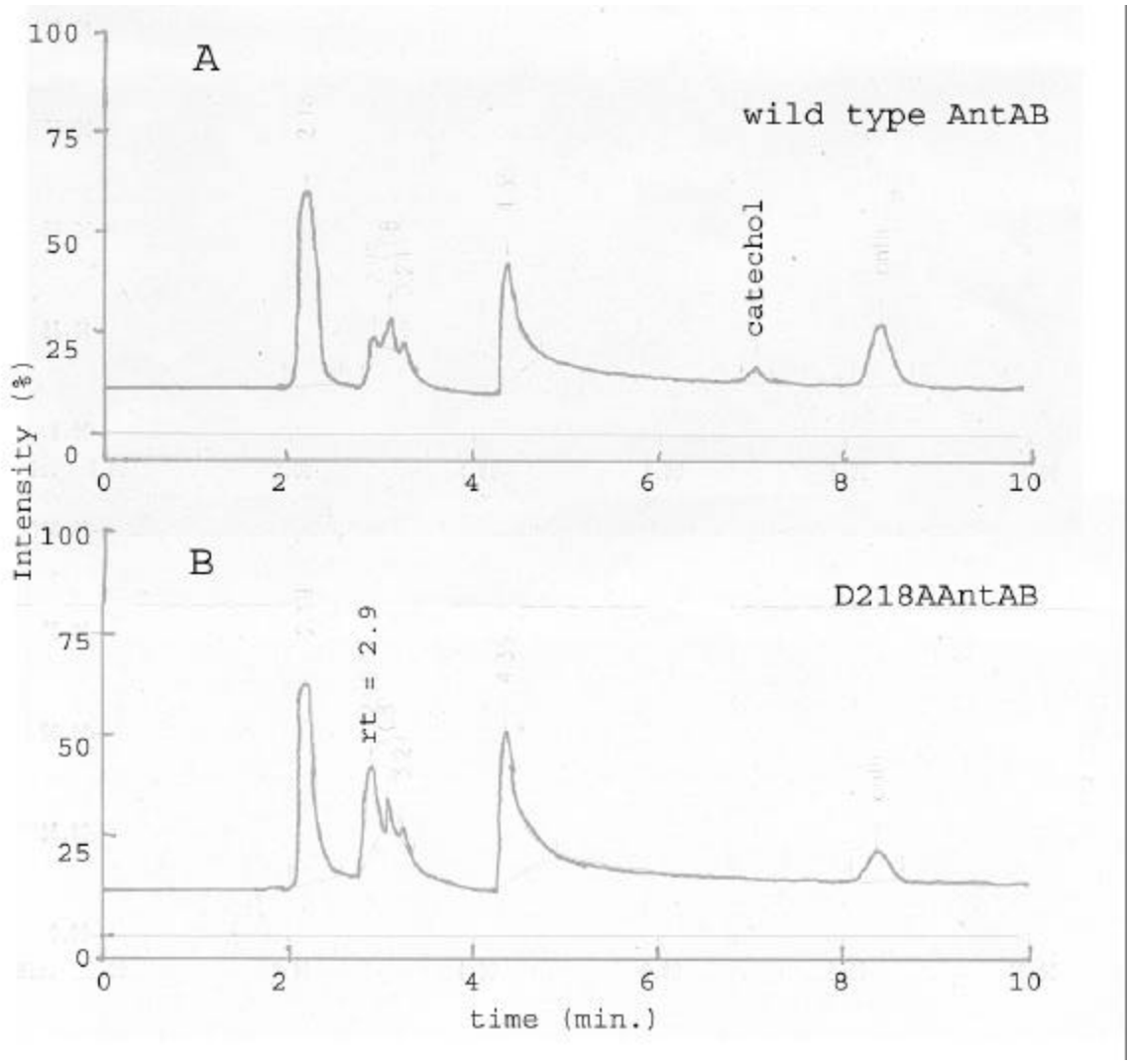

Figure 4.11. HPLC chromatograms of single turnover reactions (similar reaction conditions as described in Fig. 4.9) containing 50 μM reduced Rieske [2Fe-2S]/mononuclear iron sites of wild type AntAB (A) and D218AAntAB (B). Reactions were stopped after 5 minutes using concentrated phosphoric acid (1 % v/v). Peaks corresponding to products of the reactions are labeled as catechol (A) and unidentified product at retention time = 2.9 (rt = 2.9, B).

conditions. The retention of wild type oligomeric structure and ability to receive electrons from AntC, but complete lack of either dioxygenase or oxidase activity in the D218 variant AntABs demonstrates that D218 plays an important catalytic role within the $\alpha_3\beta_3$ oligomer. However, as discussed below, the results do not support an essential role for D218 in electron transfer between Rieske and mononuclear sites as had been proposed for the corresponding residue in NDO (*1*).

Comparisons of the kinetics of O_2 oxidation of Rieske-reduced AntABs indicated that a similar percentage of Rieske sites could be rapidly oxidized by O_2 in a substrate-dependent fashion for both wild type and D218A AntABs. Since this rapid phase (~ 350 s^{-1}) did not occur in either apo or Co(II)-substituted AntABs (with or without anthranilate), and was accompanied by mononuclear site oxidation, the rapid Rieske re-oxidation most likely occurs via electron transfer to the mononuclear iron site during the latter's reaction with O_2. The rapid phase accounts for oxidation of ~46% of wild type and ~31% of D218A AntAB Rieske sites. The remaining portion of reduced Rieske sites oxidized over the course of several minutes. These kinetic phases, which are similar in wild type and D218A AntABs, parallel those observed for wild type NDO single-turnover turnover studies (*18*). Since the as-isolated wild type and D218A AntABs contained their full complement of 9Fe/$\alpha_3\beta_3$, the slower phase of Rieske site oxidations in AntDO cannot be attributed to unoccupied mononuclear sites. The origin of the faster and slower phases may instead lie in anti-cooperativity, which could modulate either substrate binding or redox potentials of the iron sites.

The $[FeNO]^7$ EPR spectra of wild type and D218A AntABs (Figure 4.5) are consistent with an interaction of D218 with substrate but not with the mononuclear site.

The mononuclear Fe(II) site of D218A AntAB retained the ability to bind nitric oxide, and the $[FeNO]^7$ adduct was perturbed by substrate addition in a manner similar to but to a lesser degree than that of wild type. Although we cannot rule out the possibility that anthranilate coordinates to the mononuclear iron of AntAB, in NDO and several other RDOs (*2*), the nature of the substrate renders coordination to the mononuclear iron impossible. Therefore, it is presumed that anthranilate binds near but not to the mononuclear iron of AntAB.

Mechanistic implications

The mechanism of aromatic dihydroxylation catalyzed by RDOs has not been delineated. Que and Ho (*5*) proposed an oxygen activation/insertion mechanism based on the cytochrome P450 reaction cycle, as shown by the solid arrows in Figure 4.12. In this mechanism, addition of dioxygen to the enzyme-substrate complex yields a transient ferrous-oxy/ferric-superoxo complex. Electron transfer from the reductase via the Rieske site would then generate a formally ferric-peroxo mononuclear site, which could undergo proton-induced heterolytic cleavage of the O-O bond yielding a high-valent perferryl (Fe(V)=O) species. Transfer of a second electron from the reductase via the Rieske site to the mononuclear site would return the enzyme to the resting state. Que and Ho proposed, alternatively, that the ferric-peroxo species could be the intermediate responsible for substrate hydroxylation. None of the species except for the ferrous resting state in Figure 4.12 has ever been observed in any RDO.

The use of altered substrates or site-directed enzyme variants of RDOs typically leads to catalysis of dioxygen reduction to hydrogen peroxide via the uncoupling reaction

Figure 4.12. Schematic representation of the RDO reaction cycle (solid arrows) and uncoupling pathways (dashed arrows) leading to the formation of H_2O_2 and H_2O. Adapted from (*5*).

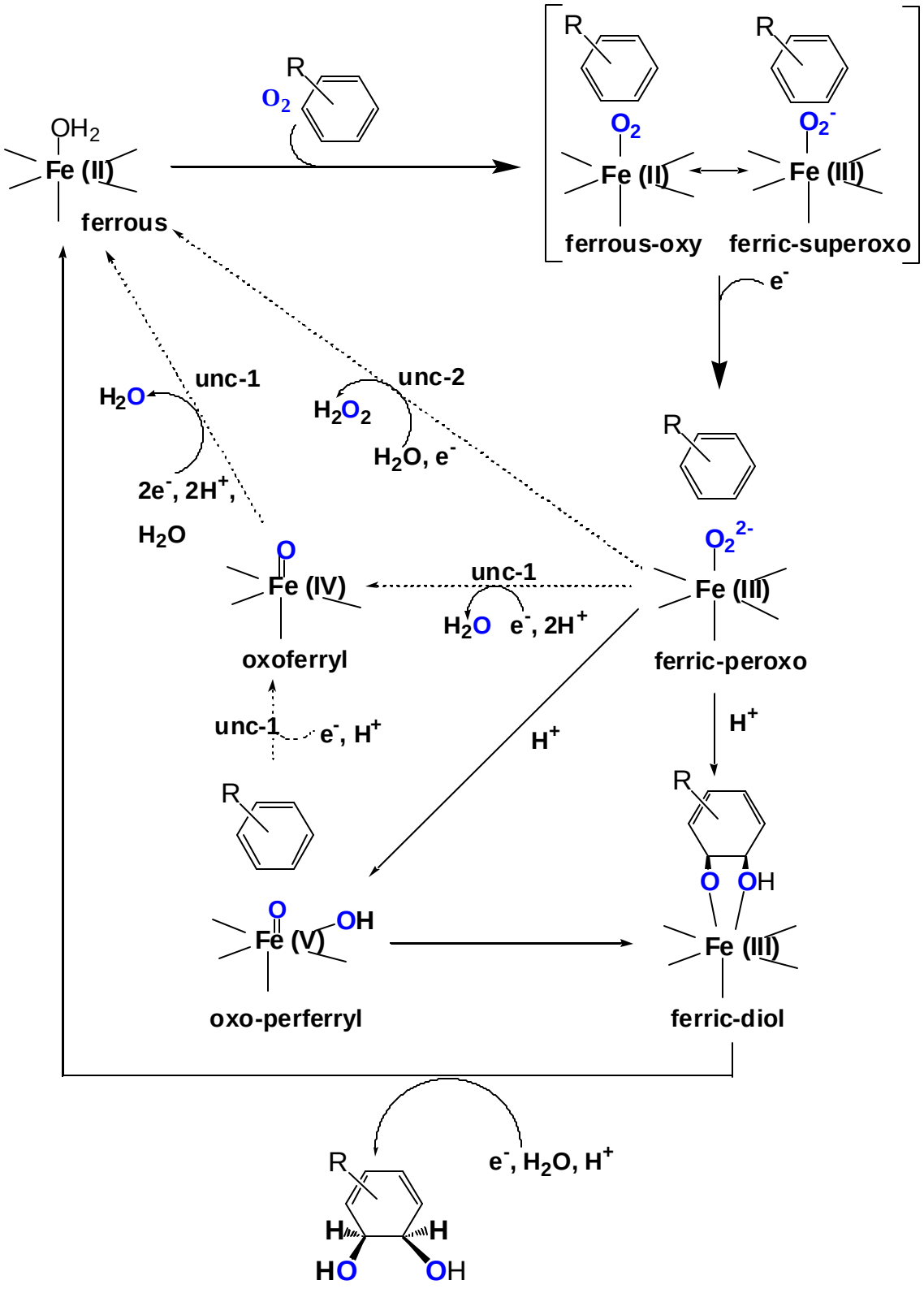
OH2
Fe (II)
ferrous
R
O2
R
O2
Fe (II)
ferrous-oxy
R
O2-
Fe (III)
ferric-superoxo
e-
unc-1
H2O
2e-, 2H+,
H2O
unc-2
H2O2
H2O, e-
R
O2 2-
Fe (III)
ferric-peroxo
O
Fe (IV)
oxoferryl
unc-1
H2O e-, 2H+
unc-1
e-, H+
H+
H+
R
O OH
Fe (III)
ferric-diol
O
OH
Fe (V)
oxo-perferryl
e-, H2O, H+
R
H
H
HO
OH

4.2 with no hydroxylation of substrate (*21*, *22*). This uncoupling reaction, in fact, occurs for the M43K variant of AntDO (*9*).

$$NAD(P)H + H^+ + O_2 \rightarrow H_2O_2 + NAD(P)^+ \qquad \textbf{(4.2)}$$

Reaction 4.2 could occur by the pathway labeled "unc-2" in Figure 4.12. This uncoupling is invariably substrate dependent, i.e., reaction 4.2 has not been reported for any RDO in the absence of either a substrate or a substrate analog. D218A AntAB apparently catalyzes neither substrate hydroxylation nor reaction 4.2 under standard assay conditions. However, a new product peak was observed in single turnover reactions of D218A AntAB that did not correspond to catechol, the product of wild type AntAB single turnover. Thus, proximal substrate binding must still trigger reaction of O_2 with the mononuclear ferrous site in the D218A AntAB. The crystal structure of NDO in the presence of the alternative substrate indole, showed that indole is oriented within the NDO active site such that its NH forms a hydrogen bond to the main chain carbonyl oxygen of Asp205, and is ideally positioned for dihydroxylation at C2 and C3 (*23*). Asp218 may, therefore, be involved in proper positioning of anthranilate in the AntAB active site for dihydroxylation at C1 and C2. Replacement of Asp218 by Ala may affect the position(s) at which anthranilate is hydroxylated, resulting in a product other than catechol. However, this Asp residue is highly conserved in the RDOs and, therefore, it seems unlikely it would function solely in proper positioning of substrate, given that the substrates that RDOs act upon vary so greatly. Therefore, it is proposed that Asp218 participates in and perhaps even orchestrates a sequence of electron and proton transfers

that channels the substrate-dependent Fe-O_2 reaction at the mononuclear site towards substrate dihydroxylation.

Reaction 4.2 has been cited as evidence that a ferric-peroxo intermediate is generated during O_2 activation in the RDOs (*22*). Figure 4.12 suggests that this intermediate is a key branch point leading to either substrate hydroxylation or uncoupled reduction of dioxygen. Figure 4.12 also indicates that a key step leading to substrate hydroxylation is protonation of the ferric-peroxo species. The fast phase of D218A AntAB Rieske reoxidation in the presence of anthranilate suggests that electron transfer to the mononuclear site is still able to occur and, according to Figure 4.12, generates the ferric-peroxo species. While the active oxygenating species in the RDO reaction cycle has not been determined, evidence for the participation of an oxo-perferryl intermediate in *cis* dihydroxylation reactions has been obtained with synthetic complexes (*24-26*). Product formation and lack of H_2O_2 generation in the D218A AntAB single turnover reactions could be the result of hydroxylation of anthranilate by the ferric-peroxo species, which is unable to form the expected product catechol. Therefore, it is proposed that Asp218 (and the homologous aspartate residues in other RDOs) is involved in proton delivery to the ferric-peroxo during coupled substrate hydroxylation. The hydrogen bonding pattern in the crystal structure of NDO is consistent with this aspartate being protonated in the Rieske reduced form (cf. Figure 1.11). Proton delivery from this carboxylic acid side chain could be triggered by delivery of the electron from the reduced Rieske site to the ferrous-oxy/ferric-superoxo in the preceding step of Figure 4.12. This oxidation of the Rieske site would increase the acidity of the hydrogen-bonded carboxylic acid, thereby triggering proton delivery. Protonation of the ferric peroxo would thus, be

coupled to the internal electron transfer event that created it and would not require participation of solvent. These mechanistic features would tend to minimize uncoupling of dioxygen activation from substrate hydroxylation. It is therefore proposed that this conserved aspartate residue between Rieske and mononuclear sites in RDOs is essential for efficient proton delivery to the activated oxygen species leading to substrate hydroxylation. Even the D218E variant showed no activity and this variant shows the same perturbed Rieske site absorption as the other D218 variants. The extra carbon in the Glu218 side chain is apparently sufficient to prevent optimal hydrogen bonding to the Rieske site.

References

1. Nam, J. W., Nojiri, H., Yoshida, T., Habe, H., Yamane, H., and Omori, T. (2001) *Biosci Biotechnol Biochem 65*, 254-263.
2. Bertini, I., Cremonini, M.A., Ferretti, S., Lozzi, I., Luchinat, C., and Viezzoli, M.S. (1996) *Coord. Chem. Rev.* ***151***, 145-160.
3. Butler, C. S., and Mason, J.R. (1997) *Adv. Microb. Physiol.* ***38***, 47-84.
4. Que, L. and Ho, R.Y.N. (1996) *Chem. Rev. 96*, 2607-2624.
5. Kauppi, B., Lee, K., Carredano, E., Parales, R. E., Gibson, D. T., Eklund, H., and Ramaswamy, S. (1998) *Structure* ***6***, 571-586.
6. Parales, R. E., Parales, J.V. and Gibson, D.T. (1999) *J. Bacteriol. 175*, 5877-5881.
7. Taniuchi, H., Hatanaka, M., Kuno, S., Hayaishi, O., Nakajima, M., and Kurihara, N. (1964) *J. Biol. Chem.* ***239***, 2204-2211.
8. Kobayashi, S., and Hayaishi, O. (1970) *Methods Enzymol.* ***17A***, 505-510.
9. Eby, D. M., Beharry, Z.M., Coulter, E.D., Kurtz, D.M., and Neidle, E.L. (2001) *J. Bacteriol.* ***183***, 109-118.
10. Bundy, B. M., Campbell, A. L., and Neidle, E. L. (1998) *J. Bacteriol.* ***180***, 4466-4474.
11. Schagger, H., and Jagow, G. von. (1987) *Anal. Biochem.* ***166***, 368-379.
12. Sambrook, J., Fritsch, E.F., and Maniatis, T. (1989) , Cold Spring Harbor Laboratory Press, Cold Spring Harbor, N.Y.
13. Ausubel, F. A., Brent, R., Kingston, R.E., Moore, D.D., Seidman, J.G., Smith, J.A. and Struhl, K. (1990) *Current Protocols in Molecular Biology*, Green Publishing and Wiley-Interscience, New York, NY.

14. Neidle, E. L. and Ornston, L.N. (1986) *J. Bacteriol. 168*, 815-820.

15. Shanley, M. S., Neidle, E.L., Parales, R.E. and Ornston, L.N. (1986) *J. Bacterol. 165*, 557-563.

16. Rocklin, A. M., Tierney, D.L., Kofman, V., Brunhuber, N.M., Hoffman, B.M., Christoffersen, R.E., Reich, N.O., Lipscomb, J.D. and Que, L. (1999) *Proc. Natl. Acad. Sci. U.S.A. 96*, 7905-7909.

17. Wolfe, M. D., Parales, J.V., Gibson, D.T., and Lipscomb, J.D. (2001) *J. Biol. Chem. 276*, 1945-1953.

18. Harpel, M. R. and Lipscomb, J.D. (1990) *J. Biol. Chem. 265*, 6301-6311.

19. Hegg, E. L., Whiting, A.K., Saari, R.E., McCracken, J., Hausinger, R.P., and Que, L. (1999) *Biochemistry 38*, 16714-16726.

20. Lee, K. (1999) *J. Bacteriol.* ***181***, 2719-2725.

21. Twilfer, H., Sandfort, G. and Bernhardt, F.H. (2000) *Eur. J. Biochem. 267*, 5926-5934.

22. Carredano, E., Karlsson, A., Kauppi, B., Choudhury, D., Parales, R. E., Parales, J. V., Lee, K., Gibson, D. T., Eklund, H., and Ramaswamy, S. (2000) *J Mol Biol 296*, 701-12.

23. Chen, K. C., and Que, L. (1999) *Angew. Chem. Int. Ed. 38*, 2227-2229.

24. Chen, K., Costas, M., Kim, J., Tipton, A.K., and Que, L. (2002) *J. Am. Chem. Soc. 124*, 3026-3035.

25. Wolfe, M. D., and Lipscomb, J.D. (2001) *J. Inorg. Biochem. 86*, 481.

CHAPTER 5

CONCLUSIONS

The studies presented in this dissertation have provided insight into the substrate specificity and reaction cycle of anthranilate 1,2-dioxygenase (AntDO) and benzoate 1,2-dioxygenase (BenDO) from *Acinetobacter* sp. strain ADP1. Previous studies determined that AntDO and BenDO cannot substitute for each other in vivo (*1*). However, the results presented herein have shown that AntDO and BenDO are able to dihydroxylate both anthranilate and benzoate to the expected in vivo products. In addition, both AntDO and BenDO in vitro were able to dihydroxylate many other substituted benzoates, which contradicts the notion that plasmid-encoded RDOs have a wider substrate specificity than their chromosomally-encoded counterparts (*2*, *3*). Possible explanations for the conflicting in vivo and in vitro results may lie in metabolic constraints of aromatic hydrocarbon degradation in vivo resulting from either lack of or insufficient induction of the necessary catabolic operons for mineralization of a given aromatic compound. Further studies are needed to elucidate the identity and mechanisms of the regulatory elements that control transcription of the *ant* and *ben* operons in response to aromatic inducers. Once characterized, these regulatory elements may be genetically altered in an effort to increase the range of substrates *Acinetobacter* sp. strain ADP1 can degrade. Similar experiments have been done to expand the range of aromatic compounds degraded by *Pseudomonas* (*4*).

The use of alternative substrates and protein variants can provide clues to intermediates involved in the RDO reaction cycle. Electron transfer was uncoupled from substrate dihydroxylation to form H_2O_2 and/or H_2O in AntDO and BenDO reactions with several of the substrates tested, most likely as a result of the decomposition of intermediates in the RDO reaction cycle. The formation of H_2O_2 and H_2O in addition to dihydroxylated product with some of the substrates suggests the involvement of ferric-peroxo and/or oxo-perferryl species, reminiscent of the cytochrome P450CAM reaction cycle (*5*). The importance of a highly conserved aspartate residue throughout the RDOs (*6*) was demonstrated and proposed to function in proton transfer to activated intermediates in RDO catalysis, rather than in electron transfer as was previously suggested (*7*). Future studies will be aimed at conclusively identifying intermediates in and the mechanism of the RDO reaction cycle using a variety of spectroscopic techniques. This will aid in engineering RDOs with increased catalytic efficiency.

Nature has provided many diverse enzymes whose capabilities are being exploited and perfected through protein engineering to perform a desired function. The reaction catalyzed by the Rieske dioxygenases (RDO) offers a more economically viable and safer means for the production of intermediates in the synthesis of pharmaceuticals. In addition, the RDO reaction is the initial transformation in the microbial degradation of numerous aromatic environmental pollutants (*6*, *8*, *9*). Bioremediation, therefore, is a potential cost-effective alternative to conventional processes for the removal of aromatic pollutants in the environment. Investigations into the mechanisms, structures and functions of RDOs are essential to aid protein engineering efforts to optimize their potential as biocatalysts.

References

1. Bundy, B. M., Campbell, A. L., and Neidle, E. L. (1998) *J. Bacteriol.* ***180***, 4466-4474.
2. Harayama, S., Rekik, M., Bairoch, A., Neidle, E.L., and Ornston, L.N. (1991) *J. Bacteriol. 173*, 7540-7548.
3. Neidle, E. L., Hartnett, C., Ornston, L.N., Bairoch, A., Rekik, M., and Harayama, S. (1991) *J. Bacteriol.* ***173***, 5385-5395.
4. Ramos, J. L., Stolz, A., Reineke, W., and Timmis, K.N>. (1986) *Proc. Natl. Acad. Sci. 83*, 8467-8471.
5. Sligar, S. G. (1999) *Essays in Biochemistry 34*, 71-82.
6. Nam, J. W., Nojiri, H., Yoshida, T., Habe, H., Yamane, H., and Omori, T. (2001) *Biosci Biotechnol Biochem 65*, 254-63.
7. Parales, R. E., Parales, J.V. and Gibson, D.T. (1999) *J. Bacteriol. 175*, 5877-5881.
8. Bertini, I., Cremonini, M.A., Ferretti, S., Lozzi, I., Luchinat, C., and Viezzoli, M.S. (1996) *Coord. Chem. Rev.* ***151***, 145-160.
9. Butler, C. S., and Mason, J.R. (1997) *Adv. Microb. Physiol.* ***38***, 47-84.